Structure and Molecular Dynamics of Thin Films of Homopolymers and Miscible Polymer Blends

Vorgelegt von
M.Sc.
Sherif A. Madkour
geb. in Kairo, Ägypten

von der Fakultät III - Prozesswissenschaften
der Technischen Universität Berlin
zur Erlangung des akademischen Grades

Doktor der Ingenieurwissenschaften
Dr. –Ing.

genehmigte Dissertation

Promotionsausschuss:
Vorsitzender: Prof. Dr. rer. nat. Walter Reimers (TU Berlin)
Gutachter: Prof. Dr.-Ing. Dietmar Auhl (TU Berlin)
Gutachter: Prof. Dr. rer. nat. Andreas Schönhals (BAM)

Tag der wissenschaftlichen Aussprache: 24.11.2017

Berlin 2018

TABLE OF CONTENTS

ACKNOWLEDGMENTS

I would like to express my heartfelt gratitude to Prof. Dr. Andreas Schönhals for giving me the opportunity to join his research group and finishing my PhD at BAM Bundesanstalt für Materialforschung und -prüfung. His flexibility, support, encouragement, and guidance have been my guiding stones throughout this work. During the past 4 years, he has been empowering me to become a better scientist and above all a better person. In addition, I would like to thank him for his continuous sincerity and honesty in conveying his knowledge to my colleagues and myself. I would also want to acknowledge the financial support from the German Science Foundation (DFG SCHO-470/20-2).

Moreover, I would like to express my sincere apperception to Prof. Dr. Dietmar Auhl and Prof. Dr. Manfred H. Wagner at the Technical University of Berlin (TU Berlin) for their continuous support, understanding and valuable suggestions.

I would also like to take this opportunity to thank Prof. Dr. Friedrich Kremer (Universität Leipzig), and Dr. Martin Tress (University of Tennessee) for the experimental assistance and the many fruitful discussions. In addition, I thank Prof. Dr. Heinz Sturm (BAM), Prof. Dr. Christoph Schick (Universität Rostock), Dr. Heiko Huth (Universität Rostock), for all the guidance and help. They have provided me with a lot of useful suggestions and guidance that helped me overcome many difficulties in the experimental work. Additionally, I would like to send special thanks to Prof. Dr. Simone Napolitano (Université Libre de Bruxelles), Prof. Dr. Regine von Klitzing (TU Darmstadt), Dr. Andreas Hertwig (BAM), Dr. Radnik Jörg (BAM), and Prof. Dr. Zahraa Fakhraai (University of Pennsylvania) for the valuable discussions, which have enriched my scientific knowledge as well as the pleasant and successful collaborations.

Furthermore, I would like to thank all the professors, faculty during the course of my education for giving me such valuable knowledge. Especial thanks to Prof. Dr. Wei-Heng Shih (Drexel University, PA) for introducing me to the world of research and nanotechnology and believing that I could one day become a scientist.

Last but not least, I would like to thank all the experts of BAM who kindly participated in this work. Mr. D. Neubert for his help with all the DSC measurements and Ms. Hidde and Mr. F. Milczewski for their help with the daily problems faced in the lab. I am also in debt to other labs that allowed me to use their facilities in my research. Moreover, I would like to thank all my colleagues in BAM, MSc. Paulina Szymoniak, MSc. Arda Yildirim, MSc.

Marcel Gawek, MSc. Shereen Omara, Dr. Huajie Yin, and Dr. Nora Konnertz for all the help with the day-to-day issues in the lab as well as the countless laughs and priceless memories though out the years.

At the end, I would like to thank my family and friends around the world for their love and support throughout my years of studying. Most importantly, I would like to thank my fiancée, Fairouz Gaber, whom I found through the motivation and strength. She patiently supported me to achieve my goals and brought me so much happiness, love, courage and strength. Finally, I would like to send my sincere thanks and gratitude to my parents, Aly Madkour and Salwa Taha, as well as my brother, Karim Madkour, for all their financial and incorporeal support throughout the years. There are no words that could possibly describe what they have done for me. The success of this work, and where I am today, is the result of their love, patience, trust, and encouragement throughout my entire life.

ZUSAMMENFASSUNG

In den letzten Jahren hat die Forschung auf dem Gebiet des Confinements auf der Nanometerskala zu vielen Versuchen geführt, die Eigenschaften von Polymeren für spezielle Anwendungen zu verändern. Eines der am häufigsten untersuchten Systeme mit Confinement im Nanometerbereich sind dünne Filme, bei dem ein 1-dimensionales Confinement aus der Verringerung der Filmdicke resultiert. Für derartige Systeme ist es wichtig zu verstehen, wie das Confinement den Glasübergang und die dazugehörige Glasdynamik im Vergleich zu einer räumlich ausgedehnten Probe beeinflusst. So kann es bei dünnen Filmen mit einigen Nanometern Dicke sein, dass innere und die Luft/Polymer Grenzfläche zu einer Änderung des Glasübergangs und der Glasdynamik führen, welches letztlich zu einer Veränderung von makroskopischen Eigenschaften wie z.B. Adhäsion, Biokompabilität oder/und Entnetzung führen kann.

Die Untersuchungen, die in dieser Dissertation dargestellt sind, konzentrieren sich auf das Verständnis, wie das Confinement in dünnen Filmen (200 nm - 7 nm) die Glasübergangstemperatur (T_g^{therm}) und die zugehörige Segmentdynamik (α-Relaxation, charakterisiert durch eine dynamische Glasübergangstemperatur, T_g^{dyn}) bei Homopolymeren und mischbaren Polymerblends beeinflussen. Die Ergebnisse wurden über das 3-Layer-Modell hinaus diskutiert, wobei weitere Parameter wie das Molekulargewicht, die Heizrate, die kompositionelle Heterogenität, geometrische Frustration, etc. mit einbezogen worden. Sich ergänzende experimentelle Methoden wie die spektroskopische Ellipsometrie, dielektrische Spektroskopie (BDS), auch unter Nutzung neuartiger Probengeometrien welche die Messung von dünnen Filmen mit freier Oberfläche erlauben, und der spezifischen Wärmespektroskopie (SHS) wurden angewandt, um den Glasübergang dünner Polymerfilme sowohl vom thermodynamischen als auch vom kinetischen Standpunkt zu untersuchen.

Im ersten Teil der Dissertation wurden dünne Filme aus Poly(2-vinyl pyridine) (P2VP) mit hohem Molekulargewicht mittels der SHS untersucht, um die in der Literatur lang andauernde Diskussion der Unabhängigkeit von T_g^{dyn} von der Schichtdicke dünner Filme von Homopolymeren und ihre Ursachen zu verifizieren. Mittels einer neu entwickelten Analysemethode wurde gezeigt, dass die Messdaten neue Einsichten über den Einfluss der Polymer/Luft- und der Polymer/Substrat-Grenzfläche auf die Dynamik des gesamten Films

liefern. Diese neu entwickelte Methode wurde dann angewandt, um alle SHS-Messdaten die in der Dissertationen dargestellt sind, zu analysieren.

Obwohl die Ergebnisse der Messungen von dünnen Filmen von P2VP einen leichten Confinement-Effekt zeigen, konnte dennoch nicht bestätigt werden, ob dieser Effekt auf die höhere molekulare Beweglichkeit an der Polymeroberfläche (d.h. die Polymer/Luft-Grenzfläche) oder einer Erhöhung des freien Volumens an der Polymer-Substrat-Grenzfläche auf Grund der geringeren Konditionierungszeit im Vergleich zur terminalen Relaxationszeit des Polymers zurückzuführen ist. Aus diesem Grund wurde der Fokus auf die Untersuchung dünner Filme von Poly(vinyl methyl ether) (PVME) mit niedrigem Molekulargewicht gelegt. Dünne Filme von PVME wurden sowohl mit der SHS als auch mit der BDS untersucht. Mittels angepasster Probenanordnungen wurden die Ergebnisse der Messungen von BDS und SHS quantitativ verglichen. Mit der BDS wurden zwei Prozesse beobachtet. Der erste Prozess wurde den kooperativen Segmentfluktuationen der α-Relaxation zugeordnet, verursacht durch die volumeartige Schicht. Dieses Ergebnis ist in übereinstimmung mit den Ergebnissen der SHS. Der zweite Prozess dagegen, wurde lokalisierten segmentellen Fluktuationen innerhalb einer irreversibel am Substrat adsorbierten Schicht zugeordnet, Diese konnte für dünne Filmen erstmalig in dieser Arbeit untersucht wurde.

Die Ergebnisse der Untersuchungen dünner Filme von P2VP und PVME weisen darauf hin, dass der Effekt der Schicht an der Polymer/Luft-Grenzfläche auf die segmentelle Dynamik des gesamten Films schwierig zu untersuchen bzw. zu verifizieren ist. Dies lässt sich damit begründen, dass oberhalb von T_g^{therm}, die segmentelle Dynamik der Oberflächenschicht sich an die Segmentdynamik räumlich ausgedehnter Proben angleicht. Indem eine asymmetrische Polymermischung ausgewählt wurde, bei der es zur Anreicherung einer Polymerkomponente an der Oberfläche kommt, konnte der Einfluss der Oberflächenschicht auf die segmentelle Dynamik de gesamten Films geuntersucht werden.

Im zweiten Teil der Dissertation wurde das gleiche PVME, welches bereits oben als Homopolymer untersucht wurde, mit Polystyrol (PS) in zwei Gewichtsanteilen (50:50 wt% und 25:75 wt%) gemischt. Untersuchungen dünner Filme dieser Polymermischungen mittels der SHS zeigten zum ersten Mal eine deutliche Dickenabhängigkeit von T_g^{dyn}. Während Filme der 50:50 wt%-Probe eine monotone Verringerung von T_g^{dyn} mit abnehmender Filmdicke zeigen, weisen Filme der 25:75 wt%-Probe ein nicht-monotones Verhalten von T_g^{dyn} auf, welche bei 30 nm ein Maximum hat. Die Abnahme von T_g^{dyn} für

kleinere Schichtdicken als 30 nm wurde auf die Anreicherung von PVME an der Oberflächenschicht zurückgeführt, welche bei filmdicken unter 30 nm das Verhalten des gesamten Filmes dominiert.

Darüber hinaus lieferten die SHS und Ellipsometrie weiter Möglichkeiten, sowohl den Glasübergang als auch die Glasdynamik für dünne Filme der 25:75 wt% Mischung zu untersuchen. Untersuchungen der Schichtdickenabhängigkeit von T_g^{therm} und der Vogel-Temperatur (T_0) für die Mischung 25:75 wt % ergaben, dass beide letztgenannten Temperaturen im Unterschied zu T_g^{dyn} einen systematischen Anstieg mit abnehmender Filmdicke Größen. Dieses wurde im Rahmen verschiedener Kooperations-Längenskalen für jede Temperatur diskutiert, welche in verschiedenen Empfindlichkeiten bzgl. der Zusammensetzung und der Dicke resultieren. Überraschenderweise konnte gezeigt werden, dass die Schichtdickenabhängigkeit von T_g^{dyn} tatsächlich die Dickenabhängigkeit von T_g^{therm} und T_0 bei Frequenzen die für T_0 charakteristisch sind, abbilden konnte.

Des weiteren wurde die Röntgen-Photoelektronen-Spektroskopie (XPS) angewandt, um die Existenz einer PVME-angereicherten Schicht nachzuweisen und ihre Zusammensetzung abzuschätzen. Dadurch wurde die dickenabhängige kompositionelle Heterogenität bestätigt.

Abschließend wurden dünne Filme des 50:50 wt% Systems mit der BDS untersucht. Die Ergebnisse wurden quantitativ sowohl mit den SHS-Ergebnissen sowie mit den Ergebnissen von Messungen reinen dünnen PVME-Filme diskutiert. Die Kombination von BDS und SHS bietet dabei ein leistungsfähiges Werkzeug, um die verschiedenen Aspekte der Glasdynamik und ihre Beziehung zu den kompositionellen Heterogenitäten zu betrachten. Bei dünnen Filmen von PVME/PS-Blends ist die BDS aufgrund der starken Asymmetrie der Dipolmomente von PVME und PS nur empfindlich auf die Segmentdynamik von PVME, die durch das PS beeinflusst wird. Währenddessen ist die SHS auf mobile Segmente von PVME und PS empfindlich. Der Vergleich der Daten aus beider Methoden zeigte die kompositionelle Heterogenität innerhalb des Polymerblends. Zusätzlich zeigten die Ergebnisse der BDS eine schichtdickenabhängige Veränderung der kompositionellen Heterogenität (in molekularen Größenordnungen) auf. Diese Änderungen beeinflussen direkt die Moleküldynamik des gesamten Films und sollten als zusätzlicher Parameter betrachtet werden, wenn der Confinement-Effekt auf den Glasübergang und die Glasdynamik von dünnen Filmen aus mischbaren Polymerblends diskutiert wird. Darüber hinaus wurde, ähnlich wie bei den dünnen Filmen aus reinen PVME, ein vollständig unabhängiger thermisch aktivierter Relaxationsprozess beobachtet Dieser Prozess wird

Fluktuationen innerhalb der adsorbierten Schicht molekular zu geortnet. Es wurde der Schluss gezogen, dass dieser Prozess zusätzlich zu der Dickenverminderung zwei zusätzliche Confinementeffekte erfährt. I) Confinement zwischen einem stark gebundenen Teil in der adsorbierten Schicht und der volumenartigen Schicht. II) Confinement aufgrund immobiler PS-Segmente innerhalb der adsorbierten Schicht.

ABSTRACT

In recent years, research on nanoscale confinement of polymers has witnessed topical investigations in attempt to tune polymer properties on demand. One of the most studied forms of nanoconfinement are thin films, where 1D confinement results from the reduction of the film thickness. For these systems, it is crucial to understand how confinement affects the glass transition phenomenon and the associated glassy dynamics, compared to the bulk behavior. This is due to the direct impact of these phenomena on many thin film-based technologies. For instance, for films of few nanometers in thickness, solid interfaces and free surfaces could alter glass transition and glassy dynamics, which could, in return, change macroscopic properties like adhesion, biocompatibility and dewetting.

The research work presented in this dissertation is focused on understanding how the confinement in thin films (200 nm – 7 nm) influences the glass transition temperature (T_g^{therm}) and the related segmental dynamics (α-relaxation process, related to a so-called dynamic glass transition temperature T_g^{dyn}) in both homopolymers and miscible polymer blends. The results were discussed beyond the idealized three-layer model, taking into account other parameters like molecular weight, annealing time, compositional heterogeneities, packing frustration, etc. This goal is achieved through careful choosing of the polymeric systems as well as combining different characterization methods with different sensitivities and frequency windows. Complementary experimental techniques including Spectroscopic ellipsometry, Broadband Dielectric Spectroscopy (BDS), employing a novel sample geometry that allows the measurement of supported films, and Specific Heat Spectroscopy (SHS) were used to investigate the glass transition phenomena of thin polymer films, from the thermodynamic and the kinetic point of views.

First, thin films of high molecular weight Poly(2-vinyl pyridine) were studied by SHS to confirm the long-standing discussion in literature regarding the thickness independency of T_g^{dyn} of thin homopolymer film and molecular reasons behind it. Through a newly developed analysis method, a slight decrease in T_g^{dyn} with decreasing the film thickness was evidenced for the first time. It was shown that SHS data, if analysis errors were avoided, could indeed be an insightful tool to study confinement effects on the overall dynamics of the film. This new analysis method was then employed to analyze the SHS data for the entire work presented in this dissertation.

Although the results of the P2VP thin films showed a slight confinement effect, it could not be confirmed whether the evidenced confinement effect was due to a free surface (the layer at the polymer/air interface) or an increase in the free volume, at the polymer/substrate interface, due to the lower annealing time, compared to the terminal relaxation time of the polymer. Therefore, the attention was switched to a low molecular weight Poly(vinyl methyl ether) PVME thin films, to insure good annealing conditions within a reasonable time. PVME thin films were then investigated by both SHS and BDS. Through adapting a new sample arrangement that allows the measuring supported films, the results from BDS and SHS were quantitatively compared. This study revealed that the molecular dynamics of the thin films had two dielectrically active processes. The first process was assigned to the cooperative segmental fluctuations of the α-relaxation, originating from a bulk-like layer, also confirmed by SHS. However, the second process was assigned to localized segmental dynamics within an irreversibly adsorbed layer, reporting the first probing of the molecular dynamics of an adsorbed layer within thin films.

The results of both studies on P2VP and PVME thin films suggested that the effect of the layer at the polymer/substrate interface on the overall segmental dynamics would be very difficult to probe and/or confirm. This is due to the fact that above T_g^{therm}, which is the temperature range at which the segmental dynamics are probed, the segmental dynamics of the free surface layer become indistinguishable from that of the bulk. However, by carefully choosing an asymmetric polymer blend system, the effect of the free surface layer on the overall segmental dynamics could be probed. This is due to the surface enrichment phenomenon, which results in a different composition at the polymer/air interface, compared to the bulk.

Consequently, in the second part of this dissertation, an identical PVME, to the one studied above, was then blended with the well-studied Polystyrene (PS) in two weight fractions 50:50 wt% and 25:75 wt%. SHS investigations of the thin films of the two blends revealed for the first time an unexpected thickness dependence of T_g^{dyn} (related to the α-relaxation). While thin films of the 50:50 wt% blend showed a systematic decrease in T_g^{dyn} with decreasing film thickness, thin films of the 25:75 wt% blend showed a non-monotonous behavior, which peaks at 30 nm. For the former blend, the systematic decrease was traced to a PVME-rich layer at the polymer/air interface, which becomes dominant with decreasing the film thickness. On the other hand, the non-monotonous behavior of the latter blend was traced back to compositional heterogeneities, which is thickness dependent and results in an

increase in T_g^{dyn} to 30 nm, followed by a drop in the T_g^{dyn} down to 10 nm. The drop in T_g^{dyn} was traced back to the effect of a PVME-rich layer at the polymer/air interface, becoming dominate for thicknesses below 30 nm.

Furthermore, combing SHS and spectroscopic ellipsometry provided a window to study both the glass transition and the glassy dynamics of the thin films of the 25:75 wt% blend. Investigations of the thickness dependence of T_g^{therm} and the Vogel temperature (T_0) for the 25:75 wt% blend revealed that the latter temperatures showed a systematic increase with decreasing film thickness, in difference to that of T_g^{dyn}. This was discussed through elaborating the different cooperativity length scales corresponding to each temperature, which would result in different sensitivities to composition and thickness. Surprisingly, it was shown that the thickness dependence of T_g^{dyn} could indeed recover the thickness dependence of both T_g^{therm} and T_0, at frequencies related to T_0.

X-ray photoelectron spectroscopy (XPS) was then utilized to affirm the existence and estimate the composition of the PVME-rich interfaces. In addition, it confirmed the thickness dependent compositional heterogeneity and supported the above mentioned findings.

Finally, thin films of the 50:50 wt% blend were investigated by BDS. The results were quantitatively discussed with the SHS ones as well as that of pure PVME thin films. The combination of BDS and SHS provides a powerful tool to look at the different aspects of the glassy dynamics and its relationship to the dynamic heterogeneities. For PVME/PS blends, BDS is only sensitive to the segmental dynamics of PVME, as affect by PS, due to the strong asymmetry in the dipole moments of PVME and PS. Whereas, SHS is sensitive to all the mobile segments of PVME and PS. Comparing that data from both methods elaborated the dynamics heterogeneity within the blend samples. In addition, BDS results evidenced thicknesses dependent changes in the compositional heterogeneities (at a molecular level) within the films. These changes directly affect the molecular dynamics of the overall film and should be considered as an extra parameter, when discussing the confinement effect on the glass transition and glassy dynamics of miscible polymer blends. Moreover, similar to the pure PVME thin films, a completely independent thermally activated relaxation process, related to the molecular fluctuations within the adsorbed layer, was observed for films below 30 nm. For the latter process it was concluded that this process undergoes two extra confinement effects, in addition to the thickness reduction. I)

Confinement between a strongly bounded part in the adsorbed layer and the bulk-like layer.

II) Confinement due to frozen PS segments within the adsorbed layer.

CHAPTER 1 – Introduction

Humankind has been producing and developing glasses for a few millennia. Throughout the years, glasses have been extremely versatile; from hunting tools to stained glass windows, to thin films in smart phones screens. Under the genetic name "glasses", this class of materials exhibits a solid-like response, though lacking the long-range order of crystals. In general, rapid cooling of a glass-forming liquid (e.g. amorphous polymers, which is the focus of this work) induces the decrease of the molecular mobility of the system. Subsequently, the molecules lose their ability to rearrange themselves in a thermodynamic equilibrium. This transition from a liquid-like equilibrium state to a non-equilibrium glassy state is called glass transition. This transition takes place over a certain temperature range, which is characterized by the so-called thermal glass transition temperature (T_g^{therm}).

For more than a century now, glass transition has been considered one of the most interesting phenomena in soft matter physics.[1-7] Despite the wealth of knowledge present on this topic, a complete and unified understanding of the phenomena still remains. For instance, to this date, it is not understood *why the viscosity of a glass-forming liquid, which cannot crystalize, increases by almost 10-orders of magnitude, within a limited temperature range, while the density varies only by 5%.*[8] For amorphous polymers, the glass transition is accompanied by an increase in the shear modulus with decreasing temperature, related to the segmental dynamics (α-relaxation), which makes it a very important phenomenon for polymers processing.[9]

Furthermore, the past three decades have witnessed an increasing interest in glass transition and the related α-relaxation for confined polymers at the nanoscale. Nowadays, thin polymer films (<100 nm) have been attracting the most attention due to their high demand in functional coatings, batteries, innovative organic electronics, and hybrid materials. Advances in these fields depend strongly on organic and/or polymeric materials confined in thin films or adsorbed at surfaces.[6,10] For thin films of few nanometers in thickness, solid interfaces and free surfaces could alter for instance entanglements, segmental dynamics, and T_g^{therm}, compared to their bulk values. Consequently, this could change macroscopic quantities of thin films like adhesion, wettability, friction, and reactivity, which are, for instance, essential properties for hybrid materials.[11] Therefore, for optimized innovative applications of thin polymer films, an understanding of the molecular reasons for the

possible deviations of the properties of confined polymers from that of their bulk is essential.[10]

The aim of this work is to achieve a deeper understanding of how the surfaces, the interfaces (especially the polymer/substrate interface), and the film thickness influence T_g^{therm} and the segmental dynamics of the whole film. In addition, it aims to understand the molecular mechanism behind the possible deviations from the bulk properties, beyond a trivial surface/volume ratio parameter. The research work presented in this dissertation, considers especially selected systems, including thin films of homopolymer and miscible polymer blends, as well as their bulk films. This goal is approached by attempting to simplify the topic through two parallel methodologies I) careful choosing of the polymeric systems, which allows the enhancement of the effect of a certain parameter (e.g. optimizing M_w and annealing times affects the thickness of the layer at the polymer/substrate interface) on the glass transition and glassy dynamics of the whole film. II) Combining different characterization methods with different sensitivities and frequency windows, which could allow selective probing of a polymer (in the case of polymer blends) and/or a property (glass transition versus segmental dynamics) of the measured systems. A detailed discussion of the idea and the line of thought behind this work is presented in chapter 5.

To investigate the thin polymer films, a combination of surface analytical techniques and volume sensitive methods was utilized. The surface analytical techniques, concluded in Atomic Force Microscopy (AFM), ellipsometry, and X-ray photoelectron spectroscopy (XPS) were employed to control the quality and thicknesses of the films, as well as their chemical composition. Whereas the volume sensitive methods, concluded in Broadband Dielectric Spectroscopy (BDS), Specific Heat Spectroscopy (SHS), and spectroscopic ellipsometry, were used to investigate the influence of the film thickness on the glassy dynamics and the glass transition behavior of the polymer thin films, from both the kinetic and the thermodynamic point of views.

This dissertation is arranged as follows. *Chapter 1* gives a short introduction to the glass transition phenomena as well as the motivation behind the research on glass transition and thin polymer films. This is then followed by an overview of the glass transition and the related relaxation behavior in amorphous polymers, as presented in *Chapter 2*. It begins with the discussion of bulk polymers, covering the topics of the glass transition temperature, the segmental dynamics, and some models utilized to relate the glass transition phenomena to the segmental dynamics.

Chapter 3 provides fundamental information on miscible polymer blends. It discusses the miscibility of polymer blend, covering the topics of the glass transition temperature, the segmental dynamics, the dynamic heterogeneity, and some models describing the intrinsic features and anomalies found for these especial systems.

Chapter 4 provides a literature review, theories and suggested model to discuss the glass transition and glassy dynamics of thin polymer films and the possible deviation from their bulk values. This is conferred in the framework of the three-layer model as well as the packing frustration, which is built on the free volume concepts. It also pays attention to the recent research on of the so-called irreversible adsorbed layers (the layer at the polymer/substrate interface).

Chapter 5 provides the idea behind all the experimental work presented here. It starts with the core aim of this work and how the idea behind this work was developed. It explains why the investigated systems where of choosing and why the employed characterization methods were used, in the exact combination. This chapter connects all the experimental work that follows. Afterwards, *Chapter 6* provides fundamental principles about the main experimental techniques used in this work. Moreover, it briefly introduces all the materials used in the study as well as all the methods and conditions used to prepare and characterize the samples.

The results and discussion are then presented in an accumulative manner, in chapters 7 through 11. *Chapter 7* presents and discusses the results of homopolymers poly(2-vinyl pyridine) (P2VP), where a new analysis method was developed, resulting in an enhanced sensitivity of the SHS data, in addition to evidencing the first confinement effect on the segmental dynamics of homopolymer thin films.[13] This analysis method was then employed to analyze all SHS data presented in this dissertation. *Chapter 8* presents a study on the dynamics of poly(vinyl methyl ether) (PVME) thin films, from both the thermal and dielectric perspectives.[14] This was carried out using SHS and BDS. For the latter method, a recently developed nanostructured electrode capacitors was utilized to measure supported polymer films.[15]

Further, PVME was then blended with the well-studied Polystyrene (PS) in an asymmetric miscible-in-bulk blend with two different concertation; PVME/PS 50:50 wt% and PVME/PS 25:75 wt%. Multiple studies were carried out to study the glassy dynamics and glass transition of the blends. *Chapter 9* presents a calorimetric investigation on thin films of PVME/PS with a concentration of 25:75 wt%, employing SHS.[16] Furthermore, the results

were further quantitatively compared to those of the 50:50 wt% blend.[17] *Chapter 10* presents a study on the decoupling phenomena of T_g^{therm} (obtained by spectroscopic ellipsometry), T_g^{dyn}, and the so-called Vogel temperature (T_0), for the 25:75 wt% blend.[18] The results and conclusions were supported by X-ray photoelectron spectroscopy (XPS) study of the interfaces of the thin films.

Last but not least, *Chapter 11* presents a studies on the dielectric response of the segmental dynamics of PVME/PS blend with a concentration of 50:50 wt%.[19] These results were further quantitatively compared to that of pure PVME thin films, chapter 7.[14] Finally, *Chapter 12* gives a short summary to the research work presented, connecting all the above-mentioned studies, followed by a short outlook on the next interesting challenges in the field.

References

1 Debenedetti, P.; Stillinger, F. *Nature* **2001**, 410, 259–267.
2 Anderson, P. W. *Science* **1995**, 267, 1617.
3 Ediger, M.; Horrowell, P. *J. Chem. Phys.* **2012**, 137, 080901.
4 Sastry, S.; Debendetti, PG.; Stillinger, FH. *Nature* **1998**, 393, 554-557.
5 Yin, H.; Madkour, S.; Schönhals, A. Dynamics in confinement: Progress in Dielectrics*, Springer vol. 2*. **2014**, Kremer, F. (Ed.).
6 McKenna, G.; Simon, S. *Macromolecules* **2017**, 50, 6333–6361.
7 Russell, T.; Chai, Y. *Macromolecules* **2017**, 50, 4597-4609.
8 Napolitano, S.; Glynos, E.; Tito, N. *Reports on Progress in Physics* **2017**, 80, 036602.
9 Young, R.; Lovell, P. The Amorphous State in Introduction to Polymers, *CRC press* **2011,** 3rd eds, Florida.
10 Ediger, M.; Forrest, J. A. *Macromolecules* **2014**, 47, 471-478.
11 Napolitano, S.; Pilleri, A.; Rolla, P.; Wübbenhorst, M. *ACS Nano* **2010**, 4, 841-848.
12 Anderson, P. Through the Glass Lightly. *Science* **1995**, 267, 1615-1616.
13 Madkour, S.; Yin, H.; Füllbrandt, M.; Schönhals, A. *Soft Matter* **2015**, 11, 7942-7952.
14 Madkour, S.; Szymoniak, P.; Heidari, M.; von Klitzing, R.; A. Schönhals. *ACS Appl. Mater. Interfaces*. **2017**, 9, 7535-7546.
15 Tress, M.; Mapesa, E. U.; Kossack, W.; Kipnusu, W. K.; Reiche, M.; Kremer, F. *Science* **2013**, 341, 1371−1374.
16 Madkour, S.; Szymoniak, P.; Schick, C.; Schönhals. A. *J. Chem. Phys*. **2017**, 146, 203321.
17 Yin, H.; Madkour, Schönhals, A. *Macromolecules* **2015**, 48, 4936.
18 Madkour, S.; Szymoniak, P.; Hertwig, A.; Heidari, M.; von Klitzing, R.; Napolitano, S.; Sferrazza, M.; A. Schönhals. *ACS Macro Letters* **2017**, 6, 1156-1161.
19 Madkour, S.; Szymoniak, P.; Radnik, J.; A. Schönhals. *ACS Appl. Mater. Interfaces*. **2017,** 9, 37289-27299.

CHAPTER 2 – Glass Transition and Glassy Dynamics

2.1. Glass Transition

Cooling a glass-forming liquid or polymer, without crystallizing, induces an increase in their density and viscosity. Consequently, the molecular motions slowdown with decreasing temperature. Within a certain temperature range, the characteristic time required for the molecules to structurally rearrange themselves into a thermodynamic equilibrium will become much longer than the timescale of the experiment. Consequently, the system will fall out of equilibrium and freeze into a non-equilibrium glassy state. This continues to temperatures, at which the viscosity is exceedingly high and the material can be considered as glass.[1] This process takes place over a given temperature range, called the glass transition region, which is characterized by the thermal glass transition temperature (T_g^{therm}). It is worth to note that T_g^{therm} could be determined by different methods,[1] for example T_g^{therm} could be taken as the midpoint temperature of the glass transition region. For instance, the glass transition shows no abrupt change in the volume, but rather a continuous change in the temperature dependence of the specific volume, see figure 2.1. It shifts from higher values in the rubbery state to lower ones in the glassy state. It is important to point out that due to the continuity of this change, glass transition is not a phase transition of any order. In fact, the glass transition is considered as a thermo-kinetic phenomenon.[2]

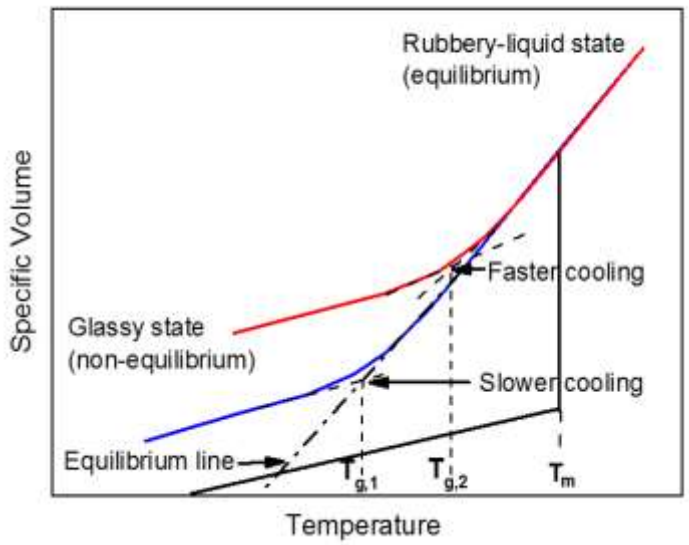

Figure 2.1. *A schematic of the temperature dependence of specific volume or enthalpy for an amorphous polymer, exposed to different cooling rates. Taken and modified from reference [3].*

Furthermore, T_g^{therm} is cooling-rate dependent. The higher the cooling rate, the higher the temperature range at which the system falls out of equilibrium, see figure. 2.1. Thus, resulting in a higher T_g^{therm} with increasing cooling rate. In the following discussion, T_g^{therm} defines the thermodynamic point of view of the glass transition phenomenon measured by the so-called static methods. These methods include Differential Scanning Calorimetry (DSC), spectroscopic ellipsometry,[4] fluorescence spectroscopy,[5] Capacitive Scanning Dilatometry (CSD),[6,7] etc. These techniques measure the temperature dependence of a physical property (heat capacity, volume, etc.), which undergoes a change as a function of temperature, at T_g^{therm}.

It is important to note that T_g^{therm} is different from the so-called dynamic glass transition temperature T_g^{dyn}, which is directly related to the segmental dynamics of polymers, discussed in the following section.

2.2. Molecular Dynamics

Amorphous polymers are well known to have complex mechanical behavior. This behavior is partially a result of a number of different motional processes within the system, occurring at the molecular and intermolecular level.[8] Due to the complex chemical structures of the polymer chains, i.e. for isolated chains, a large number of conformational-changes could take place within. These molecular processes involve localized fluctuations, segmental dynamics, which are related to the glass transition, and even collective chain motions encompassing the whole macromolecule. The former two molecular processes are the focus of this work. From the physical point of view, the aforementioned molecular dynamics depends on the structural units, hence their sizes, involved in the process, see figure 2.2. The different size-scales within the polymer result in different relaxation times (reorientation times), which is related to the different modes of motion (mobility). These modes reflect the relaxation behavior (the dynamics) of specific parts within the polymer.

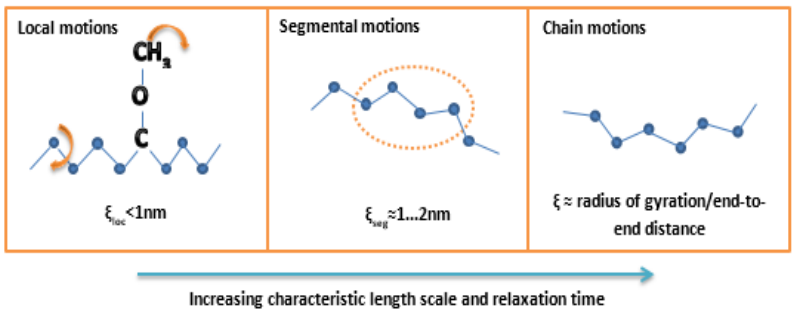

Figure 2.2. *Schematic representation of the characteristic length scales and relaxation times for the relaxation processes in polymeric systems. Taken from reference 9*

The above mentioned active molecular dynamics could be probed by applying an external disturbance (e.g. small oscillating electric field), given the right frequency and temperature window. In principle, above T_g^{therm}, the segmental dynamics are active and the whole system is in a thermodynamic equilibrium. In this temperature range, the segmental relaxation times decrease with increasing temperature and the glass transition phenomena is regarded as a dynamic phenomenon in an equilibrium state. Whereas, below T_g^{therm}, the segmental dynamics are more or less frozen. Though, other localized fluctuations might still be thermally active. It is worth to note that, from the kinetics point of view, the empirical value of T_g^{therm} is often found in a good agreement with the temperature at which the segmental relaxation time is $\tau = 10^2$ s, figures 2.4A and B. [10]

Various methods, introducing a wide range of frequency windows, are used to probe the molecular dynamics of amorphous polymers; for instance, Dynamic Mechanical Analysis (DMA),[11] neutron scattering,[12] light scattering,[13,14] Broadband Dielectric Spectroscopy (BDS),[15] and Specific Heat Spectroscopy (SHS).[16] The latter two methods were the main characterization techniques used in this work.

To understand the different relaxation time scale, resulting from the relaxation of the different structural units, the dielectric loss spectra obtained from BDS, of an amorphous polymer, is considered, see figure 2.3. In general, BDS shows two common molecular motions for most amorphous polymers I) the localized motions, i.e. fluctuations of side group(s) of the segments II) the fluctuations of the segments themselves (i.e. α-relaxation), which are typically correlated to cooperative rearrangement with respect to their environment, see figures 2.2 and 2.3. For most amorphous polymer, the dielectric spectra show a peak at high frequencies (low temperatures), which is related to the β-relaxation process. At lower frequencies (high temperatures), the α-relaxation can be observed as an asymmetric broad peak. It is important to note that the shape of the α-relaxation peak is not related to the distribution of the relaxation times, due to local spatial heterogeneities, discussed below. Therefore, the shape of the peak is considered to be an intrinsic feature of the segmental dynamics of glass-forming system.[17] This is contrary to the case of the β-relaxation.

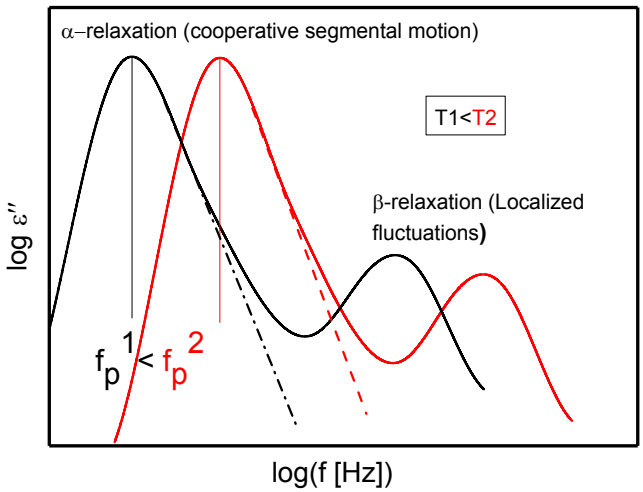

Figure 2.3. *Schematic representation of a typical dielectric loss spectra in a broad frequency range for two temperatures T_1 – black solid line - and T_2 –red solid line. Two relaxation processes, the α-relaxation (dynamic glass transition) and the β-relaxation, are indicated. Figure was taken and adapted from Reference [21].*

Through analyzing the relaxation peaks in the dielectric spectra, the frequency at which the loss is maximum is related to the relaxation process and is defined as the relaxation rate f_p or relaxation time $\tau_p = 1/(2\pi f_p)$ of the process. Through quantitative analysis of the temperature dependencies of these relaxation times (rates), information about the nature of the dielectric processes can be obtained. This is commonly presented in a relaxation map (also called activation plot); where the relaxation times are plotted as a function of reciprocal temperature, figure 2.4A. The temperature dependences of localized and segmental dynamics are discussed in detail in the next two subsections.

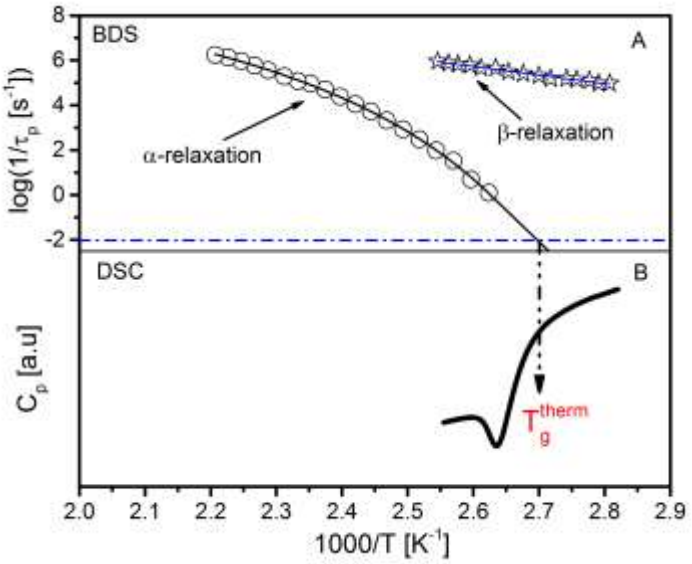

Figure 2.4. (**A**) *Relaxation map of typical segmental times τ_p versus inverse temperature as obtained by BDS showing the α and β relaxation for Poly(2-vinyl Pyridine) (P2VP). The solid black and blue lines are VFT Arrhenius fits to the data, respectively. The blue dashed dotted line mark the segmental dynamics at 100 secs, which corresponds to T_g^{therm}* (**B**) *DSC thermogram of P2VP, measured at 10 K/min. The dashed dotted arrow marks T_g^{therm}. The data are taken and adapted from reference [18].*

2.2.1. Local Fluctuations

Localized fluctuations refer to the motions (change of conformation) of structural units, which does not result in a change in conformation of the "environment" around it. Therefore, the motion is localized (isolated) from the neighboring units. An example for localized fluctuations is the β-relaxation process, which arises from intramolecular fluctuations or localized rotational fluctuations of side groups or parts of them.[19]

In general, the temperature dependence of the relaxation rates of any localized process $f_{p,loc}$ is expected to follow an Arrhenius-type equation[20]

$$f_{p,loc} = f_{\infty,loc} \exp\left[\frac{-E_a}{k_B T}\right] \tag{2.1}$$

where E_a is the activation energy and k_B is the Boltzmann constant. The value of the activation energy depends on both internal rotational barriers and the "environment" of the fluctuating unit. For instance, the typical values of E_a for β-relaxations are in the range of 20-50 kJ/mol.

2.2.2. Segmental Dynamics (α-Relaxation)

The segmental dynamics (α-relaxation) refers to the motions of the segments, which result in a change in the conformation of the segments within the environment around it. For example, it is directly related to conformational changes, like gauche-trans transitions. The α-relaxation process controls the diffusion, the viscosity and the rotation of segments.[21]. This molecular motion is, for instance, the main structural relaxation in most amorphous polymer, as probed by BDS.

For these conformational changes, the temperature dependence of their relaxation rates $f_{p,\alpha}$ cannot be well described with the Arrhenius equation (equation 2.1), as they are curved when plotted versus 1/T. The temperature dependence of $f_{p,\alpha}$ could be described by the empirical Vogel/Fulcher/Tammann (VFT) formula[22,23,24]

$$f_{p,\alpha}(T) = \frac{1}{2\pi\tau_{p,\alpha}(T)} = f_{\infty}\exp(-\frac{DT_0}{T-T_0}) \qquad (2.2)$$

where f_{∞} is the frequency in the high temperature limit and T_0 denotes the Vogel temperature, which is found 30-70 K below T_g^{therm}.[20] D is the so-called fragility parameter and provides a way to classify glass-forming systems into fragile and strong glasses. This classification depends on how strongly the temperature dependence of the relaxation rates deviates from the Arrhenius-type behavior. It is worth to note that this equation is valid only in the temperature range of T_g^{therm}. to T_g^{therm} +100 K.[25,26]

2.3. Models Relating Segmental Dynamics to Glass Transition

A number of models have been proposed in the past [27-34] to explain the molecular reasons behind the glass transition phenomenon. Nonetheless, to this date, no model could univocally describe all facts of the glass transition phenomenon. The empirical VFT dependence could be justified by different theoretical approaches. However, the following subsection presents only two possible theoretical approaches to describe the scaling of the dynamics in amorphous polymers. For a detailed review on this topic, the reader is referred to references [20 and 35].

2.3.1. Adam-Gibbs Theory

The core idea of Adam and Gibbs model is based on defining a cooperatively rearranging region (CRR), which is the smallest volume that could change its configuration independently from its neighboring environment.[31] Briefly, the model concluded that the

temperature-dependence of the α-relaxation process and that of the size of a CRR are related. It assumes that the length of the cooperative dynamic length scale would increase with decreasing temperature (T). Therefore, the segmental relaxation time at a given temperature $\tau(T)$ of a number of segments z(T) per CRR can be described as

$$\frac{1}{\tau(T)} \sim exp\left(-\frac{z(T)\Delta E}{k_B T}\right) \tag{2.3}$$

Where $z(\mathrm{T}) = \frac{S_C}{Nk_B \ln 2}$ and S_c is the total configurational entropy. N is the total number of particles and $k_B \ln 2$ is the minimum entropy of a CRR. ΔE is the free energy barrier for a segment to change its conformation. S_c can be related to the change in specific heat capacity Δc_p, at the glass transition with the following equation

$$S_c(T) = \int_{T_2}^{T} \frac{\Delta c_p}{T} dT \tag{2.4}$$

At $T_2=T_0$ and $\Delta c_p \approx C/T$, equations 2.4 results in a VFT dependence. At T_0, the configurational entropy becomes zero and the size of the CRR diverges as $z(\mathrm{T}) \approx \frac{1}{C(T-T_0)}$. Nevertheless, the Adam-Gibbs model does not provide information about the absolute size of a CRR at T_g^{therm}.

The Adam-Gibbs model was further extended by Donth [36-37], with the so-called fluctuations approach presented in equation 2.5, where the correlation length ξ was related to the step height of c_p and the temperature fluctuations δT of a CRR at T_g (T_g^{therm}) through equation 2.3.

$$\xi^3 \sim V_{CRR} = \frac{k_B T_g^2 \Delta \frac{1}{c_p}}{\rho \delta T} \tag{2.5}$$

where ρ is the density, $\Delta \frac{1}{c_p}$ is the step of the reciprocal specific heat capacity where $c_v \approx c_p$ was assumed. Experimentally, the δT can be extracted from the width of the glass transition. It is worth to note that the size of the CRR was estimated for several polymers to be in the range of 1-3 nm, corresponding to ca. 100 segments.[38]

2.3.2. Free Volume Theory

In parallel to the Adams-Gibbs model, Doolittle and Cohen [21,39,40] developed a theoretical free volume model with no characteristic length. This model is based on the idea

that in amorphous polymers, insufficient packing of disordered segments would result in free volume. They defined the free volume (V_f) concept by

$$V_f = V - V_0 \tag{2.6}$$

where V is the actual volume and V_0 is the theoretical volume based on the actual chemical structure and the van der Waals radii of the segments. Doolittle then related the free volume to the viscosity of the polymer as follows [39]:

$$\eta = A \exp[\frac{B(V - V_f)}{V_f}] \tag{2.7}$$

where A and B are fitting parameters and η is viscosity. Further assuming that the free volume increases linearly with temperature, the fractional free volume *f* would then read

$$f = f_g + \Delta\alpha(T - T_g) \tag{2.8}$$

where $f=V_f/(V_f+V_0)$, f_g is the fractional free volume at T_g (T_g^{therm}) and Δα is the difference in thermal expansion coefficients above and below T_g^{therm}. The Doolittle Equation (equation 2.7) could then be employed to rationalize the so-called WLF-equation, which is analogous to the VFT equation described above, in the frame of the free volume theory:

$$\log(\alpha_T) = \log\left[\frac{<\tau(T)>}{<\tau(T_R)>}\right] \approx \log\left[\frac{\eta(T)}{<\eta(T_g)>}\right] = \frac{B}{\left(\frac{1}{\log(e)}\right)}\left(\frac{1}{f} - \frac{1}{f_g}\right) \tag{2.9}$$

$$= \frac{-C_1(T - T_g)}{C_2 + (T - T_g)}$$

where $C_1=B/2.303f_g$ and $C_2=f_g/\Delta\alpha$.

Generally, the free volume model could also be used to describe the temperature dependence of α-relaxation times. Nevertheless, the fractional free volume cannot be determined forehand.

Furthermore, the relationship between free volume and the glass transition was recently reviewed in detail in references [41,42]. The reviews provide a thorough survey on the modern applications of free volume in experimental, theoretical, and simulation investigations. White et al.[43] recently reviewed this topic, where 50 different polymers, systematically-studied in literature, were correlated in terms of the effect of the free volume to T_g^{therm}. There, it was shown that for every polymer, a critical free volume value exists, at which the polymer becomes glassy. These critical free volume values follow a master

curve across the 50 polymers considered, revealing a close correlation/dependence on T_g^{therm}, see figure 2.5.

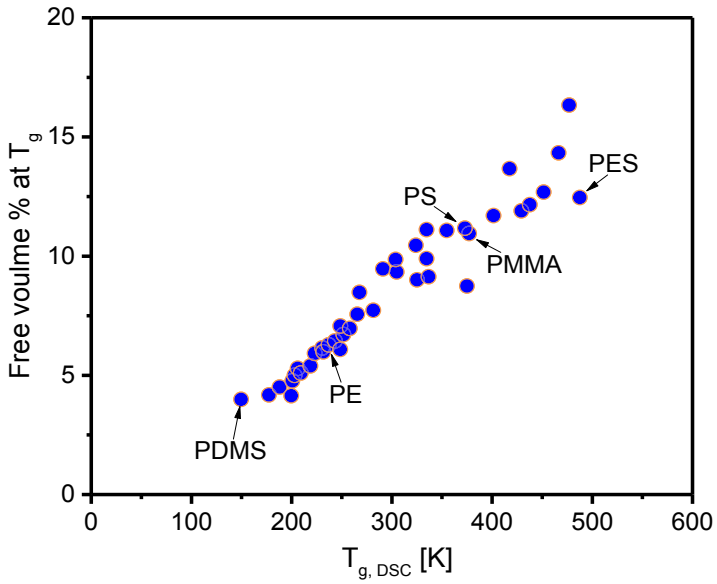

Figure 2.5. *Free volume percentage computed at T = Tg (T_g^{therm}) in the "locally-correlated lattice" (LCL) model, plotted as a function of T_g^{therm}, for 50 different polymer melts. Data for selected polymers are labeled in the figure. Adapted from reference [43].*

References

1 Young, R.; Lovell, P. The Amorphous State in Introduction to Polymers. *CRC press,* **2011***,* 3rd eds, Florida.
2 Kanaya, T.; Rintaro, I.; Kazuko, K.; Tsukasa, M.; Itaru, T.; Kaoru, S.; Go, M.; Koji, N.; Masahiro, H. *Journal of the Physical Society of Japan* **2009**, 78, 041004.
3 Donth, E.-J. Glasübergang. *Akademie-Verlag*, **1981**, Berlin.
4 Keddie, J.L.; Jones, R.A.L.; Cory, R.A. *Euro. Phys. Lett.* **1994**, 27, 59-64.
5 Ellison, C.J.; Torkelson, J.M. *Nat. Mater.* **2003**, 2, 695-700.
6 Napolitano, S.; Pilleri, A.; Rolla, P.; Wübbenhorst, M. *ACS Nano* **2010**, 4, 841-848.
7 Lupaşcu, V.; Picken, SJ.; Wübbenhorst, M. *Journal of Non-Crystalline Solids* **2006**, 352, 5594-5600.
8 Schönhals, A., Molecular Dynamics in Polymer Model Systems in Broadband Dielectric Spectroscopy. Kremer, F.; Schönhals, A., eds., *Springer*: Berlin, **2002**, p. 226.
9 Schönhals, A. Novocontrol, *Application Note Dielectrics.***1998**,1.
10 Debenedetti, P.; Stillinger, F. *Nature*, **2001**, 410:259–267.
11 Mijović, J., Lee, H., Kenny, J., Mays, J. *Macromolecules* **2006**, 39, 2172-2182.
12 Frick, B., Richter, D. *Science*, **1995**, 267, 1939-1945.
13 Fitz, B. D., Mijovic, J. *Macromolecules*, **1999**, 32, 4134-4140.
14 Frick, B.; Richter, D. *Science*, **1995**, 267, 1939-1945.
15 Schönhals, A.; Kremer, F. Theory of Dielectric Relaxation and Broadband Dielectric Measurement Techniques. In Broadband Dielectric Spectroscopy; Kremer, F.; Schönhals, A., Eds.; 1st ed; *Springer*: Berlin, **2002**; 01-57.
16 Birge, N. O., Nagel, S. R. *Physical Review Letters* **1985**, 54, 2674-267.
17 Yin, H., Schönhals, A., Dielectric Properties of Polymer Blends in Polymer Blend Handbook. Wilkie, Charles A.; Utracki, L. A., eds., *Springer*, **2014.**
18 Madkour, S.; Yin, H.; Füllbrandt, M.; Schönhals, A. *Soft Matter* **2015**, 11, 7942-7952.
19 Heijboer, J. Molecular basis of transitions and relaxation. In: Meier DJ, Ed. Gordon and Breach, **1978**.
20 Schönhals, A.; Kremer, F. The Scaling of the Dynamics of Glasses and Supercooled Liquids. In Broadband Dielectric Spectroscopy; Kremer, F.; Schönhals, A., Eds.; *Springer*, Berlin, **2002**, 99-137.
21 Cohen, M.; Turnbull, D. *Journal of Chemical Physics* **1959**, 31, 1164-1169.
22 Vogel, H. *Physikalische Zeitschrift* **1919**, 22, 645-646.
23 Fulcher, G. S. *Journal of the American Ceramic Society*, **1925**, 8, 339-355.
24 Tammann, G.; Hesse, W. *Zeitschrift für anorganische und allgemeine Chemie*, **1926**, 156, 245-257.
25 Ferry, J. D., Viscoelastic properties of polymers. 3d ed.; *Wiley*: New York, **1980.**
26 Jing, Z.; Simon, S.; Mckenna, G. *Nature Communications* **2013**, 4, 41783.
27Fox, T.; Flory, T. *Journal of Applied Physics* **1950**, 21, 581.
28 Fox, T.; Flory, T. *Journal of Physical Chemistry* **1951**, 55, 221.
29 Fox, T.; Flory, T. *Journal of Polymer Science* 1954, 14, 315.
30 Turnbull, D.; Cohen, M. *Journal of Chemical Physics* 1958, 29, 1049.
31 Adam, G.; Gibbs, J. *Journal of Chemical Physics* **1965**, 46:139.
32 Leutheuser, E. *Physical Review A*, **1984**, 29, 2765.
33Dyre, J. C.; Niels, B.; Tage, C. *Phys. Rev. B* **1996***,* 53:2171–2174.
34 Dyre, J. C. *Colloquium. Rev. Mod. Phys*. **2006**, 78:953–972.
35 Ngai, K.; Capaccioli, S. *J. Chem. Phys.* **2013**,138, 054903.
36 Donth, E. The glass transition: relaxation dynamics in liquids and disordered materials. *Springer*: Berlin, **2001.**
37 Donth, E. Relaxation and thermodynamics in polymers: glass transition. 1st ed.; *Akademie Verlag*: Berlin, **1992**.
38 Schönhals, A.; Kremer, F., Amorphous Polymers in Polymer Science: A Comprehensive Reference, Volume 1. Matyjaszewski, K.; Möller, M., eds., Elsevier, **2012**, 201-226.
39 Doolittle, A. *Journal of Applied Physics* **1951,** 22, 1471-1475.
40 Cohen, M.; Grest, G. *Physical Review B* **1979,** 20, 1077-1098.
41 White, R. P. & Lipson, J. E. G. *Macromolecules* **2016**, 49, 3987-4007.
42 Napolitano, S.; Glynos, E.; Tito, N. B. *Rep. Prog. Phys.* **2017**, *80*, 036602.
43 White, R. P.; Lipson, J. E. G. *ACS Macro Letters* 2**015**, *4*, 588–592.

CHAPTER 3 – Polymer Blends

For the past century, obtaining new materials by blending two homopolymers has been an active topic, not only from a scientific point of view, but also for technological applications. Due to the understandable difficulties in regularly commercializing new polymers, industry has thrived to blend polymers with different properties for tailor-made materials with optimized end-use properties (e.g. mechanical and rheological). Nevertheless, most polymers do not favor miscible blending, as it often comes at the expense of the total entropy of the whole system. Therefore, achieving miscible blending requires understanding of the thermodynamics of blending as well as the glassy dynamics of the blend at the molecular level.

3.1. Miscibility of Binary Polymer Blends

Despite the wealth of knowledge about the thermodynamics and structure of bulk binary miscible polymer blends[1-13], a number of questions regarding the molecular mobility remain; i.e. *how the segmental dynamics of each component of the blend is affected by blending and by changing the composition*?

In principle, the macroscopic miscible blending is governed by the thermodynamic Gibbs free energy of mixing ΔG_M.

$$\Delta G_M = \Delta H_M - T\Delta S_M \tag{3.1}$$

where ΔH_M is the enthalpy and ΔS_M is the entropy of mixing. For polymer blends, the contribution of the the entropy of mixing to the free enthalpy of mixing is small. In the framework of the lattice model of Flory/Huggins free energy [14], the Gibbs free energy for a polymer blends with A and B components is given as

$$\frac{\Delta G_M}{RT} = \frac{\phi_A}{N_A}\ln\phi_A + \frac{\phi_B}{N_B}\ln\phi_B + \chi\phi_A\phi_B \tag{3.2}$$

where R is the universal gas constant. ϕ_A and ϕ_B are the partial composition (volume) fractions of the components and χ is the interaction parameter between component A and B. N_A and N_B and the degrees of polymerization of both components, respectively. Accordingly, to achieve thermodynamic miscibility of both homopolymers, the following criterion have to be maintained:

$$\frac{\Delta G_M}{RT} < 0 \tag{3.3}$$

$$\frac{\partial^2 \Delta G_M}{\partial \phi_A^2} = \frac{\partial^2 \Delta G_M}{\partial \phi_B^2} = RT\left[\frac{1}{\phi_A N_A} + \frac{1}{\phi_B N_B} - 2\chi\right] > 0 \qquad (3.4)$$

In general the Flory/Huggins theory could only be used to describe systems with an upper critical solution temperature. This means that above a critical temperatures, T_C, the two components are miscible on a molecular level, whereas below T_c, phase separation occurs. This suggests that the composition of the separated phases is bimodal. In other words, for these systems, even in the phase separated state there will still be a certain degree of mixing resulting in two enriched phases of the two components of the blend.

The characterization of the miscibility of polymer blends is often carried out by Differential Scanning Calorimetry (DSC). For an immiscible polymer blend, two transitions, hence two T_g^{therm}s, corresponding to both components of the blend is observed. On the contrary, for miscible polymer blends, a single glass transition extending over the whole glass transition regions of both component is detected, hence single T_g^{therm}, see figure 3.1.[15]

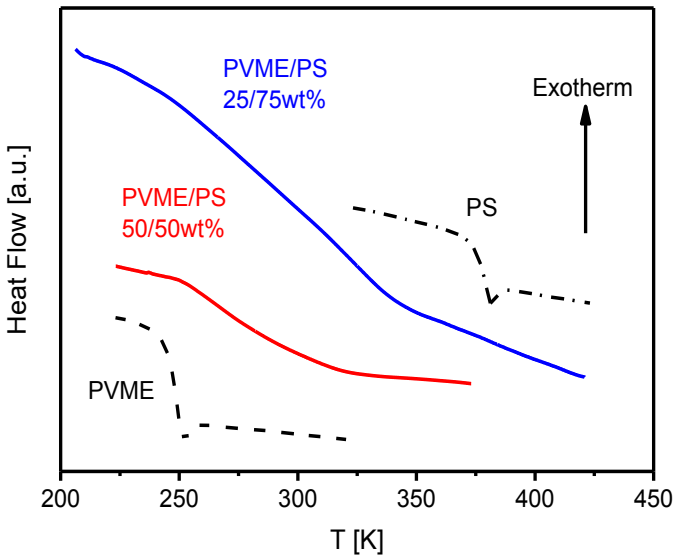

Figure 3.1. *DSC trace (second heating run; rate: 10 K/min) for PVME (dashed), PS (dashed dotted), PVME/PS (50:50 wt%, red solid), all taken from reference [16] and PVME/PS 25:75 wt%, blue solid. Figure was taken and adapted from reference [15].*

It is also important to note that the single T_g^{therm} for miscible blends is an intrinsic feature of these systems. In fact, for bulk samples, the composition dependence of the T_g^{therm} of miscible polymer blends could be described, for instance, by the Fox equation[17]

$$\frac{1}{T_{g,Blend}} = \frac{(1 - w_B)}{T_{g,A}} + \frac{w_B}{T_{g,B}} \qquad (3.5)$$

where w_B is the weight fraction of component B.

3.2. Asymmetric Miscible Polymer Blends

Asymmetric miscible blends, in which the difference between the glass transition temperatures of the two components is large, have attracted a large number of studies in the past few decades. In this case, the polymer with the lower mobility, at temperatures below its glass transition temperature, strongly affects the dynamics of the component with the higher mobility. This has been elaborated for Poly(Methyl Ethyl Ether) (PVME)/Polystyrene (PS) blends.[12,13,18-20] Here the main anomalies and intrinsic features of miscible polymer blends are shortly discussed, from the dynamics and kinetic point of view. For a detailed discussion on the anomalies of the glass transition and glassy dynamics of the components of the blend, the reader is referred to references [21 and 22].

3.3. Segmental Dynamics of Miscible Polymer Blends

It is well accepted that the molecular composition of a miscible A/B polymer blend, is not completely random. It is more likely that a segment of component A is surrounded by segments of the same kind, than by segments of component B. This means that on a molecular scale, the effective composition of a binary miscible blend is different from the macroscopic one, which would reflect on the segmental dynamics of the polymer blends.[1-13]

In general, the segmental dynamics of miscible polymer blends is affected in two major ways.[22]

I) Unlike the single T_g^{therm} obtained for miscible blends, measured by DSC, the molecular dynamics are known to be *spatially dynamically heterogeneous*.

II) *Symmetric broadening* of the relaxation functions in the frequency domain with respect to the corresponding homopolymers is observed.

It is worth to note that there is no unified theory that can explain these experimental findings in polymer blends. Nevertheless, the current understanding of these findings is often explained through the combined effect of chain connectivity, which results in a *self-concentration* mechanism,[7] and *thermally driven concentration fluctuations*.[22] These mechanisms give rise to spatial regions, which have different local compositions than the mean one with their own local relaxation behavior, and subsequently local T_g^{therm}, as discussed in the upcoming subsections.

3.3.1. Dynamic Heterogeneity

For an ideal molecularly homogenous blend system, one would expect a single averaged relaxation process, much like the single averaged T_g^{therm}, obtained from the DSC measurements for miscible blends. Nonetheless, probing the segmental dynamics of a polymer blend by BDS with dielectrically visible components, have shown that even for miscible blend systems, two processes are detected. This means that at the molecular level, their segmental dynamics is heterogeneous. Figure 3.2 elucidates this behavior through the dielectric loss spectra for Poly(Vinyl Ether)/Poly(isoprene) PVE/PI of 50:50 wt%.

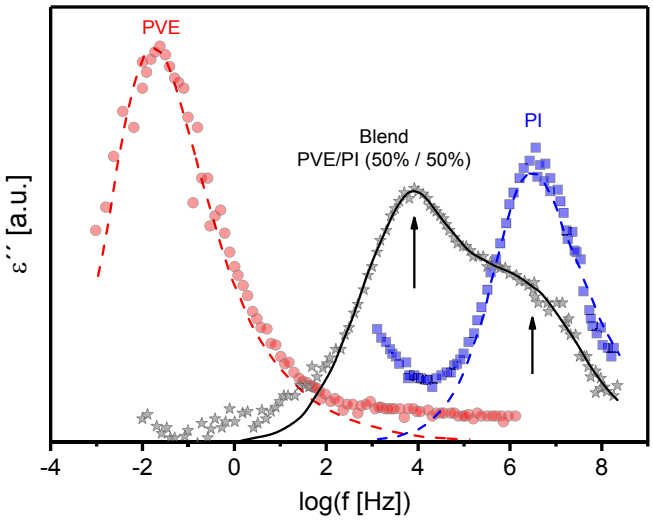

Figure 3.2. *Dielectric loss versus frequency at 270 K for the PVE/PI blend at a composition of PVE/PI 50:50 wt%. Circles – pure PVE; Squares – pure PI; stares – blend PVE/PI. Lines are HN-function fits to the active processes in the dielectric spectra. Figure was taken and adapted from reference [28].*

In addition, it is important to note that the existence of the two processes in the loss spectrum is independent from the α-peak broadening discussed below. This heterogeneity phenomena could be clearly elaborated from the combination of DSC and Thermal Simulated Currents measurement (TSC), figure 3.3. There, T_g^{therm} of pure PVME and PVME/PS blend were depicted; keeping in mind that PVME has a much stronger dipole moment, compared to that of PS.[22] Consequently, since DSC is sensitive to the molecular dynamics of the whole blend, while TSC is only sensitive to the polar component of the blend as influenced by PS, comparing the data of the two measurements could elucidate the compositional heterogeneity phenomena. A closer look on figure 3.3, reveals that T_g^{therm} from TSC is observed at a lower temperature compared to that obtained from DSC.[23] In other words, the local T_g^{therm} due to the polar PVME segments is observed at much lower temperatures than

the overall T_g^{therm}, which proves that $T_{g,eff}^{therm}$ is different from the mean T_g^{therm}.

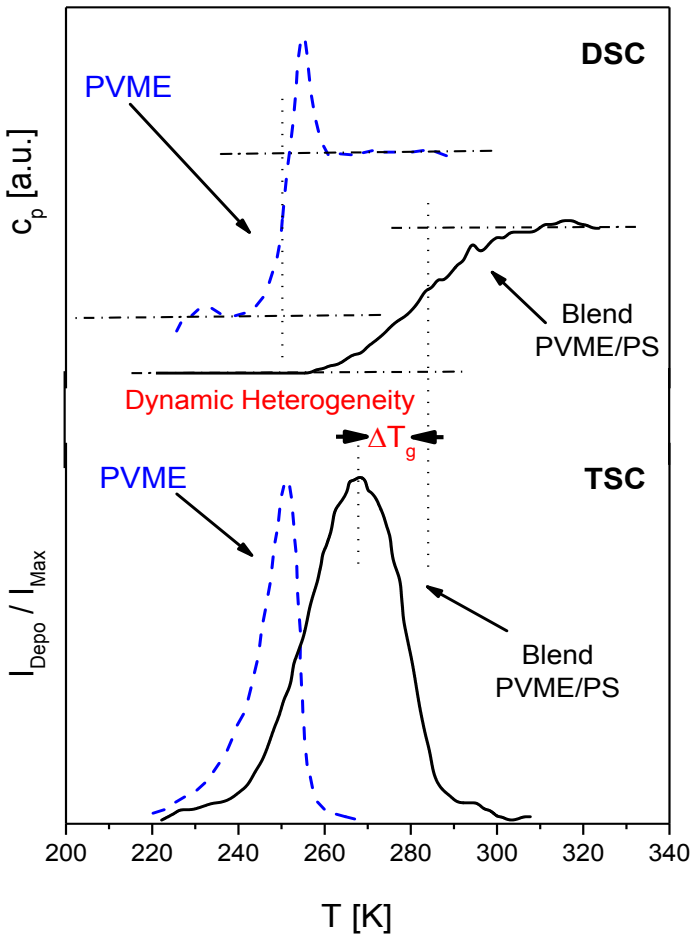

Figure 3.3. *Comparison of DSC and TSC measurements for pure PVME (dashed lines) and a PVME/PS (solid lines) at a composition of PVME/PS 50:50 wt%. Dotted vertical lines indicate the glass transition temperatures. Figure was taken and adapted from reference [28]*

A similar conclusion could be drawn from figure 3.4, where the temperature dependence of the segmental relaxation rate of the PVME/PS blend and that of the PVME, measured by BDS and SHS are depicted. It is worth to note that, similar to TSC, for PVME/PS, BDS is only be sensitive to the molecular dynamics of PVME (as affect by PS), due to the negligible dipole moment of PS compared to that of PVME. Nevertheless, SHS is sensitive to the entropy fluctuations resulting from the mobile segments of both PVME and PS. Therefore, combing both methods could provide deep insights into the dynamic heterogeneity.

For PVME/PS 50:50 wt%, despite the fact that both SHS and BDS probe the segmental dynamics, the relaxation rates measured by SHS are shifted by 13 K to higher temperatures,

compared to the dielectric data. This is contrary to the case of pure PVME, where both data coincide, within the experimental error. In other words, this shift in the rates of the segmental dynamics of the polymer blend, measured by the two different methods, is an expression of the dynamic heterogeneity within the bulk blend sample.

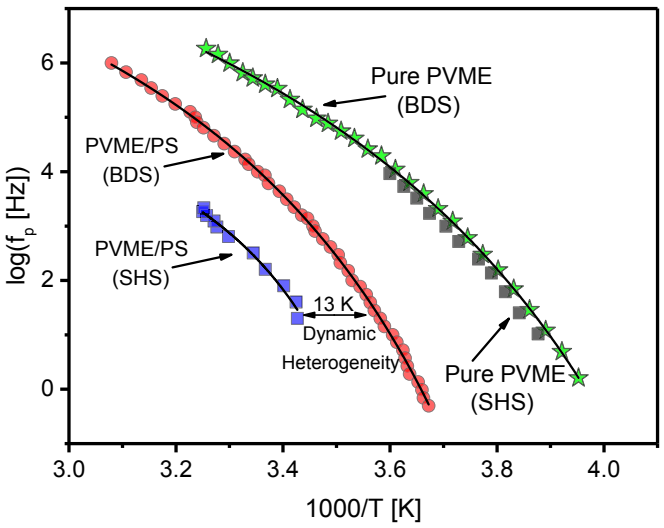

Figure 3.4. *Relaxation map for bulk PVME/PS 50:50 wt%: red circles - α-relaxation; blue squares - bulk PVME/PS measured by SHS,[43] green stars - α-relaxation pure PVME measured by BDS and SHS – black squares[24] The solid lines are VFT fits to the data. Figure was taken and adapted from reference [25].*

The Self-concentration (SC) model is usually used to discuss the dynamic heterogeneity.[26] In short, the SC model considers the segments of each component in its local environment, contrary to the TCF model, which only takes into account the local composition of certain volume. The SC model assumes that every segment is enriched by the same kind of segments in its environment, due to chains connectivity. This would lead to an averaged local composition, thus local glass transition temperatures. Subsequently, it would lead to average relaxation times for segments of both components. Further, this gives rise to the double peaks of the dynamic heterogeneity, seen in figure 3.2.

3.3.2. Symmetric Broadening

As mentioned above, the segmental relaxation process measured for miscible blends shows notable broadening compared to that of the homopolymer components. The dielectric loss spectrum for PVME/PS 65:35 wt% versus pure PVME elucidates this behavior, see figure 3.5. In general the broadening of the loss peak of the blend is temperature dependent in two main ways.

I) The broadening of the loss peaks decreases with increasing temperature, as depicted in figure 3.5.

II) The broadening of the loss peaks increases with increasing the difference between T_g^{therm} of both components.

This broadening phenomenon can be described by the *Temperature driven concentration fluctuations (TCF)* model.[27.]

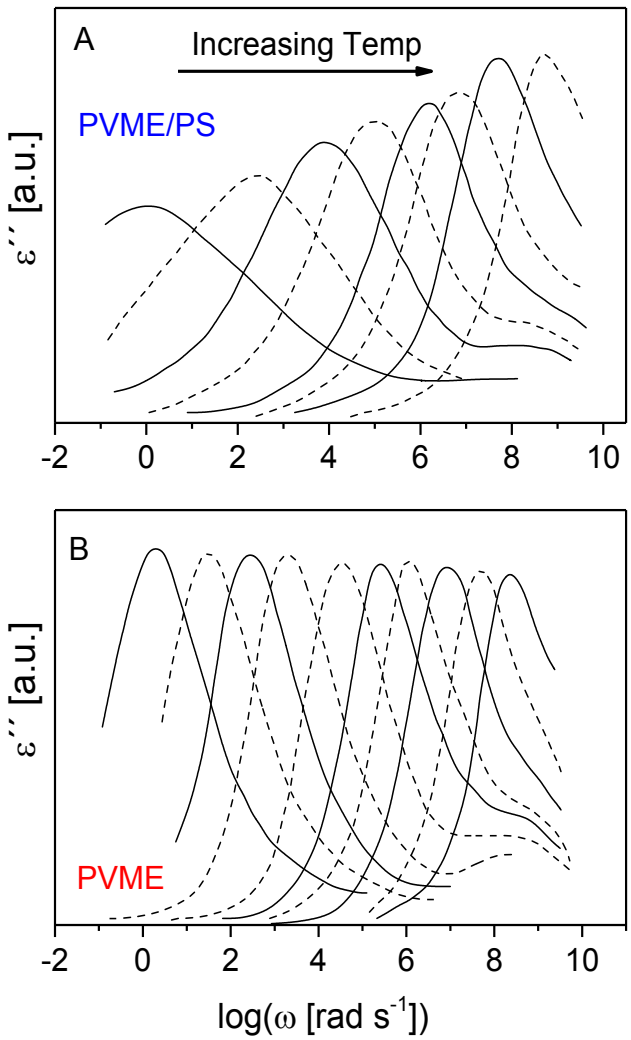

Figure 3.5. *Dielectric loss for the PVME/PS blend 65:35 wt%.* **(A)** *Dielectric loss versus frequency for PVME/PS blend: (T=263, 273, 283, 293, 308, 318, 338, and 368 K)* **(B)** *Dielectric loss versus frequency for pure PVME: (T=253, 258, 263 , 268 , 278 , 288, 298, 308, 328,and 348 K). Figure was taken and adapted from reference [28].*

The *Temperature driven concentration fluctuations (TCF)* model assumes that the sample consists of i subcells of volume V with composition ϕ_i and thus a local glass transition $T_g^i(\phi_i)$.

On the molecular level, local concentration of these sub cells, which is different from the macroscopic concentration, will lead to different local glass transition $T_g^i(\phi_i)$. Consequently, this will give rise to local relaxation times, which is also different from the mean relaxation time. Eventually, the statistical distribution of these different relaxation times, see figure 3.6, yields the broadening of the loss peak, see figure 3.5.

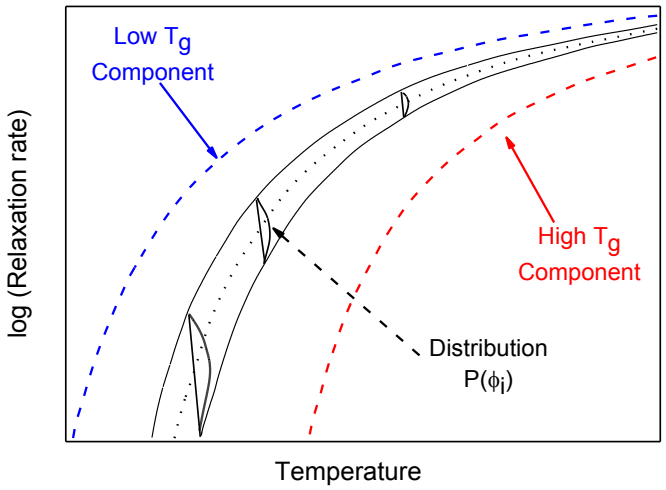

Figure 3.6. *Scheme of the temperature driven concentration fluctuation approach to binary miscible blends. Figure was taken and adapted from reference [28].*

3.4. Surface Enrichment

Polymer blends undergo another special phenomenon due to the different surface tensions of the blend components. This is especially significant for asymmetric polymer blends. A part of the component with lower surface tension will diffuse to the surface to minimize the free energy of the system, which is thermodynamically favorable.[29] Therefore, the composition at the interfaces is different than that of the bulk.

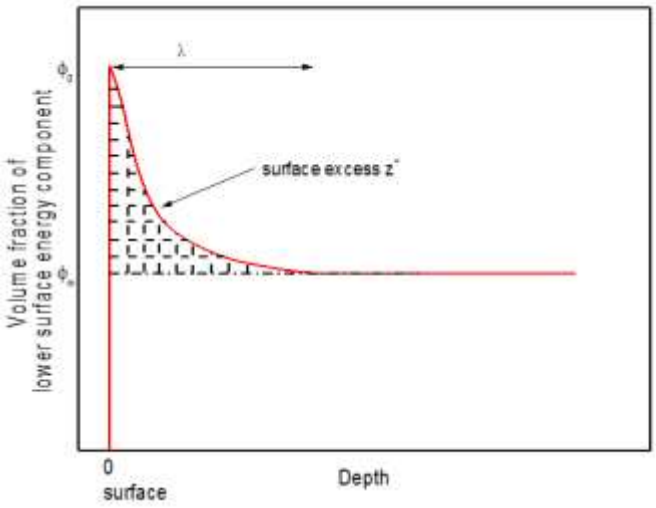

Figure 3.7. *Schematic diagram of the surface composition profile in a binary polymer blend. Figure taken and adapted from reference [29].*

The composition difference of the surface composition ϕ_0 to the bulk composition ϕ_∞ is described by the composition profile $\phi(z)$. This composition profile is extended throughout a characteristic length λ, in the order of magnitude of 10 nm, figure 3.7. Equation 3.6 describes the surface excess (Z*), by integrating the composition profile when the system is at a thermodynamic equilibrium.

$$Z^* = \int_0^\infty [\emptyset(z) - \emptyset_\infty]\, dz \tag{3.6}$$

At Z*=0, there is no segregation, whereas at Z*>0 would indicate preferential segregation to the surface. In fact, this phenomenon is more or less negligible for bulk samples. However, it becomes of great importance with confining the polymer blend films into thin films, where the interfaces can no longer be ignored. This will be discussed in detail in the next chapter.

References

1 Alegria, A.; Colmenero, J.; Ngai, K.; Roland, C. *Macromolecules* **1994,** 27, 4486.
2 Cendoya, I. Alegria, A. Alberdi, J. M. Colmenero, J. Grimm, H. Richter, D. Frick, B. *Macromolecules* **1999,** 32 4065.
3 Takeno, H.; Kobayashi, M.; Aikawa, T. *Macromolecules* **2006**, 39, 2183.
4 Watanabe, H.; Urakawa, O. *Korean-Australian Rheol. J.* **2009**, 21, 235.
5 Green, P.; Adolf, D.; Gilliom, L. *Macromolecules* **1991**, 24, 3377.
6 Colby, R.; Lipson, J. *Macromolecules* **2005**, 38, 4919.
7 Urakawa, O.; Fuse, Y.; Hori, H.; Tran-Cong, Q.; Yano, O. *Polymer* **2001**, 42, 765.
8 Chung, G.; Kornfield, J.; Smith, S. *Macromolecules* **1994**, 27, 5729.
9 Wang, D.; Ishida, H. *Macromol. Chem. Phys.* **2007**, 208, 2222.
10 Dionisio, M.; Fernandes, A.; Mano, J.; Correia, N.; Sousa, R. *Macromolecules* **2000**, 33, 1002.
11 Wang, J.; Roland, C. *Polymer* **2005**, 46, 4160.
12 Alvarez, F.; A. Alegria, A.; Colmenero, J. *Macromolecules* **1997**, 30, 597
13 Arbe, A.; Alegria, A.; Colmenero, J.; Hoffmann, S.; Willner, L.; Richter, D. *Macromolecules* **1999**, 32, 7572.
14 Sperling, L.H. *Introduction to Physical Polymer Science*, **1986**, *John Wiley & Sons*, New York.
15 Madkour, S.; Szymoniak, P.; Schick, C.; Schönhals. A. *J. Chem. Phys*. **2017**, 146, 203321.
16 Yin, H.; Madkour, S.; Schönhals, A. *Macromolecules* **2015**, 48, 4936.
17 Hiemenz, P.; Lodge, T. *Polymer Chemistry (second Edition)*. (CRC Press, Boca Raton, Florida, **2007**).
18 Schwartz, G. A.; Colmenero, J.; Alegria, A. *Macromolecules* **2007**, 40, 3246.
19 He, Y.; Lutz, T. R.; Ediger, M. D. *J. Chem. Phys.* **2003**, 119, 9956.
20 Gotzen, N.-A.; Huth, H.; Schick, C.; Van Assche, G.; Neus, C.; Van Mele, B. *Polymer* 2010, **51,** 647.
21 Ngai, K.; Capaccioli, S. *J. Chem. Phys.* 2013, **138**, 054903.
22 Colmenero; J.; Arbe, A. *Soft Matter*, **2007**, 3, 1474-1480.
23 Leroy, E.; Alegria, A.; Colmenero, J. *Macromolecules*, **2002**, 35, 5587.
24 Madkour, S.; Szymoniak, P.; Heidari, M.; von Klitzing, R.; A. Schönhals. *ACS Appl. Mater. Interfaces*. **2017**, 9, 7535-7546.
25 Madkour, S.; Szymoniak, P.; Radnik, J.; A. Schönhals. *ACS Appl. Mater. Interfaces*. **2017,** 9, 37289-27299.
26 Lodge, T.P.; Mcleish, T. *Macromolecules*, **2000**, 33, 6332.
27 Wetton, R.E.; Macknight, W.J.; Fried, J.R.; Karasz, F.E. *Macromolecules*, **1978**, 11, 158-164.
28 Yin, H.; Schönhals, A. *Broadband Dielectric Spectroscopy of Polymer Blends in Polymer Blends Handbook*, **2014**, L.A. Utracki, Ch., Wilkie, (Eds.), *Springer*.
29 Jones, R. A.L.; Kramer, J. *Polymer* **1993**, 34, 115-118.

CHAPTER 4 – 1D Confinement (Thin Films)

Nowadays, modern technology frequently employs polymers and/or their blends confined at the nanoscale. In general, confinement can take place in 1D (thin films), 2D (cylindrical nanopores), or 3D (nanoporous glasses). At the present time, thin polymer films (<200 nm), have been attracting a lot of attention due to their high demand in thin-film based technologies.[1-6] In principle, thin films could have three different configurations, supported, capped and freestanding films. However, this work only focuses on the former two configurations. In the capped sample geometry, the substrate has two polymer/substrate interfaces, while for supported films; the samples are allowed a free surface at the polymer/air interface, in addition to the one at the polymer/substrate interface.

4.1. Effect of 1D Confinement on the Glass transition

Two decades ago, the pioneering work of Keddie et al.[7,8] showed that the thickness dependence of T_g^{therm} of supported PS (figure 4.1) and Poly(methyl methacrylate) PMMA films deviates from their bulk values depending on their supporting substrates. Since then, the interest in this topic has been on the rise, exponentially. In fact, despite the wealth of knowledge present on this topic now, there are still a lot of open questions. For instance, *what are the molecular reasons behind the possible deviations in the properties (e.g. glass transition) of confined polymers, compared to that of the bulk?*

In general, the discussion on this topic is still controversial, where divergent results were published, even for the same polymer/substrate systems.[9,10] These results show both a depression[11-14] or an increase in T_g^{therm},[15-17] with decreasing film thickness. Furthermore, a similar behavior was also reported for capped films. For instance, Al-capped Polystyrene films experience a T_g^{therm} depression, with decreasing film thickness.[10] Nevertheless, for Al-capped PC films, an elevation of T_g^{therm} with decreasing film thickness, was observed.[9] This was related to the fact that the fact that the interfacial energy of PS/Al is much higher than that of PC/Al.

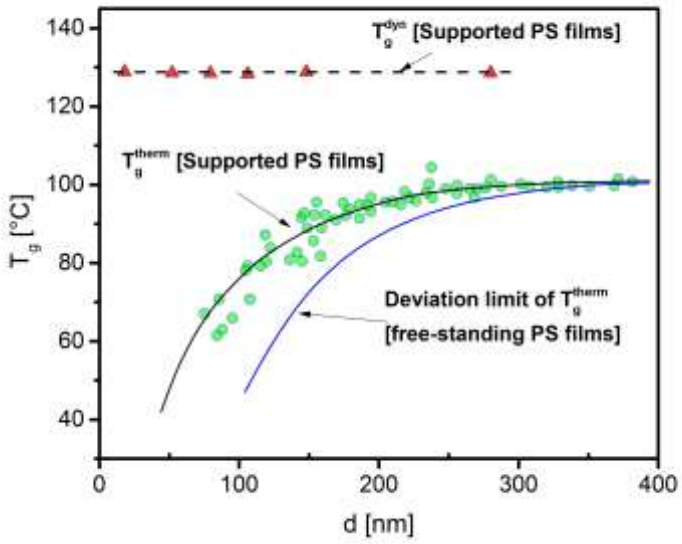

Figure 4.1. *T_g^{therm}- green circles and T_g^{dyn}- red triangles as a function of film thickness for thin PS films supported on silicon wafer. The black dashed and solid lines are guides for the eyes. The Blue solid line marks the limit of the deviation from the bulk value, which is observed for free standing PS films. The figure and data were taken and adapted from reference [18].*

In a perspective review by Ediger et al.,[19] the progress made in the last years was thoroughly discussed, the reader is also referred to references [20-28] for a deeper insight in this topic.

4.1.1. Three Layer Model

Nowadays, the thickness dependence of T_g^{therm} of supported thin films is usually discussed in the framework of an idealized three-layer model. This model elaborates a sensitive balance between the effects of a spatial dynamically heterogeneous structure across the whole film, see figure 4.2. For supported films, this structure is composed of a free surface layer (polymer/air interface), a bulk-like layer with bulk properties (in the middle of the film), and a layer adsorbed at the substrate (polymer/substrate interface).

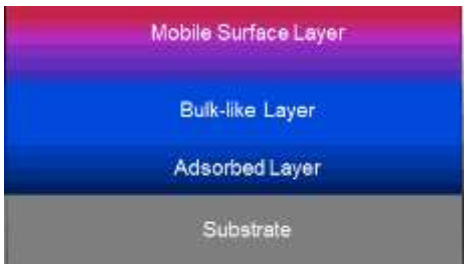

Figure 4.2. *Schematic representation of the idealized three-layer model of thin films. Figure was taken and modified from reference [21].*

Upon decreasing the total film thickness, the thickness of the bulk-like layer decreases.[15] However, at the polymer/air interface, due to the missing segment-segment interactions, compared to the bulk, a mobile surface layer will always be formed. Consequently, for a repulsive polymer/substrate interactions, the free surface layer becomes more dominant, yielding a reduction in T_g^{therm}. For non-repulsive polymer/substrate interactions, segments can get adsorbed at the polymer/substrate interface. Within this adsorbed layer, the segments have a reduced mobility and may result in an elevation of T_g^{therm}, compared to that of the bulk. Consequently, the measured T_g^{therm} is a complicated average reflecting the effect of the aforementioned layers.

Furthermore, recent studies on linear [29,30] and star shaped polymers [31] revealed that the three-layer model and interfacial interactions are not adequate to univocally describe the deviations of T_g^{therm}, form its bulk value, observed for polymer under confinement. Thus, suggesting that more parameters should also be taken into account.

For instance, one has to bear in mind that the diffusive mobility of a polymer chain depends on molecular weight (M_w). The higher the M_w, the longer the time needed for the chains to reach an equilibrate confirmation. This process (annealing) is necessary to form an adsorbed layer. Therefore, the formation of the adsorbed layer (at the polymer/substrate interface) requires a given time (longer than the terminal relaxation time). Consequently, this insinuates that the effect of the adsorbed layer, and thus the possible decrease or increase of T_g^{therm} of a thin film, is also influenced by the annealing condition, which is a function of the M_w.[32] This was concluded from investigations by ellipsometry on polystyrene thin films[32,33] as well as broadband dielectric spectroscopy (BDS) of isolated, semi-isolated,[28] and brushes of high M_w poly(2-vinyl pyridine) (P2VP) films.[34]

In addition, Burroughs et al. have confirmed a correlation between the change of T_g^{therm} and the thickness of the adsorbed layer. Their data was quantitatively rationalized through the free volume hole diffusion model, see references [35,36]. The shift in T_g^{therm} was explained as a result of the diffusion of free volume sites toward interfacial "sinks", causing packing frustration at the polymer/substrate interface. This concept is explained in the following subsection.

4.1.2. Free Volume under Confinement (Packing Frustration)

The relationship between the free volume and the glass transition has been an active topic not only for bulk polymers, as discussed in section 2.3.2, but also for confined polymeric

films. In recent years, the concept of packing frustration, which is due to the change in the free volume within the system, has gained popularity in explaining the effect of confinement on the glass transition phenomenon. In general, the increase of the free volume sites would translate into a reduction in T_g^{therm}. For thin films, the free surface and the adsorbed layer could act as a source and/or sink of free volume sites.

The mechanism of how the free surface could introduce free volume sites to the system was first proposed by deGennes.[37-39] Through the suggested model, deGennes theorized that at the free surface, kinks along the polymer chains could generate a free volume site, which could then diffuse into the films along the chain back bone. Since the radius of gyration of the polymer chains is related to the molecular weight of the chains, this model would then imply that the free volume sites would be able to diffuse deeper into the film, for polymers with higher M_W. Nevertheless, investigations on the local distributions of T_g^{therm} in freestanding films[40] disagrees with this model. Whereas, T_g^{therm} of thin supported films of poly(α-methyl styrene), PaMS, showed no confinement effects on T_g^{therm} for shortest chains (1.3 kg/mol),[41] contrary to a 20 K drop in T_g^{therm} for 420 kg/mol samples, in agreement with the model. A similar behavior was observed for different molecular weights of PS supported films.[10] Further explanation for these contradicting results could be deduced from reference [42]. There, it was discussed that for short chains, the excess in free volume could be promptly supplied by their relatively abundant chain ends. Nonetheless, for longer chains the excess must be created, which would result in the reduction of T_g^{therm}. Nevertheless, to verify this concept this model, further investigations are necessary due to the controversial results in literature.

In reference [43], this behavior was further discussed in the framework of the Gibbs-Di Marzio Model. This model introduced the chain rigidity as factor in determining the impact of the free volume on T_g^{therm}. If $k_B T_g^{therm} > E_{conf}$ applies, conformational changes of the chains will take place, where E_{conf} is the energy barrier related to a conformational change possible via free volume. In the light of this model, polymer with rigid backbones, would not evidence a reduction in T_g^{therm} unless their $k_B T_g^{therm}$ is higher than E_{conf}. Consequently, this behavior would not apply for shorter chains, due to their low T_g^{therm}. For instance, this trend is in a good agreement with the results obtained for PMMA thin films.[44]

Alternatively, excess free volume sites could also be introduced in the vicinity of an adsorbing interface, for instance in poorly annealed polymer films supported on non-

repulsive substrates. There, packing frustration results in the reduction of the local density of the segments at the interface; between the adsorbed and the non-adsorbed layer. As expected, this packing frustration would get enhances in the presence of bulky side groups. This was shown for the case of poly(4-tertbutyl styrene) films, with bulky tertbutyl moieties.[11] This is in agreement with reference [45], where it was shown, for freestanding films, that the yielded packing frustration could be quantitatively recovered, as the excess in free volume.[45] Furthermore, Cangialosi and Napolitano evidenced a proportionality of T_g^{therm} with the excess in interfacial free volume.[36]

In the light of these findings, the aforementioned consideration should all be taken into account when discussing T_g^{therm} reductions in the vicinity of free surfaces and weakly adsorbing interfaces.

4.1.3. Adsorbed Layer

Polymer systems with non-repulsive polymer/substrate interfacial interactions, present further challenges to the understanding of the deviations of T_g^{therm} from its bulk value. For a well annealed polymer thin films with non-repulsive polymer/substrate interactions, it was shown that an adsorbed layer is expected to form. In this layer, the chains get trapped into non-equilibrium conformations, which reduces their effective viscosity. To achieve equilibrated conformations, the reptation model[46] predicted that the annealing times should be longer than the terminal relaxation time. This was found for PS[47], PMMA, and PVAc.[48] Rotella et al.[49] showed that only the molecules in direct contact with an adsorbing surface are influenced, resulting in changes in the local T_g^{therm}. It was further suggested in reference [49] that at the molecular level, these alterations have a finite lifetime. Furthermore, these changes correspond to metastable conformations of the polymer chain corresponding to local minima in the free energy landscape rather than a global one.

The current understanding of the behavior and growth kinetic of the adsorbed layer was recently concluded from solvent leaching (also called Guiselin brushes) experiments,[29] where the free surface and the bulk-like layers are removed. Through combing spectroscopic ellipsometry and AFM imaging, it was recently shown that for a well-annealed sample, an irreversibly adsorbed thin layer is formed at the polymer/substrate interface, with a thickness compared to the radius of gyration (R_g) of the polymer. This was shown for a number of polymers, as reported in references [50,51], where the segment/surface interaction energies are in the order of k_BT. The connectivity of the chains further stabilizes this layer, as the

detachment would require cooperative rearrangement of a larger set of the adsorbed segments.[52]

Housmans et al. showed that for well annealed atactic PS supported films, the adsorption process takes place in two different regimes having different time dependencies, figure 4.3A.[32] At short times, the polymer chains thrive to pin as many segments as possible to the substrate, lowering its free energy. The growth kinetics of this adsorption process follows a linear time dependence and the polymer segments are directly adsorbed at the substrate forming a dense strongly bounded adsorbed layer.[53,54] This layer is mainly formed of trains strongly bounded to the substrate, hence, it is assumed to be completely immobilized (dead layer). This part of the adsorbed layer is referred to as "strongly bounded layer" in the following discussion.

However, at longer times, the adsorption growth kinetics is characterized by logarithmic time dependence. The adsorbed layer further grows by the diffusion of segments through the already existing layer, on the expense of their entropy. The structure of this part of the adsorbed layer is less dense, compared to the strongly bounded layer, as it is mainly formed out of loops and tails. Theses loops and tails allow for some molecular mobility, compared to the trains of the strongly bounded layer, see figure 4.3A and B. This part of the adsorbed layer is referred to in the following discussion as "loosely bounded layer". For further details, see references [55,56].

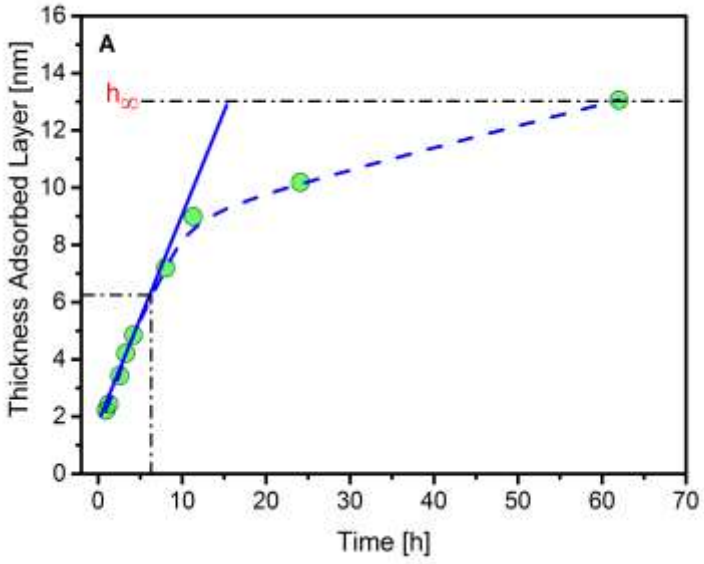

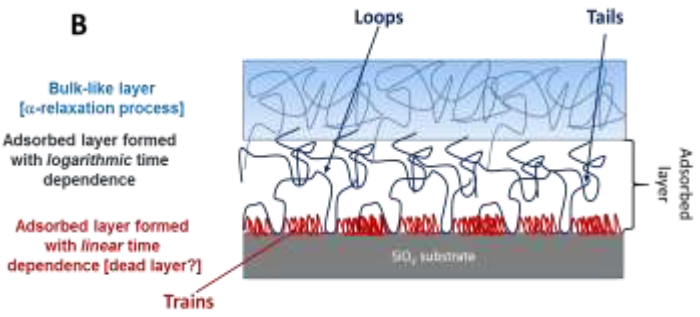

Figure 4.3. (**A**) *Kinetics of irreversible chain adsorption of melts of PS of constant M_w and different temperatures. Figure regenerated from the reference [32].* (**B**) *A schematic cartoon of a two-layer structure (adsorbed layer and a bulk-like layer) as deduced from the data and literature, taken from reference [57].*

The picture of the heterogeneous structure within the irreversibly adsorbed layer suggests that the number of the adsorbed segments is also dependent on the annealing time. Hence, the more adsorbed segments, the higher the thickness of the adsorbed layer (h_{ads}), where a plateau is reached at $h_{ads} \approx R_g$. This would mean that at short annealing times/low number of adsorbed segments, the system is comparable to the polymer/substrate repulsive system, explained in the previous section. Consequently, one could conclude that even for capped films with non-repulsive polymer/substrate interfaces, if the film is not well annealed, a reduction in T_g^{therm} could be evidenced. This is in a good agreement with studies on linear[29,30] and star-shaped polymers.[31]

4.2. Effect of Thin Film Confinement on Segmental Dynamics

The segmental dynamics and the related T_g^{dyn} of most homopolymers confined into thin films show no thickness dependency, see figure 4.1. This is considered to be a combined effect of a number of reasons with different origins. First, as discussed in chapter 2, T_g^{therm} is measured at lower temperatures (lower frequencies), compared to the T_g^{dyn}, where the system is not in a thermodynamic equilibrium. Whereas at T_g^{dyn} (higher frequencies) the system is already in equilibrium. At both temperatures, the correlation length scales are different and so are their sensitivities to thickness changes. Secondly, dynamic glass transition is measured at temperatures above T_g^{therm}, where it was found that the segmental dynamics of the mobile surface layer becomes similar to that of the bulk-like layer.[22] Thus, the influence of the surface layer on T_g^{dyn} becomes less pronounced with increasing temperature above T_g^{therm}. This effect could be the reason why dynamic methods show no thickness dependency of T_g^{dyn}, while T_g^{therm} deviates from its bulk value, with decreasing

film thickness. This suggests that if a thickness dependence is observed for the T_g^{dyn}, it is more likely that this confinement effect would be due to the effect of the adsorbed layer on the overall segmental dynamics. Therefore, understanding of the molecular dynamics of the adsorbed layer is essential for understanding the effect of confinement on the overall segmental dynamics of the whole film.

Despite the existing evidence for the irreversible adsorbed layer in well-annealed polymer films, little is known about their glassy dynamics, due to the hard accessibility of this layer and their low intensity.[57] Nevertheless, experiments on systems related to thin films, for instance polymer nanocomposites of P2VP,[58] PVAc[59], and PDMS[60] with embedded silica nanoparticles, successfully probed the glassy dynamics of the adsorbed layer. In general, it was found that the adsorbed layer showed slowed down segmental dynamics, compared to that of the bulk.

Further, it was recently found that the cooperativity of the segmental dynamics of the adsorbed layer in these system could also be M_w dependent. For instance, for PDMS with embedded silica nanoparticles[60] the segmental dynamics of PDMS in the adsorbed layer loses its cooperative nature with decreasing the M_W. Where the temperature dependence of the segmental rates switches from a VFT behaviour to an Arrhenius one, with decreasing the M_W below the entanglement M_W (M_c). This could be rationalized by taking into account that with decreasing the M_W, h_{ads} would have to decrease, due to the lower R_g. The decrease in the h_{ads} would have to take place first on the expense of the loosely bounded layer. Consequently, at a certain thickness (estimated to be 1 nm in this work), the adsorbed layer would be mainly formed out of the strongly bounded layer, which is mainly formed out of trains with very low mobility. Therefore, the segmental dynamics becomes localized and lose their cooperative nature. The localization of the segmental dynamics (degeneration of their cooperative nature) was also observed for other systems confined within a hard or frozen host.

For instance, PDMS confined into nonporous glass[61,62] showed the degeneration of the segmental dynamics of PDMS (α-relaxation) with decreasing the pore sizes to a similar length scale to that of V_{CRR}. For pore sizes >> V_{CRR}, the segmental dynamics are cooperative, whereas for pore sizes ≈ V_{CRR} (or smaller), they are localized. This was evidenced by the transition of the temperature dependence of the relaxation rates of the segmental dynamics from a VFT to an Arrhenius behavior, upon decreasing the reaching a similar length scale compared to that of the V_{CRR}, see figure 4.4A. Consequently, the glassy

dynamics was assigned to a degenerated α-relaxation of the PDMS segments. Interestingly, probing the glassy dynamics of the same system employing temperature modulated DSC (TMDSC), which is a SHS technique, showed a decrease in Δc_p with decreasing the pore size. Further, Δc_p was found to be zero exactly at the pore size ,where the temperature dependence of the segmental dynamics changes from a VFT to an Arrhenius behavior, see figure 4.4B. This suggests that SHS is not sensitive to localized molecular dynamics and could only probe the cooperative mobility of the polymer segments. This is in agreement with reference [57].

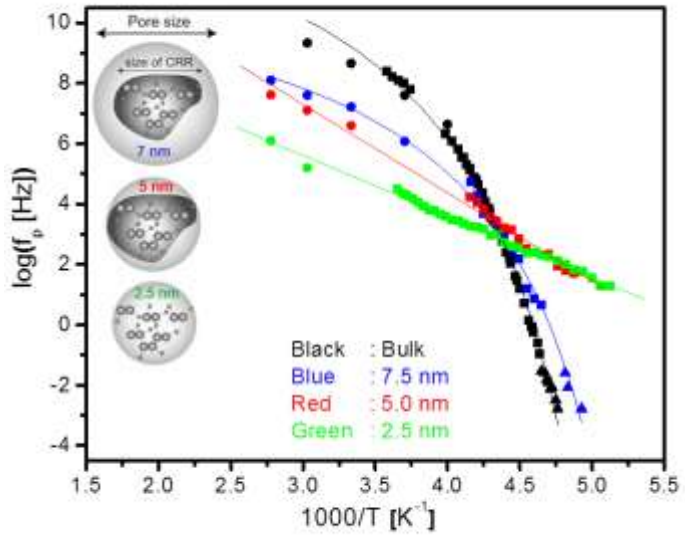

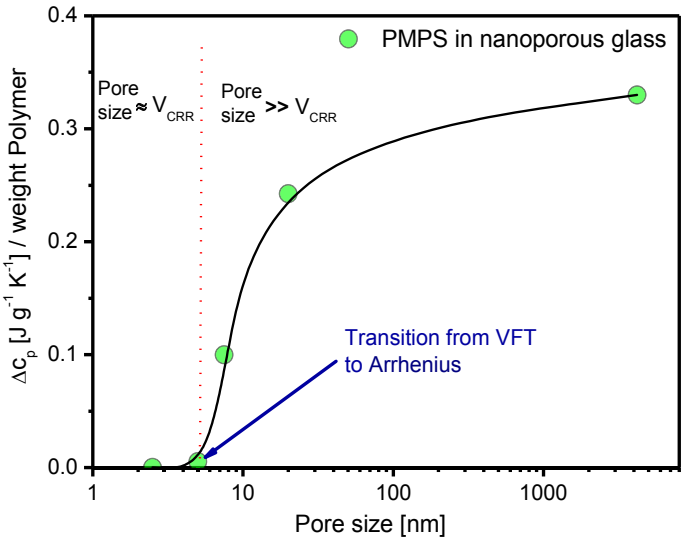

Figure 4.4. (A) *Relaxation map of segmental dynamics of PDMS confined into nanoporous glass. Inset: cartoon representation of polymer segment confined into a host, such as nanopores. Figure adapted from the References [61,62].* **(B)** *Δc_p (measured by TMSDC) of PMPS confined into nanoporous glass as a function of the pore sizes. The dashed red line represents the pore size at which the transition from VFT to Arrhenius occurs. The solid black like is a guide for the eyes. Figure taken and adapted from the references [61,62].*

References

1 Delcambre, S.; Riggleman, R.; de Pablo, J.; Nealey, P. *Soft Matter* **2010**, 6, 2475−2483.
2 Ediger, M.; Forrest, J. A. *Macromolecules* **2014**, 47, 471-478.
3 Napolitano, S.; Pilleri, A.; Rolla, P.; Wübbenhorst, M. *ACS Nano* **2010**, 4, 841-848.
4 Debenedetti, P.; Stillinger, F. *Nature* **2001**, 410, 259–267.
5 Anderson, P. *Science* **1995**, 267, 1615-1616.
6 Ediger, M.; Horrowell, P. *J. Chem. Phys.* **2012**, 137, 080901.
7 Keddie, J.L.; Jones, R.A.L.; Cory, R.A. *Faraday Discussions* **1994**, 98, 219-230.
8 Keddie, J.L.; Jones, R.A.L.; Cory, R.A. *Euro. Phys. Lett.* **1994**, 27, 59-64
9 Yin, H.; Napolitano, S.; Schönhals, A. Macromolecules 2012, 45, 1652-1662.
10 Yin, H.; Cangialosi, D.; Schönhals, A. *Thermochimica Acta* **2013**, 566, 186-192.
11 Dalnoki-Veress, K.; Forrest, J. A.; Murray, C.; Gigault, C.; Dutcher, J. *R. Phys. Rev. E* **2001**, 63, 031801-031811.
12 Lupaşcu, V.; Picken, SJ.; Wübbenhorst, M. *Journal of Non-Crystalline Solids* **2006**, 352, 5594-5600.
13 Fakhraai, Z.; Forrest, J. A. *Phys. Rev. Lett.* **2005**, 95, 025701-025705.
14 Sharp, J. S.; Forrest, J. A. *Phys. Rev. Lett.* **2003**, 91, 235701-235705.
15 Paeng, K.; Richert, R.; Eidger, M.D. *Soft Matter* **2012**, 8, 819-826.
16 Qi, D.; Ilton, M.; Forrest, J. A. *Eur. Phys. J. E* **2011**, 34, 56-63.
17 Qi, D.; Daley, C. R.; Chai, Y.; Forrest, J. A. *Soft Matter* **2013**, 9, 8958−8964.
18 Yin, H.; Cangialosi, D.; Schönhals, A. *Thermochimica Acta **2013, 566, 1**86.*
19 Ediger, M.; Forrest, J. A. *Macromolecules* **2014**, 47, 471-478.
20 Forrest, J.; Dalnoki-Veress, K. *ACS Macro Letters* **2014**, 3, 310−314
21 O'Connell, P. A.; McKenna, G. B. *Science* **2005**, 307, 1760–1763.
22 Paeng, K.; Swallen, S. F.; Ediger, M. D. *J. Am. Chem. Soc.* **2011**, 133, 8444–8447.
23 Forrest, J. A.; Dalnoki-Veress, K.; Coll.; J. *Int. Sci*. **2001**, 94, 167–195.
24 Forrest, J. A.; *Eur. Phys. J. E* **2002**, 8, 261–266.
25 Fakhraai, Z.; Forrest, J. A. *Science* **2008**, 319, *600-604*.
26 Chai, Y.; Salez, T.; McGraw, J. D.; Benzaquen, M.; Dalnoki-Veress, K.; Raphaël, E.; Forrest, J. A. *Science* **2014**, 343, 994-999.
27 Tress, M.; Erber, M.; Mapesa, E. U.; Huth, H.; Müller, J.; Serghei, A.; Schick, C.; Eichhorn, K.-J.; Voit, B.; Kremer, F. *Macromolecules* **2010**, 43, 9937−9944.
28 Tress, M.; Mapesa, E. U.; Kossack, W.; Kipnusu, W. K.; Reiche, M.; Kremer, F. *Science* **2013**, 341, 1371−1374.
29 Napolitano, S.; Wübbenhorst, M. *Nat. Comm.* **2011**, 2, 260.
30 Tarnacka, M.; Kaminski, K.; Mapesa, E. U.; Kaminska, E; Paluch, M. *Macromolecules* **2016**, 49, 3415–3426.
31 Glynos, E.; Frieberg, B.; Chremos, A.; Sakellariou, G.; Gidley, D.; Green, P. *Macromolecules* **2015**, 48, 2305-2312.
32 Housmans, C.; Sferrazza, M.; Napolitano, S. *Macromolecules* **2014,** 47, 3390-3393.
33 Burroughs, M.; Napolitano, S.; Cangialosi, D.; Priestley, R. *Macromolecules* **2016**, 49, 4647-4655.
34 Neubauer, N.; Winkler, R.; Tress, M.; Uhlmann, P.; Reiche, M.; Kipnusua, W.; Kremer, F. *Soft Matter* **2015**, 11, 3062-3066.
35 Cangialosi, D.; Boucher, V. M.; Alegria, A.; Colmenero, J. *Journal of Chemical Physics* **2013**, 135, 95362.
36 Napolitano, S.; Cangialosi, D. *Macromolecules* **2013***,* 46, 8051-8053.
37 Dalnoki-Veress, K.; Forrest, J. A.; de Gennes, P. G.; Dutcher, J. R. *Journal de Physique* **2000**, 10, 221-226.
38 de Gennes, P-G. Glass transitions of freely suspended polymer films. *Comptes Rendus de L'Academie Des Sciences Serie Iv Physique Astrophysique* **2000**, 1, 1179-1186.
39 de Gennes, P-G. *European Physical Journal E* **2000***,* 2, 201-203.
40 Martinez-Tong, D. *Macromolecules* **2013**, 46, 4698–705.
41 Ellison, C. J., Mundra, M. K.; Torkelson, J. M. *Macromolecules* 2005, 38, 1767-1778.
42 Wang, H.; Tongxin, C.; Xiaohui, L.; Zhijun, H.; Alain, J. *Nanoscale* **2016**, 8, 14950-14955.
43 Gibbs, J. H.; DiMarzio, E. A. *Journal of Chemical Physics* **1958**, 28, 373.
44 Geng, K.; Tsui, O. K. C. *Macromolecules* **2016**, 49, 2671-2678.
45 Xu, J. Tongxin, C.; Xiaohui, L. *Macromolecules* **2011**, 44, 7445-7450.
46 de Gennes, P-G.. *J. Chem. Phys.* **1971**, 55, 572-578.
47 Barber, D. R.; Steiner, U. *Phys. Rev. Letter*. **2007**, 98, 227801-227808.
48 Serghei, A,; Kremer, F. *Macrom. Chem. Phys*. **2008**, 209, 810-819.

49 Rotella, C.; Napolitano, S.; De Cremer, L.; Koeckelberghs, G.; Wübbenhorst, M. *Macromolecules* **2010**, 43, 8686-8691.
50 Santore, M. *Curr. Opin. Colloid Interface Sci.* **2005**, 10, 176−183.
51 Granick, S. *Eur. Phys. J. E* **2002**, 9, 421−424.
52 O'Shaughnessy, B.; Vavylonis, D. *J. Phys.: Condens. Matter* **2005**,17, R63−R99.
53 Gin, P.; Jiang, N.; Liang, C.; Taniguchi, T.; Akgun, B.; Satija, S.K.; Endoh, M.K.; Koga, T. *Phys. Rev. Lett.* **2012**, 109, 265501.
54 Asada, M.; Jiang, N.; Sendogdular, L.; Gin, P.; Wang, Y.; Endoh, M.K.; Koga, T.; Fukuto, M.; Schultz, D.; Lee, M.; Li, X.; Wang, J.; Kikuchi, M.; Takahara, A. *Macromolecules* **2012**, 45, 7098–7106.
55 Jiang, N.; Shang, J.; Di, X.; Endoh, M.K.; Koga, T. *Macromolecules* **2014**, 47, 2682–2689.
56 Jiang, N.; Endoh, M.; Koga, T. Structures and Dynamics of Adsorbed Polymer Nanolayers on Planar Solids: Non-equilibrium Phenomena in Confined Soft Matter. vol.*1*. *Springer* **2015**, Napolitano, S. (Ed.).
57 Madkour, S.; Szymoniak, P.; Heidari, M.; von Klitzing, R.; A. Schönhals. *ACS Appl. Mater. Interfaces.* **2017**, 9, 7535-7546.
58 Holt, A.; Bocharova, V.; Cheng, S.; Kisliuk, A.; White, B.; Saito, T.; Uhrig, D.; Mahalik, J.; Kumar, R.; Imel, A.; Etampawala, T., Martin, H.; Sikes,N.; Sumpter, B.; Dadmun, M.; Sokolov, A. *ACS Nano* **2016,** 10, 6843-6852.
59 Füllbrandt, M.; Purohit, P.; Schönhals, A. *Macromolecules* **2013**, 46, 4626-4632.
60 Klonos, P. et al. *Macromolecules* **2016**, 49, 9457-9473
61 Schönhals, A.; Goering, H.; Schick, C.; Frick, B.; Zorn, R. *J. Non-Cryst. Solids* **2005**, 351, 2668 – 2677.
62 Schönhals, A.; Zorn, R.; Frick, B. *Polymer* **2016**, 105, 393-406.

CHAPTER 5 –The Idea Behind This Work

As discussed in chapters 1 and 4, since the pioneering work of Keddie et al. [1,2], the thickness dependence of the glass transition temperature has been controversially discussed in the literature.[3-12] The current understanding behind the deviations of the glass transition temperature for polymer thin films, from their bulk values, is commonly discussed in the framework of an idealized three-layer model. Nevertheless, it was recently shown that parameters like M_w, annealing time, interfacial interaction and packing frustration could directly influence the overall glass transition and the glassy dynamics of the thin films, as discussed in chapter 4. Consequently, it was concluded that the effects of nanoconfinement on the glass transition and glassy dynamics go beyond an idealized three-layer model, which mainly considers the surface to volume ratio effects.

The aim of this work is to achieve a deeper understanding of the nanoconfinement effects on the glass transition and the glassy dynamics of polymer films and the molecular mechanism behind the possible deviations from the bulk properties. This goal is achieved by simplifying the topic through two main parallel approaches I) carefully chosen polymeric systems, which allows the enhancement of the effect of a certain parameter (e.g. M_w and annealing times effect on the growth to the adsorbed layer) on the glass transition and glassy dynamics of the whole film. II) Combining different characterization methods with different sensitivities and frequency windows, which could allow selective probing of a polymer (in the case of polymer blends) or a property (glass transition versus segmental dynamics) of the measured systems. A schematic summarizing the especially selected system and the different characterization methods employed to study them is given in figure 5.1.

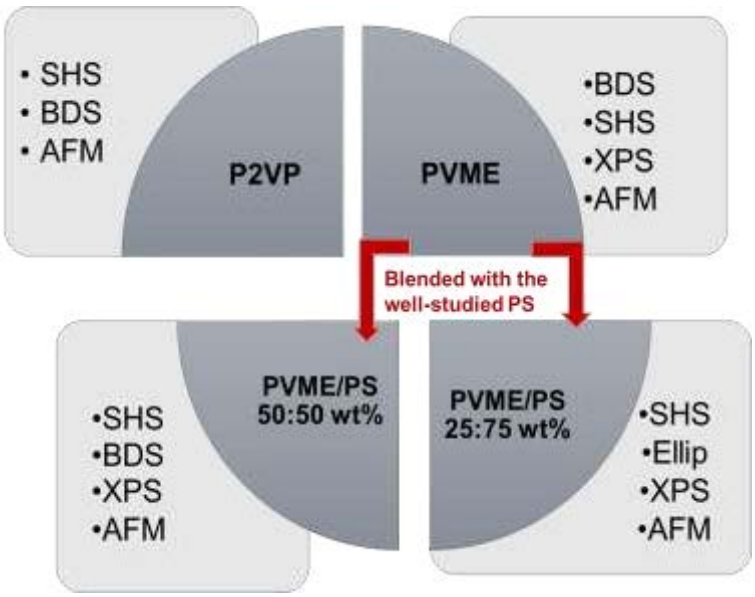

Figure 5.1. *A schematic summarizing the especially selected systems studied in this dissertation. In addition, the selected combination of the characeterization methods used for every system are given.*

The experimental work presented here starts with a SHS study on thin films of high Molecular weight (M_w) Poly(2-vinly pyridine) (P2VP), *Chapter 7*.[13] This study was carried out to confirm what has been controversially discussed in literature regarding the thickness independency of T_g^{dyn} of thin polymer film and molecular reasons behind it. Through developing a new derivative-based analysis method, which reduces the analysis error, a slight deviation, from the bulk value, of T_g^{dyn} with decreasing the film thickness was surprisingly evidenced for the first time. A closer look on the data revealed that the temperature dependence of the heat capacity in the glassy and liquid states changes with film thickness, which was considered as a confinement effect. Although the decrease in T_g^{dyn} with decreasing the film thickness was related to the effect of the free surface, it could not be excluded that this temperature dependence could also be a result of an increase in the free volume at the polymer/substrate interface, as explained in 4.1.2. This could also be expected, as the annealing time required to equilibrate segments for a high M_w polymer, which is necessary to form an adsorbed layer, could be much longer than the annealing time used for this work (48 hrs).

Consequently, to exclude the latter possibility, the attention was directed to a lower M_w polymer, namely Poly(Vinyl methyl ether) (PVME). The annealing time was increased to 72 hrs, which is expected to be longer than the terminal relaxation times, as suggested by the reptation model. Therefore, ensuring the presence of an adsorbed layer and eliminating the effect of an increased free volume at the polymer/substrate interface. *Chapter 8* then

presents a detailed SHS and BDS study on thin films of PVME.[14] First, to avoid the long-standing argument on the effect of the different sample arrangements and substrates on the glassy dynamics, measure by BDS and SHS, the following approach was followed. First, the recently developed Nanostructured Capacitor (NSC) was adapted and employed.[15] This sample arrangement allowed BDS measurements of supported films with a free polymer/air interface, rather than capped one, commonly measured by Crossed Electrode Capacitor (CEC). By comparing identically prepared films measured by both arrangements, it was concluded that for this system, the free surface layer has no effect on the overall segmental dynamics. On the other hand, due to the stronger interfacial interaction of PVME with SiO_2 compared to AlO_x (as confirmed by Contact Angle Measurements (CAM)), a thicker PVME adsorbed layer at the polymer/substrate interface was evidenced. Utilizing NSC, the glassy dynamics of this adsorbed layer, within the thin films, was reported for the first time and was found to be completely independent from that of the bulk-like layer.

The results of the homopolymer thin films, presented in chapters 7 and 8, suggested that the effect of the free surface layer on the overall segmental dynamics cannot be probed with dynamic methods, due to the measurement conditions. This is in line with reference [16], where it was shown that the segmental dynamics of the free surface layer becomes indistinguishable from that of the bulk-like layer, at temperatures above T_g^{therm}. Nevertheless, by carefully choosing a polymer blend system, a contrast in the segmental dynamics between the free surface and bulk-like layer could be created, utilizing the so-called surface enrichment phenomenon.

Therefore, the second part of this work focuses on polymer blends. An identical PVME, to the one used in the above mentioned study, was blended with the well-studied PS to form a blend miscible-in-bulk, with a composition of PVME/PS 50:50 wt% and 25:75 wt%. These asymmetric polymer blends experience an enhanced surface enrichment phenomenon, due to the large difference between in the surface tensions of PVME and PS. This results in the segregation of PVME at the free surface, forming a PVME rich-layer at the polymer/air interface. Since large differences in surface tensions is related to large differences in viscosity, which translates into large differences in the segmental dynamics, having a PVME-rich layer at the free surface would induce enough contrast in the segmental dynamics, with respect to that of the bulk-like layer. Subsequently, allowing the probing of the effect of the free surface layer on the overall segmental dynamics, as a function of the film thickness. It is worth to note that for these blend systems, there is no unified theory to

explain molecular mechanism behind the compositional heterogeneities even for bulk samples, see chapter 3. In addition, the glassy dynamics of thin polymer blend films and the effect of thin film confinement on the compositional heterogeneities and the segmental dynamics is considered rare in literature.

The thickness dependence of the glassy dynamics and glass transition of thin films of PVME/PS blends were studied by BDS, SHS, spectroscopic ellipsometry as well as X-ray Photoelectron Spectroscopy (XPS), AFM in *Chapters 9* through *11*.[17-19] The choosing of these systems as well as the exact combinations of the characterization methods were carefully selected based on a number of reasons.

I) These polymer blends are asymmetric with respect of the T_g^{therm}s of both components (ΔT_g^{therm} =130 K) and M_w (1:50 folds), which enhances the compositional heterogeneities as well as the preferential segregation of the PVME at the interfaces, [20] see section 3.4.

II) For these polymer blends, there is an additional asymmetry with respect to the dipole moments of both components. For BDS measurements, this feature allows the selective probing of the PVME dynamics as affected by PS. This is due to the fact that PS has a negligible dipole moment, compared to PVME. Therefore, by comparing the glassy dynamics of the blend to that of pure PVME, as a function of film thickness, different aspects of the nanoconfinement effect on the compositional heterogeneities within the polymer blend film, and the molecular mechanism behind it, was elaborated. For instance, this methodology helped in deciding whether a confinement effect was due to frozen PS segments or PVME adsorbed at the substrate.

III) Combing BDS and SHS provided a powerful tool to look at the different aspects of the glassy dynamics and its relationship to the dynamic heterogeneities.[21] While BDS would only be sensitive to the PVME segments, as affect by PS, SHS measures the entropy fluctuations all mobile segments of both PVME and PS. By comparing the temperature dependence of the segmental relaxation rates, various aspects of the nanoconfinement effects on the glassy dynamics as well as the compositional heterogeneity was displayed.

IV) In addition, the combination of BDS measurements using NSC and SHS allowed the studying of the influence of the mobile surface layer as well as the surface enrichment phenomena on the segmental dynamics, which could not be probed for thin films of homopolymers, as discussed above.

V) Combining ellipsometry (Ellip.) with SHS provides a window to look at the glass transition and the related segmental dynamics in a large frequency spectrum. Choosing this system, which shows a thickness dependence of T_g^{dyn}, allows for the comparison with the thickness dependence of T_g^{therm}. Utilizing this behavior, a direct evidence was provided on the coupling/decoupling phenomena of T_g^{dyn} and T_g^{therm}, which withstands a two-decade controversial discussion.

VI) Finally, XPS measurements on the free surface as well as the leached adsorbed layer (utilizing recently developed solvent leaching experiments), provided for the first time direct evidence of the compositional heterogeneities at the interfaces. Due to the mass conservation of the measured film, educated assumptions about the overall compositional heterogeneities was then concluded. By combing the XPS results to that of the BDS, the molecular mechanism behind the effect of the compositional heterogeneities on the glassy dynamics of the polymer blend were discussed.

References

1 Keddie, J.L.; Jones, R.A.L.; Cory, R.A. *Faraday Discussions* **1994**, 98, 219-230.
2 Keddie, J.L.; Jones, R.A.L.; Cory, R.A. *Euro. Phys. Lett.* **1994**, 27, 59-64.
3 Ediger, M.; Forrest, J. A. *Macromolecules* **2014**, 47, 471-478.
4 Forrest, J.; Dalnoki-Veress, K. *ACS Macro Letters* **2014**, 3, 310−314
5 O'Connell, P. A.; McKenna, G. B. *Science* **2005**, 307, 1760–1763.
6 Paeng, K.; Swallen, S. F.; Ediger, M. D. *J. Am. Chem. Soc.* **2011**, 133, 8444–8447.
7 Forrest, J. A.; Dalnoki-Veress, K.; Coll.; J. *Int. Sci*. **2001**, 94, 167–195.
8 Forrest, J. A.; *Eur. Phys. J. E* **2002**, 8, 261–266.
9 Fakhraai, Z.; Forrest, J. A. *Science* **2008**, 319, *600-604*.
10 Chai, Y.; Salez, T.; McGraw, J. D.; Benzaquen, M.; Dalnoki-Veress, K.; Raphaël, E.; Forrest, J. A. *Science* **2014**, 343, 994-999.
11 Tress, M.; Erber, M.; Mapesa, E. U.; Huth, H.; Müller, J.; Serghei, A.; Schick, C.; Eichhorn, K.-J.; Voit, B.; Kremer, F. *Macromolecules* **2010**, 43, 9937−9944.
12 Tress, M.; Mapesa, E. U.; Kossack, W.; Kipnusu, W. K.; Reiche, M.; Kremer, F. *Science* **2013**, 341, 1371−1374.
13 Madkour, S.; Yin, H.; Füllbrandt, M.; Schönhals, A. *Soft Matter* **2015**, 11, 7942-7952.
14 Madkour, S.; Szymoniak, P.; Heidari, M.; von Klitzing, R.; A. Schönhals. *ACS Appl. Mater. Interfaces*. **2017**, 9, 7535-7546.
15 Tress, M.; Mapesa, E. U.; Kossack, W.; Kipnusu, W. K.; Reiche, M.; Kremer, F. *Science* **2013**, 341, 1371−1374.
16 Paeng, K.; Swallen, S. F.; Ediger, M. D. *J. Am. Chem. Soc.* **2011**, 133, 8444–8447.
17 Madkour, S.; Szymoniak, P.; Schick, C.; Schönhals. A. *J. Chem. Phys*. **2017**, 146, 203321.
18 Madkour, S.; Szymoniak, P.; Hertwig, A.; Heidari, M.; von Klitzing, R.; Napolitano, S.; Sferrazza, M.; A. Schönhals. *ACS Macro Letters* **2017**, 6, 1156-1161.
19 Madkour, S.; Szymoniak, P.; Radnik, J.; A. Schönhals. *ACS Appl. Mater. Interfaces*. **2017,** 9, 37289-27299.
20 Jones, R. A. L.; Kramer, J. *Polymer* **1993**, *34*, 115-118.
21 Yin, H.; Madkour, S.; Schönhals. A. *Macromolecules* **2015**, 48, 4936-4941.

CHAPTER 6 - Experimental Techniques (Principles and Preparation)

The idea behind the characterization techniques used in this work is combing different volume sensitive methods with surface analytical techniques. The main volume sensitive methods employed here were Broadband Dielectric Spectroscopy (BDS), Specific Heat Spectroscopy (SHS) and spectroscopic ellipsometry. These different techniques reveal the different aspects of the glass transition and the related glassy dynamics, as illustrated in this section. As for the surface analytical techniques, Atomic Force Microscopy (AFM), Contact Angle Measurements (CAM), and X-ray Photoelectron Spectroscopy (XPS) were carried out to control and affirm the quality, the thickness, and the molecular composition of the prepared thin films. This chapter is arranged as follows. First, the principles of the main characterization methods (BDS and SHS) used in this work are briefly introduced. This is then followed by a brief description of all the other complementary techniques used in this work. Finally, a short summary of the sample preparation and the different samples arrangements is given.

6.1. Principles of the Main Experimental Techniques

Broadband Dielectric Spectroscopy (BDS) and Specific Heat Spectroscopy (SHS) were the two main characterization methods used. Both methods follow the linear response theory (LRT).[1,2] In general, LRT states that if an outer disturbance x(t) (applied perturbation) acts on a system, a response y(t) may be caused. If the observed response of the system is proportional to the applied perturbation, the linear response theory[3] can be applied. In that case, the time-dependent response of the system, following an applied disturbance, can be described by a linear equation. By applying for instance a small external disturbance to the system under investigation, the time-dependent response of the system, e.g. molecular fluctuations already present in the system, can be probed. The applied disturbance can be for example modulations of temperature, electric field, shear force, etc. By changing the source of the external disturbance, the yielded the proportional response will also differ. Consequently, allowing to probe different aspects of the same process. This is for instance one of the advantages of combing BDS and SHS in a complementary manner, figure 6.1.

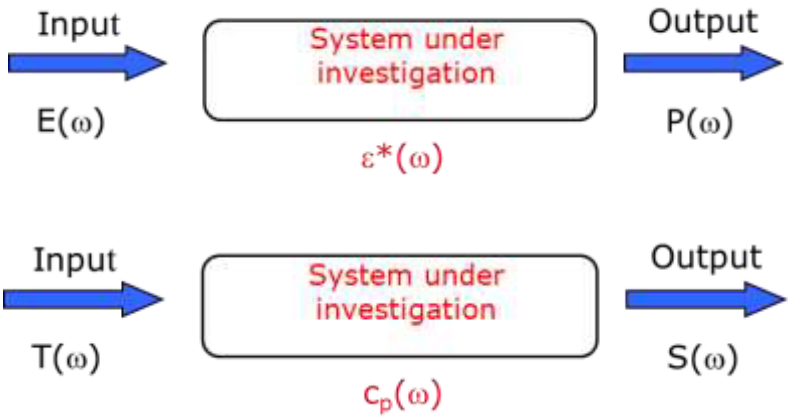

Figure 6.1. *A schematic of the applied external disturbance and the yielded proportional response of the system in the case of Broadband Dielectric Spectroscopy (BDS) – upper panel- and Specific Heat Spectroscopy (SHS) – bottom panel.*

6.1.1. Broadband Dielectric Spectroscopy

Broadband Dielectric Spectroscopy (BDS) refers to the measurement of a sample using electromagnetic fields, in the frequency range from 10^{-4} Hz to 10^{12} Hz. The interactions of these electromagnetic fields with the matter are based on different processes, such as restricted molecular and/or cooperative fluctuations, as well as charge transport and polarization effects at the interfaces. For polymeric system, different dynamic processes occur over an extremely broad time and temperature scales. Therefore, BDS is a useful and efficient tool to probe the different molecular dynamics of polymers. The section is based on references [3-6].

6.1.1.1. Electrostatics

In an isotropic system, for small electric field strength *E,* the dielectric displacement *D* can be expressed as:

$$D = \varepsilon^* \varepsilon_0 E \tag{6.1}$$

where ε_0 is the dielectric permittivity of vacuum ($\varepsilon_0 = 8.854\ 10^{-12}\ AsV^{-1}m^{-1}$). When a time-dependent process is present, the time dependencies of the applied electric field and the resulting dielectric displacement are phase shifted.

In the case of a periodic electric field E(t) with small strength, $E(t) = E_0 exp(-i\ \omega\ t)$; where $\omega = 2\pi f$ and $i = \sqrt{-1}$ symbolizes an imaginary unit, this phase shift can be described by the complex dielectric function

$$\varepsilon^*(\omega) = \varepsilon'(\omega) - i\varepsilon''(\omega) \tag{6.2}$$

where $\varepsilon'(\omega)$ is the real part and $\varepsilon''(\omega)$ is the imaginary (loss) part of the complex dielectric function.

Polarization P is the part of the dielectric displacement, which is specifically attributed to the reaction of the material under study

$$P = D - D_0 = (\varepsilon^* - 1)\varepsilon_0 E \quad \text{with } \chi^* = (\varepsilon^* - 1) \tag{6.3}$$

where χ^* defines the dielectric susceptibility

In general, the macroscopic Polarization P is a yield of microscopic dipole moments p_i in the volume V. Since p_i could have a permanent or induced character. The latter is due to a local field E_{loc}, which disturbs the neutral charge distribution. For small field strengths, the linear relation $P = \alpha.E_{loc}$; where α denotes the polarizability. The polarization effects that occur on very short time scales are induced polarization P_∞, which are typically

I) Electronic polarization: resonant process occurring when the electron cloud of an atom (or molecule) is shifted with respect to the positive nucleus.

II) Atomic polarization: This process is observed when an agglomeration of positive and negative ions is deformed under the force of the applied field.

Additionally, due to the chemical structure, many molecules carry a permanent dipole moment $\bar{\mu}$. If there is only one type of N permanent dipoles in the system, with the mean dipole moment $\langle\bar{\mu}\rangle$, P then reads

$$P = \frac{1}{V}\sum \mu_i + p_\infty = \text{N/V } \langle\mu_i\rangle + P_\infty \tag{6.4}$$

where μ_i defines the dipole moment of the repeating unit and N/V denotes the number density of the dipoles involved in the time-dependent process present.

Assuming that the dipoles do not interact with each other (isolated dipoles) and the E_{loc} (at the permeant dipoles) is equal to the outer electric field, one can derive the contribution of the orientational polarization originating from the electric field[7-9] as

$$\Delta\varepsilon = \Delta\varepsilon_s - \Delta\varepsilon_\infty = \frac{1}{3\varepsilon_0}\,\frac{\mu^2}{k_B T}\,\frac{N}{V} \tag{6.5}$$

where $\varepsilon_s = \lim_{\omega\to 0} \varepsilon'(\omega)$. $\varepsilon_\infty = \lim_{\omega\to\infty} \varepsilon'(\omega)$ covers all contributions to the dielectric function, which are due to induced polarization P_∞ and $\Delta\varepsilon$ is also called the dielectric strength.[3]

6.1.1.2. Dielectric Relaxation

For small applied electric field strength, the dielectric relaxation theory can be described in the framework of the linear response theory. In dielectric spectroscopy, the external electric field E(t) corresponds to the perturbation, and the polarization P(t) is the response of the system and they are linked together as follows,[1]

$$P(t) = P_\infty + \varepsilon_0 \int_{-\infty}^{t} \varepsilon(t-t') \frac{dE(t')}{dt'} dt' \tag{6.6}$$

where $\varepsilon(t)$ is the time dependent dielectric function. Consequently, the time-dependent dielectric function can be directly measured as a response of the system exposed to a step-like change of the external electric field $\frac{dE(t)}{dt} = E_0\delta(t)$, as shown in the figure 6.2. Thus, according to equation 6.6, the response of the system can be described by $\varepsilon(t)$, where $\varepsilon(t) = \frac{P(t)-P_\infty}{E_0\varepsilon_0}$.

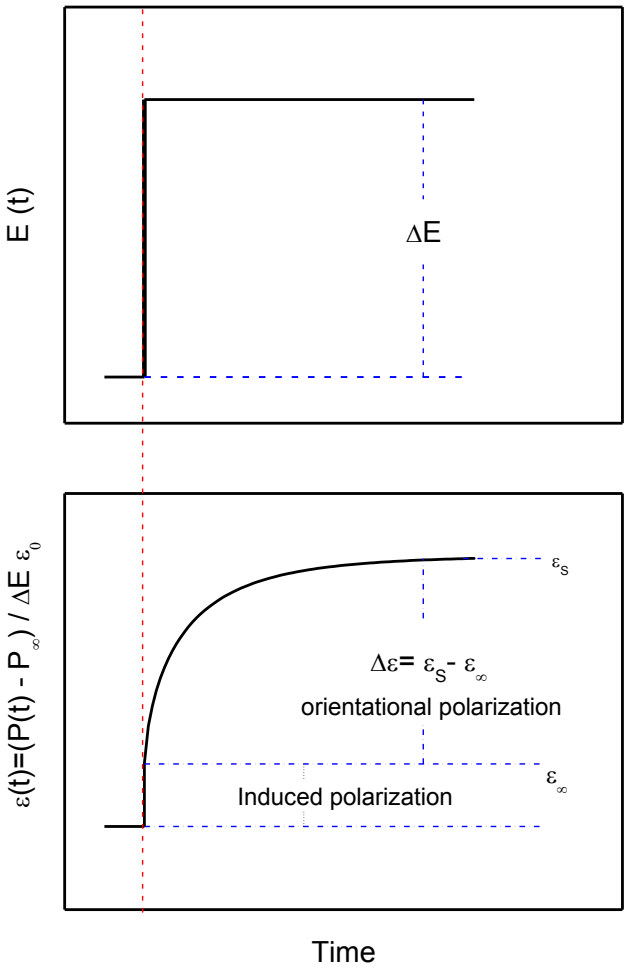

Figure 6.2. *Schematic representation of the polarization, and the time-dependent dielectric relaxation function (right panel) as well as the time dependence of the electric field* (**inset**). *Reproduced and adapted from the reference [3].*

When the applied electric field is periodic in a stationary state, the induced polarization from equation 6.6. becomes

$$P^*(\omega) = \varepsilon_0(\varepsilon^*(\omega) - 1)E^*(\omega) \tag{6.7}$$

where $\varepsilon^*(\omega)$ is related to $\varepsilon(t)$ with the following equation

$$\varepsilon^*(\omega) = \varepsilon'(\omega) - i\varepsilon''(\omega) = \varepsilon_\infty - \int_0^\infty \frac{d\varepsilon(t)}{dt} exp(-i\omega t)\, dt\ , \tag{6.8}$$

6.1.1.3. Analysis of the Dielectric Spectra

In principle, the analysis of the dielectric relaxation processes is usually done using model functions. Starting with the theoretically well-founded Debye function, several formulas for both the frequency and time domain, which were suggested to described the experimentally observed dielectric spectra. Here, only the important approaches are discussed.

Debye Behavior

Debye relaxation is a theoretically well-grounded model for dielectric relaxation. It assumes that the change in polarization is proportional to its actual value.[9,10] The time dependence of a dielectric process, where τ_D is the relaxation time of the process, is given as follows

$$\frac{dP(t)}{dt} = -\frac{1}{\tau_D} P(t) \tag{6.9}$$

This model was firstly derived by Debye, leading to a dielectric function in the frequency domain, which reads

$$\varepsilon^*(\omega) = \varepsilon'(\omega) - i\varepsilon''(\omega) = \varepsilon_\infty + \frac{\Delta\varepsilon}{1 + i\omega\tau_D} \tag{6.10}$$

With real and imaginary parts, figure 6.3, given as

$$\varepsilon'(\omega) = \varepsilon_\infty + \frac{\Delta\varepsilon}{1 + (\omega\tau_D)^2} \tag{6.11 a}$$

$$\varepsilon''(\omega) = \frac{\Delta\varepsilon\omega\tau_D}{1 + (\omega\tau_D)^2} \tag{6.11 b}$$

In the frequency domain, the real part shows a stepwise decrease, with increasing frequency, while the imaginary part shows a symmetric loss peak. The maximal loss position provides an information about the relaxation rate $f_p = \frac{\omega_p}{2\pi}$ or relaxation time $\tau_D = \frac{1}{2\pi f_p} = \frac{1}{\omega_p}$. In addition, the step height of the real part of the relaxation process or the area under the loss peak gives the dielectric strength $\Delta\varepsilon$.

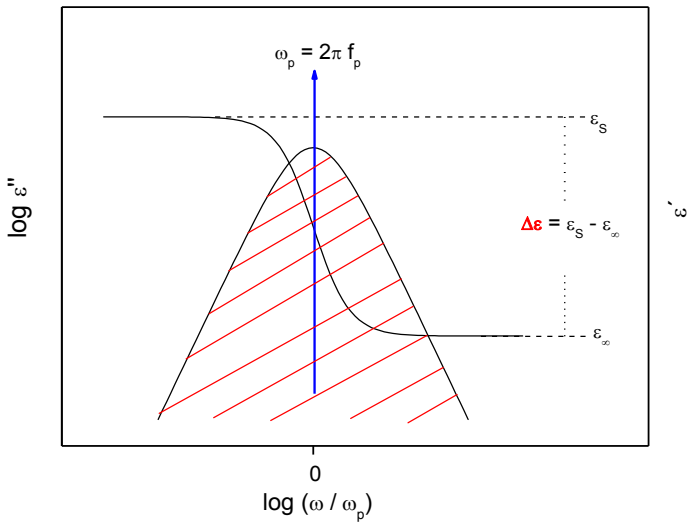

Figure 6.3. *Frequency dependence of the real part and the imaginary part of the complex dielectric function according to the Debye function. Figure reproduced from reference [5].*

6.1.1.4. Non-Debye Behavior

In practice, the Debye function is not sufficient to describe the experimental results obtained from complex systems like amorphous polymers. In most cases, the measured loss peaks have a half width that is much broader than what is predicted by equation 6.10. Moreover, their shapes are asymmetric with a high frequency tail. This is called non-Debye behavior.

The broadening of the symmetric relaxation peak is described by Cole/Cole (CC) function[11]

$$\varepsilon^*(\omega) = \varepsilon_\infty + \frac{\Delta\varepsilon}{(1 + i\omega\tau_{CC})^{\beta}} \tag{6.12}$$

where β value characterizes the symmetric broadening of the relaxation peaks within the boundary conditions of ($0<\beta\leq1$) and τ_{CC} is the characteristic relaxation time.

The relaxation peaks can also have an asymmetric broadening, which can be described by the Cole/Davidson (CD) function[12,13]

$$\varepsilon^*(\omega) = \varepsilon_\infty + \frac{\Delta\varepsilon}{(1 + i\omega\tau_{CD})^{\gamma}} \tag{6.13}$$

where γ value characterizes the asymmetric broadening of the relaxation peaks within the boundary conditions of ($0<\gamma\leq1$) and τ_{CD} is the characteristic relaxation time.

In general, most non-Debye relaxation processes can be well described by Havrilian/Negami (HN) function developed, which is the most generalized form of the Debye function, taking into account both the asymmetry and the broadening of the peak.

$$\varepsilon^*(\omega) = \varepsilon_\infty + \frac{\Delta\varepsilon}{((1 + i\omega\tau_{CD})^{\beta})^{\gamma}} \tag{6.14}$$

where and τ_{HN} is the characteristic relaxation time. The fractional shape parameters β and γ ($0 < \beta,\ \beta\gamma \leq 1$) determine the deviation from the Debye function. Their effect on the dielectric relaxation spectra is illustrated in figure 6.4. From the experimental point of view, all of the relevant parameters, such as dielectric strength, relaxation time and the shape parameters can be estimated by fitting the HN function to the obtained data.[16]

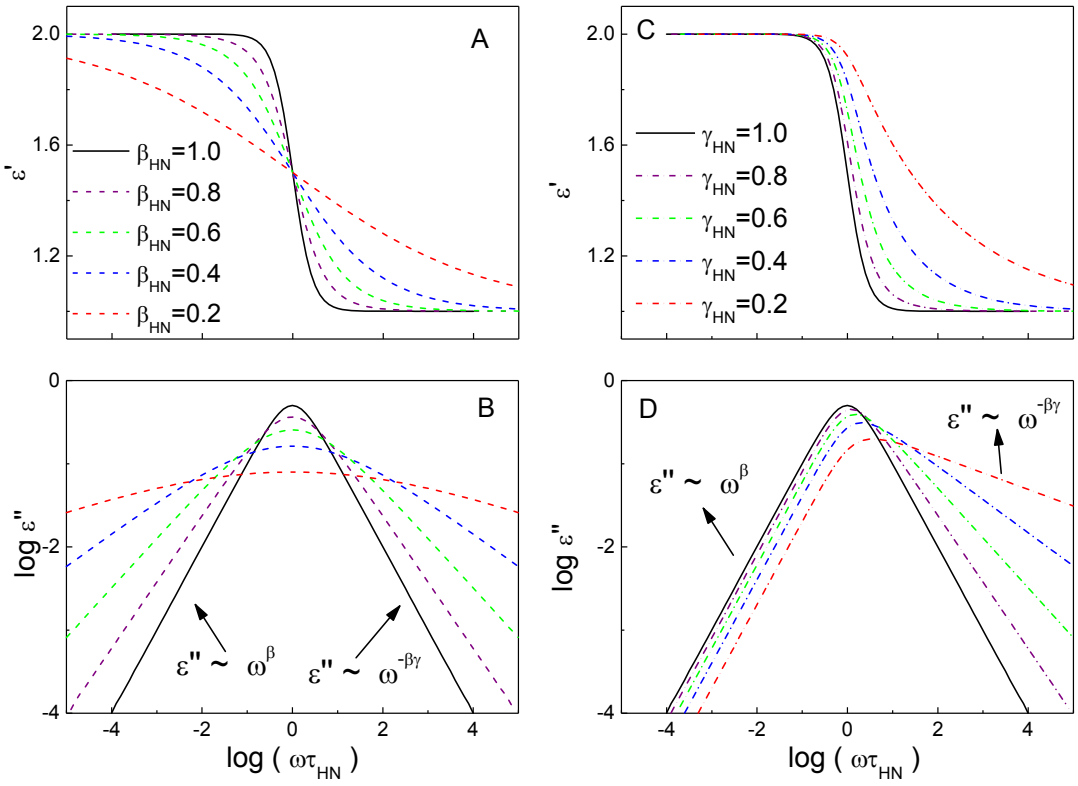

Figure 6.4. *Complex dielectric permittivity for the HN-function with fixed β=1 and γ=1 and decreasing till before 0 (0< β, βγ =<1.). Figure was taken and adapted from reference [5].*

6.1.1.5. Fitting HN Function to Experimental Data

From the experimental point of view, the dielectric spectra of a complex system do not show isolated loss peaks. In addition to the relaxation processes (one or more could be dielectrically active), other parasitic contributions are often observed, such as the

conductivity contributions due to the conductivity of the electrode. The conductivity contribution to the dielectric loss can be described as $\varepsilon'' = \sigma/(\omega^s \varepsilon_0)$, where σ is connected to the DC conductivity, s is a parameter to model non-Ohmic effects, s = 1 for Ohmic contacts, and s<1 holds for a non-Ohmic behavior. It is worth to note that the conductivity contribution is taken into account during the data analysis, in addition to the relaxation processes, which can be well-described by the HN-function. For bulk samples, the following equation was obtained for the whole fit function[5]

$$\varepsilon^*_{Fit} = \varepsilon^*_{HN}(\omega) - i\frac{\sigma}{\omega^s \varepsilon_0} \tag{6.15}$$

6.1.2. Specific Heat Spectroscopy

In the frame work of the LRT,[1,2] analogously to BDS, in Specific Heat Spectroscopy (SHS) the complex heat capacity function can be regarded as the response of the system to an external periodic disturbance (temperature modulations), figure 6.1.

6.1.2.1. Complex Heat Capacity

Many thermal processes are related to the time-dependent entropy/enthalpy changes, e.g. glass transition. If the applied disturbance is also time-dependent and adequately small, the resultant time-dependent heat capacity C(t) can be considered as the response of the system, within the framework of the linear response theory.[14]

The time dependent enthalpy and temperature is described as follows

$$\partial H(t) = \int_{-\infty}^{t} \frac{dC(t-t')}{dt} \partial T(t')\, dt' \tag{6.16}$$

If this equation is then Fourier transformed, it would yield

$$H(\omega) = C^*(\omega)\, T(\omega) \tag{6.17}$$

where $C^*(\omega) = C'(\omega) - iC''(\omega)$, with a real and imaginary part.

The time-dependent complex heat capacity C*(ω) could then be related to a time-dependent relaxation process,[15] as

$$C^*(\omega) = C_\infty + i\omega \int_0^t \frac{dC(t)}{dt} exp\ (-i\omega t)\, dt \tag{6.18}$$

6.1.2.2. Differential AC-Chip Calorimetry

The basic principle of this method is based on utilizing a commercially available AC-chip calorimeter in a differential set-up, which result in a boost in the sensitivity by two orders of magnitude. By applying an alternating current (AC) with frequency ν, through a small heating area, where the system under investigation is placed, a small periodic heat flow with frequency ω is measured, where ω = 2ν.

For the differential AC-Chip calorimetry, calorimetric chip XEN 39390 (Xensor Integration, NI) was used as measuring cell, see figure 6.5. It has optimized heater and thermometer on a sub-micrometer-thick silicon nitride membrane, which dramatically reduces the addenda heat capacity, allowing accurate measurements of ng samples. The sensor has a heater located in the center of a freestanding thin silicon nitride membrane (thickness 1 μm) supported by a Si-frame with a window. It has a theoretical heated hot spot area of about 30 x 30 μm^2, with an integrated 6-couple thermopiles and two-four-wire heaters (bias and guard heater), as shown in reference [16]. Please note that in addition to the 30 x 30 μm^2 hot spot, the heater strips also contribute to the heated area. A SiO_2 layer with a thickness of 0.5 - 1 μm protects the heaters and thermopiles. The thin films are spin coated over the whole sensor, but only the small heated area is sensed, thus considered as a point heat source. For further details, the reader is referred to references [17-20].

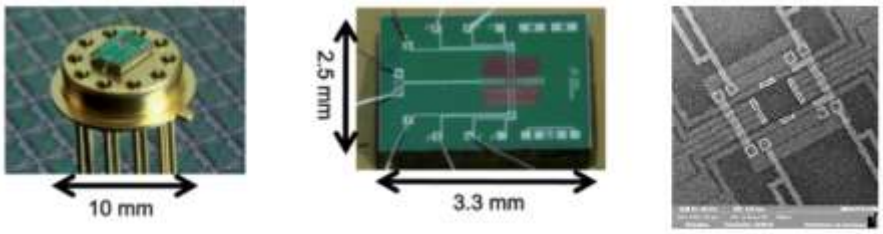

Figure 6.5. *Pictures of* (**left**) *XEN 39390AC-chip sensor* (**middle**) *Silicon nitride membrane fixed on a rectangular silicone substrate. Pictures were adapted from reference [5]* (**right**) *SEM images of the 30 X 30 μm^2 heating area.*

In the differential approach to AC-chip calorimetry, the contribution of the heat capacity of the empty sensor to the measured signal is minimized. This approach boosts the sensitivity of the measurement to reach pJ/K. In the approximation of thin films (submicron), the heat capacity of the sample C_S is then given by [21,22]

$$C_S = i\omega\overline{C}^2(\Delta U - \Delta U_0)/SP_0 \tag{6.19}$$

where ω is the angular frequency. $\overline{C} \equiv C_0 + G/i\omega$ describes the effective heat capacity of the empty sensor (C_0 – heat capacity of the sensor; G/iω is the heat loss through the surrounding atmosphere), S is the sensitivity of the thermopile, P_0 is the applied heating power, and ΔU is the complex differential thermopile signal for an empty reference sensor and a chip with a sample, where ΔU_0 is the complex differential voltage measured for two empty sensors. A more detailed description of the calorimetric chip, its differential setup and the experimental method can be found in reference [21]. Absolute values of the heat capacity can be obtained by calibration procedures.[22]

6.2. Methods and Experimental Techniques

6.2.1. Broadband Dielectric Spectroscopy (BDS)

The dielectric properties of samples were measured by a high-resolution ALPHA analyzer (Novocontrol) including a sample holder with an active head. Dielectric measurements were carried out, employing a small sinusoidal changing electric field, where the voltage is in the linear regime for all film thicknesses (0.1 V), in a broad frequency range (10^{-2}-10^{7} Hz). A Quatro cryosystem (Novocontrol) was interfaced to the cryostat to control the sample temperature with a temperature stability better than 0.1 K. The impendence $Z^*(\omega)$ of the sample was measured, which is directly related to the complex dielectric function with the following equation

$$\varepsilon^*(\omega) = \frac{1}{i\omega Z^*(\omega) C_0} \tag{6.20}$$

where C_0 is the capacitance of an empty capacitor. C_0 for a parallel plate capacitor with a dielectric material in between can be represented as

$$C_0 = \frac{\varepsilon_0 \epsilon_r A}{d} \tag{6.21}$$

where A is the area of the capacitor (area between the two electrode plates) and d is the distance between the two electrodes. It is also important to note that all samples were purged with dry nitrogen during the course of the measurement. For more experimental details the reader is referred to ref [5].

6.2.2. Specific Heat Spectroscopy (SHS)

SHS was employed utilizing *differential AC chip calorimetry*. The experiments were carried out in the temperature scan mode, which means that the frequency was increased step-wise,

while the temperature was ramped throughout the whole temperature range, for every frequency step. To ensure stationary conditions during the measurement, the scanning rate was varied in the range from 1 K/min to 2.0 K/min, depending on the programmed frequency. The power for temperature modulation was kept constant at about 25 μW. This value ensures that the maximum amplitude of the temperature oscillation is smaller than 0.25 K and so the response takes place in the linear regime.

It is worth to note that before the measurement, the PT-100 of the thermostat chamber was calibrated by measuring the phase transition temperatures for five different calibration substances, covering the whole temperature range of the calorimeter (173-573 K). The calibration equation obtained was then used to correct all the collected temperature data. Due to the lag between the cryostat temperature and the temperature at the chip membrane, an additional temperature correction was applied to the collected data. With the assumption of symmetric conditions for heating and cooling, the temperature lag was determined as ΔT, with the $2\Delta T$, being the temperature difference for same resistance at heating and cooling at the same rate [23].

6.2.3. Differential Scanning Calorimetry (DSC)

The glass transition temperature of all bulk samples were determined by DSC. Measurements were carried out on a Seiko Instrument DSC 220C attached to a liquid-nitrogen cooling system. All measurements were run at heating/cooling rate of 10 K/min, with nitrogen as the purging gas. The glass transition temperature of the samples was taken as the inflection point of the heat flow of the second heating run.

6.2.4. Ellipsometry

Ellipsometry is an optical technique for investigating the dielectric properties (complex refractive index also related to the dielectric function) of thin films. Ellipsometry measures the change of polarization upon reflection or transmission and compares it to a model.

The measured signal is the change in polarization of the incident beam, in a known polarized state, after it interacts (e.g. reflected, absorbed, etc.) with the structure of the material under investigation. The polarization change is quantified by the amplitude ratio, Ψ, and the phase difference, Δ.

Upon the analysis of the change in polarization of light, given the right model, the thickness of the thin films can be estimated with great accuracy. In this work, the analysis model employed a simplified multilayer model, consisting of air/polymer film/SiO_2/Si-substrate.

To reduce the number of free fit parameters, the thickness of the natural SiO_2 layer was determined and this value (1.7 nm) was kept constant during the data analysis of the polymer film.

Furthermore, for a polymer thin film, if the temperature is ramped during the measurement, the temperature dependence of the thickness (related to the thermal expansion coefficient of the film) can be determined. At T_g^{therm}, the temperature dependence of the thickness changes. T_g^{therm} is defined as the intersection of the linear dependencies of the thickness in the supercooled and glassy regimes in accordance with literature procedures.[24]

During the course of this work, two ellipsometry machines were used, which are discussed below. The laser ellipsometry was used to measure T_g^{therm} of thin films in the range of 0 K < T_g^{therm} < 373 K. However, for films with lower T_g^{therm}, a spectroscopic ellipsometer allowing measurements in the temperature range of 173 K - 373 K was utilized.

Laser Ellipsometry

To measure the film thickness as well as T_g^{therm} of thin films, an ellipsometer with polarizer-compensator sample analyzer (PCSA) (Optrel GbR, Sinzing, Germany) was utilized. This ellipsometer has a laser light with an average wavelength λ = 632.8 nm. The samples were measured at a set angle of incidence of 70 degrees. The analysis of the raw data was done employing the above-mentioned analysis model.

For the temperature measurements, the films were mounted onto a heating stage in ambient atmosphere. Water was used as the heating liquid, hence the limited heating/cooling range of 0 K < T_g^{therm} < 373 K, while the heating/cooling rate was fixed to 1 K/min.

Spectroscopic Ellipsometry

Secondly, the spectroscopic ellipsometer used is this work was M-2000 VI, J. A. Wollam. The raw ellipsometric angles Ψ and Δ data were fitted to a Cauchy model ($n(\lambda)=A + B/\lambda^2 + C/\lambda^4$, $K \cong 0$). Where n and K are the real and imaginary parts of the complex index of refraction. For 10 nm (±1 nm) films, B was also fixed to 0 due to the short path length of the light passing through the sample and reduced resolution. The analysis of the measurements employed the multilayer model discussed above.

For the temperature measurements, the films were mounted onto a heating stage, inside a chamber, connected to a liquid nitrogen cooling system interfaced with the ellipsometer. The closed chamber with the heating stage was purged with dry nitrogen gas throughout the experiment. The heating/cooling rate was fixed to1 K/min.

6.2.5. Atomic Force Microscopy

Atomic forces microscopy (AFM) - Cypher (Asylum Research, Santa Barbara, CA, USA, Silicon cantilevers with a reflective coating of aluminum (AC160TS, Oxford Instruments) were used to control the quality, topography and thickness of the film. In general, the thickness of the films were determined by estimating the step height of a scratch across the film. For all films considered here in this work, AFM pictures showed low roughness and no dewetting, down to the lowest film thicknesses. It is worth to note that the thicknesses were further confirmed by ellipsometry.

6.2.6. Contact Angle Measurements (CAM)

The measurements were carried out using the automated contact angle system OCA20 (Dataphysics, Germany), equipped with halogen lamps to ensure a homogeneous back lighting, a six-fold power zoom lens and a CCD camera. The contact angle (CA) was determined using the tangent fitting method. The used test liquids were Glycerol, n-hexadecane, n-tetradecane, and polyethylene glycol with a molecular weight of 200 g/mol. The measurements were carried out in an atmosphere saturated by the vapor of the test liquid. To insure the complete saturation of the atmosphere, samples were place in cuvette with the test liquid for 15 mins prior to the measurements. 3 drops with a volume of 4 µl were dropped onto the surface of a well-annealed 200 nm thick polymer film. Mean contact angles were calculated from averaging the angles of both sides of the drop over 10 minutes. The data for SiO_2 and AlO_x were taken from references [25 and 26], respectively.

6.2.7. X-ray Photoelectron Spectroscopy (XPS)

XPS investigations were carried out with an ESCALAB 220iXL (ThermoFisher) using monochromatic Al K α radiation (1486.6 eV). The samples were fixed with a double adhesive Carbon tape on a stainless steel sample holder. The peaks were fitted by Gaussian−Lorentzian curves after Shirley background subtraction. The electron binding energy was referenced to the Ti 2p3/2 peak of TiO_2 at 458.8 eV. The areas of the peaks were determined from the Gaussian−Lorentzian fits and divided by the element-specific Scofield factor and the analysator-depending transmission function.

6.3. Sample Preparation

6.3.1. Materials

The glass transition and glassy dynamics of different homopolymers and their blends in the thin film geometry was investigated by the different characterization methods, discussed above. The materials used in this work described in the following subsections. The chemical structure of all the homopolymers used are given in figure 6.6, as well as their DSC thermograms are shown in figure 6.7 and its inset.

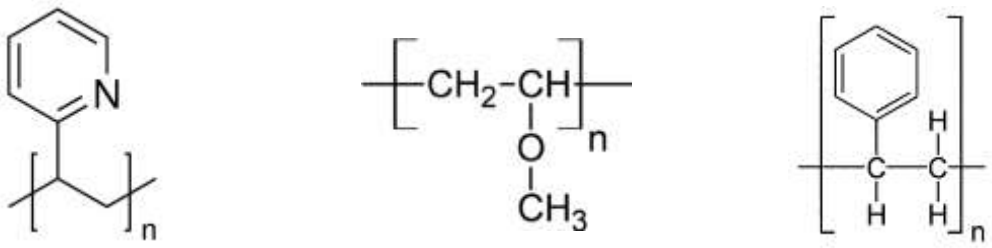

Figure 6.6. *Chemical structure of* (**left**) *Poly(2 vinyl pyridine)(P2VP)* (**middle**) *poly(vinyl methyl ether)(PVME)* (**right**) *polystyrene (PS).*

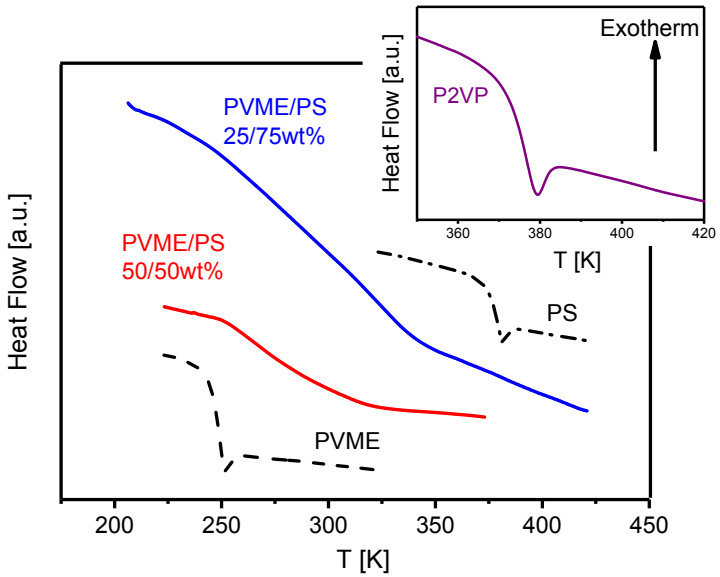

Figure 6.7. *DSC Thermograms (second heating run; rate: 10 K/min) for PVME –dashed, PS -dashed dotted, PVME/PS 50:50 wt% - red solid, and PVME/PS 25:75 wt% - blue solid.* **Inset***: DSC thermograms of P2VP – Purple solid line.*

6.3.1.1. Poly(2 Vinyl Pyridine) (P2VP)

P2VP was purchased from Polymer Standards Services GmbH (Germany) with a M_w of 1020 kg/mol and a polydispersity index (PDI) of 1.33. T_g^{therm} was found to be 373 K, estimated by DSC. Chloroform (≥ 99.9%) was used as a solvent to prepare a master polymer

solution. This solution was further diluted by Chloroform to prepare different concentrations, used to attune the films thicknesses.

6.3.1.2. Poly(Vinyl Methyl Ether) (PVME)

PVME was purchased (Aldrich, Inc.) as an aqueous solution (50 wt%) with a M_w of 10 kg/mol, which is lower than the entanglement M_w, and a PDI of 3. To obtain the dried PVME, the aqueous polymer solution was dried and annealed in an oil free vacuum for 72 h at 303 K, then for another 96 h at 323 K. T_g^{therm} of the dried PVME was estimated by DSC and found to be 246 K. A concentrated solution of the dried PVME in toluene was prepared as a master solution. This solution was further diluted by Toluene to prepare different concentrations, used to attune the films thicknesses.

6.3.1.3. Polystyrene (PS)

PS was purchased from Aldrich Inc. with a M_w of 524 kg/mol and a PDI of 1.04. T_g^{therm} of the bulk PS estimated by DSC, was found to be to be 376 K.

6.3.1.4. PVME/PS Blend

A concentrated polymer solution of the dried PVME and PS with the weight ratio of the polymers of 50:50 wt% and 25:75 wt% was prepared as master solution using toluene. A bulk film was prepared by casting from the master solution. This solution was further diluted by Toluene to prepare different concentrations, used to attune the films thicknesses. The films were then dried and annealed in an oil free vacuum for 72 h at 313 K, then for another 96 h at 343 K. The T_g^{therm} of the bulk materials were determined by DSC to be 273 K and 293 K for the 50:50 wt% and 25:75 wt% blends, respectively.

6.3.2. Sample Preparation

6.3.2.1. Spin Coating

In this work, all thin polymer films were prepared by spin-coating (SPIN150, SPS-Europe). The spin coater was placed in a laminar flow box during the sample preparation to avoid any possible contamination. Attuned film thicknesses were prepared from varying concentrations of the solution, after filtration (Minipore, 0.2 μm). Meanwhile, both rotation speed and time (3000 rpm, 60 s) were kept constant. It is worth to note that spin coating is an efficient approach to form uniform thin polymer films, with well-controlled thicknesses.

6.3.2.2 Annealing

After the spin coating process, the samples were annealed at temperatures $T_{ann} > T_{g,Bulk}$ for time t_{ann}. Table 6.1 illustrates the annealing conditions for all the samples prepared in this work. This annealing procedure insures two main points: I) the removal of the solvent, II) the release of the induced stress during spin coating.[27]

Table 6.1. *T_g^{therm} measured by DSC and annealing condition - temperatures (T_{ann}) and time (t_{ann}) employed for all polymer thin films measured in this work.*

Polymers	T_g^{therm} [K]	T_{ann} [K]	t_{ann} [hr]
P2VP	373	398	48
PVME	246	313	72
PS	376	423	72
PVME/PS 50:50 wt%	273	323	72
PVME/PS 25:75 wt%	293	338	72

6.3.2.3 Plasma Oven

The surface of all the Silicon wafers and AC-chip sensors (explained below) used in this work were activated, except for the work done on thin films of P2VP. Samples were placed in a plasma oven in a pure oxygen atmosphere (20 W, 300 sec). This process insures the removal of any organic contaminations and further activate the natural silica. It is important to note that this process was the main cleaning procedure for the AC-chip sensors, whereas, for the silicon wafers, it was a step within a longer cleaning protocol, as discussed below.

6.3.2.4. Solvent Leaching (Guiselin brushes experiments)

Preparation of the irreversibly adsorbed layer (PVME, PS, PVME/PS blends) was done employing solvent-leaching experiments. Toluene was used as the leaching-solvent, for all samples. First, all samples were dipped into separate toluene baths for 20 mins. This was then followed by a two-step process I) resining with toluene II) fast drying with dry nitrogen. Finally, the samples were annealed for 20 mins at $T = T_g + 50$ K. For a more detailed explanation, the reader is referred to reference [28]. The yielded adsorbed layers were then checked by AFM, where no sign of dewetting was observed. The thickness of this layer was found to be ca. 4 nm for PVME and PVME/PS blend, whereas it was found to be ca. 9 nm for PS.

6.3.2.4. Broadband Dielectric Spectroscopy

6.3.2.4.1. Bulk Sample

Bulk sample was prepared by melting the polymer on a gold plated brass electrode. The thickness was controlled by employing fused silica spacers with fixed diameter of 50 μm. After that, the polymer was covered with a smaller top gold electrode. Area of the molten polymer on the bottom electrode has to be larger than the upper electrode to avoid air gaps between the capacitor plates. A schematic representation of the bulk sample is shown in the figure 6.8.

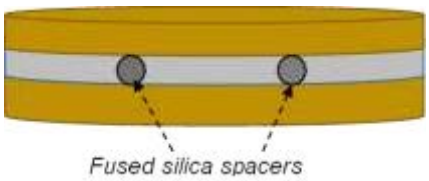

Figure 6.8. *Schematic of a bulk sample capped between two gold plated electrodes with 50μm fused silica spacers.*

6.3.2.4.2. Crossed Electrodes Capacitors

In this work, Crossed Electrodes Capacitors (CEC) were used to measure thin films A schematic representation of a CEC is given in figure 6.9. Here, the polymer film is capped between two thin aluminum electrodes. Glass substrates (10 x 10 mm) were cleaned in an ultrasonic alkaline bath at 333 K for 15 min. Subsequently, glass substrates were washed with ultrahigh purified water (Millipore, resistivity > 18 MΩ/cm), rinsed with acetone and dried in an inert gas flow. First, an aluminum electrode (2 mm width, ca. 60 nm thickness) was deposited on the glass substrate via thermal evaporation in ultrahigh vacuum (10^{-5} mbar). To minimize the risk of creating electrical shortcuts, a so-called flash evaporation was employed (> 30 nm/s), which allows for a smooth and defined metal/polymer interface.[29,30] After spin-coating and annealing of the film, the second aluminum strip was evaporated perpendicularly to the bottom electrode. This means that the capacitor was at the cross-section of the two strips.

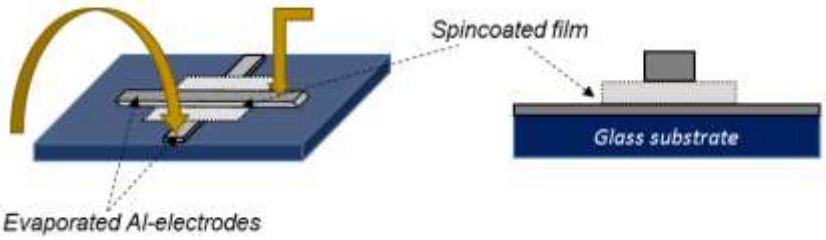

Figure 6.9. *Schematic representation of a Crossed Electrodes Capacitor sample.*

6.3.2.4.3. Nanostructured Capacitors

In the case of Nanostructured Capacitors (NSC),[31] both electrodes consist of highly doped conductive silicon wafers with a specific resistance $\rho < 0.003$ Ωcm and 0.23 nm roughness of RMS. On the backside of the electrodes a 200 nm Al-electrode was deposited. Bottom electrode additionally consists of a native oxide layer of ca. 2 nm. The sizes of the electrodes are 4 x 10 mm and 1 x 1 mm for the bottom and top electrode, respectively. The top electrode consists of an array of highly insulating silica spacers with the height of 35 or 70 nm and a cross-section of 5 x 5 µm and a fixed separation. Figure 6.10 represents a schematic of the NSC and an AFM image of the top nanostructured electrode. The preparation of thin films was carried out as follows. Silicon wafers were initially rinsed with acetone to remove the photoresist layer and dried with an inert gas flow (N_2). Subsequently, the substrates were cleaned and activated in O_2 plasma, as discussed above. As a final stage of the wafers cleaning, a snow jet gun was used (30 Gunjet Spraying Systems CO., Wheaton, USA), which purges super critical CO_2 through a nozzle, generating a jet flow of CO_2. This procedure was done while heating the substrate, to insure the sublimation of the solid CO_2 into gas, and thus polishing the surface with CO_2 solid particles and removing of any contaminating particles.

Polymer films were spin-coated on a these thoroughly cleaned bottom electrodes and thermally annealed as described in the section 6.3.2.2. In the last step, the top electrode was assembled on the counter planar wafer.[31]

In this sample geometry, thin films remain in contact with air, allowing polymer/air interaction at the free surface. It is important to note that the spacer heights must be ca. twice as large as the film thickness, to allow a free surface, even in the case spacers sinking into the film.

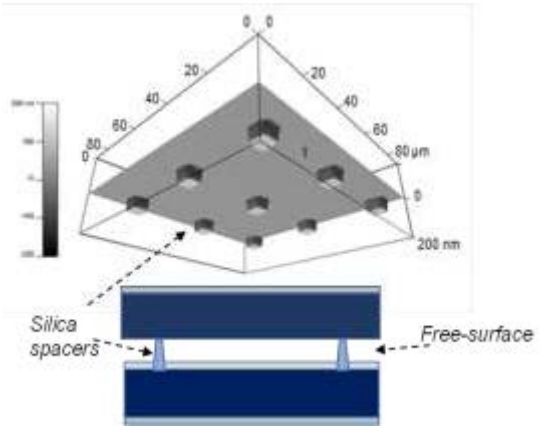

Figure 6.10. *AFM picture of the top electrode with 70nm spacers (upper panel), side view schematic of the nanostructured capacitor (bottom panel).*

6.3.2.5. AC-Chip Calorimetry

AC-Chip sensors were cleaned by exposing them to oxygen plasma, see section 6.3.2.3. Afterwards, polymer solutions were spin coated and annealed according to the protocol described in sections 6.3.2.1 and 6.3.2.2. Thickness of the films could not be measured directly on the sensor, due to the size limitations. Therefore, spin coated films (prepared under identical conditions) on silicon substrates with similar surface properties to the sensor were used to estimate the film thicknesses by ellipsometry and/or AFM.

References

1 Landau, L. D,; Lifschitz, E. M., Course of Theoretical Physics, vol. 5. Statistical Physics. Akademie-Verlag: Berlin, **1979**.
2 Kubo, R. *Reports on Progress in Physics* **1966,** 29, 255.
3 Schönhals, A.; Kremer, F. Broadband Dielectric Measurement Techniques and Theory of Dielectric Relaxation. In Broadband Dielectric Spectroscopy; Kremer, F.; Schönhals, A., Eds.; 1st ed; *Springer*: Berlin, **2002**; 01-34.
4 Schönhals, A.; Kremer, F. Broadband Dielectric Measurement Techniques. In Broadband Dielectric Spectroscopy; Kremer, F.; Schönhals, A., Eds.; 1st ed; *Springer*: Berlin, **2002**; 35-57.
5 Schönhals, A.; Kremer, F. Analysis of Dielectric Spectra In Broadband Dielectric Spectroscopy; Kremer, F.; Schönhals, A., Eds.; *Springer*, Berlin, **2002**; 59-96.
6 Schönhals, A.; Kremer, F. The Scaling of the Dynamics of Glasses and Supercooled Liquids. In Broadband Dielectric Spectroscopy; Kremer, F.; Schönhals, A., Eds.; *Springer*, Berlin, **2002,** 99-127.
7 Kirkwood, J. G. *The Journal of Chemical Physics* **1939**, 7, 911-919.
8 Kirkwood, J. G. *Annals of the New York Academy of Sciences* **1940,** 40, 315-320.
9 Fröhlich, H., Theory of dielectrics: dielectric constant and dielectric loss. 2d ed.; Clarendon Press: Oxford, **1958**.
10 Debye, P. J. W., *Polar molecules*. The Chemical Catalog Company, Inc.: New York, **1929**.
11 Cole, K. S.; Cole, R. H. The Journal of Chemical Physics **1941**, 9, 341-351.
12 Davidson, D. W.; Cole, R. H. *The Journal of Chemical Physics* **1950,** 18, 1417-1417.
13 Davidson, D. W.; Cole, R. H. *The Journal of Chemical Physics* **1951,** 19, 1484-1490.
14 H. Yin, S. Madkour and A. Schönhals, Glass transition of ultra-thin polymer films: A combination of relaxation spectroscopy with surface analytics in *Dynamics in confinement: Progress in Dielectrics,* Kremer, F. (Ed.) *Springer*, Berlin **2014**, pp17-59
15 Haase, R., Thermodynamics of irreversible processes. Dover: New York, **1990**.
16 van Herwaaden, S.; Application note for Xsensor's calorimeter chips of XEN-39390 series http://www.xensor.nl/pdffiles/sheets/nanogas3939.pdf
17 Huth, H.; Minakov, A. A.; Serghei, A.; Kremer, F.; Schick, C. *The European Physical Journal Special Topics* **2007**, 141, 153-160.
18 Efremov, M. Y.; Warren, J. T.; Olson, E. A.; Zhang, M.; Kwan, A. T.; Allen, L. H. *Macromolecules* **2002,** 35, 1481-1483.
19 Yin, H.; Schönhals, A. *Soft Matter* **2012,** 8, 9132-9139.
20 Madkour, S.; Yin, H.; Füllbrandt, M.; Schönhals, A. *Soft Matter* **2015**, 11, 7942-7952.
21 H. Huth, A. Minakov and C. Schick, *J. Polym. Sci. B: Polym. Phys*. **2006**, 44, 2996-3005.
22 D.S. Zhou, H. Huth, Y. Gao, G. Xue and C. Schick, *Macromolecules,* **2008**, 41,7662-7666.
23 Huth, H.; Schick, C. *Personal Communication*.
24 Glor, R.; Composto, J.; Fakhraai, Z. *Macromolecules*, **2015**, 48, 6682–6689.
25 Madkour, S.; Yin, H.; Füllbrandt, M.; Schönhals, A. *Soft Matter* **2015**, 11, 7942-7952.
26 Yin, H.; Napolitano, S.; Schönhals, A. *Macromolecules* **2012**, 45, 1652-1662.
27 Reiter, G.; Hamieh, M.; Damman, P.; Sclavons, S.; Gabriele, S.; Vilmin, T.; Raphael, E. *Nat. Mater*. **2005,** *4*, 754-758.
28 Napolitano, S.; Wubbenhorst, M. *Nature Communications* **2011**, 2, 260.
29 Amarandei, G.; Clancy, I.; O'Dwyer, C.; Arshak, A.; Corcoran, D. *ACS Appl. Mater. Interfaces* **2014**, 6, 20758-20766.
30 Zaporojtchenko, V.; Strunskus, T.; Erichsen, J.; Faupel, F. *Macromolecules* **2001**, 34, 1125–1127.
31 Tress, M.; Mapesa, E.; Kossack, W.; Kipnusu, W.; Reiche, M.; Kremer, F. *Science* **2013**, 341, 1371−1374.

CHAPTER 7 - Calorimetric Evidence for a Mobile Surface Layer in Ultrathin Polymeric Films: Poly(2-vinyl pyridine)

DOI: http://dx.doi.org/10.1039/C5SM01558H

Abstract

Specific heat spectroscopy was used to study the dynamic glass transition of ultrathin poly(2-vinyl pyridine) films (thicknesses: 405 - 10 nm). The amplitude and the phase angle of the differential voltage were obtained as a measure of the complex heat capacity. In a traditional data analysis, the dynamic glass transition temperature T_g is estimated from the phase angle. These data showed no thickness dependency on T_g down to 22 nm (error of the measurement of ± 3 K). A derivative-based method was established, evidencing a decrease in T_g with decreasing thickness up to 7 K, which can be explained by a surface layer. For ultrathin films, data showed broadening at the lower temperature side of the spectra, supporting the existence of a surface layer. Finally, temperature dependence of the heat capacity in the glassy and liquid states changes with film thickness, which can be considered as a confinement effect.

7.1 Introduction

The characterization of the glass transition temperature, T_g, of ultrathin polymer films has been of great interest due to their numerous applications in fields like coatings, membranes, and innovative organic electronics. Scientifically, ultrathin films provide ideal sample geometry for studying the confinement effects on the glass transition of polymers; as film thicknesses can be easily tuned by spin coating.[1] Generally, glass transition is a topical problem of soft matter research (see for instance [2-7]). Investigations on highly confined systems may help to evidence the existing of a dynamical length scale[8] corresponding to the glass transition, which is difficult to measure by other approaches.

Since the pioneering work of Keddie et al.,[9,10] the thickness dependence of the glass transition temperature has been controversially discussed in the literature. For the same polymer/substrate systems, divergent results have been published. In a recent perspective discussion by Ediger et al.,[11] the progress made in the last years was discussed (see for instance [12-20]). For polymers supported by a non-attractive substrate (see for instance [10,21-27]) a depression of the thermal glass transition temperature T_g with decreasing film thickness is widely observed. This T_g depression is discussed to originate as a result of a free polymer/air surface having a higher molecular mobility than the bulk due to missing polymer-polymer segment interactions and also due to structural differences.[19,23] Recently, optical photobleaching experiments,[22,28] as well as the embedding of gold nanospheres into a polymer surface,[29,30] provided some evidence for a highly mobile surface layer.

For polymers having a strong interaction with the substrate, T_g may increase with the reduction of the film thickness.[31-33] These experimental results were explained by the formation of an adsorbed boundary layer, in which the polymer segments have a lower molecular mobility; hence a higher glass transition temperature.[34] For that reason, attempts are made to correlate depression or increase of the glass transition temperature with the interaction energy between the surface of the substrate and the polymer γ_{SP}.[35] A depression of T_g should be observed for values of γ_{SP} smaller than a critical value γ_c, because the influence of the mobile surface layer should be dominant in this case. For $\gamma_{SP}>\gamma_c$ the reduced mobility layer at the substrate will dominate and an increase of T_g should be expected. This concept was critically considered by Tsui et al.,[36] with the conclusion that the interaction energy between the polymer segments and the surface of the substrate is not the only relevant parameter. Also the packing of the segments at the interface might play a role. In general, no correlation between γ_{SP} and the change of T_g with the film thickness was found.[7]

Nowadays, there is growing consensus that the T_g shifts observed in ultrathin films compared to the bulk are related to the combined influence of the free surface (polymer-air) and the polymer-substrate interfacial interaction.[19] Even though the free surface is assumed to speed up the segmental dynamics, at temperatures near T_g, the effect of the polymer-substrate interaction can either increase or decrease the dynamics, and consequently the relaxation times of the adjacent polymer segments.

Generally, there are two different experimental approaches to investigate the glass transition of ultrathin polymer films. In the first approach (also called static experiments), the temperature is ramped and a thermodynamic property (or an associated quantity) is measured. A change in the temperature dependence of this quantity is interpreted as thermal glass transition, where a corresponding thermal glass transition temperature (T_g) can be extracted. Examples for these methods are ellipsometry,[10,23] DSC[43] or Flash DSC,[26] fluorescence spectroscopy,[37] dielectric expansion dilatometry,[12,32] or X-ray reflectivity,[38] just to mention a few. In the second approach, techniques that directly explore the segmental mobility, like dielectric (see for instance [19,32,33]) or specific heat spectroscopy[27,39-42] have been employed. In these cases, a dynamic glass transition temperature is measured which is higher than the thermal one. So far, all investigations carried out by specific heat spectroscopy did not show a thickness dependence of the dynamic glass transition temperature, even in cases where simultaneous dilatometric experiments evidenced a decrease of the thermal glass transition temperature.[43] A possible reason for that is discussed in reference [19]. Moreover by employing cooling rate dependent experiments like ellipsometric,[23,25] photobleaching[22] or Flash DSC[26] experiments it was evidenced that there is a limiting cooling for the depression of the thermal T_g. For instance, for polystyrene the value of this limiting cooling rate was found to be higher than 90 K/min.[25]

This study focuses on the investigation of the dynamic glass transition of thin films of poly(2-vinyl pyridine) (P2VP), as contradicting results exist in the literature. In an X-ray reflectivity study of P2VP films on acid cleaned SiO_2 surface, the thermal glass transition temperature T_g increases with decreasing film thickness up to 20 – 50 K compared to the bulk value.[38] These results are also consistent with more recent data[44,45] and were explained assuming strong interactions of the polymer segments with surface of the substrates. Moreover, a similar behavior was observed for thin P2VP films capped between aluminum layers in a dielectric study.[46] Moll and Kumar found only a small shift in T_g for P2VP/ silica nanocomposites.[47]. Holt et al.[48] report also a study on P2VP filled with silica nanoparticles.

An adsorbed boundary layer around the nanoparticles with a thickness of ca. 4 nm was found having a two-order of magnitude reduced mobility compared to the bulk P2VP, hence a higher glass transition temperature consistent with findings discussed above. A similar result was reported for poly(vinyl acetate) filled with silica nanoparticles.[49] These results are in contradiction to an investigation of P2VP films spin coated on a highly doped Si wafer by broadband dielectric spectroscopy[50] where the dynamic glass transition was found to be independent of the film thickness. Also semi-isolated P2VP chains adsorbed on a doped Si wafer seem to resemble bulk like dynamics.[28] These results are also consistent with data obtained by high speed chip calorimetry where also a thickness independent T_g value for ultrathin P2VP films was found.[51] Paeng et al. employed photobleaching techniques to explore the dynamics of thin P2VP films on the cleaned native surface of a SiO_2 wafer.[52] A highly mobile surface layer at the polymer/air interface was evidenced. However, indications for a reduced mobility layer at the surface of the substrate were also reported.

Here specific heat spectroscopy is employed utilizing AC-chip calorimetry[39] to investigate the dynamic glass transition of thin P2VP films. These measurements are accompanied by contact angle measurements in order to quantify the interaction of the P2VP segment with a SiO_2 surface used as substrate. Additionally, broadband dielectric spectroscopy is used to measure the molecular dynamics of the bulk material for comparison.

7. 2. Experimental Section

7.2.1. Methods

Specific heat spectroscopy: Specific heat spectroscopy is employed using differential AC-chip calorimetry [39]. The calorimetric chip XEN 39390 (Xensor Integration, NI) was used as measuring cell. The heater is located in the center of a freestanding thin silicon nitride membrane (thickness 1 μm) supported by a Si-frame with a window. This nanocalorimeter chip has a theoretical heated hot spot area of about 30 x 30 μm^2, with an integrated 6-couple thermopiles and two-four-wire heaters (bias and guard heater), as shown in reference [53]. Please note that in addition to the 30 x 30 μm^2 hot spot, the heater strips also contribute to the heated area. A SiO_2 layer with a thickness of 0.5 - 1 μm protects the heaters and thermopiles. The thin films are spin coated over the whole chip area, but only the small heated area was sensed and considered as a point heat source. Pictures of the sensor can be found in reference [41].

In principle the chip itself will contribute to the measured heat capacity. In the differential approach to AC-chip calorimetry, the contribution of the heat capacity of the empty sensor (without a sample) to the measured signal is minimized. In the approximation of thin films (submicron), the heat capacity of the sample C_S is then given by[39,40]

$$C_S = \frac{i\omega \bar{C}^2 (\Delta U - \Delta U_0)}{S P_0} \tag{7.1}$$

where ω is the angular frequency and i=(-1)$^{1/2}$ the imaginary unit. $\bar{C} \equiv C_0 + G/i\omega$ describes the effective heat capacity of the empty sensor (C_0 – heat capacity of the sensor; G/iω is the heat loss through the surrounding atmosphere), S is the sensitivity of the thermopile, P_0 is the applied heating power, and ΔU is the complex differential thermopile signal for an empty reference sensor and a chip with a sample, where ΔU_0 is the complex differential voltage measured for two empty sensors. A more detailed description of the calorimetric chip, its differential setup and the experimental method can be found in reference [39]. Absolute values of the heat capacity can be obtained by calibration procedures.[40]

For the calorimetric measurement, the temperature scan mode was used. The temperature was scanned using a heating/cooling rate of 2.0 K/min at fixed frequency. After each heating/cooling run the frequency was changed stepwise in the range of 1 Hz - 10^4 Hz. The selected scanning rate and the used frequency range ensure stationary conditions for the measurement.[54] The heating power for the modulation was kept constant at about 25 µW, which ensures that the amplitude of the temperature modulation is less than 0.5 K[39] and so a linear regime. It is important to note that the measurements are carried out in the frame of the linear response theory. The estimated glass transition temperatures are dynamic glass transition temperatures and are taken in the equilibrium state. As discussed in detail in the introduction this is different form the temperature ramping experiments carried out in DSC[43], Flash DSC[26] or ellipsometric studies.[23,25]

The PT-100 of the cryostat was calibrated by measuring phase transition temperatures for five different calibration substances, covering the whole temperature range of the calorimeter (173-573 K). The calibration equation obtained was then used to correct the collected temperature data.[55]

Contact angle measurements: The measurements were carried out using the automated contact angle system G2 (Krüss) employing the static sessile drop method. The used test liquids were ethylene glycol, formamide, water and diiodomethane. Usually, 8 drops with a

volume of 3 µl were dropped onto the surface of a thick sample film treated in a similar way as the thin layers. The mean contact angles were calculated from the average of at least 6 drops. The data for SiO_2 were taken from reference [41].

Broadband dielectric spectroscopy: For comparison, the dielectric properties of a bulk sample (50 µm) were measured by a high resolution Alpha analyzer with an active sample head (Novocontrol GmbH). The temperature was controlled by a Quatro cryosystem with a stability of 0.1 K. The sample for the dielectric measurements was obtained by melting P2VP between two gold plated brass electrodes (diameter 20 mm). Fused silica spacers controlled its thickness to be 50 µm.

7.2.2. Materials and Sample Preparation

P2VP was purchased from Polymer Standards Services GmbH (Germany) with a M_w of 1020 kg/mol and a PDI of 1.33. The thermal glass transition temperature is 373 K estimated by Differential Scanning Calorimetry (DSC, 10 K/min, second heating run). The selected polymer here is similar to the material used in reference [28] and allows therefore a direct comparison of the dielectric data. For the AC-chip calorimetry, the sensors were first mounted on the spincoater, a few drops of chloroform were added in the center, and then spin coated to rinse dust and organic contaminations. This procedure was repeated twice, followed by an annealing process of the empty chip at 473 K in vacuum for two hours to cure the epoxy resin completely, which is used to glue the chip to the housing.

P2VP was dissolved in chloroform with different weight percentages. The solutions were spincoated (3000 rpm, 60 s) onto the central part of the sensors. The film thickness was varied by adjusting the concentration of the solution. Note that all spin coating processes were carried out in a laminar flow box to minimize any possible contamination. Further, the films were annealed at 398 K ($T_{ann}=T_{g,Bulk}+25$ K) in an oil-free vacuum for 48 h, in order to remove the residual solvent and relax the stress induced by the spin coating procedure.[56]

The thicknesses were measured for films identically prepared on silicon wafers with a native SiO_2 surface, because the film thicknesses cannot be directly measured at the sensor. Assuming that the surface of the silicon wafer has similar properties as the surface of the sensor, under identical spin coating and annealing conditions, corresponding film thicknesses will be obtained. To proof this assumption in more detail a XPS study is in preparation. The film thickness d was measured by the step height of a scratch across the film down to the wafer surface by an AFM Nanopics 2100 (see figure 7.1).

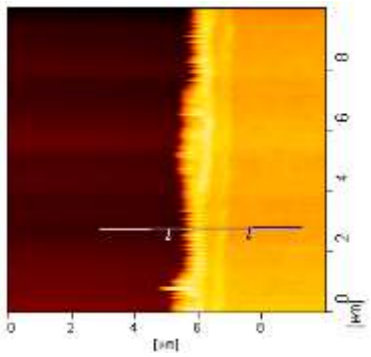

Figure 7.1 *AFM image of a scratch across a P2VP layer with a thickness of 50 nm on a silicon wafer.*

Figure 7.2 gives the estimated film thicknesses versus the concentration of the solution. A linear dependence is observed, which goes to the point of origin as expected.

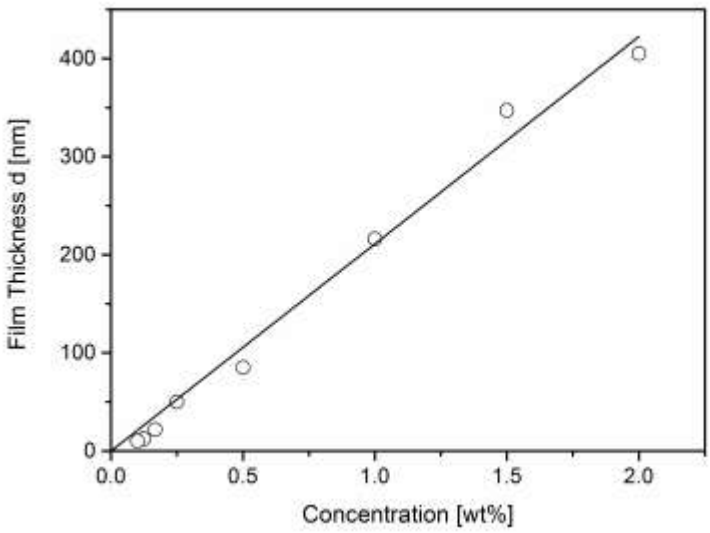

Figure 7.2. *Estimated film thickness d versus the concentration of the solution. The solid line is a linear regression to the data. The error bar is smaller than symbols used.*

Moreover, the AFM topography image (figure 7.1) reveals no inhomogeneities and/or dewetting at the surface of the films. Also, a low surface roughness is observed. The root mean square (rms) roughness in the central area of the empty sensor was estimated to be about 3.5 nm.[40] The roughness of the film spin coated onto the surface of the sensor is lower and decreases with increasing film thickness. For a film thickness of ca. 10 nm, the roughness of the film on the sensor is comparable with that of a film prepared on a wafer.[57]

7.3. Results and Discussion

The result of an AC calorimetry measurement yields a complex differential voltage as a function of frequency and temperature, which is proportional to the complex heat capacity

(C^*_P) of the film. Here the real part of the complex differential voltage U_R and the phase angle ϕ are taken as measures of C^*_P. At the dynamic glass transition, U_R increases stepwise with increasing temperature (Figure. 7.3a) and ϕ shows a peak (figure 7.3b).

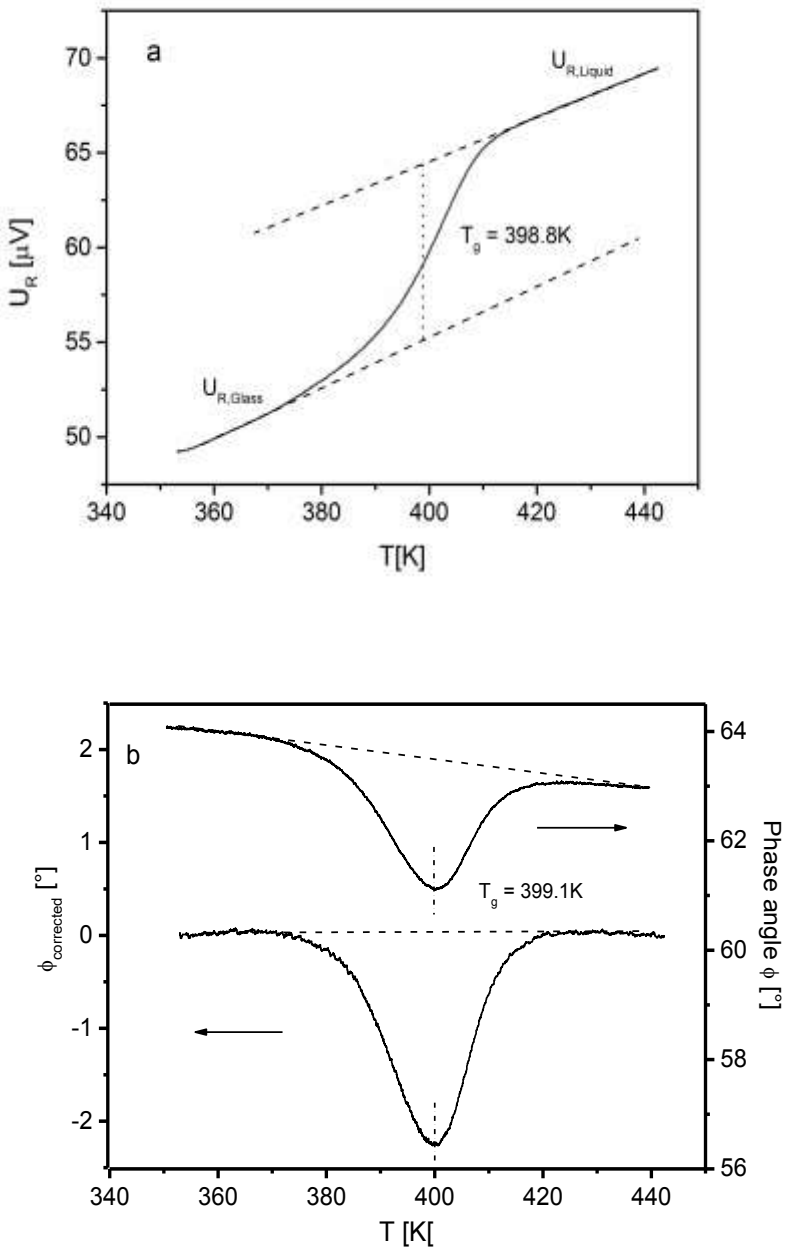

Figure 7.3. *Real part* **(A)** *and phase angle* **(B)** *of the complex differential voltage of a thin P2VP polymer film (347 nm) measured at a frequency of 160 Hz. The contribution of the underlying step in the heat capacity in the raw data of the phase angle (upper panel) was subtracted from the all over curve (lower panel).*

A dynamic glass transition temperature can be determined as either the half step temperature of U_R or as the maximum temperature of the peak of the corrected phase angle. In the raw data of the phase angle (figure 7.3B, upper panel), there is an underlying step in the signal,

which is proportional to the real part. Hence, the phase angle is corrected by subtracting this contribution. According to equation 7.1 and assuming that the density of the film is the same as in the bulk, the step high of the heat capacity at the glass transition is given by[40]

$$C_{S,Liquid} - C_{S,Glass} = \frac{i\omega\bar{C}^2\left(U_{R,Liquid} - U_{R,Glass}\right)}{SP_0} \sim m \sim d \qquad (7.2)$$

where m is the mass of the film. Therefore, $U_{R,Liquid}$ - $U_{R,Glass}$ = ΔU_R should be proportional to the thickness of the film. In figure 7.4, ΔU_R is plotted versus d. The expected linear dependence is confirmed. Moreover, the data can be described by a regression line going through the point of origin. From those results, one might conclude that the whole sample material on the chip takes part in the dynamic glass transition and no boundary layer with a reduced mobility is present.

7.3.1. Conventional Analysis of Specific Heat Spectroscopy Data

Figure 7.5 gives the normalized phase angle versus temperature for different film thicknesses for a frequency of 160 Hz. For all values of d the data collapse into a common curve. This means that the dynamic glass transition temperature is independent of the film thickness. Similar results were obtained by AC-chip calorimetry for PS,[27,39] PMMA,[50,58] poly(2,6-dimethyl-1,5-phenylene oxide),[40] polycarbonate[41] and also poly(vinyl methyl ether).[42] At the first glance the results obtained here are in accordance with the dielectric data given in references [28,50] but disagree with findings discussed in [38,48].

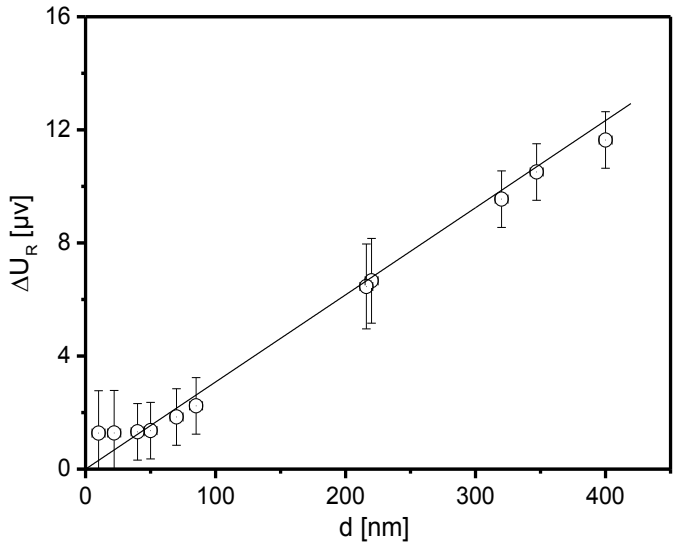

Figure 7.4 *ΔU_R versus the film thickness d for a frequency of 160 Hz. The solid line is a linear regression to the data. For low film thickness, the error is somewhat larger. Therefore, the data points for the lowest film thickness might deviate slightly from the regression line.*

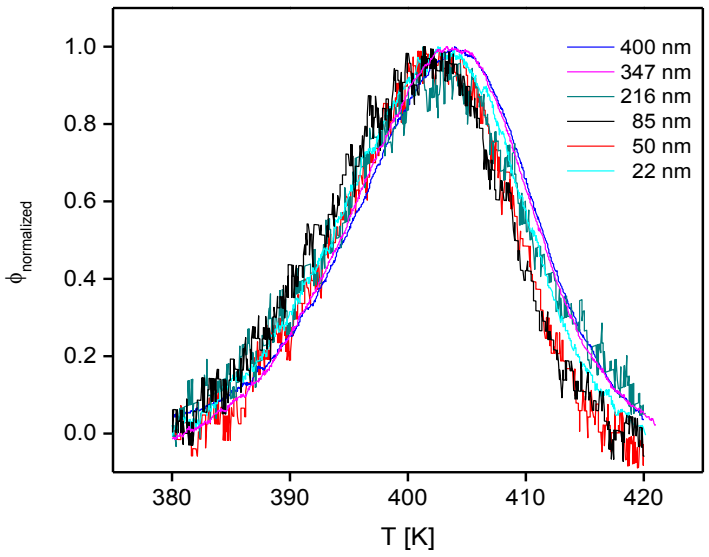

Figure 7.5. *Normalized phase angle of the complex differential voltage versus temperature measured for thin P2VP films at a frequency of 160 Hz for selected thicknesses of 400, 347, 216, 85, 50, and 22 nm.*

To analyse the data in more detail, Gaussians were fitted to the normalized phase angle as depicted in inset A of figure 7.5.[40] From such analysis, the maximum temperature of the normalized phase angle is estimated at the given frequency and the relaxation map can be constructed (see Figure 7.4). Within the experimental error of ±3 K, the data for all film thicknesses collapse into one chart. As mentioned above, this is in agreement with AC-chip calorimetry studies on other polymers.[27,39-42,58]

The temperature dependence of the relaxation rates can be described by the Vogel/Fulcher/Tammann- (VFT-) equation[59-61]

$$log\ f_p = \log f_\infty - \frac{A}{T - T_0} \tag{7.3}$$

where f_∞ and A are fitting parameters and T_0 is called ideal glass transition or Vogel temperature, which is found to be 30-70 K below the thermal T_g. For all film thicknesses the data can be described by a common VFT-fit (see figure 7.4). Due to the limited frequency range of the specific heat spectroscopy, the prefactor f_∞ was taken from the dielectric results (see below) and kept constant during the fit procedure.

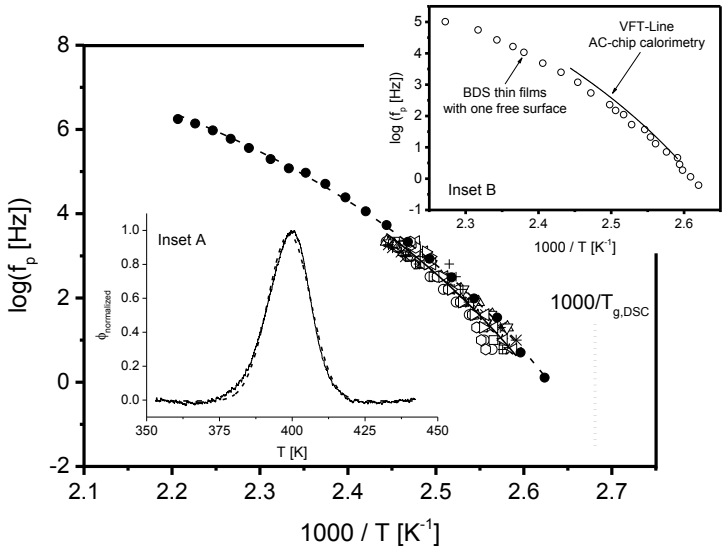

Figure 7.6. *Relaxation rates versus inverse temperature for different film thicknesses estimated from the normalized phase angle (open symbols): circles – 405 nm, squares – 349 nm, up sited triangles – 230 nm, down sited triangles -216 nm, stars – 150 nm, asterisks – 120 nm, left sited triangles – 85 nm, hexagons – 50 nm, right sited triangles – 22 nm, crosses – 10 nm. The solid circles are data from dielectric spectroscopy for a bulk sample. Solid lines are fits of the VFT equation to the corresponding data with following parameters. Dielectric data (dashed line): log (f_∞ [Hz])=12, A=779 K, T_0=315.4 K; Thermal data (solid line): log (f_∞ [Hz])=12, A=774.6 K, T_0=317.8 K. The dotted line gives the thermal glass transition temperature measured by DSC.* **Inset A.** *gives the normalized phase angle for a film with a thickness of 347 nm at a frequency of 160 Hz (solid line). The dashed line is a fit of a Gaussian to the data. The solid line is the averaged value of the given data points.* **Inset B.** *compares dielectric data for ultrathin P2VP films measured with one free surface taken from reference [50] with the VFT-fit taken from the AC-chip calorimetry. The dielectric data are averaged data in the thickness range from 172 nm down to 8 nm because the data for all film thicknesses collapse into one chart.*

In figure 7.6, the data for a bulk sample measured by dielectric spectroscopy are included as well. Further, the temperature dependence of these data can be described by the VFT equation where the estimated value for the Vogel temperature T_0 is close to that estimated from the thermal data (see caption figure 7.6). The dielectric and thermal data overlap more or less, which is a bit uncommon for most materials. The thermal and dielectric data usually exhibits a systematic shift, as previously found for different homopolymers,[41,42] and also for low molecular compounds.[62]

The inset B of figure 7.6 compares dielectric data measured for thin films of P2VP with the VFT fit line extracted from the specific heat spectroscopy data. The dielectric data are the averaged data in the thickness range of 172 nm down to 8 nm, taken form reference [50]. The free surface was implemented by the use of insulating colloids as spacers. For more details see reference [50]. Both sets of data, where samples have one free surface, agree nicely with each other and both sets of relaxation have the same temperature dependence.

A similar behaviour should be expected for mechanical measurements, which are hard to conduct in the case of ultrathin films.

7.3.2. Contact angle measurements

To characterize the interaction of the P2VP segments with the SiO_2 surface of the substrate contact angle measurements were carried out. It is assumed that a silicon wafer with 500 nm native SiO_2 layer has the same surface properties than the used AC-chip. The estimated contact angles obtained for the different test liquids are summarized in Table 7.1.

Table 7.1. *Contact angle values of the test liquids for poly(2-vinyl pyridine). Data for SiO_2 were taken from reference [41]. The errors result from the average of measurements on 6 drops.*

	Water	*Formamide*	*Ethylene glycol*	Diiodomethane
P2VP	67.5°±0.9°	65.5°±0.8°	46.6°±1.1°	40.0°±0.9°
SiO_2	61.0°±1.0°	48.2°±1.0°	39.0°±0.6°	28.9°±1.2°

The total surface energy γ^{Total} of a sample is expressed by $\gamma^{Total} = \gamma^{LW} + \gamma^{P}$ where γ^{LW} and γ^{P} are the dispersive and polar components of the surface energy, respectively.[63,64] The measured contact angles θ_i for the liquid i are related by the Owens/Wendt theory,[65,66] which is a combination of Young's relation with Good's equation (for details see [67]) to the polar and dispersive components of the surface energies of the solid and liquid by

$$\frac{(1+\cos\theta_i)\,\gamma_{L,i}}{2\sqrt{\gamma_{L,i}^{LW}}} = \sqrt{\gamma_S^P}\,\frac{\sqrt{\gamma_{L,i}^P}}{\sqrt{\gamma_{L,i}^{LW}}} + \sqrt{\gamma_S^{LW}} \qquad (7.4)$$

where γ_S^P and γ_S^{LW} are the dispersive and polar components of the surface energy of the polymer or the substrate (S=P2VP, SiO_2). The values for the surface tension of the test liquids were taken from reference [63]. Using at least 3 test liquids, an Owens/Wendt plot according to equation 7.4 is created and the polar and dispersive components of the solid surface energy are estimated by linear regression. Results are presented in table 7.2.

Table 7.2. *Total surface energy γ^{Total} and its dispersive γ^{LW} and polar γ^{P} components for P2VP and the SiO_2 surface of the silicon wafer.*

	γ^{Total} [mJ m^{-2}]	γ^{LW} [mJ m^{-2}]	γ^{P} [mJ m^{-2}]
P2VP	39.5	29.8	9.7
SiO_2	47.0	44.6	2.3

The rule of Fowkes[64] was applied to estimate the interfacial energy γ_{SP} between P2VP and SiO_2, which reads

$$\gamma_{SP} = (\gamma_A + \gamma_{B)} - 2\left[\left(\gamma_A^{LW}\gamma_B^{LW}\right)^{\frac{1}{2}} + \left(\gamma_A^{p}\gamma_B^{p}\right)^{1/2}\right] \tag{7.5}$$

where A and B refer to the substrate and the polymer, respectively.

Using Equation 7.5, the total interfacial energy between P2VP and SiO_2 is 4.1 mJ m^{-2}. According to reference [35], this is a strong interaction between the polymer segments and the surface of the substrate. Therefore an adsorbed layer with a reduced mobility should be formed at the surface of the substrate in agreement with results published in reference [48]. Likewise, for other polymers, which interact strongly with the substrate, an increase of the glass transition temperature should be observed. But however, no change in dynamic T_g was observed here by specific heat spectroscopy. One possible reason for this result might be the high molecular weight of the used P2VP. As it was shown in reference [31,71] the formation of the reduced mobility layer depends on time and the diffusive mobility of the polymer chains. For a high molecular weight, the chain mobility is lower than for a lower one. It might be that under the selected experimental condition the annealing time above T_g was not long enough to form a reduced mobility at the substrate, which is thick enough to influence the dynamic glass transition of the whole film.

Attempts to correlate the change in the glass transition temperature with the interaction energy between the substrate and the polymer surface γ_{SP} are made in reference [35]. In figure 7.7, the difference of the glass transition temperature for 20 nm thick films and the bulk value versus the interfacial energy are plotted for polystyrene and poly(methyl methacrylate) spin coated on modified octadecyltrichlorosilane (OTS) surfaces according to reference [35]. For γ_{SP}<2 mJ m^{-2} a depression of the glass transition temperatures should be observed while for γ_{SP}>2 mJ m^{-2} an increase of T_g should be observed. In this figure, data for different polymer substrate combinations, with comparable film thicknesses, taken from the literature, were added. (A similar figure but with less data points is given in reference [68] too). This concept is able to describe the variation of the T_g with interaction energy for polystyrene and poly(methyl methacrylate) on the modified octadecyltrichlorosilane surfaces. Also for some other polymers like polycarbonate on SiO_2 or AlO_X[32,41] or poly(ethylene terephthalate),[69] this correlation seems (partially) valid. However, it is not generically true for all polymer/substrate combinations.

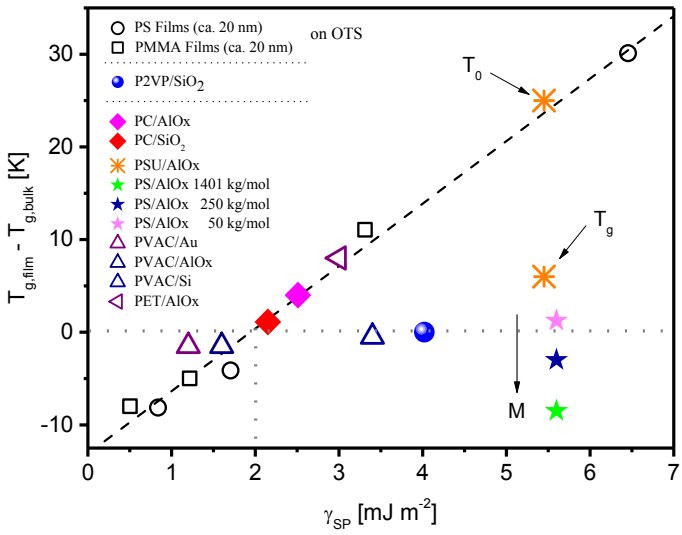

Figure 7.7. *Difference of the glass transition temperature for 20-nm-thick films and the corresponding bulk value versus the interfacial energy. The open symbols for poly(methyl methacrylate) (squares) and polystyrene (circles) are taken together with the (dashed) correlation line from reference [35]. The grey dotted lines gives $\Delta T_g=0$ and critical value for γ_c. The data for polycarbonate (PC,diamonds) are taken from reference [32] (AlOx) and [41] (SiO_2). The asterisks represent data for polysulfone (PSU) taken from reference [33]. The value for PET (left pointed triangle) are taken form reference [69]. The data for poly(vinyl acetate) (PVAC, triangels) prepared on the indicated surfaces are taken from reference [70]. The values for polystyrene (PS, green stars) are drawn from [71]. P2VP (solid circle) – this work.*

For instance, for polysulfone, the interaction energy between the segments and the substrate surface was estimated to be γ_{SP}= 5.45 mJ m^{-2}, taken from reference [33]. This value is much larger than the value of polycarbonate/AlO_X, where a similar increase of the glass transition temperature of about 5 K (for a ca. 20 nm thick film) was found. However, the corresponding point for polysulfone is located far away from the correlation line between the polymer-substrate interaction energy and the change in the glass transition temperature. However, by taking the Vogel temperature, T_0, as a measure for the thermal glass transition temperature, the correlation between the change in the glass transition temperature and the polymer-substrate interaction energy[31,35] seems to be fulfilled.

For poly(vinyl acetate) films prepared on different surfaces,[70] this correlation is found to be invalid as well. Data for polystyrene samples having different molecular weights were also added,[71] whereas the interaction energy between the AlO_X surface of the substrate and the polystyrene segments is taken from reference [31]. These data points are located also far away from the correlation line between the polymer / substrate interaction energy and the change in the glass transition temperature. The observed dependence on the molecular weight is in contradiction to the assumption that the interaction energy between the polymer

segments and the surface of the substrate is the only parameter, which determines the value of the glass transition temperature of ultrathin polystyrene films as well. This regards also the observed time dependence of the depression of T_g.[31] In conclusion, the polymer/substrate interaction energy seems to be not the only parameter, which is responsible for the change in the thermal glass transition temperature with the film thickness for ultrathin films. Packing effects and/or densifications of the reduced mobility layer at the surface, which can be time and molecular weight dependent, might also play a role. This is discussed also in detail in reference [31].

7.3.3. Derivative analysis of specific heat spectroscopy data

As discussed above, all AC-chip calorimetry studies on ultrathin films of homopolymers, including P2VP used in this work concluded that the dynamic T_g is thickness independent, in many cases, contradicting the findings of other studies using different characterization techniques. For P2VP, one shall expect to see a rather strong reduced mobile layer as speculated from the contact angle measurements, shown above. The reduced mobile layer for this polymer has also been detected by other methods, e.g. X-ray reflectivity[38] and different BDS studies.[46,48] On the other hand, also the existence of a high mobile free surface layer has been evidenced for P2VP.[52] To resolve the systematic contradiction of AC-chip calorimetry from the other characterization method, an advanced analysis of the calorimetric data might be useful.

From the technical point of view, there are a few problems with the conventional data analysis of AC-chip calorimetry. Firstly, the theoretical treatment of the method assumes that the reference and the sample sensor are identical. In that theoretical case, one shall expect to see a constant baseline at zero level for the differential voltage for all frequencies and temperatures. Because of the fact that the sensors are not completely identical, an extra contribution will be added up to the signal coming from the film. This extra contribution to the differential voltage is not large but depends on both temperature and frequency. It can be ignored for relatively thick films (>50 nm). However, for thinner films, the difference between the two empty sensors is in the same order of magnitude as the measured U_R, which might induce artifacts.

The other problem in estimating the dynamic glass transition temperature from the maximum position of the phase angle is related to the fact that the measured phase angle has also an underlying contribution that is proportional to the step of the heat capacity.[39] This effect will not affect the T_g peak position for thick samples. However, for ultrathin

films (<20 nm), the values of the phase angle become small and comparable to the noise level of the instrument.[40] Thus, the correction and estimation of the phase angle cannot be done unambiguously.

For these reasons here the temperature dependence of the complex differential voltage is analysed in more detail for some selected sample thicknesses, which was investigated with an optimized sensitivity. First, the sensitivity of the lock-in amplifier of the AC-chip calorimeter was set to be between two and three times the value of U_R of the sample at 160 Hz and the corresponding $T_{g,160\ Hz}$, to assure an optimal signal and a reduced noise. Second, pairs of empty sensors were first measured in the identical frequency and temperature range as for the samples to obtain the excess contribution of the sensors. Third, after the measurement of the films spin coated on one of the analyzed empty sensors, the real part of the complex voltage obtained for the two empty sensors was subtracted from the corresponding U_R recorded for the films. This procedure leads to a corrected U_R.

Instead of analysing the temperature dependence of the phase angle, the derivative of the corrected real part of the complex voltage versus temperature was employed. Since U_R changes step-like at the dynamic glass transition, its first derivative will result in a peak. The temperature of the peak maximum can be taken as the dynamic glass transition temperature at 160 Hz. The derivative method will also allow estimating dU_R/dT which is related to dc_p/dT for both the glassy and the liquid state. To calculate the derivative of the corrected real part of the complex voltage was adjacent-point averaged (over 300 points; for the two thinnest films over 500 points) in the whole measured temperature range. This will result in a smoothed signal. To have equidistant points, U_R (T) was interpolated (1000 points). After that the derivative was calculated. It is worth to mention that the difference in the smoothing methods and parameters was previously reported to result in about ±2 K difference in the T_g values, which is within the uncertainty of the measurement.[40] The advantage of this method is strong when analyzing measurements of ultrathin films, where the signal is weak and changes of the phase angle are hardly to detect. For films thinner than 15 nm, one can usually still see a small step in U_R, yet it is not unambiguously to determine where the step starts and ends. Moreover, in a first crude approximation the derivative can be considered as a representation of the relaxation time spectra.[72]

Four new samples were prepared (10 nm, 20 nm, 85 nm and 220 nm) and the measurements were analyzed as described above.

Figure 7.8 shows the derivative calculated as described versus temperature for three different sample thicknesses at a frequency of 160 Hz. For each value of the thicknesses a well-defined peak is visible indicating the dynamic glass transition. With decreasing thickness, a systematic shift of the dynamic glass transition to lower temperatures is observed. This shift up to 7 K is essentially larger than the error of the AC-chip calorimetric measurement.

The derivative method was also applied to the other samples prepared previously and a dynamic glass transition temperature at 160 Hz was estimated from the maximum position of the derivative. These data were plotted in figure 7.9 versus the thickness of the film. The dynamic glass transition temperature of the bulk sample is taken as the average value of the dynamic glass transition temperature for the five samples with the highest thicknesses.

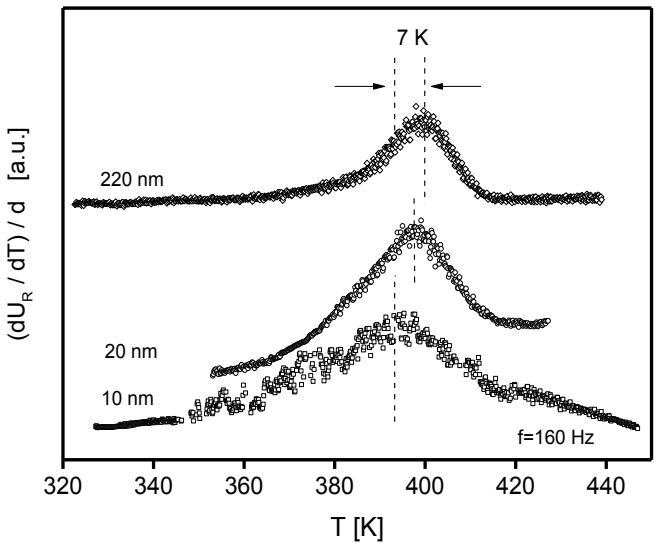

Figure 7.8. *Derivative of the corrected real part of the complex differential voltage with regard to temperature versus temperature for the indicated film thicknesses at the frequency of 160 Hz. For sake of clearness the curves were shifted along the y-scale.*

For small film thicknesses, the value of the dynamic glass transition is below this average value and further decreases with decreasing film thickness. Because a decrease of the dynamic glass temperature is considered as the influence of a free surface,[19] this result can be considered as an evidence for a free surface with a higher molecular mobility from calorimetric measurements.

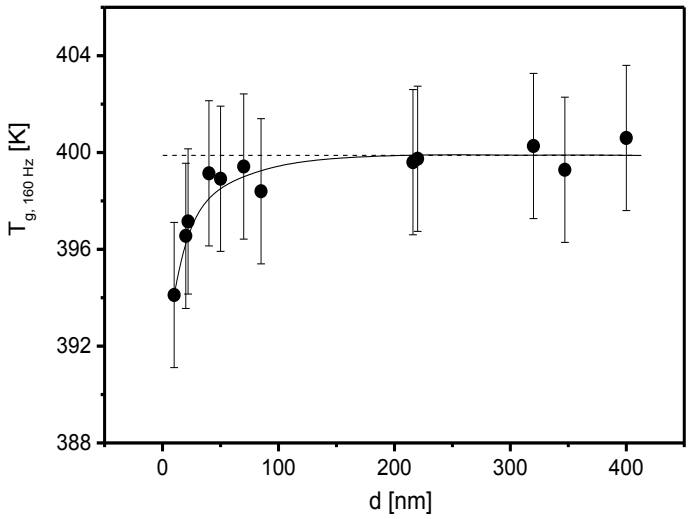

Figure 7.9. *Dynamic glass transition temperature measured at 160 Hz versus film thickness d. The dashed line is the average value of the five data points with largest thicknesses.*

It should be shortly summarized why the traditional and the derivative based data analysis give different results. Firstly, in the phase angle two different quantities with well-defined physical meanings are mixed up, the real and the loss part of the complex differential voltage. The correction of the phase angle for the real part of the complex voltage cannot be done unambiguously especially for low film thickness as discussed above. Secondly, the derivative of the real part of the complex differential voltage can be considered as an estimation of the underlying relaxation time spectra.[72] This means both quantities weight the underlying dynamics in a different way. This fact in unimportant for thick films but might become relevant for low film thicknesses. A closer inspection of figure 7.5 that also the phase angle measured for higher thickness seem to be located at somewhat higher temperatures which is consistent with the derivative analysis.

Some further evidence for a mobile surface layer comes from the shape of dU_R/dT versus temperature. A more detailed inspection of figure 7.8 reveals that the width of the derivative for a thin film (for instance see 10 nm) is broader than that measured for a larger thickness. This fact is illustrated in more detail in figure 7.10, where the derivative for a 10 nm and a 40 nm thick film are compared. Therefore, the derivative is normalized with respect to both its intensity and peak temperature. Figure 7.10 reveals that the peak for the 10 nm thick film is much broader than that for the 40 nm one. Firstly, compared to the 40 nm thick layer, the film with a thickness of 10 nm shows a considerable broadening at the lower temperature

side. In the sense of distribution of relaxation times, this corresponds to an increased contribution of relaxation modes having shorter relaxation times. With decreasing film thickness, the influence of a surface layer with a higher mobility will increase. Therefore, in addition to the decrease of the dynamic glass transition with decreasing film thickness, the broadening of the relaxation spectra on the low temperature side gives further evidence for the existence of a surface layer with a higher molecular mobility at the polymer air interface.

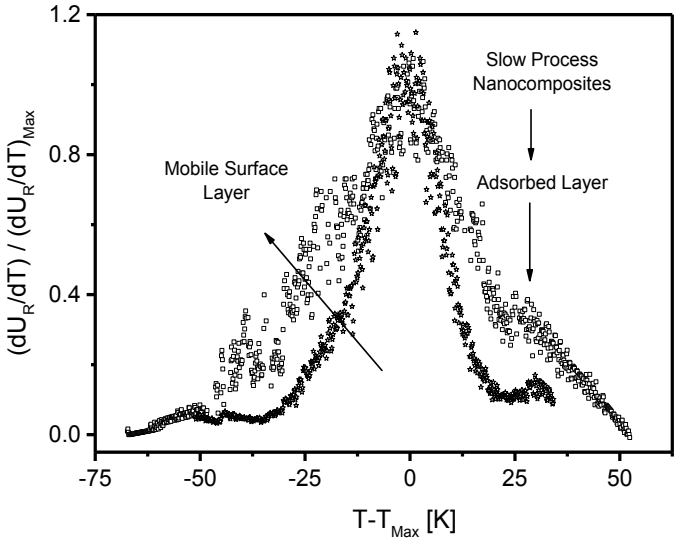

Figure 7.10. *Normalized derivative $(dU_R / dT) / (dU_R / dT)_{Max}$ versus temperature at a frequency of 160 Hz for a 10 nm (open squares) and a 40 nm (open stars) thick film.*

Besides the broadening of the spectra at the low temperature side for the thin film for the 10 nm thin film there is also a broadening of the derivative at temperatures above the dynamic glass transition temperature. This broadening at the high temperature side of the spectra is due to relaxation modes having a reduced mobility. As shown by the contact angle measurements, discussed above, the P2VP segments should strongly interact with the SiO_2 surface of the sensor, which should result in slowing down of the molecular dynamics of the polymer segments close to the surface. Therefore, the broadening of the spectra at high temperatures is assigned to polymer segments, which are in interaction with the SiO_2 surface of the sensor. A corresponding broadening was observed by dielectric spectroscopy employing nanostructured electrodes.[28] A closer inspection of the data for the 10 nm thick film reveals that there is a small shoulder at $T-T_{Max}=28$ K (T=424 K). This shoulder is found at the same temperature frequency position, where for the nanocomposites of P2VP with silica nanoparticles, discussed in reference [48], the relaxation process is observed, which

was related to the fluctuations of P2VP segments adsorbed at the surface of the silica particles. This coincidence provides further evidence that a reduced mobility layer is formed at surface of the calorimeter. Probably, due to the high molecular weight of the used P2VP, the formation of this reduced mobility layer will take longer time. Under the employed experimental conditions, it is likely that the thickness of this layer is small and will not influence the dynamic glass transition behavior of the whole film. For future work, additional investigations are planned where the annealing time and temperature, during film preparation, are varied in broader ranges. This includes further a variation of the molecular weight because it was shown for instance that for polystyrene[71] the change of the glass transition temperature depends on molecular weight due to a changed adsorption kinetics.

It is well known that the specific heat capacity in the glassy state has a stronger temperature dependence than in the liquid,[73] which means $(dc_p/dT)_{Glass} > (dc_p/dT)_{Liquid}$. Close to the glass transition $c_p(T)$ can be approximated by linear dependencies in both the glassy and liquid state. In the derivative representation, this is reflected by constant values of the derivative dU_R/dT which corresponds to dc_p/dT independent of temperature below and above the dynamic glass transition. The inset of figure 7.11 depicts the derivative versus temperature for a relatively thick film of 347 nm. For this film, which can be considered as bulk-like, the expected relationship $(dc_p/dT)_{Glass} > (dc_p/dT)_{Liquid}$ is fulfilled. However, figure 7.11 shows further that with decreasing film thickness, this relationship changes. For a film with a 220 nm thickness, $(dU_R/dT)_{Glass} \approx (dU_R/dT)_{Liquid}$ holds; whereas for a thinner film with a thickness of 70 nm the relationship is reversed $(dU_R/dT)_{Glass} < (dU_R/dT)_{Liquid}$. This is not only observed for the considered thicknesses, but also for the other thicknesses as well (see figures 7.8 and 7.10). Obviously, confinement effects influence the temperature dependencies of the specific heat capacity in the liquid and glassy state. Such change in the temperature dependence of specific heat capacity before and after the dynamic glass transition region was able to be observed at relatively high thicknesses, above 220 nm in the present study. The critical thickness is possibly molecular weight dependent, which needs further quantitative measurements. It was already reported that for PS with Mw=1400 kg/mol, a change in the temperature dependence of specific heat capacity at the glass transition occurred from several hundred nm.[43] In the glassy state, $c_p(T)$ originates from vibrations. The same vibrations are also responsible for the temperature dependence of the thermal expansion. The specific heat capacity and the thermal expansion coefficient are

linked to each other.[74] It has been reported previously that the thermal expansion coefficient in the glassy state for thin films decreases with the film thickness.[75,76]

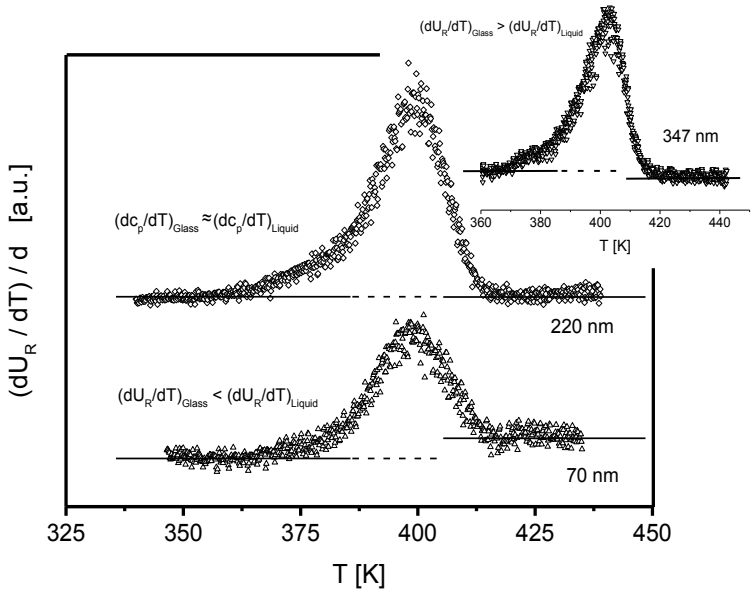

Figure 7.11. *Derivative (dU_R / dT) /d versus temperature at a frequency of 160 Hz for a 220 nm (open diamonds) and a 70 nm (open triangles) thick film. The inset shows the same for a film with a thickness of 347 nm.*

These findings are quite similar to the results found here for P2VP. Moreover, quasielastic neutron scattering experiments for thin films of polystyrene and polycarbonate[77, 78] showed that the mean square displacement $\langle r^2 \rangle$ decreases with decreasing film thickness. Also a direct investigation of the vibrational density of states in the frequency range of excess vibrations characteristic for the glassy state (Boson Peak) show a decrease of the intensity of the Boson Peak with decreasing film thickness for polystyrene for relatively high thicknesses of 100 nm.[79,80] This behavior is equivalent to a decrease of the mean square displacement. Using a harmonic approximation $\langle r^2 \rangle$ can be related to a force constant f_K by $f_K \sim 1/\langle r^2 \rangle$. A decrease of the mean square displacement can therefore be explained by an increase of the force constant. This means a change from a soft to hard potential. Taking as well as anharmonic contributions into account, the change of the temperature dependence of the specific heat capacity in the glassy state might be explained by a hardening of the potential of the vibrations. However, it is worth to note that the change of the specific heat capacity in the glassy and liquid state might also be explained by a three layer model which also applies here.[81] To differentiate between both possibilities, additional investigations on a broader range of samples and different polymers are required. Such studies are under preparation, which will also include a more quantitative discussion.

7.4. Conclusion

Specific heat spectroscopy employing differential AC-chip calorimetry in the frequency range from 1 Hz to 10^4 Hz with a sensitivity of pJ/K was used to study the dynamic glass transition behavior of ultrathin poly(2-vinyl pyridine) films with thicknesses from 405 nm down to 10 nm. To characterize the interaction of the P2VP segments with the surface of the substrate, contact angle measurements was utilized along with AFM investigation to study the topology of the films. Broadband dielectric spectroscopy was used to obtain the molecular dynamics for the bulk sample.

AC-chip calorimetry delivers the real part and the phase angle of the complex differential voltage as a measure of the complex heat capacity as function of temperature and frequency simultaneously. The data were analyzed by two different methods. In a rather traditional data analysis, the dynamic glass transition temperature is estimated from the maximum position of the measured phase angle. These data showed no thickness dependence of the dynamic glass transition temperature down to ca. 22 nm, within in the error of the measurement of ± 3 K. This result is in agreement with dielectric data obtained for samples having one free surface, yet still in disagreement to other literature data. Therefore, a second method was established which is based on the first derivative of the real part of the complex differential voltage with regard to temperature. These data show a decrease of the dynamic glass transition temperature with decreasing thickness of about 7 K. This decrease can be explained as a result of the influence of surface layer with a higher molecular mobility. Moreover, for thin films the data showed a broadening at the lower temperature side of the dynamic glass transition, which can be considered as a further prove for a surface layer.

Moreover, contact angle measurements showed that the P2VP/SiO_2 interaction was rather a strong one, 4.1 mJ m^{-2}, which suggests that an absorbed layer of reduced mobility should exist at the polymer/substrate interface. An absorbed layer was evidenced for films below 50 nm, through another broadening of the peak with the appearance of a shoulder at the higher temperature side of the spectra that superimposes with the fluctuations of P2VP segments adsorbed at the surface of the silica particles, as reported in literature.

Finally, evidence was provided the temperature dependence of the specific heat capacity in the glassy and the liquid state changes depends on the film thickness. These changes were observed for relatively high film thickness of some 100 nm and can be considered as confinement effects. For the glassy state these changes are in agreement with several neutron scattering studies and can be explained by a hardening of the potential of the vibrations, and

thus the existence of a reduced mobile layer, in agreement of the three-layer model. Nevertheless, additional investigations are required.

References

1 Hall, B.D.; Underhill, P.; Torkelson, J. *Polymer Eng. Sci*. **1998**, 38, 2039-2045.
2 Debenedetti, P.; Stillinger, F. *Nature,* **2001**, 410, 259–267.
3 Anderson, P.W. *Science,* **1995**, 267, 1617.
4 Ediger, M.; Horrowell, P. *Journal of Chemical Physics* **2012**, 137, 080901-080915.
5 Angel, C.A. *Science,* **1995**, 267, 1924-1935.
6 Sastry, S.; Debendetti, P.; Stillinger, F.H. *Nature,* **1998**, 393, 554-557.
7 Yin, H.; Madkour S.; Schönhals, A. Glass transition of ultra-thin polymer films: A combination of relaxation spectroscopy with surface analytics in *Dynamics in confinement: Progress in Dielectrics,* Kremer, F. (Ed.) *Springer*, Berlin **2014**, pp17-59
8 Alcoutlabi, M.; McKenna, G.B. *J. Phys. Condens. Matter,* **2005**, 17, 461–524.
9 Keddie, J.L.; Jones, R.A.L.; Cory, R.A. *Faraday Discussions,* **1994**, 98, 219-230.
10 Keddie, J.L.; Jones, R.A.L.; Cory, R.A. *Euro. Phys. Lett.* **1994**, 27, 59-64.
11 Ediger, M.; Forrest, J. *Macromolecules,* **2014**, 47, 471-478.
12 Forrest, J.; Dalnoki-Veress, K. *ACS Macro Letters* **2014**, 3, 310−314
13 O'Connell, P.A.; McKenna, G.B. *Science,* **2005**, 307, 1760–1763.
14 Paeng, K.; Swallen, S.F.; Ediger, M. *J. Am. Chem. Soc.* **2011**, 133, 8444–8447.
15 Forrest, J.; Dalnoki-Veress, K. *J. Coll. Int. Sci*. **2001**, 94, 167–195.
16 Forrest, J. *Eur. Phys. J. E.* **2002**, 8, 261–266.
17 Fakhraai, Z.; Forrest, J. *Science,* **2008**, 319, *600-604*.
18 Chai, Y.; Salez ,T.; McGraw, J.D.; Benzaquen, M.; Dalnoki-Veress, K.; Raphaël, E.; Forrest, J. *Science,* **2014**, 343, 994-999.
19 Tress, M. ; Erber, M.; Mapesa, E.; Huth, H.; Müller, J.; Serghei, A.; Schick, C.; Eichhorn, K.; Voit, B.; Kremer, F. *Macromolecules,* **2010**, 43, 9937−9944.
20 Tress, M.; Mapesa, E.; Kossack, W.; Kipnusu, W.; Reiche, M.; Kremer, F. *Science,* **2013**, 341, 1371−1374.
21 Dalnoki-Veress, K.; Forrest, J.; Murray, C.; Gigault, C.; Dutcher, J. *Phys. Rev. E.* **2001**, 63, 031801-031811.
22 Napolitano, S.; Pilleri, A.; Rolla, P.; Wübbenhorst, M. *ACS Nano,* **2010**, 4, 841-848.
23 Glor, E.; Fakhraai, Z. *J. Chem. Phys.* **2014**, 141, 194505.
24 Lupaşcu, V.; Picken, S.; Wübbenhorst, M. *Journal of Non-Crystalline Solids,* **2006**, 352, 5594-5600.
25 Fakhraai, Z.; Forrest, J. *Phys. Rev. Lett.* **2005**, 95, 025701-025705.
26 Shamim, N.; Koh, Y.; Somon, S.; McKenna, G. *J. Polym. Sci. Part B: Polym. Phys*. **2014**, 52, 1462-1468.
27 Sharp, J.; Forrest, J. *Phys. Rev. Lett.* **2003**, 91, 235701-235705.
28 Paeng, K.; Richert, R.; Eidger, M.D. *Softmatter,* **2012**, 8, 819-826.
29 Qi, D.; Ilton, M.; Forrest, J. A. *Eur. Phys. J. E,* **2011**, 34, 56-63.
30 Qi, D.; Daley, C.R.; Chai, Y.; Forrest. J.A. *Soft Matter,* **2013**, 9, 8958−8964.
31 Napolitano, S.; Wübbenhorst, M. *Nature Communications,* **2011**, 2, 260-267.
32 Yin, H.; Napolitano, S.; Schönhals, A. *Macromolecules,* **2012**, 45, 1652-1662.
33 Labahn, D.; Mix, R.; Schönhals, A. *Physical Review E,* **2009**, 79, 011801-011810.
34 Rotella, C.; Wübbenhorst, M.; Napolitano, S. *Soft Matter,* **2011**, 7,5260-5266.
35 Fryer, D.S.; Peters, R.D.; Kim, K.J.; Tomaszewski, J.; de Pablo, J.; Nealey, P.F. *Macromolecules,* **2001**, 34, 5627-5634.
36 Clough, A.; Peng, D.; Yang, Z.; Tsui, K. *Macromolecules,* **2011**, 44, 1649–1653.
37 Ellison, C.J.; Torkelson, J.M. *Nat Mater.* **2003**, 2, 695-700.
38 van Zanten, J.H.; Wallace, W.; Wu, W. *Physical Review E,* **1996**, 53, R2053-R2056.
39 Huth, H.; Minakov, A.; Schick, C. *J. Polym. Sci. B: Polym. Phys*. **2006**, 44, 2996-3005.
40 Zhou, D.S.; Huth, H.; Gao, Y.; Xue, G.; Schick, C. *Macromolecules,* **2008**, 41,7662-7666.
41 Yin, H.; Schönhals, A. *Soft Matter,* **2012**, 8, 9132-9139.
42 Yin, H.; Schönhals, A.*Polymer,* **2013**, 45, 2067-2070.
43 Boucher, V.M.; Cangialosi, D.; Yin, H.; Schönhals, A.; Alegria, A.; Colmenero, J. *Soft Matter,* **2012**, 8, 5119-5122.
44 Park, C.H.; Kim, J.H.; Ree, M.; Sohn, B.; Jung, J.; Zin, W. *Polymer*, **2004**, 45, 4507–4513.
45 Roth, C.; McNerny, K.; Jager, W.; Torkelson, J. *Macromolecules,* **2007**, 40, 2568–2574.
46 Napollitano, S.; Lupaşcu, V.; Wübbenhorst, M. *Macromolecules,* **2008**, 41, 1061-1063.
47 Moll, J.; Kumar, S. *Macromolecules*, **2012**, 43, 1131-1135.

48 Holt, A.; Griffin, P.; Bocharova, V.; Agapov, A.; Imel, A.; Dadmun, M.; Sangoro, J.; Sokolov, A. *Macromolecules,* **2014**, 47, 1837–1843.
49 Füllbrandt, M.; Purohit, P.; Schönhals, A. *Macromolecules,* **2013**, 46, 4626-4632.
50 Serghei, A.; Huth, H.; Schick, C.; Kremer, F. *Macromolecules,* **2008**, 41, 3636-3639.
51 Efremov, M.; Olson, E.; Zhang, M.; Zhang, Z.; Allen, L. *Phys. Rev. Lett*. **2003**, 91, 085703-085707.
52 Paeng, K.; Richert, R.; Ediger, M.D. *Soft Matter,* **2012**, 8, 819-826.
53 van Herwaaden, S. *Application note for Xsensor's calorimtere chips of XEN-39390 series* http://www.xensor.nl/pdffiles/sheets/nanogas3939.pdf.
54 Schick, C. *Calorimetry in Polymer science: A comprehensive reference*, Matyjaszewwski, K. Möller (Eds) Elsevier B. V., Amsterdam, **2012**, pp 793-823.
55 Huth, H.; Schick, C. *Personal Communication*.
56 Reiter, G.; Hamieh, M.; Damman, P.; Sclavons, S.; Gabriele, S.; Vilmin, T.; Raphael, E.; *Nat. Mater.* **2005**, 4, 754-758.
57 Huth, H.; Schick, C. *Personal Communication*.
58 Huth, H.; Minakov, A.; Serghei, A.; Kremer, F.; Schick, C. *Eur Phys J-Spec Top,* **2007**,141,153-60.
59 H. Vogel, *Phys. Z.* **1921**, 22, 645.
60 Tammann, G.; Fulcher, G.; *J. Am. Ceram. Soc.* **1925**, 8, 339.
61 Hesse, W. *Anorg. Allg. Chem*. **1926**, 156, 245.
62 Jacobson, B.; Hecksher, T.; Christensen, T.; Olsen, N.B.; Dyre, J.; Niss, K. *J. Chem Phys*. **2012**, 136, 081102-081107.
63 Lee, L. *Langmuir,* **1996**, 12,1681-1687.
64 Good, R.; Girifalco, L. *J. Phys. Chem*. **1960**, 64, 561-565.
65 Owens, D.; Wendt, R. *J. Appl. Polym. Sci.* **1969**, 13, 1741-1747.
66 Kaelble, D.J. *Adhesion,* **1970**, 2, 66-81.
67 van Oss, C.; Chaudhury, M.; Good, R. *Chem. Rev*. **1988,** 88, 927-931.
68 Napolitano, S.; Cappoini, S.; Vanroy, B. *Eur. Phys. J. E,* **2013**, 36, 61-65.
69 Napolitano, S.; Prevosto, D.; Lucchesi, M.; Pinque, P.; D´Acunto, M.; Rolla, P. *Langmiur,* **2007**, 23, 2103-2109.
70 Nguyen, H.; Labardi, M.; Capaccioli, S.; Lucchesi, M.; Rolla, P.; Prevosto, D. *Macromolecules,* **2012**, 45, 2138-2144.
71 Yin, H.; Cangialosi, D.; Schönhals, A. *Thermochimica Acta,* **2013**, 566, 186-192.
72 van Turnhaut, J.; Wübbenhorst, M. *J. Non-Cryst. Solids,* **2002**, 305, 40-49.
73 Materials.springer.com.
74 Landau, L. D.; Lifschitz, E. M. *Textbook of theoretical physics, vol. V. Statistical physics*, **1979**, Akademie Verlag, Berlin.
75 Pochan, D.J.; Lin, E.K.; Satija, S.; Wu, W. *Macromolecules,* **2001**, 34, 3041-3045.
76 Miyazaki, T.; Nishida, K.; Kanaya, T. *Phys. Rev. E,* **2004**, 69, 061803.
77 Inoue, R.; Kanaya, T.; Yamano, H.; Nishida, K.; Tsukushi, I.; Shibata, K. *AIP Conf. Proc.* **2003**, 708, 197.
78 Soles, C.L.; Douglas, J.F.; Wu, W.; Dimeo, R. *Phys. Rev. Lett.* **2002**, 88, 037401.
79 Inoue, R.; Kanaya, T.; Yamano, H.; Nishida, K; Tsukushi, I.; Shibata, K. *Phys. Rev. Lett.* **2005**, 95, 056102.
80 Inoue, R.; Kanaya, T.; Yamano, H.; Nishida, K; Tsukushi, I.; Shibata, K. *Phys. Rev. E,* **2006**, 74, 021801.
81 Bhattacharya, M.; Sanyal, M.K.; Geue, T.H.; Pietsch, U. *Phys. Rev. E,* **2005**, 71, 041801.

CHAPTER 8 - Unveiling the Dynamics of Self-Assembled Layers of Thin Films of PVME by Nanosized Relaxation Spectroscopy

This chapter is reproduced with permission from (*Madkour, S.; Szymoniak, P.; Heidari, M.; von Klitzing, R.; Schönhals, A. Unveiling the Dynamics of Self-Assembled Layers of Thin Films of Poly(vinyl methyl ether) (PVME) by Nanosized Relaxation Spectroscopy*. *ACS Appl. Mater. Interfaces. 2017, 9, 7535-7546. DOI: 10.1021/acsami.6b14404).*

*Supporting information is given in Appendix I

DOI: http://dx.doi.org/10.1021/acsami.6b14404

Abstract

A combination of nanosized dielectric relaxation (BDS) and thermal spectroscopy (SHS) was utilized to characterize the dynamics of thin films of Poly(vinyl methyl ether) (PVME) (thicknesses: 7 nm – 160 nm). For the BDS measurements, a recently designed nano-structured electrode system is employed. A thin film is spin-coated on an ultra-flat highly conductive silicon wafer serving as the bottom electrode. As top electrode, a highly conductive wafer with non-conducting nanostructured SiO_2 nano-spacers with heights of 35 nm or 70 nm is assembled on the bottom electrode. This procedure results in thin supported films with a free polymer/air interface. The BDS measurements show two relaxation processes, which are analyzed unambiguously for thicknesses smaller than 50 nm. The relaxation rates of both processes have different temperature dependencies. One process coincidences in its position and temperature dependence with the glassy dynamics of bulk PVME and is ascribed to the dynamic glass transition of a bulk-like layer in the middle of the film. The relaxation rates were found to be thickness independent as confirmed by SHS. Unexpectedly, the relaxation rates of the second process obey an Arrhenius-like temperature dependence. This process was not observed by SHS and was related to the constrained fluctuations in a layer, which is irreversibly adsorbed at the substrate with a heterogeneous structure. Its molecular fluctuations undergo a confinement effect resulting in the localization of the segmental dynamics. To our knowledge, this is the first report on the molecular dynamics of an adsorbed layer in thin films.

8.1. Introduction

Advances in functional coatings, batteries, innovative organic electronics, and hybrid materials depend strongly on organic and/or polymeric materials confined in thin films or adsorbed at surfaces.[1-2] For innovative applications of thin polymer films, an understanding of the molecular reasons for the possible deviations of the properties of confined material from that of the bulk is essential.[3-5] In the nanometer vicinity, solid interfaces and free surfaces could alter for instance entanglements, glassy dynamics (α-relaxation), and the thermal glass transition temperature (T_g), compared to the bulk behavior. Subsequently, this could change macroscopic quantities of thin films like adhesion, wettability, friction, reactivity, and biocompatibility, which are topical problems for hybrid materials.[6] For thin films (<100 nm), local heterogeneities can be induced, which might result in local glass transition temperatures that are different from the bulk value.[7]

Scientifically, polymers in the form of thin films can be considered as sample geometry to study 1-dimentional confinement effects. For films with thicknesses of few nanometres, the question is whether or not the glass transition phenomenon deviates from the bulk behaviour and what the molecular reasons for these possible changes are. The founding work of Keddie and Jones,[8,9] was followed by a variety of studies, which investigated the dependence of T_g on the film thickness, where the results have been controversially discussed. Especially, thin films prepared from simple homopolymers have been extensively studied through the so-called *static* experiments, e.g. ellipsometry,[10,11] fluorescence spectroscopy,[7] and dielectric expansion dilatometry[11,12,13] as well as by techniques that explore the segmental mobility at temperatures above the thermal T_g, e.g. dielectric[14-16] and specific heat spectroscopy (*dynamic* experiments, see for instance references 17-19). To be precise, here a *thermal* T_g is defined as a glass transition temperature measured by a static method where the thermodynamic state of the film changes from an equilibrium liquid (melt) to a non-equilibrium glass.[10,5] Subsequently, the contradicting results existing in the literature are due to the usage of different methods (*static* or *dynamic*) and/or different preparation methods (capped versus free polymer/air interface).[10]

For thin polymeric films, the *thermal* T_g[13,20,21] and the melting temperature (T_m)[22,23] could deviate substantially from its bulk value. It is commonly accepted that the thickness dependence of the *thermal* T_g of supported thin films results as a combined effect of a self-assembled spatial dynamic heterogeneous structure across the whole film; composed of a so-called mobile surface layer (polymer/air interface), a layer having bulk-like properties

(in the middle of the film), and a layer adsorbed at the substrate.[10,30] The measured *thermal* glass transition temperature results a complicated average including all of these effects in dependence on the polymer and the interaction energy of the segments with the substrate, as well as the preparation conditions. Due to missing segment-segment interactions, compared to the bulk, a mobile surface layer is formed at the interface of the polymer with air. For non-attractive polymer/substrate interactions, this free surface layer becomes more dominant, yielding a lower *thermal* T_g. For attractive polymer/substrate interactions, segments can adsorb at the polymer/substrate interface. In this adsorbed layer the segments have a reduced mobility and may result in a higher *thermal* T_g compared to the bulk. One has to bear in mind that the formation of this adsorbed layer requires a given time. The diffusive mobility of a polymer chain depends on molecular weight (M_w).[14] The higher the M_w, the longer the time is needed to form an adsorbed layer. This means that the decrease or increase of the *thermal* T_g of a thin film can be also be due to the annealing condition during film preparation. This was concluded from investigations by ellipsometry on polystyrene[24,25] as well as broadband dielectric spectroscopy (BDS) of isolated, semi-isolated,[26] and brushes of high M_w poly(2-vinyl pyridine) (P2VP) films.[27]

In contrast to *static* experiments, results obtained by *dynamic* methods often show that the glassy dynamics (α-relaxation, *dynamic* T_g) is independent of film thickness. (Please note, a *dynamic* T_g is measured in equilibrium, above the *thermal* T_g at a given measurement frequency). These results are discussed as a combination of multiple measurement and sample preparation effects. For instance, at temperatures above the *thermal* T_g, the thickness of the mobile surface layer becomes smaller with increasing temperature.[28] Therefore, its influence on a measured *dynamic* T_g diminishes with increasing temperature. This effect might be the reason that *dynamic* methods do not show a change of the *dynamic* T_g, while the *thermal* T_g estimated in *static* experiments decreases or increases with decreasing film thickness.[29-30]

A mobile surface layer was evidenced by several experiments like by photobleaching experiments, the sinking of gold nanospheres into a surface[31], measurements on polymer blends[32] and a recent study on P2VP thin films.[33] On the contrary, little is known about the molecular fluctuations in the adsorbed layer of thin films. Although, related systems like nanocomposites of P2VP,[34] poly(vinyl acetate) (PVAc),[35] and poly(dimethyl siloxane) (PDMS)[36-37] filled with silica nanoparticles show some dynamics of an adsorbed interface layer, there is no direct measurement that probes the dynamics of this reduced mobility

layer, independently from the bulk-like dynamics, in thin films till now. This is due to the hard accessibility of the dynamics of the polymer/substrate interface and its weak intensity.[14]

Of particular interest here is the dynamics in the irreversible adsorbed layer, which is formed at the polymer/substrate, where the chains get trapped into non-equilibrium conformations that reduces their effective viscosity. To achieve equilibrated conformations, the reptation model[38] predicted that the annealing times should be longer than the terminal relaxation time. This was found for PS[39], PMMA, and PVAc.[40] Rotella et al.[41] showed that only the molecules in direct contact with an adsorbing surface are influenced resulting in changes of the local T_g. It was further suggested[14] that, at the molecular level, these alterations have a finite lifetime. Furthermore, these changes correspond to metastable conformations of the polymer chain corresponding local minima in the free energy landscape rather than a global one.

In this study, well-annealed thin films of low molecular weight (M_w) PVME (film thicknesses from the bulk down to 7 nm) were investigated by combining surface analytical techniques with two volume sensitive methods. As surface sensitive tools, contact angle measurements (CAM), atomic force microscopy (AFM), as well as ellipsometry were used. As volume sensitive experiments, BDS and SHS, utilizing a recently developed capacitor with a nanostructured spacer arrangement[26,42] and a pJ/K sensitive AC-nanochip calorimeter, respectively. Nano-size relaxation spectroscopy that probed the dynamics of the adsorbed layer of PVME thin films showed for the first time, that the segments adsorbed at the polymer/subtract interface have constraint segmental fluctuations. These fluctuations are independent of the film thickness.

8.2. Experimental Section

Materials

PVME was obtained from Aldrich Inc. as an aqueous solution (50 wt %) with a M_w of 10,455 g/mol (~ lower than the PVME entanglement M_w[43]). The polydispersity index is 3. To remove the water before the preparation of the films, the obtained PVME solution was kept in an oil free vacuum at 303 K for 72 h, then at 323 K for another 96 h. Differential scanning calorimetry (DSC) was used to estimate the thermal glass transition temperature T_g for the bulk sample to be 246 K (10 K/min, second heating run). A concentrated solution of the dried PVME in toluene was prepared as a master solution. This solution was further diluted

by toluene to prepare different polymer solution with different concentrations, which were used to control the films thicknesses.

Spin coating and annealing procedure

Thin films were prepared by spin coating in a flow box to insure a dust-free atmosphere. The filtered (Minipore, 0.2 µm) diluted solutions were spin coated with rotational speed 3000 rpm for 60 s. The concentration of the solution was varied to adjust the film thicknesses. After spin coating process, the samples were dried in vacuum (10^{-4} mbar, oil-free) and annealed at 313 K ($T_{ann}=T_{g,Bulk}+67$ K) for 72 h. This annealing procedure insures firstly the removal of the solvent. Secondly, the induced stress during spin coating was also released.[44] It is important to note that AFM topography images revealed that films have low roughness down to 7 nm, as shown in Figure S1. Further, no inhomogeneities nor dewetting was observed.

An important point is that the spin coating and annealing procedures and conditions we kept identical for all thin film samples; AC chip sensors, nanostructured capacitors, and crossed electrode capacitors (see below).

Volume sensitive methods and Sample preparation

Broadband dielectric spectroscopy (BDS): The dielectric properties of samples were characterized by a high-resolution ALPHA analyzer (Novocontrol) including a sample holder with an active head. The complex dielectric permittivity $\varepsilon^*(f) = \varepsilon'(f) - i\varepsilon''(f)$ were measured at frequencies between 10^{-1} and 10^{7} Hz. Here f denotes the frequency where ε' and ε'' are the real and imaginary (loss) part of the complex dielectric function. $i = \sqrt{-1}$ symbolizes the imaginary unit. A Quatro cryosystem (Novocontrol) was interfaced to the cryostat to control the sample temperature (temperature stability better than 0.1 K.). For more experimental details the reader is referred to ref [45]. It is important to note the sample was purged with dry nitrogen during the course of the measurement.

BDS sample preparation:

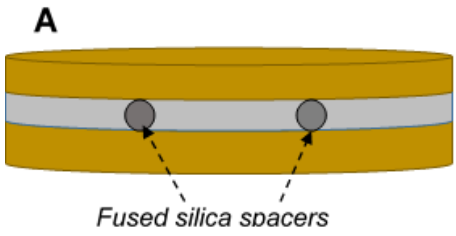

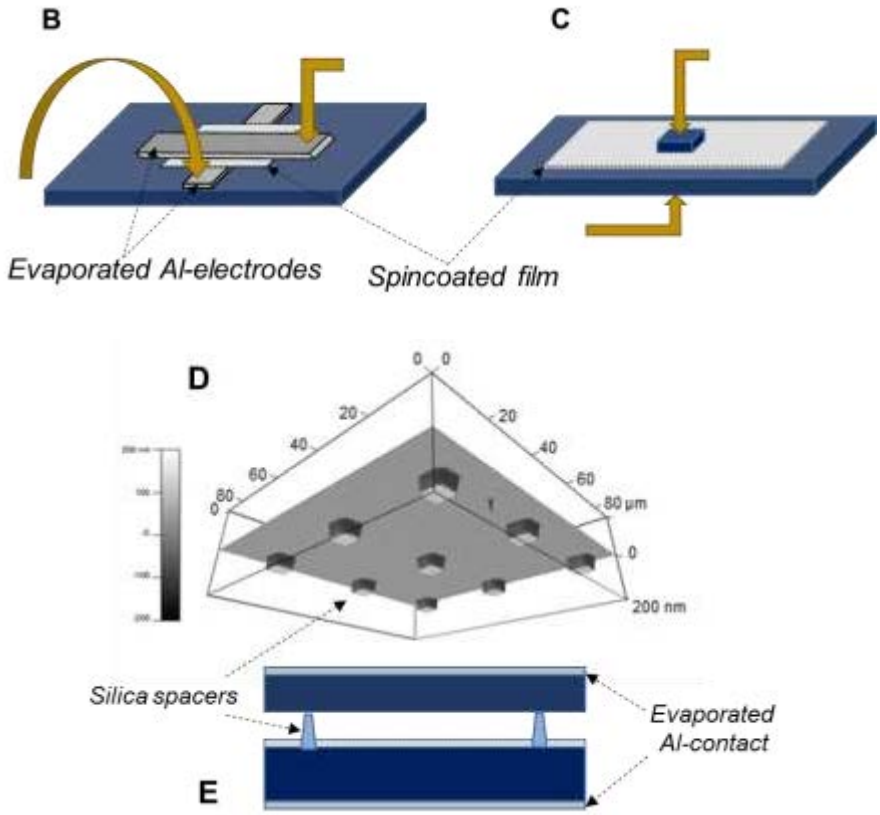

Figure 8.1. (A) *Schematic of a bulk sample in parallel plate arrangement with spacers. 3D* **(B)** *-view of the crossed electrode sample and,* **(C)** *nanostructured capacitor sample.* **(D)** *AFM picture of the nanostructured top electrode with 70nm spacers.* **(E)** *Side view schematic of the nanostructured capacitor*.

Bulk samples (figure 8.1A): The bulk sample was prepared by melting the PVME between the contacting electrodes (two round gold plated brass electrodes with a diameter of 20 mm) in parallel plate geometry. Fused silica spacers were employed to control the sample thickness to be 50 µm.

Crossed electrodes capacitors (CEC, figure 8.1B and 8.1C): For these dielectric experiments, thin films were prepared between two thin evaporated aluminum strips as described in detail in reference [12]. In short, the used glass substrates were first cleaned in an ultrasound bath using alkaline solution at 333 K for 15 min. This treatment was followed by a further ultrasound bath treatment employing Millipore water (resistivity >18 MΩ/cm). After that, the substrates were flushed in acetone (Uvasol quality) and further dried under nitrogen. As bottom electrode on the substrate, served a 2 mm wide aluminum strip with thickness ca. 60 nm, which was prepared by thermal deposition.[12] This step was followed by a further cleaning step, where the substrate was ~~is~~ rinsed again with acetone. After that, thin films were prepared by spin-coating and further annealed, as described above. As final step of the preparation of this sample capacitor a top electrode (width 2 mm, thickness ca.

60 nm) on the polymer film as described above oriented perpendicular to the bottom electrode (figure 8.1B and 8.1C). In general, the evaporation of metals could damage the polymer surface,[21] although this is not always the case[46,47]. Nevertheless, to minimize this risk and to avoid a diffusion of metal atoms into the film, a so-called flash evaporation (deposition rate >30 nm/s) was applied. Such method, as well as the Aluminum used, allows for a smooth and defined metal/polymer interface.[48,49]

Nanostructured capacitors (NEC, figure 8.1D and 8.1E): Here the sample capacitor was prepared by two doped silicon wafers, which are highly conductive with a specific resistance $\rho < 0.003$ Ωcm. The RMS roughness is 0.23 nm. An ultra-flat wafer with a size of 3 x 8 mm^2 is used as the bottom electrode and the substrate for spin coating the thin films. (The thickness of the native oxide layer is about 1–2 nm.) This electrode is first dipped in acetone for 2 minutes to remove the photoresist layer. It was then placed in a plasma oven in a pure oxygen atmosphere (20 W, 300 sec) to clean the substrate and further to activate the natural silica. As final step, before spin coating, a CO_2 snow jet gun was applied to further clean the surface, down to the microscale. Further cleaning and assembly details can be found in reference [26]. Spin coating under the exact same conditions was employed to prepare the thin films, which were further annealed as described above. A silicon wafer dice with a size of 1 x 1 mm^2 was used as the top electrode. It has an array of highly insulating silica spacers. These silica spacers have quadratic cross sections of 5 x 5 μm^2 and heights of 35 nm or 70 nm (Figure 1D). The nanostructured electrodes were prepared by a microlithographic process. For details see ref [26,42]. Identical cleaning procedures, as described for the bottom electrodes, were also applied for the nanostructures. This means acetone flushing and plasma treatment finalized by CO_2 snow jet cleaning. As a final step for the capacitor assembly, the top electrode was carefully placed on the wafer with the spin coated film. To avoid dust-contamination all described procedures were done in a flow box.

Differential *AC chip calorimetry: For* specific heat spectroscopy the nano calorimeter chip XEN 39390 (Xensor integrations, Nl) was employed. At this chip, two 4-wire heaters heater are located in the middle of a free standing thin silicon nitride membrane (thickness 1 μm) supported by a Si frame. The theoretical heated area is about 30 μm ×30 μm, where an integrated 6-couple thermopile senses the temperature[50]. Note that the heater-connecting lines can contribute slightly to the heated area, in addition to the hot spot. A 0.5 to 1 μm thick SiO_2 layer protects the described microstructure. Although the thin film was spin

coated across the whole sensor, only the small heated area is analyzed. Theoretically, it could be modelled and treated as point heat source.

Further, one has to consider that the empty sensor itself contributes to measured heat capacity. The differential approach to AC chip calorimetry minimizes this effect under the assumption of identical chips.[17] In the thin film limit (submicron film thicknesses), the heat capacity of the sample C_S is then calculated to

$$C_s = \frac{i\omega C_{eff}(\Delta U - \Delta U_0)}{P_0 S} \tag{8.1}$$

where ω - radial frequency, S - sensitivity of the thermopile, P_0 P_0- applied heating power.[17] The effective heat capacity of the empty sensor is given by $C_{eff} = C_0 + G/i\omega$, where G/iω models the heat loss by the surrounding atmosphere. Additionally, ΔU denotes the complex differential voltage measured for a sample and an empty reference sensor. Analogously, ΔU_0 is the thermopile signal obtained for two empty sensors. Absolute values of C_S can be deduced using calibration techniques.[51] Nevertheless, the real part of the complex differential voltage and the corresponding phase angle can be considered as measure for the complex heat capacity[17].

The experiments were carried out in the temperature scan mode. This means that during the measurement, the frequency was fixed while the temperature was ramped. To ensure stationary conditions during the measurement, the scanning rate was varied in the range from 1 K/min to 2.0 K/min depending on the programmed frequency. The theoretical basis for AC chip calorimetry is founded on having the response taking place in the linear regime. Therefore, the power for temperature modulation was kept constant at about 25 μW. This value ensures that the maximum amplitude of the temperature oscillation is smaller than 0.25 K and so a linear regime. A frequency range from 10 to 10^4 Hz is considered here for AC chip calorimetry. Further details can be found in reference [17].

AC-chip Film preparation: The sensors were placed in an oxygen plasma, for 300 sec at 20 W to clean the surface and activate the silica. Thin films were obtained by spin coating the filtered solution of PVME on the sensor. Finally, the samples were annealed according to the procedure described above (see section spin coating and annealing procedure).

Surface analytical methods

Contact angle measurements: The automated contact angle system OCA20 (Dataphysics, Germany) was applied to conducted the contact angle measurements. This system is equipped with a six-fold power zoom lens and a CCD camera. Halogen lamps were used to ensure a homogeneous back lighting. The contact angle (CA) was determined using the tangent fitting method. The used test liquids were Glycerol, n-hexadecane, n-tetradecane, and a polyethylene glycol (M_w=200g/mol). The measurements were carried out in an atmosphere saturated by the vapor of the test liquid. To insure the complete saturation of the atmosphere, samples were place in a cuvette with the test liquid for 15 mins prior to the measurements. 3 drops were dropped at the surface of a PVME film with a thickness of 200 nm. The film was treated identically to what is discussed above. The drops had volume of 4 µl. Mean values of the contact angles values were estimated by averaging the angles of both sides of the drop over 10 minutes. The data for SiO_2 and AlO_x were taken from reference [33] and [12], respectively.

Film thickness estimation:

CEC: Ellipsometric measurements could not be carried out for the CEC samples, due to transparency of glass. Therefore, after the deposition of the bottom Al-electrode, its thickness was measured by atomic forces microscopy (Nanopics 2100) by estimating the height of a step resulting from a scratch across the Al-electrode. After spin coating and annealing the film, similarly, the step height of a gap, obtained by cutting through the film on top of the Al-electrode, was measured. The film thickness was estimated as the difference between these two measurements.

NSC: Film thicknesses were estimated by ellipsometry using the procedure described below.

Film thickness determination for AC chip sensors: The films thicknesses could not be measured on the sensor directly. This is due to the small dimensions of the chip and the light reflected by connecting bond wires. Therefore, a further series of films were re-prepared on a silicon wafer to estimate the thickness by ellipsometry. The same solutions and identical conditions were used as for the preparation of AC chips. Assuming that the silicon wafer has similar surface properties as the sensor, the film on silicon wafer should have the same thickness as that supported on the sensor.[17-19,32-33]

Ellipsometry: The films thicknesses were measured using an ellipsometer based on a polarizer-compensator sample analyser (PCSA) (Optrel GbR, Sinzing, Germany). The wavelength of the laser light was 632.8 nm and the measurements were done at an angle of

incidence of 70 degrees. The analysis of the measurements employed a multilayer model; consisting of air/PVME/SiO_2/Si-substrate. In order to reduce the number of fit parameters, firstly the thickness of the SiO_2 layer was estimated before spin coating the polymer film. This value (ca. 1.7 nm) was kept constant during the data analysis for the polymer film. A linear increase of the film thickness with the concentration was obtained (Figure S2), which is expected. Furthermore, the ellipsometric measurements agree with the AFM data.

8.3. Results and Discussion

Contact angle measurements (CAM) were conducted to estimate the interaction of the polymer with the substrates. During the course of this investigation, two different substrate materials SiO_2 (nanostructured capacitors, AC nanochip calorimetry) and AlO_x (crossed electrodes capacitors) were used. To insure that PVME segments interact with both SiO_2 and AlO_x, the interfacial energies between PVME and both substrate systems were estimated. To estimate the interfacial tension of PVME, Owens/Wendt approach was utilized. It combines the Young relation with the Good equation (for details see [52]). Using this approach, the polar (γ^P) and dispersive (γ^{LW}) components of the surface energy of the solid (S=PVME) and the test liquid (L) can be extracted by

$$\frac{(1+\cos\theta_i)\,\gamma_{L,i}}{2\sqrt{\gamma_{L,i}^{LW}}} = \sqrt{\gamma_S^P}\,\frac{\sqrt{\gamma_{L,i}^{p}}}{\sqrt{\gamma_{L,i}^{LW}}} + \sqrt{\gamma_S^{LW}} \qquad (8.2)$$

(θ_i – contact angle, i counts the different test liquids). Literature values are used for the surface tensions of the test liquids.[53] Applying at least four test liquids, from the Owens/Wendt plot (see Figure S7) according to Equ. (1), γ^P and γ^{LW} of the surface energy of the sample were obtained. Using the Fowkes equation (*see the supporting information, Table S1 and S2*), the interfacial energy γ^{Total} of PVME/SiO_2 was found to be 2.73 mJ/m^2 while for PVME/AlO_x γ^{Total} =0.66 mJ/m^2 was obtained.

These values of the interfacial energy confirm that PVME interacts with both surfaces, which provide one basis for the formation of an adsorbed surface layer. Further, as discussed above, the formation of an adsorbed layer requires time, which is determined by both the molecular weight and annealing temperature. Both quantities are related to the longest reptation time, which is found to be relevant for the adsorption of chain segments at solid interfaces building an adsorbed layer [24,25]. To allow for an adsorption process here,

firstly, a PVME with a relative low molecular weight was chosen, which has shorter reptation time than a sample with a higher molecular weight. Secondly, the films were annealed at a high temperature (T_g+67 K, see preparation conditions) providing a high enough molecular mobility. Comparing these conditions to a recent study,[24] where a fully developed adsorbed layer was found for polystyrene on silica, which has a ca. 100 times higher molecular weight and was annealed only at T_g+40 K, the 72 h employed as annealing time is much longer than what would be expected for the formation of an adsorbed layer of PVME on silica. Further, preliminary ellipsometric investigations have started for samples; where the bulk-like layer of the films is removed by a solvent-leaching approach. These measurements give first direct evidence for an adsorbed layer in the system considered here. These studies are ongoing and will be published elsewhere.

Dielectric spectroscopy senses the fluctuations of dipoles within a sample. For the bulk material, which had to be measured for comparison, the polymer was measured in conventional parallel plate arrangement between two gold-plated electrodes. This measurement displays one relaxation process observed as a peak in the dielectric loss. As expected, this peak is observed for higher temperatures at higher frequencies (see Figure S3). It is due to the α-relaxation connected to segmental fluctuations (dynamic glass transition) and agrees with literature data [54]. Conductivity contributions due to mobile charge carriers cause the increase of ε″ at low frequencies.

The empirical formula of Havriliak/Negami (HN-function)[45] is employed to quantitatively characterize the α-relaxation process. It reads

$$\varepsilon^*_{HN}(\omega) = \varepsilon_\infty + \frac{\Delta\varepsilon}{(1+(\frac{i\omega}{\omega_0}))^\beta)^\gamma} \tag{8.3}$$

where ω_0 is a rate connected to the frequency of maximal loss f_p of the peak (relaxation rate). β and γ are shape parameters ($0<\beta\leq 1$ and $0<\beta\gamma\leq 1$) characterizing the width and the asymmetry of the process, where Δε expresses the dielectric strength. ε_∞ models ε′ for $\omega>>\omega_0$ ($\omega=2\pi f$). The conductivity contribution is described by adding $\varepsilon'' = \sigma/(\omega^s\varepsilon_0)$ to the loss part of the dielectric spectra. Here σ is connected to the DC conductivity, s is a parameter to model non-Ohmic effects s is one for Ohmic contacts, $s<1$ holds for a non-Ohmic behavior. ε_0 is the permittivity of vacuum. The reader is referred to reference [45] for further details.

For thin polymer films, the crossed electrode capacitors (CEC, *see experimental section*) were used to characterize films, with thicknesses of 160, 110, 80 and 50 nm. By this preparation technique, the polymer film is capped between two thermally deposited Aluminum electrode strips (see Figures 8.1B and 8.1C). However, this approach has two disadvantages. Firstly, the preparation of the upper electrode by thermal evaporation can attack the structure of the polymer chemically and/or the metal atoms can diffuse into polymer film, thereby leading to ill-defined interfaces and also electrical short cuts. Secondly, this sample geometry does not allow for a free surface at the polymer/air interface. Therefore, comparisons with other techniques are questionable, due to the different geometrical constrains and the different interfacial energy of the samples.

To overcome these limitations, a recently developed nanostructured capacitor (NSC) arrangement (Figures 8.1D and 8.1E), was employed.[26,42] In this geometry, the polymer film has a free surface at the polymer/air interface. For more details, see experimental section and references [26,27,42]. Samples with thicknesses between 50 nm and 7 nm were prepared in this arrangement. For film thickness of 50 nm, 36 nm, and 26 nm, nanostructured electrodes with 70 nm high SiO_2 nanospacers were employed, while the films with 15 nm and 7 nm thickness were prepared with 35 nm high nanostructured SiO_2 spacers. It is important to note that the height of the employed nanostructured spacers should be at least around twice as the thickness of the films, to insure a free surface even in the case when the silica spacers sinking into the film. However, due to the limited available spacer heights, CECs were used for films, which are thicker than 50 nm, as described above. To ensure that both methods will lead to consistent results, to samples with a thickness of 50 nm were prepared by both crossed electrodes and nanostructured capacitors. The results of the different measurements overlap (*see Figure S4*). This means that the two different surface conditions (capped - free) does not influence the dynamics of the PVME segments significantly.

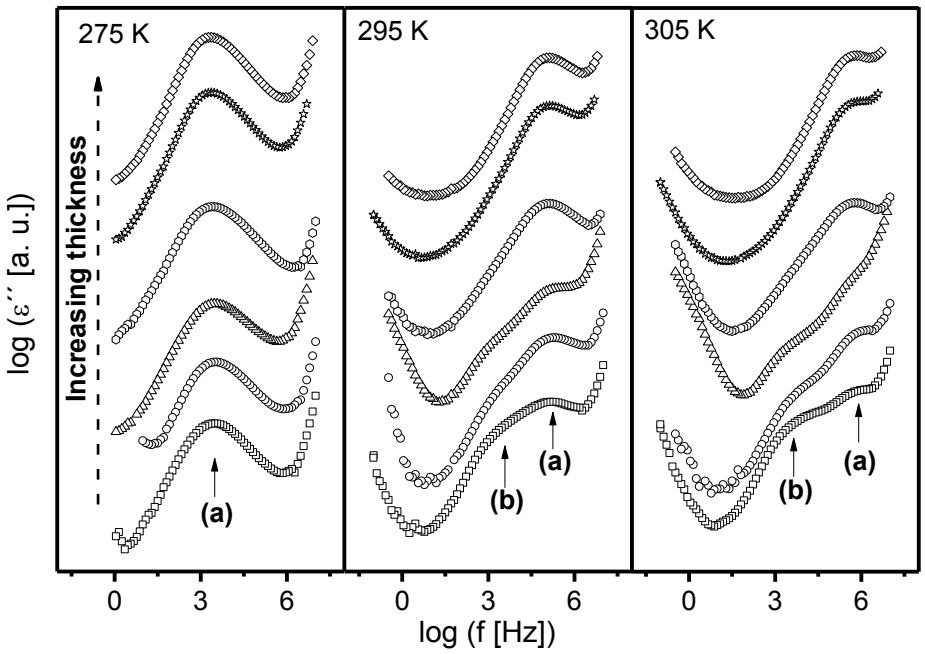

Figure 8.2. *Dielectric spectra versus frequency at the indicated three different temperatures for PVME thin films: squares – 15 nm, circles – 26 nm, triangles – 36 nm, hexagons – 50 nm, stars – 110 nm, and rhombuses – 160 nm. (a) α-relaxation of PVME, (b) the relaxation of an adsorbed interfacial layer. For sake of clearness, the data are shifted along the y-scale.*

Figure 8.2 shows the dielectric loss ε'' spectra at three different temperatures (275, 295 and 305 K) for PVME thin films with thicknesses of 15, 26, 36, 50, 110, and 160 nm. Two parasitic features are observed in the spectra. Firstly, similar to the bulk, for all temperatures at lower frequencies a conductivity contribution is detected. Secondly, for thin films, one has to take into account the limited resistance R of the Al- and/or that of the highly doped silicon electrodes. This resistance causes an additional parasitic loss peak (here called electrode peak) located at the high-frequency side of the spectra having a characteristic time constant τ_{Res} = R*C (C = sample capacitance). The electrode peak obeys a Debye function in its frequency dependence. The maximum position of this electrode peak $f_{Res} \sim 1/\tau_{Res}$ can be moved for optimized sample geometries outside the experimental frequency window.[12] For this reason, the Debye function is modeled by its low frequency tail. These contributions have to be added during the data analysis. Describing the relaxation process by the HN-function, the following equation is obtained for the whole fit function

$$\varepsilon^*_{Fit} = \varepsilon^*_{HN}(\omega) - i\frac{\sigma}{\omega^s \varepsilon_0} + iA\omega \qquad (8.4)$$

A is a parameter mainly due to τ_{Res}.

As a first result, a relaxation peak (a) is detected at the same frequency as the one measured for the bulk, for the lowest temperature. Its position does not change with lowering the film thicknesses, indicating that the relaxation rate of the process (a) is thicknesses independent. As a second result, with increasing temperature, a further peak (b) becomes visible at lower frequencies than process (a). With increasing temperature, the separation of both processes becomes more pronounced. Similarly, to process (a), the relaxation frequency of peak (b) is also thickness independent.

By increasing the temperature by 30 K, the maximum frequency of peak (a) shifts by ca. 3 orders of magnitude to higher frequencies, whereas process (b) only shifts by ca. 1.5 orders of magnitude, for the same temperature change (see Figure S5). This result indicates, that the temperature dependence of the relaxation rate of process (b) is weaker, compared to that of process (a).

Specific heat spectroscopy detects the thermal response of the films. Figure 8.3A depicts a result of an AC-nanocalorimetry measurement for a 100 nm thick PVME film. The real part U_R as well as the phase angle ϕ of the complex differential voltage are depicted at a frequency of 160 Hz as a function of temperature. The dynamic glass transition is indicated by a step-like change in U_R together with a peak in ϕ. A *dynamic* glass transition temperature can be defined in dependence on the measuring frequency as temperature of the half step height of U_R as well as the maximum temperature of the peak of ϕ. The as-measured phase angle data has to be corrected for an underlying step in the signal, which is proportional to the real part[17]. However, this subtraction process is somewhat ambiguous. Therefore, a recently developed method was applied for estimating the *dynamic* T_g in dependence on frequency, as described in reference [33]. In this approach, the stepwise function of the real part U_R (Figure 8.3A) is differentiated with respect to temperature, which results in a peak in the derivative. A Gaussian is fitted to these data and the maximum temperature of that peak is taken as *dynamic* T_g (Figure 8.3B). ±2 K can be considered as the typical error in the estimation of the T_g by AC-chip calorimetry. For further details see references [17,33].

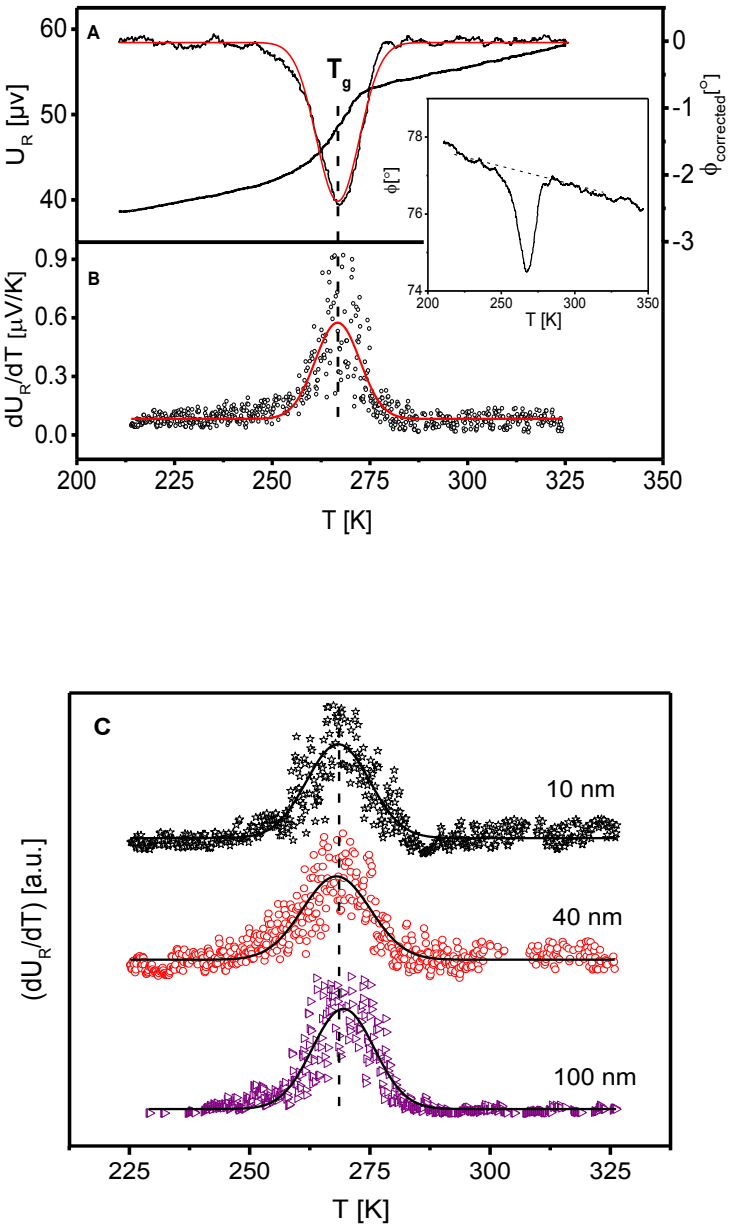

Figure 8.3. (**A**) *Real part as well as the corrected phase angle of the complex differential voltage versus temperature at 160 Hz for a 100 nm thick film. The contribution of U_R in the raw data of $\phi-$ (see inset) was subtracted.* (**B**) *First derivative of the U_R data given in A versus temperature. The red solid lines in A and B are fits of Gaussians to the data.* (**C**) *Normalized first derivative of the real part at a frequency of 160 Hz for the indicated different film thickness. For clearness, the curves were systematically moved along the y-scale. The solid lines are nonlinear regressions of Gaussians to the data as guides for the eyes.*

Figure 8.3c shows the temperature dependence of first derivatives of U_R versus temperature, for several film thicknesses normalized to its maximum heights. Two main observations could be made. 1) Only one relaxation process is detected for all film thicknesses in difference to the dielectric measurements. It is related to the dynamic glass transition of PVME (α-relaxation, cooperative segmental motion. 2) Down to the lowest film thicknesses

of 10 nm, all curves have a maxima at the same temperature position, which means that the *dynamic* T_g is thickness independent.

Discussing all results in quantitative way, a so-called relaxation map is used. In this representation, the relaxation rate f_p is plotted versus 1/T (see Figure 8.4).

For an α-process, the temperature dependence of the relaxation rate f_p is expected to be non-linear in such a plot, where this dependence can be approximated by the well-known Vogel/Fulcher/Tammann- (VFT-) equation[45]

$$\log f_p = \log f_\infty - \frac{B}{T - T_0} \tag{8.5}$$

f_∞ and B are fitting parameters. T_0 is a parameter known as ideal glass transition or Vogel temperature. Empirically T_0 is found to be 30-70 K below the conventional thermal T_g measured by DSC.

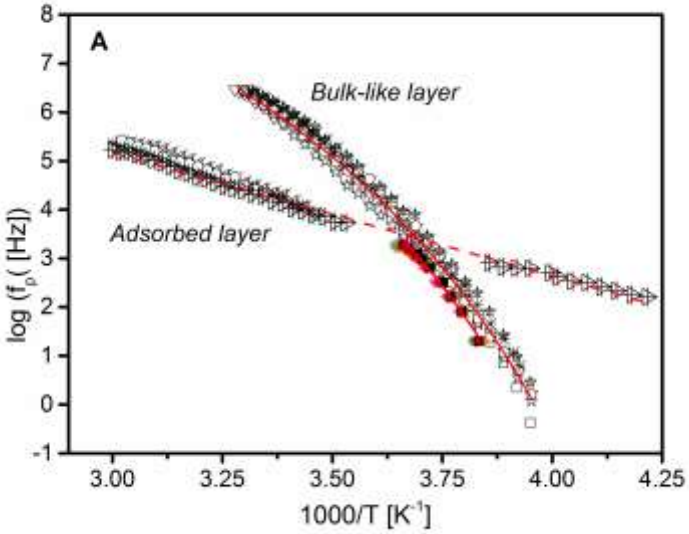

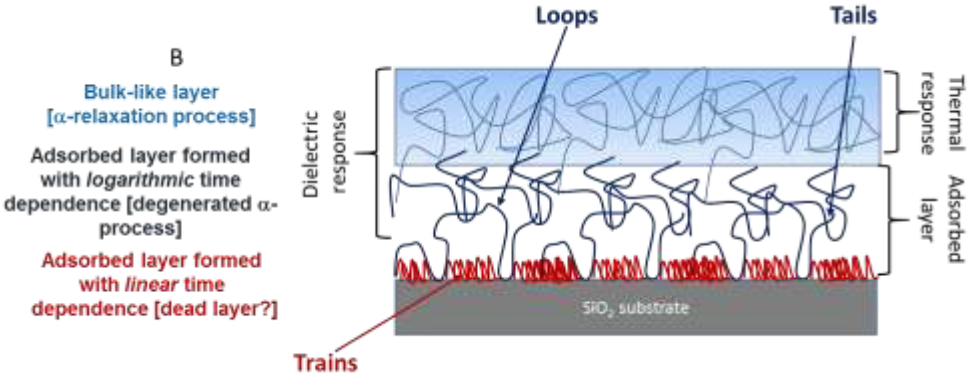

Figure 8.4: (A) *Open symbols: f_p versus 1/T for different film thicknesses measured by BDS: down sited triangles – bulk, stars - 160 nm, squares – 110 nm, hexagonal - 47 nm, asterisks – 36 nm, circles – 26 nm, crossed stars –15 nm and crossed-right sited triangles – 7 nm. Solid symbols: f_p versus 1/T for different estimated by SHS for different film thicknesses: squares - 140 nm, stars - 100 nm, rhombuses – 40 nm, circles – 30 nm, right sited triangles – 20 nm, up-sited triangles – 10nm. The red solid lines correspond to fits of the VFT formula to the different data. BDS (bulk-like): log (f_∞ [Hz])=12, B=646 K, T_0=202 K; SHS: log (f_∞ [Hz])=12, B=560 K, T_0=208 K. The dotted line is an fit of the Arrhenius equation to the dielectric data of process (b) (the part of the adsorbed layer with logarithmic time dependence).* **(B)** *A schematic cartoon of a two-layer structure (adsorbed layer and a bulk-like layer) as deduced from the data and literature.*

For the BDS measurements, the process (a), coincidence in its frequency position as well as in its temperature dependence with the α–relaxation of bulk PVME. Therefore, process (a) is ascribed to the dynamic glass transition of a bulk-like layer in the central part of the film. As discussed above, the temperature dependence of the relaxation rate of process (a) is thickness independent and can be well described by a common (including all film thicknesses) VFT-fit. This is further confirmed by the SHS data, which approximately superimpose, within the experimental error discussed above, with the BDS results, independent of film thickness. Similar results were found in AC-chip calorimetric studies for other polymers.[17-19,30,33]

Although process (b) can still be observed for larger film thicknesses as a shoulder to process (a), it can only be unambiguously analyzed for thicknesses of 40 nm and below, as it becomes more pronounced with decreasing film thickness. This result gives first evidence, that process (b) is related to a layer, which is relatively independent from the bulk-like layer. Further, it is worth to note that process (b) is observed only by BDS, but not by specific heat spectroscopy, despite of the fact that for both measurements the samples were prepared under identical conditions (see method section). Compared to process (a), the relaxation rates of process (b) obey an essentially different temperature dependence. It is well described by an Arrhenius equation. The estimated activation energy of 62.4 ± 2.6 kJ/mol is independent of film thickness. Dielectric investigation shows that PVME also has a conventional β-relaxation, which is found for 1 Hz to be around 120 K, with an activation energy of 21.7 kJ/mol.[55] Process (b) is observed at essentially higher temperatures, and as discussed above its activation energy is ca. three times higher. Therefore, process (b) cannot be assigned to the β-relaxation of PVME.

To assign this process, one has to recall that the selected experimental conditions during sample preparation will allow for the existence of an irreversibly adsorbed layer on the attractive silica. Since relaxation process (b), compared to the α-process due to the bulk-

like layer, is observed independently, has slower relaxation rates at higher temperatures, and is still observed at temperatures below the T_g, it is ascribed for that reason to molecular fluctuations in the adsorbed layer. The existence of such a layer is shown for most polymers as reported in references [56,57], where the segment/surface interaction energies are in the order of k_BT (k_B-Boltzmann constant). The connectivity of the chains further stabilizes this layer since the detachment would require cooperative rearrangement of a larger set of the adsorbed segments.[58]

To understand the origin of process (b) in more detail, it is necessary to discuss growth kinetics of the adsorbed layer, according to literature results. Recently, it was shown that the adsorption process takes place in two different regimes having different time dependencies.[24] At short times, the kinetics of the adsorption process follows a linear time dependence and the polymer segments are directly adsorbed at the substrate forming a dense strongly bounded adsorbed layer.[59,60] This layer is probably completely immobilized and cannot be detected by dielectric spectroscopy. This part of the layer consists mainly of the so-called trains. [61,62] At longer times, the adsorption kinetics is changed to a logarithmic time dependence. The adsorbed layer further grows by diffusion of segments through the already existing layer, on the expense of their entropy. The structure of this part of the adsorbed layer is consisting of loops and tails[61,62] and is thus less dense than the immobilized part. Therefore, its structure should allow for some molecular fluctuations, which can be monitored by dielectric spectroscopy (see figure 8.4B). According to these literature results, relaxation process (b) is therefore ascribed to molecular mobility or fluctuations within the part of the adsorbed layer, which is formed mainly during the logarithmic stage of the adsorption, leading to constrained PVME segments.

The results reveal that the molecular dynamics in the adsorbed layer is not directly a cooperative segmental motion with a slowed down relaxation time, as it was observed for nanoparticles embedded for instance in PVAc[35]and P2VP[34] formed by a solution casting process. This means that spin-coating leads to different polymer substrate interfaces compared to the solution casting. In the solution casting route, a long time is employed to remove the solvent from the system, whereas during the spin coating process, most of the solvent is removed from the system in few seconds. These different time regimes for solution casting versus spin coating will result in different adsorbed layers with different structures and dynamics. Whereas in the former case, probably an equilibrated layer is

formed, while the latter procedure will lead to a non-equilibrated adsorbed layer with constrained dynamics.

The found activation energy for the constrained fluctuation in the adsorbed layer of 62.4 kJ/mol seems, at the first glance, to be similar to the value of the activation energy found by Housmanns for the adsorption of polystyrene at a SiO_2 substrate.[24] On the one side, this agreement could be accidental. Nevertheless, the adsorption/desorption process must also be related to some molecular mobility. To prove this, further experiments, including other polymers, are necessary.

A phenomenologically analogous behavior is observed for two polysiloxanes - poly(dimethyl siloxane) (PDMS) and poly(methyl phenyl siloxane) (PMPS) – which are embedded into nanoporous glasses.[63,64] With decreasing confining pore size, a transition from a VFT behavior, indicating glassy dynamics, to an Arrhenius law was observed. Further, the estimated apparent activation energies decrease with decreasing the pore size. Also a crossing of the temperature dependencies of the relaxation rates, which are characteristic for the bulk by that in confinement, is found. For polymers embedded into nanoporous glasses, the transition from the VFT to the Arrhenius behavior is interpreted as an effect of the spatial confinement due to the pores on the molecular fluctuations of the α-relaxation. Hence, the observed process with an Arrhenius-like temperature dependence is considered as a degenerated α-relaxation within the pores. This means that due to the confining effect of the pores, including interaction effects with the walls, the cooperative segmental dynamics degenerates from a cooperative to constrained localized molecular fluctuation. In the case of thin PVME films, an analogously comparable interpretation is suggested. Here, the confinement originates from the adsorption at the substrate together with the structure of the formed adsorbed layer, as discussed above. A similar discussion has been made for polystyrene films investigated by neutron scattering.[65]

In a recent study, Burroughs and coworkers[25] evidenced that there is a critical annealing time after which the thickness of the adsorbed layer becomes constant with a value h_∞. In the case of polystyrene, h_∞ was found to be on the order of 0.55 to 0.47 R_g. Here, R_g is the radius of gyration of the polymer.[66] For PVME, with similar M_W to the one used in this work, the radius of gyration was found to be 4.7 nm.[67] The above mentioned scaling factor might be used to get an estimation for the thickness of the whole adsorbed layer, which gives $h_\infty = 2.4 \pm 0.15$ nm for PVME. For this estimation, one has to keep in mind that the applied scaling factor was obtained for a weakly interacting system. Here, the polymer segments

and the substrate have an attractive interaction. This means that the estimated value of h_∞=2.4 nm has to be considered only as a lower bound. This means that the part of the adsorbed layer formed in the logarithmic regime has even smaller thickness. It is worth to note that this value corresponds to the range of pore sizes, where the change from a VFT to an Arrhenius behavior was found. [63,64]

Moreover, as discussed above, AC chip calorimetry measures the averaged thermal response of only the mobile segments throughout the whole film. However, this response is sensitive to the total mass (thickness) of the film, down to ng. Using Equation (8.1) the change of the heat capacity at the glass transition can be expressed by[17,51]

$$C_{S,Liquid} - C_{S,Glass} = i\omega\overline{C}^2 (U_{R,Liquid} - U_{R,Glass}) / SP_0 \sim m \sim d \qquad (8.6)$$

Here m is the mass of the film. To derive this equation, it was further assumed that the density of the film is the same as in the bulk. According to Equation (8.6), $U_{R,Liquid}$ - $U_{R,Glass}$ = ΔU_R should scale linearly with the thickness of the film. In Figure 8.5, ΔU_R is given versus d. The data can be well described by a linear regression line. However, this line does not go through the origin, as expected when the whole sample mass contributes to the dynamic glass transition. It intercepts the x-axis at ca. 3.5 ± 0.8 nm. From this result, one might conclude that there is ca. 3.5 nm thick layer of the film immobilized at the substrate with regard to molecular fluctuations, which cannot be sensed by specific heat spectroscopy. Therefore, it does not contribute to the dynamic glass transition. This value includes both parts of the adsorbed layer; formed during the linear and the logarithmic adsorption regime.[24] Within the experimental error, this value is in good agreement with the 2.4 nm, evaluated from the adsorption kinetics of polystyrene.

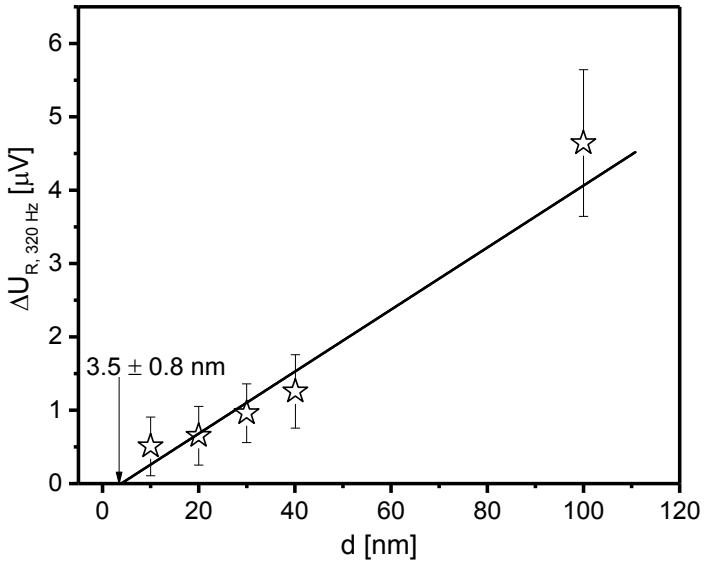

Figure 8.5. *ΔU_R versus d for thin PVME films at a frequency of 320 Hz. The solid line is a fit to the data.*

Furthermore, the cooperativity approach to the glass transition predicts a value for the cooperativity length scale smaller than 3 nm,[68] which was experimentally evidenced [see for instance 69,70]. The calculated thickness of the adsorbed layer is smaller than 3 nm. This might mean that no glass transition can take place in this layer. To be complete, the value of 2.4 nm means that for a film with a thickness 7 nm, more than one third of the film is the adsorbed layer.

For PDMS and PMPS confined into nanoporous glasses, at the change from the VFT to the Arrhenius behavior, the step-like increase of the specific heat capacity at the thermal glass transition vanishes [63,64]. This indicates that no glass transition takes place for smaller pore sizes. This is consistent with the observation that the specific heat spectroscopy shows only one peak related to the glassy dynamics of the bulk-like layer, yet no process due to the dynamics of the adsorbed layer.

A closer look on Figure 8.2 reveals that the dielectric intensity of the process due to the adsorbed layer increases with decreasing film thickness compared to the bulk-like layer. Therefore, the inset of Figure 8.6 depicts the ratio of the dielectric strength due to the adsorbed layer $\Delta\varepsilon_b$ to the total dielectric strength $\Delta\varepsilon_a+\Delta\varepsilon_b$ versus film thickness. Although the data show considerable scattering, this ratio decreases by trend. This indicates that the influence of the adsorbed layer on the properties of the whole film increases with decreasing thickness.

It is important to note that due to the increasing complexity and inhomogeneity of the setup of the NSC, an accurate extraction of the net dielectric strength requires a consideration of the geometry of the capacitors. An equivalent circuit analysis is necessary, to mimic the thin film, the air gap, the spacers etc. of the nanostructured capacitor,[26,27] for the extraction of the net dielectric strength from the data measured by NSC. This means that only the trend of the extracted relaxation strength from the NSC measurements can be considered, when comparing different film thicknesses measured by NSC and/or when comparing NSC to CEC, and not their estimated values. Furthermore, it is worth to mention that these equivalent circuits are complex and have to be adapted from one system to another. However, such an analysis will be presented elsewhere.

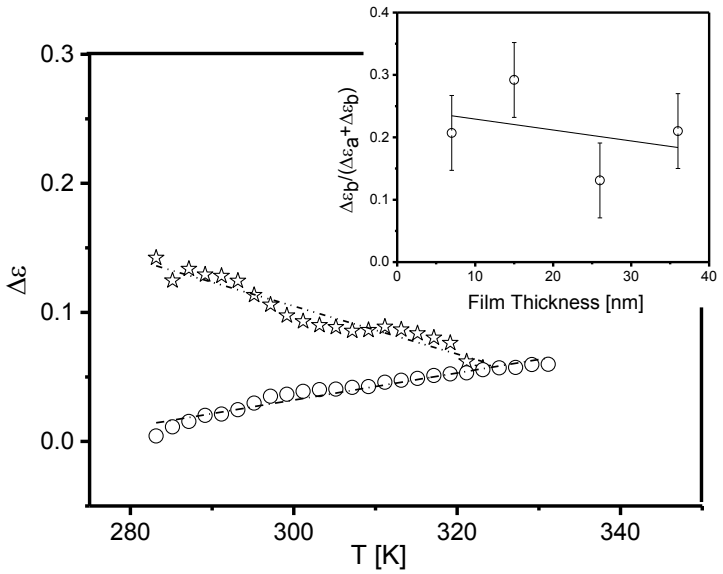

Figure 8.6. *Dielectric strength of the bulk-like layer (stars) and interfacial layer (circles) versus temperature for the 7 nm PVME film. The inset shows the dielectric strength of the adsorbed layer $\Delta\varepsilon_b$ divided the total dielectric strength $\Delta\varepsilon_a+\Delta\varepsilon_b$ versus film thickness.*

Figure 8.6 shows $\Delta\varepsilon_a$ and $\Delta\varepsilon_b$ as a function of temperature for the film which is 7 nm thick. While $\Delta\varepsilon_a$ decreases with temperature, the dielectric strength of peak (b) increases.

The Debye theory of dielectric relaxation gives for the dielectric strength $\Delta\varepsilon$[45]

$$\Delta\varepsilon = \frac{1}{3\varepsilon_0} g \frac{\mu^2}{k_B T} \left(\frac{N}{V}\right) \tag{8.7}$$

Here μ is the dipole, N the number of fluctuating dipoles in the volume V. Static correlations between the dipoles are described by the so-called Kirkwood correlation factor g. The Onsager factor is omitted for the sake of simplicity.[35] Generally, the dielectric strength

decreases with increasing temperature[45] for glassy dynamics, as it is also observed for bulk PVME as well as PVME films measured by CEC (see Figure S6). This is also observed for the temperature dependence of $\Delta\varepsilon_a$ of the bulk-like relaxation in thin films. In difference, $\Delta\varepsilon_b$ of the relaxation process ascribed to the adsorbed layer increases with increasing temperature. This can be understood by taking into account that the interaction strength of the segments with the substrate decreases with increasing temperature. This will increase the number of mobile dipoles in the adsorbed layers and hence, according to Eq. 4, the dielectric strength.

Finally, as recently illustrated in previous work,[33] AC-chip calorimetry was proven to be a sensitive tool to detect adsorbed and/or surface layers by examining the shape and/or the broadening of the processes. Upon a closer look at Figure 8.3C, one notices that the peaks broaden with decreasing film thickness. To clarify that, Figure 8.7 shows the normalized Gaussian fits to the first derivative of U_R versus normalized temperature (with the corresponding dynamic T_gs). This normalization was done to exclude the error of SHS which is ±3 K and further elucidate the broadening process. From the Gaussians to the data, the full width at half maximum (FWHM) can be calculated, which can be considered as a parameter to characterize the broadening of the curves.

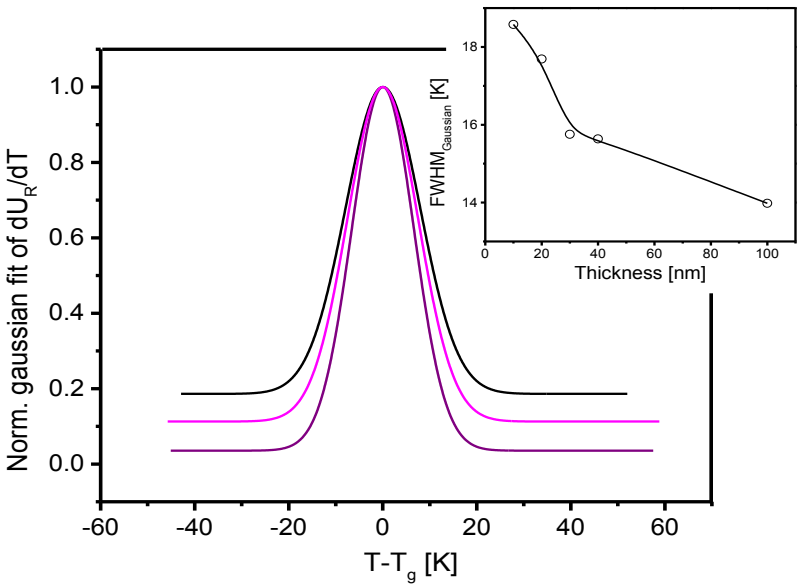

Figure 8.7. *The Gaussian fits to the normalized first derivative of the real part at 160 Hz versus temperature. Purple - 100 nm, magenta - 20 nm, and black - 10nm.* **The inset** *shows the full width at half maximum for the Gaussian fits versus the sample thickness.*

Figure 8.7 shows that there is a systematic broadening of the peaks with decreasing thickness. If one assumes that the peak is due to a distribution function of the relaxation

times, a broadening to lower temperatures would correspond to increased contribution of fluctuations with shorter relaxation times, while a broadening to higher temperatures is related to an increased amount of molecular mobility having longer relaxation times. In other words, as the thickness of the bulk-like layer decreases with decreasing the thickness, the influence of the mobile surface layer and an adsorbed layer increases. This is in agreement with reference [28] and further confirms the existence of the adsorbed layer observed by BDS.

8.4. Conclusion

The molecular dynamics of low M_w PVME thin films (160 nm down to 7 nm) was investigated via a combination of volume sensitive methods and surface analytical techniques. Volume sensitive techniques like broadband dielectric spectroscopy, utilizing nanostructured capacitors (NSC) with a nanostructured electrode sample arrangement and crossed-electrode capacitors (CEC), as well as specific heat spectroscopy using a nanochip calorimeter were employed. In addition, contact angle investigations proved the interaction of PVME segments with SiO_2 and AlO_X. For films with thicknesses up to 50 nm, measured by NSC, BDS measurements showed two relaxation processes, which can be analyzed for these film thicknesses in details. One process coincides in its frequency position as well as in its temperature dependence, with the α-relaxation of bulk PVME. For this reasons, it is assigned to the dynamic glass transition of a bulk-like layer located in the center of the film. Furthermore, the temperature dependence of the relaxation rates of this process is independent of film thickness. This was further confirmed by the SHS investigations, which superimpose in its temperature dependence with the BDS results independent of film thickness.

On the other hand, the relaxation rates of the second process, which became more pounced with decreasing film thickness, showed an essentially different temperature dependence. Its dielectric strength increases with temperature, in contrast to that of the bulk-like layer. This was explained by assuming that with increasing temperature, the segments substrate interaction becomes weaker, and hence the number of contributing mobile dipoles increases. Furthermore, the second process did not show a rather slowed down segmental dynamics, as it was the case for a layer absorbed at silica embedded in PVAc[35] and P2VP.[34] However, the behavior of its relaxation rates as a function of temperature resembles that of PMPS and PDMS confined into nanoporous glass. Therefore, this process was assigned to a degenerated constrained α-relaxation of an irreversible adsorbed layer at the

polymer/substrate interface, which undergoes a confinement effect resulting in the localization of the segmental dynamics. This was further confirmed by SHS, where a systematic symmetric broadening was observed with decreasing thickness, as well as an immobilized 3.5 nm, which does not contributing to the total thermal response of the film. To our knowledge, this is the first probing of the molecular dynamics of an adsorbed layer in thin films. Further work will concentrate on evidencing such an adsorbed layer for other systems as well.

References

1 Delcambre, S.; Riggleman, R.; de Pablo, J.; Nealey, P. *Soft Matter* **2010**, 6, 2475−2483.
2 Ediger, M.; Forrest, J. A. *Macromolecules* **2014**, 47, 471-478.
3 Debenedetti, P.; Stillinger, F. *Nature* **2001**, 410, 259–267.
4 Anderson, P. *Science* **1995**, 267, 1615-1616.
5 Ediger, M.; Horrowell, P. *J. Chem. Phys.* **2012**, 137, 080901-080914.
6 Napolitano, S.; Pilleri, A.; Rolla, P.; Wübbenhorst, M. *ACS Nano* **2010**, 4, 841-848.
7 Ellison, C.; Torkelson, J. *Nat Mater.* **2003**, 2, 695-700.
8 Keddie, J.; Jones, R.; Cory, R. *Faraday Discuss.* **1994**, 98, 219-230.
9 Keddie, J.; Jones, R; Cory, R. *Europhys. Lett*. **1994**, 27, 59-64.
10 Forrest, J.; Dalnoki-Veress, K. *Adv. Colloid Interface Sci.* **2001**, 94, 167-196.
11 Efremov, M.; Kiyanova, A.; Last, J.; Soofi, S.; Thode, C.; Nealey, P. *Phys. Rev. E.* **2012**, 86, 021501-021505.
12 Yin, H.; Napolitano, S.; Schönhals, A. *Macromolecules* **2012**, 45, 1652-1662.
13 Lupaşcu, V.; Picken, S.; Wübbenhorst, M. *J. Non-Cryst. Solids* **2006**, 352, 5594-5600.
14 Napolitano, S.; Wübbenhorst, M. *Nat. Commun.* **2011**, 2, 260.
15 Tress, M.; Erber, M.; Mapesa, E.; Huth, H.; Müller, J.; Serghei, A.; Schick, C.; Eichhorn, K.; Voit, B.; Kremer, F. *Macromolecules* **2010**, 43, 9937−9944.
16 Labahn, D.; Mix, R.; Schönhals, A. *Phys. Rev. E.* **2009**. 79, 011801-011809.
17 Huth, H.; Minakov, A.; Schick, C. *J. Polym. Sci., Part B: Polym. Phys*. **2006**, 44, 2996–3005.
18 Yin, H.; Schönhals, A. *Soft Matter* **2012**, 8, 9132-9139.
19 Yin, H.; Schönhals, A. *Polymer* **2013**, 54, 2067-2070.
20 Fakhraai, Z.; Forrest, J. *Phys. Rev. Lett.* **2005**, 95, 025701-025707.
21 Sharp, J. S.; Forrest, J. A. *Phys. Rev. Lett.* **2003**, 91, 235701-235711.
22 Wang, Y.; Rafailovich, M.; Sokolov, J.; Gersappe, D.; Araki, T.; Zou,Y.; Kilcoyne, A., Ade, H.; Marom, G.; Lustiger. A. *Phys. Rev. Lett.* **2006**, 96, 028303-028304.
23 Pandit, P.; Gupta, A.; Kuma, D.; Banerjee, M.; Bernstorff, S. *Langmuir* **2013**, 29, 3950-3956.
24 Housmans, C.; Sferrazza, M.; Napolitano, S. *Macromolecules* **2014,** 47, 3390-3393.
25 Burroughs, M.; Napolitano, S.; Cangialosi, D.; Priestley, R. *Macromolecules* **2016**, 49, 4647-4655.
26 Tress, M.; Mapesa, E.; Kossack, W.; Kipnusu, W.; Reiche, M.; Kremer, F. *Science* **2013**, 341, 1371−1374.
27 Neubauer, N.; Winkler, R.; Tress, M.; Uhlmann, P.; Reiche, M.; Kipnusua, W.; Kremer, F. *Soft Matter* **2015**, 11, 3062-3066.
28 Paeng, K.; Swallen, S.; Ediger, M. *J. Am. Chem. Soc.* **2011**, 133, 8444–8447.
29 Boucher, V.; Cangialosi, D.; Yin, H.; Schönhals, A.; Alegria, A.; Colmenero, J. *Soft Matter* **2012**, 8, 5119-5122.
30 Yin, H.; Cangialosi, D.; Schönhals, A. *Thermochim. Acta* **2013**, 566, 186-192.
31 Qi, D.; Daley, C.; Chai, Y.; Forrest, J. *Soft Matter* **2013**, 9, 8958−8964.
32 Yin, H.; Madkour, S.; Schönhals, A. *Macromolecules* **2015**, 48, 4936– 4941.
33 Madkour, S.; Yin, H.; Füllbrandt, M.; Schönhals, A. *Soft Matter* **2015**, 11, 7942-7952.
34 Holt, A.; Bocharova, V.; Cheng, S.; Kisliuk, A.; White, B.; Saito, T.; Uhrig, D.; Mahalik, J.; Kumar, R.; Imel, A.; Etampawala, T., Martin, H.; Sikes,N.; Sumpter, B.; Dadmun, M.; Sokolov, A. *ACS Nano* **2016,** 10, 6843-6852.
35 Füllbrandt, M.; Purohit, P.; Schönhals, A. *Macromolecules* **2013**, 46, 4626-4632.
36 Fragiadakis, D.; Pissis, P.; Bokobza, L. *Polymer* **2005**, 46, 6001-6008.
37 Klonos, P.; Kyritsis, A.; Pissis, P. *Polymer* **2016**, 84, 38–51.
38 De Gennes, P. *J. Chem. Phys.* **1971**, 55, 572-578.
39 Barber, D. R.; Steiner, U. *Phys. Rev. Letter*. **2007**, 98, 227801-227808.
40 Serghei, A,; Kremer, F. *Macromol. Chem. Phys*. **2008**, 209, 810-819.
41 Rotella, C.; Napolitano, S.; De Cremer, L.; Koeckelberghs, G.; Wübbenhorst, M. *Macromolecules* **2010**, 43, 8686-8691.
42 Serghei, A.; Kremer, F. *Rev. Sci. Instrum.* **2008**, 79, 026101-026107.
43 Takahashi, Y.; Suzuki; H.; Nakagawa, Y.; Yamaguchi, M.; Noda, I. *Polymer* **1991**, 23, 1333-1337.
44 Reiter, G.; Hamieh, M.; Damman, P.; Sclavons, S.; Gabriele, S.; Vilmin, T.; Raphael, E. *Nat. Mater.* **2005**, 4, 754-758.
45 Schönhals, A.; Kremer, F. Broadband Dielectric Measurement Techniques and Theory of Dielectric Relaxation. In Broadband Dielectric Spectroscopy; Kremer, F.; Schönhals, A., Eds.; 1st ed; *Springer*: Berlin, **2002**; 01-57.

46 Amarandei, G.; Clancy, I.; O'Dwyer, C.; Arshak, A.; Corcoran, D. *ACS Appl. Mater. Interfaces* **2014**, 6, 20758-20766.
47 Zaporojtchenko, V.; Strunskus, T.; Erichsen, J.; Faupel, F. *Macromolecules* **2001**, 34, 1125–1127.
48 Strunskus, T.; Zaporojtchenko, V.; Behnke, K.; Bechtolsheim, C.; Faupel, F. *Adv. Eng. Mater.* **2000**, 2, 489−492.
49 Bébin, P.; Prud'homme, R. *Chem. Mater.* **2003**, 15, 965–973.
50 Van Herwaaden, S. Application note for Xsensor's calorimtere chips of XEN-39390 series http://www.xensor.nl/pdffiles/sheets/nanogas3939.
51 Zhou, D.; Huth, H.; Gao, Y.; Xue, G.; Schick, C. *Macromolecules* **2008**, 41, 7662-7666.
52 Van Oss, C.; Chaudhury, M.; Good, R. *Chem. Rev.* **1988**, 88, 927-931.
53 Lee, L. *Langmuir* **1996**, 12, 1681-1687.
54 Cendoya, I.; Alegria, A.; Alberdi, J.; Colmenero, J. *Macromolecules* **1999**, 32, 4065-4078.
55 Lorthioir, C.; Alegría, A.; Colmenero. J. *Phys. Rev. E* **2003**, 68, 031805-03194.
56 Santore, M. *Curr. Opin. Colloid Interface Sci.* **2005**, 10, 176−183.
57 Granick, S. *Eur. Phys. J. E* **2002**, 9, 421−424.
58 O'Shaughnessy, B.; Vavylonis, D. *J. Phys.: Condens. Matter* **2005**,17, R63−R99.
59 Gin, P.; Jiang, N.; Liang, C.; Taniguchi, T.; Akgun, B.; Satija, S.K.; Endoh, M.K.; Koga, T. *Phys. Rev. Lett.* **2012**, 109, 265501-265507.
60 Asada, M.; Jiang, N.; Sendogdular, L.; Gin, P.; Wang, Y.; Endoh, M.K.; Koga, T.; Fukuto, M.; Schultz, D.; Lee, M.; Li, X.; Wang, J.; Kikuchi, M.; Takahara, A. *Macromolecules* **2012**, 45, 7098–7106.
61 Jiang, N.; Shang, J.; Di, X.; Endoh, M.K.; Koga, T. *Macromolecules* **2014**, 47, 2682–2689.
62 Jiang, N.; Endoh, M.; Koga, T. Structures and Dynamics of Adsorbed Polymer Nanolayers on Planar Solids: Non-equilibrium Phenomena in Confined Soft Matter. vol.*1*. *Springer* **2015**, Napolitano, S. (Ed.).
63 Schönhals, A.; Goering, H.; Schick, C.; Frick, B.; Zorn, R. *J. Non-Cryst. Solids* **2005**, 351, 2668 – 2677.
64 Schönhals, A.; Zorn, R.; Frick, B. *Polymer* **2016**, 105,393-406.
65 Rintaro, I.; Kanaya, T. Heterogeneous Dynamics of Polymer Thin Films as Studied by Neutron Scattering. In Glass Transition, Dynamics and Heterogeneity of Polymer Thin Films. Kanaya, T. Eds.; 1st ed; *Springer* Berlin -Heidelberg, **2013**; 252, 107-140.
66 Fujii, Y.; Yang, Z.; Leach, J.; Atarashi, H.; Tanaka, K.; Tsui, O. *Macromolecules* **2009**, 42, 7418–7422.
67 Choi, S.; Liu, X.; Briber, R. *J. Polym. Sci. B Polym. Phys*. **1998**, 36, 1–9.
68 Adam, G.; Gibbs, J. *J. Chem. Phys.* **1965**, 43, 139-146.
69 Cangialosi, D.; Alegría, A.; Colmenero, J. *Phys. Rev. E* **2007**, 76, 011514-011522.
70 Saiter, A.; Delbreilh, L.; Couderc, H.; Arabeche, K.; Schönhals, A.; Saiter, J. *Phys: Rev. E* **2010**, 81, 041805-041812.

CHAPTER 9 - Unexpected Behavior of Ultra-Thin Films of Blends of Polystyrene/Poly(vinyl methyl ether) studied by Specific Heat Spectroscopy

The following chapter/article is reprinted from (*Madkour, S.; Szymoniak, P.; Schick, C.; Schönhals. A. Unexpected Behavior of Ultra-thin Films of Blends of Polystyrene/Poly(vinyl methyl ether) Studied by Specific Heat Spectroscopy. J. Chem. Phys. 2017, 146, 203321 and may be found at http://dx.doi.org/10.1063/1.4978505*). With the permission of American Institute of Physics (AIP) Publishing.

DOI: http://dx.doi.org/10.1063/1.4978505

Abstract

Specific heat spectroscopy (SHS) employing AC nanochip calorimetry was used to investigate the glassy dynamics of ultra-thin films (thicknesses: 10 nm – 340 nm) of a polymer blend, which is miscible in the bulk. In detail, a Poly (vinyl methyl ether) (PVME)/Polystyrene (PS) blend with the composition of 25:75 wt% was studied. The film thickness was controlled by ellipsometry while the film topography was check by AFM. The results are discussed in the framework of the balance between an adsorbed and a free surface layer on the glassy dynamics. By a self-assembling process, a layer with a reduced mobility, is irreversibly adsorbed at the polymer/substrate interface. This layer is discussed employing two different scenarios. In the first approach, it is assumed that a PS-rich layer is adsorbed at the substrate. Whereas in the second approach, a PVME-rich layer is suggested to be formed at the SiO_2. Further, due to the lower surface tension of PVME, with respect to air, a nanometer thick PVME-rich surface layer, with higher molecular mobility, is formed at the polymer/air interface. By measuring the glassy dynamics of the thin films of PVME/PS in dependence on the film thickness, it was shown that down to 30 nm thicknesses, the dynamic T_g of the whole film was strongly influenced by the adsorbed layer yielding a systematic increase in the dynamic T_g, with decreasing the film thickness. However, at a thickness of ca. 30 nm thickness, the influence of the mobile surface layer becomes more pronounced. This results in a systematic decrease in T_g with the further decrease of the film thickness, below 30 nm. These results were discussed with respect to thin films of PVME/PS blend with a composition of 50:50 wt% as well as literature results.

9.I. Introduction

For many decades, the nature of glass transitions of amorphous polymers has been considered as a topical question of soft matter-physics.[1-7] Apart from homopolymers, miscible blends of amorphous polymers have also attracted much attention in the past decades,[8-20] due to their numerous applications. From the scientific point of view, there are differences in their behavior, compared to homopolymers, which are still under discussion.[21-22] For instance, the dynamic heterogeneities observed for the segmental dynamics or dynamic glass transition of bulk blends, as discussed below. This study deals with the investigation of the dynamic glass transition (segmental dynamics, α-relaxation) of ultra-thin films of polymer blends, which are miscible in the bulk. Therefore, in the first part of the introduction, some peculiarities of the dynamic glass transition of miscible blends in the bulk are discussed, whereas in the second part some important facts about the glass transition of ultra-thin polymer films are summarized.

Despite the wealth of knowledge about the structure of bulk binary miscible polymer blends[7-20], a number of questions regarding the molecular mobility remain; i.e. how the segmental dynamics of each component of the blend is affected by blending and by changing the composition. It is well accepted that the molecular composition of a miscible polymer blend, is not completely random. It is more likely that a segment, of the component A, is surrounded by segments of the same kind than by segments of the component B. This means that on a molecular scale, the effective composition of a binary miscible blend is different from the macroscopic one.[7,13] In general, the segmental dynamics of miscible polymer blends is affected in two major ways.[7] First, a *symmetric broadening* of the relaxation functions in the frequency domain with respect to the corresponding homopolymers is observed. Secondly, unlike the fact that a single glass transition temperature (T_g) is obtained for miscible blends, as measured by differential scanning calorimetry (DSC), the molecular dynamics are known to be spatially dynamic heterogeneous. These experimental findings have been explained through the combined effect of chain connectivity, which results in a self-concentration mechanism,[7] and thermally driven concentration fluctuations.[7] These mechanisms give rise to spatial regions, which have different local compositions than the average one with their own local relaxation behavior, and subsequently local T_gs.

Asymmetric miscible blends, in which the difference between the glass transition temperatures of the two components is large, have attracted a high number of studies in the past few decades. In this case, the polymer with the lower mobility, at temperatures below

its glass transition temperature, strongly affects the dynamics of the component with the higher mobility. This has been elaborated for Poly(methyl ethyl ether) (PVME) / Polystyrene (PS) blends,[10-11,23-25]. A further detailed discussion of the segmental α-relaxation and the global chain relaxation of the faster component can be found in ref [22].

While the above discussed behavior apply for the bulk, confining polymer blends into thin films (1-dimension) introduces additional constrains to the molecular dynamics. In the nanometer vicinity, solid interfaces and free surfaces could alter for instance intermolecular entanglements, local and effective concentrations, glassy dynamics, and *thermal* glass transition temperatures of miscible polymer blends, compared to their bulk values. Subsequently, this could affect macroscopic properties such as adhesion, wettability, friction, reactivity, and biocompatibility of ultra-thin films.[26] Furthermore, for polymer blends, the surface tension of each component with respect to the air and the substrate plays an important role and could further alter the compositional heterogeneities. Consequently, for films of miscible polymer blend with thicknesses of few nanometers, the key questions become: I) Whether or not glassy dynamics and glass transition deviates from their bulk behavior and what are the molecular reasons for these possible changes? II) Could the confinement influence the local composition of the blend and/or the phase stability?

The thickness dependence of the *thermal* T_g of supported thin films of homopolymers has been probed by the so-called static measurements,[27,28] e.g. DSC, florescence spectroscopy[29] and ellipsometry.[30,31] Here a *thermal* T_g is defined as a glass transition temperature measured by a static method at the transition from the equilibrium liquid state to the non-equilibrium glassy state. These measurements have revealed that with decreasing film thickness, the *thermal* T_g of ultra-thin films can deviate substantially from their bulk values, where both an increase or a decrease of the thermal glass transition temperature could be observed with decreasing film thickness, depending on both the polymer and the substrate.[32-34] This behavior is now generally explained by a spatial dynamical heterogeneous structure across the film thickness as a combined effect of a free surface layer, (at the polymer/air interface), a bulk-like layer (in the middle of the film), and a layer adsorbed at the substrate due to substrate/polymer interactions.[30,35] At the polymer/air interface, the segments have missing interaction, compared to the bulk, which results in an enhancement of their mobility. The influence of this so-called free surface layer on the measured thermal glass transition temperature depends on the substrate/polymer interactions. For non-attractive polymer/substrate interactions the influence of the free surface layer becomes more

pronounced with decreasing film thickness, and thus a decrease in the thermal T_g is observed.[30,35] Evidence for such a free surface layer was provided by photobleaching experiments[36,37] and embedding of gold nanospheres into a polymer surface.[38,39] On the other hand, it was shown that for attractive polymer/substrate interactions, an irreversible adsorbed thin layer is expected to be formed at the substrate interface,[40,41] where the segment/surface interfacial interactions are in the order of k_BT (k_B – Boltzmann's constant). This layer is further stabilized by the chain connectivity, as cooperative detachment of the segments would be required for desorption.[42] Recently, it was shown that this adsorbed layer has within a self-assembled spatial dynamic heterogeneous structure, which is formed throughout a two-step adsorption regime with different time dependencies.[43] At shorter times, the kinetics of the adsorption process follows a linear time dependence and the polymer segments are directly adsorbed at the substrate forming strongly bounded adsorbed layer.[44,45] This layer is dense[46,47] and probably immobilized. At longer times, the adsorption kinetics is characterized by a logarithmic time dependence. Here, the adsorbed layer further grows by diffusion and changes in the conformation of the segments through the already existing layer, on the expense of their entropy. Accordingly, for an attractive polymer/substrate system, this adsorbed layer, formed at the surface of the substrate with reduced segmental mobility, could over compensate the influence of the free surface on the thermal glass transition temperature. Consequently, an increase in *thermal* T_g compared to the bulk value with decreasing film thickness would be expected.

On the other hand, measurements by dynamic methods, e.g. broadband dielectric spectroscopy (BDS) and specific heat spectroscopy (SHS), on homopolymers,[48-51] carried out at temperatures well above the *thermal* glass transition have shown no thickness dependence of the *dynamic* glass transition, in contrary to the *thermal* T_g.[52,53] On the one side, that was partially discussed by showing that the thickness of the mobile surface layer decreases with increasing temperatures above T_g, and thus probing its influence on dynamic glass transition becomes difficult.[36] On the other side, a second approach to discuss the different behavior starts from the consideration that the dynamic measurements are carried out in a linear regime, where the static measurements are related to a transition from an equilibrium to a non-equilibrium state, which can be considered as a non-linear response. For instance, the rate dependence of the thermal T_g over a wide range of cooling rates for thin polystyrene films shows a depression from the bulk T_g[54,55] in a temperature range, whereas dynamic measurements are independent of the film thickness[48,51,52]. It is important

to note that the two sets of results are obtained for films prepared on the same substrate and with the same kind of perturbation. The only difference being is that in the former case, a non-linear perturbation is applied when measuring the thermal T_g, whereas in the latter, the perturbation is linear.

However, for ultra-thin films of miscible polymer blend, due to the absence of entropic effects, the composition at the free surface is dominated by the component, which has the lower cohesive energy to air[56-57]. For PVME/PS blends this was demonstrated by X-ray photoelectron spectroscopy (XPS)[58] and ellipsometry[59]. This might allow to study the influence of the surface layer on the α-relaxation, especially in the case of asymmetric polymer blends. It has been shown recently[60] that for ultra-thin films of PVME/PS with a composition of 50:50 wt%, through a combination of SHS and X-ray photoelectron spectroscopy (XPS), that the preferential interfacial energy of PS towards SiO_2 results in a layered structure; where a PVME-rich layer is self-assembled at the free surface interface. The influence of this surface layer is detectable at temperatures well above the monotonous T_g of the blend, resulting in the decrease of T_g with decreasing thickness.

Here, as a continuation of the previous work[16,61] the dynamic glass transition of ultra-thin films of in the bulk miscible blend PVME/PS with a composition of 25:75 wt% was investigated by employing AC-chip calorimetry. Of a particular interest here is the understanding, and elaborating the sensitive balance between the adsorbed and the free surface layer. All the findings are discussed with respect to ultra-thin films of PVME/PS with an overall composition of 50:50 wt% as well as literature results. A dielectric study on the same system is in progress using a recently developed nanostructured electrode system. This study gives direct evidence for the dynamic heterogeneity for this blend system and will be published elsewhere.

9.2. Methods

Polymers were purchased from Aldrich Inc. PVME was obtained as an aqueous solution (50 wt.%) with a molecular weight (M_w) of 10,455 g/mol (lower than the entanglement M_w[62]) and a PI of 3. For sample preparation, PVME was dried in an oil free vacuum for 72 h at 303 K, then for another 96 h at 323 K. PS has a M_w of 524 kg/mol and a polydispersity index (PI) of 1.04. The thermal T_gs of materials in the bulk were determined by differential scanning calorimetry (DSC) and were found to be 246 K and 376 K (10K/min, second heating run) for PVME and PS, respectively. A concentrated polymer solution of PVME

and PS with the weight ratio of the polymers of 25 to 75 wt% was prepared as master solution using toluene. The thin films were then prepared by spin coating; where the film thickness is controlled by the concentration of the polymer solution. For that the master solution was diluted by toluene.

Differential AC chip calorimetry: Specific heat spectroscopy is employed utilizing a nano calorimeter chip. On the calorimeter chip (XEN 39390, Xensor integrations, Nl), the heater is located in the center of a free standing thin silicon nitride membrane (thickness 1 μm) supported by a Si frame. The chip has a theoretical heated hot spot area of about 30 μm ×30 μm, with an integrated 6-couple thermopile and two 4-wire heaters[63]. In addition to the hot spot, the heater strips can contribute to the heated area as well. A SiO_2 layer (thickness 0.5-1 μm) protects the heater and thermopile. The thin film was spin coated over the whole sensor, but only the small heated area is sensed and can be considered as point heat source.

The differential approach to AC chip calorimetry minimizes the contribution of the heat capacity of the empty sensor to the measured data.[48] In the approximation of thin films (submicron film thicknesses) the heat capacity of the sample C_S is then given by

$$C_s = \frac{i\omega C_{eff}(\Delta U - \Delta U_0)}{P_0 S} \qquad (9.1)$$

where ω - radial frequency, S - sensitivity of the thermopile, P_0 P_0- applied heating power.[48] $C_{eff=}C_0 + \frac{G}{i\omega}$ describes the effective heat capacity of the empty sensor were G/iω is the heat loss through the surrounding atmosphere. ΔU is the complex differential thermopile signal for an empty and a sensor with a sample, and ΔU_0 is the complex differential voltage measured for two empty sensors. Absolute values of C_S can be deduced using calibration techniques.[64] Here the real part of the complex differential voltage and the phase angle are considered as measure for the complex heat capacity.

During the measurement the frequency was kept constant while the temperature was scanned with a rate of 1… 2.0 K/min depending on the programmed frequency to guaranty a stationary state. It is known that thin PVME/PS films can undergo phase separation. Therefore, the maximum temperature reached during the measurement was kept well below the cloud temperature of PVME/PS 25:75 wt%, measured for a 100 nm thick film, which is 448 K.[20] The heating power for the modulation was kept constant at about 25 μW, which ensures that the amplitude of the temperature modulation is less than 0.25 K and so a linear

regime. The frequency is varied between 10 and 10^4 Hz. Further details can be found in reference [48].

AC-chip Film preparation: Films were prepared on the surface of the sensor. The sensors were annealed under vacuum at 473 K for 2 h to cure the epoxy resin completely, which was used to glue the chip to the housing. Then the sensors were placed in an oxygen plasma, for 300 s at 20 W to clean the surface and activate the OH-groups at the silica surface. This procedure might change the surface properties and therefore the interaction with the polymer. It is worth to note that this step was not done in related studies.[48]

Thin films were prepared by spin coating a filtered (Minipore, 0.2 μm) solution of PVME/PS with a composition of 25:75 wt% in toluene (3000 rpm, 60 s) onto the central part of the sensor. The film thickness was adjusted by the concentration of the solution. After spin coating, all samples were dried in an oil-free vacuum (10^{-4} mbar) and annealed at 313 K ($T_{ann}=T_{g,Bulk}+ 50$ K) for 72 h in order to remove the solvent and the stress induced during spin coating.[65]

The films thicknesses could not be measured on the sensor directly, due to the small size of the sensors surface. Therefore, a second set of films were prepared under identical conditions on a silicon wafer to estimate the thickness by ellipsometry. Since the silicon wafer has similar surface properties as the sensor, it is assumed that under identical spin coating conditions, the film on silicon wafer has the same thickness as that supported on the sensor.[21,6,48,50,16-66] Furthermore, to insure no phase separation or dewetting occurs during measurements, all samples were heated up to the maximum temperature used in the measurement and kept there for 24 hr. The topography of the films was checked by atomic force microscopy (AFM) before and after the treatment. The prepared films have a low surface roughness and no sign of dewetting, or phase separation was observed, even after heating to the maximum temperature reached during the measurement (see figure 9.1).

Differential scanning calorimetry (DSC): DSC was carried out for the bulk samples employing a differential scanning calorimeter (Seiko DSC 220C, rates 10 K/min). N_2 was used as a protection gas.

Ellipsometry: The films thicknesses were measured using a polarizer-compensator sample analyser (PCSA) ellipsometer (Optrel GbR, Sinzing, Germany). The wavelength of the laser light was 632.8 nm and the measurements were done at an angle of incidence of 70 degrees. The analysis of the measurements employed a multilayer model consisting of air/polymer

film/SiO_2/Si-substrate. To reduce the number of free fit parameters, the thickness of the SiO_2 layer was determined before spin coating the polymer film and then this value (ca. 1.7 nm) was kept constant during the data analysis for the polymer film.

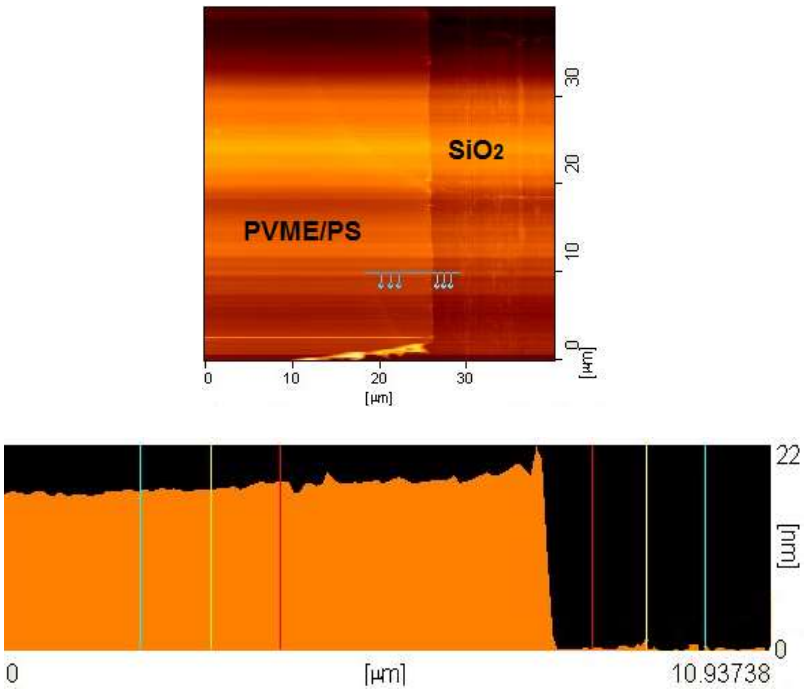

Figure 9.1. *AFM image of* **(top panel)** *top view and* **(bottom panel)** *cross section view of scratch across a PVME/PS (25:75 wt%) thin film with a thickness of ca. 18 nm after annealing at T= 338 K for 72 hours. No sign of dewetting or phase separation is observed.*

9.3. Results and Discussion

Figure 9.2 shows the result of an AC chip calorimetry measurement at a frequency of 320 Hz for a PVME/PS 25:75 wt% film with a thickness of 100 nm. The measurement gives a complex differential voltage, which is proportional to the complex heat capacity of the film (C_S; see Eq. 9.1, method section) as a function of temperature at the selected frequency. The real part of the complex differential voltage U_R and the phase angle ϕ are taken as measurements of C_S. While the real part of the complex voltage displays a step-like change, the phase angle shows a peak indicating the dynamic glass transition (α-relaxation). A dynamic glass transition temperature at the selected measuring frequency can be taken as the temperature of the half step-high of the U_R step (figure 9.2A), or the temperature at which the phase angle ϕ displays a minimum (figure 9.2B). In the raw data of ϕ (figure 9.2 – top panel), an underlying step contributes to the measured data, which is proportional to the step in U_R. Therefore, the phase angle has to be corrected by subtracting this contribution (figure 9.2B - bottom panel). However, this correction process is somehow ambiguous. Therefore, a recently developed method was employed to estimate the dynamic T_g in

dependence on frequency, as described in reference [66]. In this approach, the first derivative, with respect to temperature, of the real part U_R (figure 9.2A) is calculated, which results in a peak in the dU_R/dT. A Gaussian is fitted to these data and the dynamic T_g is determined as the maximum temperature of that peak (figure 9.2B). The typical error of the AC-chip calorimetry is ±2 K. For further details see references [48,66].

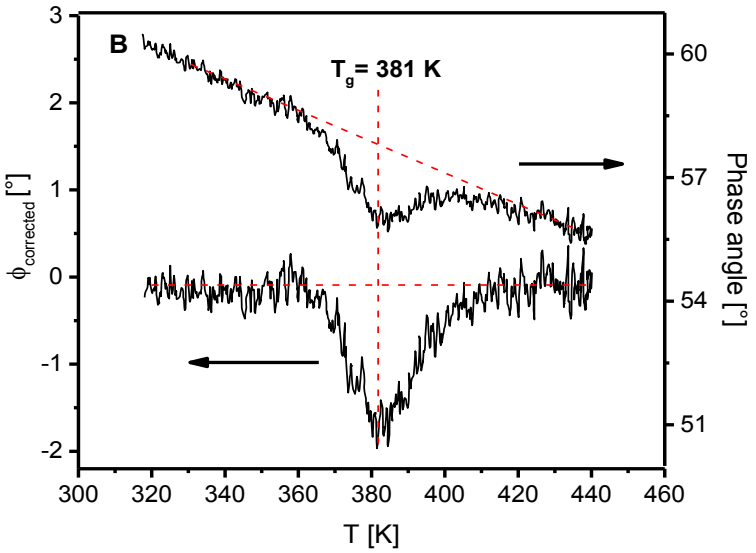

Figure 9.2. (A) *Real part U_R and its first derivative with respect to temperature as well as* **(B)** *phase angle of the complex differential voltage of a PVME/PS 25:75 wt% film (100 nm, f = 320 Hz). The contribution of the underlying step in the heat capacity in the raw data of ϕ (upper panel) was subtracted from the curve (lower panel). The dashed lines are there to guide the eyes. The red line in part (A) is a fit of a Gaussian to the data of the derivative.*

Figure 9.3A gives the DSC curves for PVME, PS, and PVME/PS 50:50 wt% taken from reference [16] and 25:75 wt%. The data show the broadening of the glass transition zone with blending and with increasing PS concentration as known form the literature,[7] which can be understood within the self-concentration as well as in the temperature driven concentration fluctuation approach.[7]

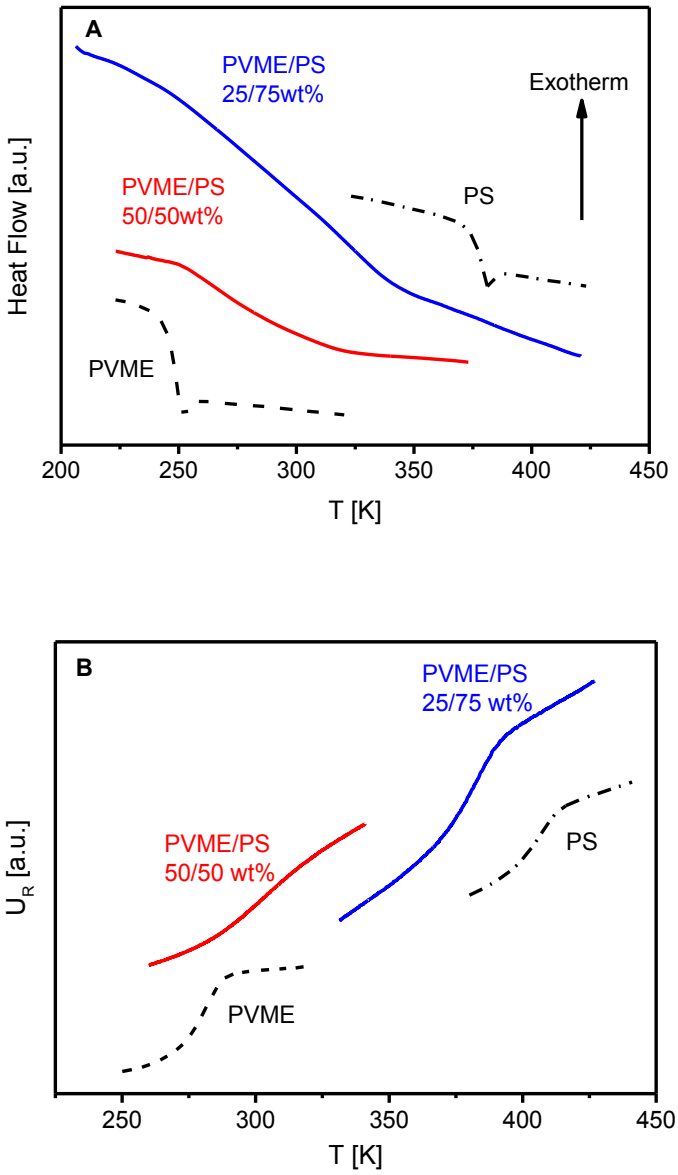

Figure 9.3. (A) *DSC trace (second heating run; rate: 10 K/min) for PVME (dashed), PS (dashed dotted), PVME/PS (50:50 wt%, red solid), all taken from reference [16] and PVME/PS 25:75 wt%, blue solid.* **(B)** *Real part of the complex differential voltage U_R versus temperature for films: dashed line – PVME, thickness 192 nm; dashed dotted line – PS, thickness 280 nm; solid line – PVME/PS 50:50 wt%, thickness 162 nm, taken from reference. [16] and PVME/PS (25:75 wt%), thickness 340 nm. The frequency of the measurement was 480 Hz and the rate 2 K/min.*

This broadening of the glass transition is also confirmed by the AC chip calorimetry on thin films (see figure 9.3B). For the blend films, the U_R shows considerable broadening of its widths, compared to the homopolymers.

AC chip calorimetry investigation for ultra-thin PS[48,52] and PVME[50,61] films show that the dynamic T_g is independent of the film thickness down to several nanometers (see figure 9.4B - inset). Figure 9.4A depicts U_R, normalized by its step height ($U_{Normalized}=U_R/(U_{R,Liquid}$

- $U_{R,Glass}$)) at the dynamic glass transition, for ultra-thin blend films with different thickness. Contrary to both homopolymers, the dynamic T_g depends on thickness. Surprisingly, the film thickness determines whether the dynamic glass transition is shifted to higher or lower temperature values. A systematic shift to higher temperatures with decreasing thickness is observed for films with thickness down to 30 nm (figure 9.4A – upper panel). For film thicknesses below 30 nm, the dynamic glass transition shifts back to lower temperatures (figure 9.4A – bottom panel). These observed shifts are much larger than the error of the AC-chip calorimeter measurement, which is typically ± 2 K.

To discuss this thickness dependence in more detail, the dynamic T_g measured at 320 Hz is plotted versus film thickness (figure 9.4B). As discussed above for both homopolymers, the dynamic T_g is independent of d (figure 9.4B -inset). For films, of the blend, thicker than 100 nm, the dynamic T_g is also independent of thickness, within the experimental error. This is in agreement with measurements on thin films of the PVME/PS blend with the composition of 50:50 wt%.[16] At around 100 nm, T_g starts to increase with decreasing film thickness, down to 30 nm, by ca. 24 K. At 30 nm, the T_g starts to decrease systematically again with decreasing the film thickness by ca. 21 K. This is different than the findings for the PVME/PS 50:50 wt% system, where for films with thicknesses below 100 nm, a decrease of the dynamic T_g with decreasing the film thickness was observed (figure 9.4C). It is worth to mention that a similar trend, to the ΔT_g dependence of the 25:75 wt% blend, was seen for star-shaped PS films, where ΔT_g displayed a non-monotonic dependence on the functionality.[67,68]

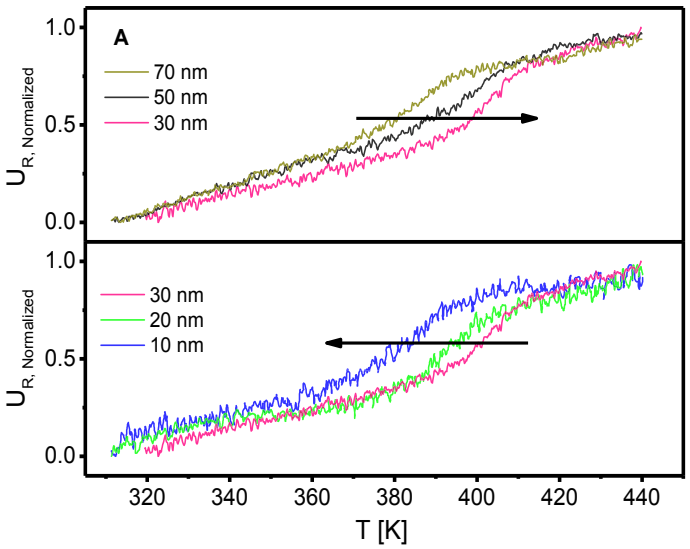
A
70 nm
50 nm
30 nm
30 nm
20 nm
10 nm
U R, Normalized
T [K]

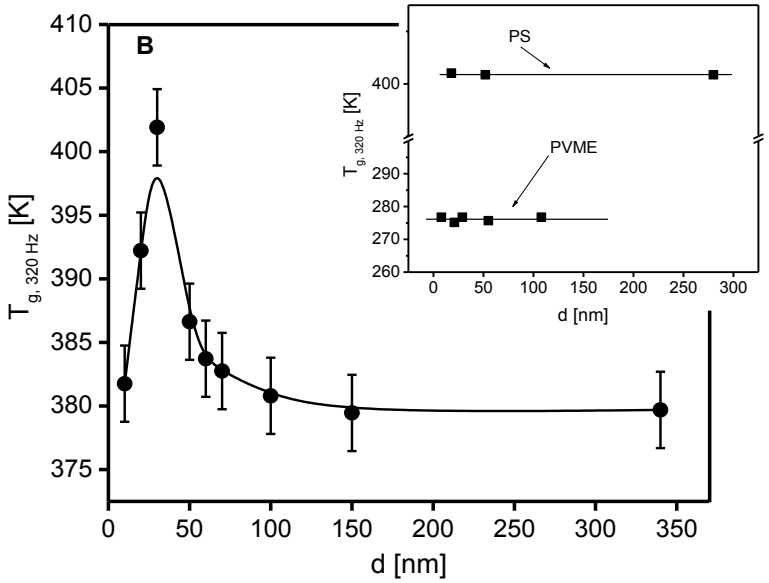
B
PS
PVME
T g, 320 Hz [K]
d [nm]

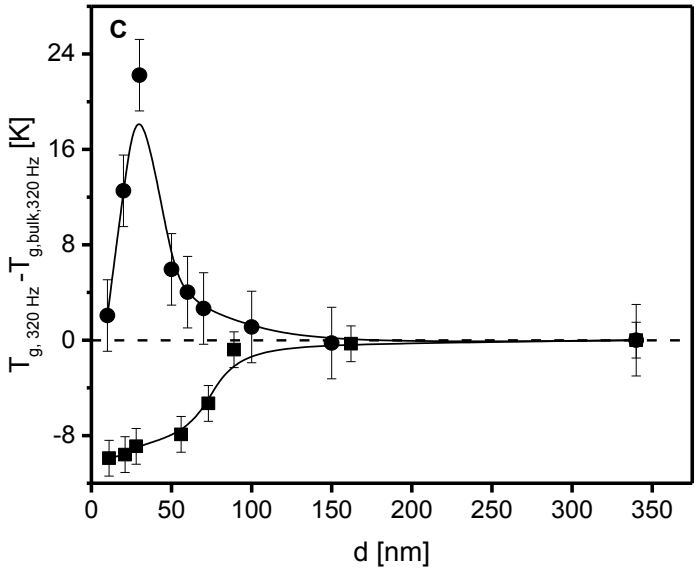

Figure 9.4. (A) *Gives the normalized U_R, normalized by its step height at the dynamic glass transition, of the complex differential voltage for thin films of the polymer blend PVME/PS (25:75 wt-%) at a frequency of 320 Hz for the indicated film thicknesses* **(B)** *Dynamic glass transition temperature measured at 320 Hz versus film thickness d for PVME/PS blend films (25:75 wt%). The line is guide for the eyes. The lines represent the average values. (**C**) Dynamic Tg, normalized by bulk Tg, versus thickness for PVME/PS blend films (25:75 wt% solid circles) and (50:50 wt% - solid squares, taken from reference [56]). Lines are guides to the eyes. The inset gives T_g measured at 320 Hz versus film thickness d for the PS and PVME, taken from reference [16].*

The data are further discussed in a so-called relaxation map, where the relaxation rate f_p is plotted as a function of the reciprocal temperature (see figure 9.5 and its inset).

For the dynamic glass transition, the temperature dependence of its relaxation rate is expected to be curved when plotted versus 1/T. This dependence can be described by the Vogel/Fulcher/Tammann (VFT-) equation[69], which reads

$$\log f_p = \log f_\infty - \frac{B}{T - T_0} \tag{9.2}$$

f_∞ and B are fitting parameters. T_0 is called ideal glass transition or Vogel temperature, which is found empirically to be 30-70 K below the thermal T_g measured by DSC. For all film thickness the data follow the VFT equation. Because all data were measured by the temperature ramping method at a fixed frequency one could further conclude that no phase separation took place during the measurement. Such a phase separation will result in measurement irregularities and deviations from the VFT behavior which is not observed.

As discussed above, for pure PVME and PS, the temperature dependence of the relaxation rates on the dynamic glass transition superimposes, for all film thicknesses down to a few

nanometers, with the corresponding bulk measurements. This is contrary to the case of PVME/PS 50:50 wt%,[16] where it was found that the dynamic T_g decreases with decreasing film thickness (see figure 9.5 -inset). This was explained through the three-layer model as discussed above. XPS showed that the free surface of the films was mainly dominated by PVME (82%), having a higher molecular mobility than the rest of the film. The influence of this PVME-rich layer at the air/polymer interface increases with decreasing the films thickness, causing the decrease of the dynamic T_g.

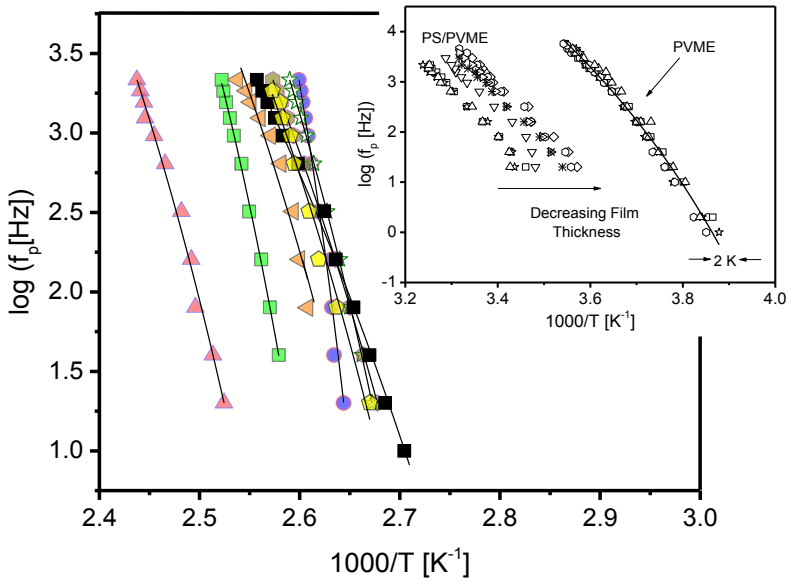

Figure 9.5. *Relaxation map of PVME/PS films (25:75 wt-%) for different film thicknesses: blue circles- 10 nm, green squares – 20 nm, pink triangles – 30 nm, orange right-sided triangles – 50 nm, yellow pentagon -60 nm, dark yellow hexagons – 70 nm, stars- 100 nm, and black squares – 340 nm. The solid black lines are VFT fits to the data.* **Inset.** *Relaxation map for PVME and for PVME/PS films (50:50 wt-%) for different film thicknesses. PVME: triangles – 12 nm, hexagons – 58 nm, stars – 168 nm, squares -192 nm, circles – 218 nm. The solid line is a fit of the VFT-equation to all data of PVME. PVME/PS blend: diamonds – 11nm, hexagons – 21 nm, right-sited triangles – 28 nm, asterisks – 56 nm, down-sited triangles – 73 nm, squares – 89 nm, stars – 162 nm, up-sited triangles – 340 nm. All taken from reference [16].*

However, for PVME/PS 25:75 wt%, a similar scenario applies, but yielding a different result. Here, the system contains a much lower amount of PVME. Nevertheless, the PVME still segregates at the surface, enhancing the PVME concentration with respect to the formulated concentration, at the polymer/air interface. This was proven by XPS,[58] where it was shown that the surface layer of PVME/PS 25:75 wt% film is ca. 60% PVME-rich. Keeping this in mind, the data could be discussed by two different assumptions concerning the formation and composition of the adsorbed layer at the SiO_2 substrate. *In the first approach*, it is assumed that a PS-rich layer is adsorbed at the substrate, so that the total concentration of the film remains as formulated. This structural model is in agreement with

the data published in Ref 70 where a polystyrene rich layer is evidenced by SIMS depth profile measurements. Furthermore, it was also found that the interaction energy between polystyrene and SiO_2 is larger than the value for the interaction between PVME and SiO_2.[70] A polystyrene rich layer at the substrate was further deduced from AC chip calorimetric measurements for a PVME/PS blend with the composition of 50:50 wt%.[16] The assumed adsorbed polystyrene-rich layer has a constrained molecular mobility, which influences the molecular fluctuations in the bulk-like layer in the middle of the film leading to an increase of the dynamic T_g with decreasing film thickness.

In the second approach it is assumed that a PVME-rich layer is formed at the SiO_2 surface. This assumption is in agreement with experimental data published in references [71-74], although different concentrations and molecular weights were employed in these studies. Keeping in mind that also a PVME-rich layer is formed at the polymer/air interface, this assumption will lead to a PS-rich layer in the middle of the film, which has a higher dynamic glass transition temperature than the formulated blend. With decreasing film thickness, the concentration of PS in the layer in the middle of the film increases, which will lead to an increase of the dynamic glass transition temperature. This model is further supported by the observation that for the film with a thickness of 30 nm its dynamic glass transition temperature is similar to that of polystyrene (see figure 9.4B).

Based on the experimental data obtained in this study, it is not possible to discriminate between the two approaches. Therefore, further experiments are necessary e.g. solvent leaching experiments, to directly investigate the adsorbed layer.[43]

To discuss the behavior of the dynamic T_g for films with thicknesses below 30 nm, a few considerations need to be taken into account. First, AC chip calorimetry measures the averaged thermal response of the mobile segments throughout the whole film. Secondly, for the investigated homopolymers, the free surface layer was proven to be more or less thickness independent, contrary to the bulk-like layer in the middle of the film, where its thickness decreases with decreasing the film thickness. This was demonstrated by fluorescence anisotropy measurements.[36] Furthermore, angle-dependent XPS measurements showed that the free surface layer has a higher PVME concentration than the as formulated, for all PVME/PS concentrations.[58] In the case of PVME/PS 25:75 wt% films, below 30 nm, a critical stage is probably reached. It is accepted that the layer in the middle of the film would decrease with decreasing film thickness. In addition, the free PVME-rich surface will still be present, due to the existence of the polymer/air interface. Here, it seems

that for film thicknesses below 30 nm, the relative influence of the PVME-rich surface layer on the measured thermal response becomes more pronounced, which consequently results in the decrease of the dynamic T_g. This can be understood by taking into account that not only the bulk-like layer decreases with film thickness. Also the thickness of the adsorbed layer, formed in the logarithmic regime of the adsorption process, could decrease with decreasing film thickness, because the whole film will not allow for the formation of this part of the layer, which has a certain restricted mobility. In other words, there will simply not be enough material to form that part of the layer. Therefore, its relative influence on the dynamic T_g decreases, compared to the mobile surface layer. In return, the influence of the PVME-rich layer becomes dominant, and thus causing the dynamic T_g to then decrease systematically with decreasing the thickness, below 30 nm. It should be noted that the results obtained will dependent on the annealing conditions of the film before the measurements. Therefore, further experimental work has started, where both annealing conditions (temperature, time) as well as the chemical nature of the surface of the substrate, are changed. The reason for this change in the thickness dependence of the dynamic T_g, taking place at around 30 nm for the selected composition, requires further investigations, including different concentrations of the blend.

In the next part, the different behavior of 25:75 wt% system compared to that of 50:50 wt% is addressed. The different thickness dependence of the dynamic T_g observed for both considered compositions is attributed to the different PVME concentrations in the surface layer at the air/polymer interface. For the system with 50:50 wt%, the concentration of PVME in that layer is much higher than that of the 25:75 wt% blend. Consequently, the dynamic T_g of that layer is relatively much lower, compared to the rest of the film. Thus, the influence of that layer on the thickness dependence of the dynamic T_g of the whole system is much stronger in the former case than for the 25:75 wt% system.

Finally, some general consideration will be made concerning the adsorbed layer at the substrate. As described above, for homopolymers, the adsorbed layer at the substrate has a self-assembled spatial dynamic heterogeneous structure. In the adsorption regime characterized by the linear time dependence, polymer segments are directly adsorbed to the surface forming a dense PS-rich layer that is immobilized. This was shown for several polymers as reported in references [40,41], where the segment/surface interactions are in the order of k_BT (k_B-Boltzmann constant). Due to the fact that this part is immobilized it cannot be measured, and/or sensed by the AC chip calorimetry. The second part of the

adsorption process, has a logarithmic time dependence. The structure of this part of the adsorbed layer is less dense than the immobilized part and allows therefore for some molecular mobility, as it is also discussed in literature.[46,47]

It is important to note here that the AC chip calorimetry measures the averaged thermal response of the mobile segments throughout the whole film. According to Equation (9.1) and assuming that the density of the film is the same as in the bulk, the step high of the heat capacity at the glass transition is given by [48,51]

$$C_{s,Liquid} - C_{s,Glass} = \frac{i\omega\overline{C^2}\left(U_{R,Liquid} - U_{R,Glass}\right)}{SP_0} \sim m \sim d \qquad (9.3)$$

where m is the mass of the film. Therefore, $U_{R,Liquid}$ - $U_{R,Glass}$ = ΔU_R should be proportional to the thickness of the film. In figure 9.6, ΔU_R is plotted versus d. The expected linear dependence is confirmed. Moreover, the data can be described by a regression line. However, this line does not go through the origin and intercepts the x-axis at ca. 4 nm ± 0.7 nm. From this result, one might conclude that there is ca. 4 nm thick layer of the film completely immobilized at the substrate and do not contribute to the dynamic glass transition. This could be the part of the boundary layer at the polymer/substrate interface self-assembled during the linear time dependence of the adsorption process, discussed above.

Regarding the *first assumption,* discussed above, where a PS-rich layer is assumed to be adsorbed at the substrate Housmann et al.[43] showed that this regime, yielding a completely immobilized layer, takes place till a given fraction of the macromolecular size is reached. For atactic PS, this was found to be ca. 5.8 nm. This value is in agreement with the ca. 4 nm deduced from figure 9.6, within the measurement error and also considering the different approaches.

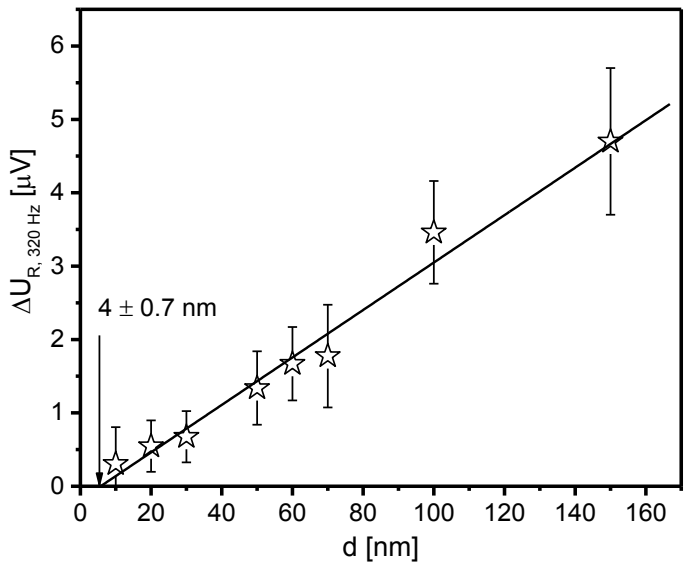

Figure 9.6. *ΔU_R versus the film thickness d for a frequency of 320 Hz for PVME/PS 25:75 wt% films. The solid line is a linear regression to the data.*

To support the second assumption that a PVME rich layer is formed at the substrate, first solvent leaching experiments have been carried out. In a first step, pure PVME was considered where the results will be discussed in detail elsewhere.[75] These first investigations show that a 3.6 nm thick irreversible adsorbed layer of PVME is formed at the SiO_2 substrate. The thickness of this layer is also in agreement with the data found by AC chip calorimetry here and in reference [61]. As discussed above, investigations will be carried out to explore nature of the adsorbed layer.

9.4. Conclusion

In conclusion, the molecular dynamics of ultra-thin films of the asymmetric polymer blend PVME/PS with the composition of 25:75 wt% which is miscible in bulk was investigated by specific heat spectroscopy. The film thicknesses (10 nm – 340 nm) were measured by ellipsometry. AFM was employed to estimate the film topography. The prepared films have low roughness, down to 10 nm. No dewetting or phase separation was observed. The calorimetric dynamic glass transition was measured in dependence of the film thickness. A completely different behavior, than that for thin films of PVME/PS with the composition 50:50 wt% was found.[16] For thin films of PVME/PS 25:75 wt%, with thicknesses down to 30 nm, the dynamic glass transition increases with decreasing the film thickness. This was assigned to the influence of an irreversibly adsorbed layer at the polymer/substrate interface.

Two assumptions were discussed for composition of this adsorbed layer. In the first approach, it was assumed that a PS-rich layer is adsorbed at the surface. This layer has reduced mobility, which influences the bulk-like layer in the middle of the film and thus an increase in T_g was observed. In the second approach, it was suggested that a PVME-rich is formed at the substrate. Because of the fact that a PVME-rich surface layer is present at the polymer/air interface, the concentration of the PS, in the middle layer of the film, increases and therefore the dynamic T_g increases. However, at a thickness of 30 nm thickness, the influence of the mobile surface layer on the dynamic glass transition increases. In return, a decrease in the dynamic glass transition, with further decrease in film thickness was observed. In contrary, ultra-thin films of PVME/PS 50:50 wt%, showed a systematic decrease in the T_g with decreasing the film thickness. This was discussed by showing that the influence of a self-assembled PVME-rich layer at the polymer/air interface, with a higher mobility, becomes more pronounced with decreasing the film thickness.

References

1 Debenedetti, P. G.; Stillinger, F. H. *Nature* **2001**, 410, 259–267..
2 Anderson, P. W. *Science* **1995**, 267, 1617.
3 Ediger, M.; Horrowell, P. *J. Chem. Phys.* **2012**, 137, 080901-080915.
4 Angell, C. A. *Science* **1995**, 267, 1924-1935.
5 Sastry, S.; Debenedetti, P.G.; Stillinger, F.H. *Nature* **1998**, 393, 554-557.
6 Yin, H.; Madkour, S.; Schönhals, A. Dynamics in Confinement: Progress in Dielectrics, Springer vol. 2. **2014**, Kremer, F. (Ed.).
7 Colmenero, J.; Arbe, A. *Soft Matter*, **2007**, *3*, 1474-1485.
8 Alegria, A.; Colmenero, J.; Ngai, K. L.; Roland, C. M. *Macromolecules* **1994**, *27*, 4486-4492.
9 Cendoya, I.; Alegria, A.; Alberdi, J. M.; Colmenero, J.; Grimm, H.; Richter, D.; Frick, B. *Macromolecules* **1999**, *32*, 4065-4078.
10 Takeno, H.; Kobayashi, M.; Aikawa, T. *Macromolecules* **2006**, *39*, 2183-2190.
11 Watanabe, H.; Urakawa, O. *Korean-Australian Rheol. J*. **2009;** *21*, 235-244
12 Green, P. F.; Adolf, D. B.; Gilliom, L. R. *Macromolecules* **1991**, *24*, 3377-3382.
13 Colby, R. H.; Lipson, J. E. G. *Macromolecules* **2005**, *38*, 4919-4928.
14 Urakawa, O.; Fuse, Y.; Hori, H.; Tran-Cong, Q.; Yano, O. *Polymer* **2001**, *42*, 765-773.
15 Chung, G. C.; Kornfield, J. A.; Smith, S. D. *Macromolecules* **1994**, *27*, 5729-5741.
16 Wang, D.; Ishida, H. *Macromol. Chem. Phys.* **2007,** *208*, 2222-2228.
17 Dionisio, M.; Fernandes, A. C.; Mano, J. F.; Correia, N. T.; Sousa, R. C. *Macromolecules* **2000**, *33*, 1002-1011.
18 Wang, J.; Roland, C. M. *Polymer* **2005**, 46, 4160-4165.
19 Alvarez, F.; Alegria, A.; Colmenero, J. *Macromolecules* **1997**, *30*, 597-604.
20 Arbe, A.; Alegria, A.; Colmenero, J.; Hoffmann, S.; Willner, L.; Richter, D. *Macromolecules* **1999**, *32*, 7572-7581.
21 Yin, H.; Schönhals, A. (Eds.) Utracki, L.; Wilkie, C. Broadband Dielectric Spectroscopy on Polymer Blends. In Polymer Blends Handbook (*Springer*, Netherlands, **2014**) p. 1299.
22 Ngai, K.; Capaccioli, S. *J. Chem. Phys*. **2013**, *138*, 054903
23 Schwartz, G. A.; Colmenero, J.; Alegria, A. *Macromolecules* **2007**, 40, 3246.
24 Y He, Y.; Lutz, T. R.; Ediger, M. D. *J. Chem. Phys.* **2003,** *119*, 9956-9965.
25 Gotzen, N.-A.; Huth, H.; Schick, C.; Van Assche, G.; Neus, C.; Van Mele, B. *Polymer* **2010**, 51, 647.
26 Napolitano, S.; Pilleri, A.; Rolla, P.; Wübbenhorst, M. *ACS Nano* **2010**, 4, 841.
27 Keddie, J. L.; Jones, R. A.; Cory, R. A. *Faraday Disc.* **1994**, 98, 219-230.
28 Keddie, J. L.; Jones, R. A; Cory, R. A. *Euro Phys Lett*. **1994**, 27, 59-64.
29 Ellison, C.; Torkelson, J. *Nat Mater.* **2003**, 2, 695-700.
30 Forrest, J.; Dalnoki-Veress, K. *Adv. Colloids Interface Sci.* **2001**, 94, 167-196.
31 Efremov, M.; Kiyanova, A.; Last, J.; Soofi, S.; Thode, C.; Nealey, P. *Phys. Rev. E.* **2012**, 86, 021501-021505.
32 Lupaşcu, V.; Picken, S.; Wübbenhorst, M. *J. Non-Cryst. Solids* **2006**, 352, 5594-5600.
33 Fakhraai, Z.; Forrest, J. *Phys. Rev. Lett.* **2005**, 95, 025701-025707
34 Sharp, J. S.; Forrest, J. A. *Phys. Rev. Lett.* **2003**, 91, 235701.
35 Ediger M.; Forrest, J. A. *Macromolecules* **2014**, 47, 471.
36 Paeng, K.; Swallen, S.; Ediger, M. *J. Am. Chem. Soc.* **2011**, *133*, 8444–8447..
37 Paeng, K.; Richert, R.; Eidger, M. Softmatter **2012**, 8, 819.
38 Qi, D.; Ilton, M.; Forrest, J. *Eur. Phys. J. E* **2011**, 34, 56.
39 Qi, D.; Daley, C.; Chai, Y.; Forrest, J. *Soft Matter* **2013**, 9, 8958.
40 Santore, M.; *Curr. Opin. Colloid Interface Sci.* **2005**, 10, 176.
41 Granick, S.; *Eur. Phys. J. E* **2002**, 9, 421.
42 O'Shaughnessy, B.; Vavylonis, D. J. *Phys.: Condens. Matter* **2005**, 17, 63.
43 Housmans, C.; Sferrazza, M.; Napolitano, S. *Macromolecules* **2014**, 47, 3390−3393.
44 Gin, P.; Jiang, N.; Liang, C.; Taniguchi, T.; Akgun, B.; Satija, S. K.; Endoh, M. K.; Koga, T. *Phys. Rev. Lett.* **2012**, 109, 265501.
45 Asada, M.; Jiang, N.; Sendogdular, L.; Gin, P.; Wang, Y.; Endoh, M. K.; Koga, T.; Fukuto, M.; Schultz, D.; Lee, M.; Li, X.; Wang, J.; Kikuchi, M.; Takahara, A. *Macromolecules* **2012**, 45, 7098-7106.
46 Jiang, N.; Shang, J.; Di, X.; Endoh, M. K.; Koga, T. *Macromolecules* **2014**, 47, 2682-2689.
47 Jiang, N.; Endoh, M.; Koga, T.; (Ed.) Napolitano, S. Structures and Dynamics of Adsorbed Polymer Nanolayers on Planar Solids: Non-equilibrium Phenomena in Confined Soft Matter, *Springer International*, Switzerland, **2015**, 129.

48 Huth, H.; Minakov, A.; Schick, C. D. *J. Polym. Sci., Part B: Polym. Phys*. **2006**, 44, 2996–3005
49 Yin, H.; Schönhals, A. *Soft Matter* **2012**, 8, 9132-9139.
50 Yin, H.; Schönhals, A. *Polymer* **2013**, 54, 2067.
51 Tress, M.; Erber, M.; Mapesa, E.; Huth, H.; Müller, J.; Serghei, A.; Schick, C.; Eichhorn, K.; Voit, B.; Kremer, F. *Macromolecules* **2010**, 43, 9937−9944.
52 Boucher, V.; Cangialosi, D.; Yin, H.; Schönhals, A.; Alegria, A.; Colmenero, J. *Soft Matter* **2012**, 8, 5119-5122.
53 Yin, H.; Cangialosi, D.; Schönhals, A. *Thermochim. Acta* **2013**, 566, 186-192.
54 Gao, S.; Koh, Y. P.; Simon, S. L. *Macromolecules* **2013**, 46, 562.
55 Cangialosi, D.; Alegria, A.; Colmenero, J. (Ed.) Schick, C.; Mathot, V. Cooling Rate Dependent Glass Transition in Thin Films and in Bulk. In Fast Scanning Calorimetry (*Springer International*, Switzerland, **2016**) p. 403.
56 Nakanishi, H.; Pincus, P. J. *Chem. Phys.* **1983**, 79, 997.
57 Schmidt, I.; Binder, K. *J. Phys.* **1985**, 46, 1631.
58 Bhatia, Q. S.; Pan, D. H.; Koberstein, J. T. *Macromolecules* **1988**, 21, 2166.
59 Thomas, K. R.; Clarke, N.; Poetes, R.; Morariu, M.; Steiner, U. *Soft Matter* **2010**, 6, 3517.
60 Yin, H.; Madkour, S.; Schönhals. A. *Macromolecules* **2015**, 48, 4936-4941.
61 Madkour, S.; Szymoniak, P.; Heidari, M.; von Klitzing, R.; A. Schönhals. *ACS Appl. Mater. Interfaces.* **2017**, 9, 7535-7546
62 Takahashi, Y.; Suzuki; H.; Nakagawa, Y.; Yamaguchi, M.; Noda, I. *Polym. J.* **1991**, 23, 1333.
63 Van Herwaaden, S. Application note for Xsensor's calorimtere chips of XEN-39390 series http://www.xensor.nl/pdffiles/sheets/nanogas3939.
64 Zhou, D.; Huth, H.; Gao, Y.; Xue, G.; Schick, C. *Macromolecules* **2008**, 41, 7662-7666.
65 Reiter, G.; Hamieh, M.; Damman, P.; Sclavons, S.; Gabriele, S.; Vilmin, T.; Raphael, E. *Nat. Mater.* **2005**, 4, 754-758.
66 S Madkour, S.; Yin, H.; Füllbrandt, M.; Schönhals, A. *Soft Matter* **2015**, 11, 7942-7952.
67 Glynos, E.; Frieberg, B.; Oh, H.; Liu, M.; Gidley, D. W.; Green, P. F. *Phys. Rev. Lett.* **2011**, 106, 128301.
68 Glynos, E.; Frieberg, B.; Chremos, A.: Sakellariou, G.; Gidley, D. W.; Green, P. F. *Macromolecules*, **2015**, 48, 2305.
69 Vogel, H. *Physikalische Zeitschrift* **1921**, 22, 645. Fulcher, G. S.; *J. Am. Cerm. Soc.* **1925**, 8, 339. Tammann, G. W; Hesse*, Anorg. Allg. Chem*. **1926**, 156, 245.
70 Tanaka, K.; Yoon, J.-S.; Takahara, A.; Kajiyama, T. *Macromolecules* **1995**, 28, 934.
71 Ogawa, H.; Kanaya, T.; Nshida, K.; Matsuba, G. *Polymer* **2008**, 49, 2553.
72 Ogawa, H.; Kanaya, T.; Nshida, K.; Matsuba, G. *Polymer Polymer* **2008**, 49, 254.
73 Ermi, B. D.; Karim, A.; Douglas, J. F. *J. Polym. Sci. Part B Polym. Phys.* **1998**, 36, 191.
74 Karim, A.; Slawecki, T. M.; Kumar, S. K.; Douglas, J. F.; Satija, S. K.; Han, C. C.; Russell, T. P.; Liu, Y.; Overney, R.; Sokolov, J.; Rafailovich, M. H. *Macromolecules* **1998**, 31, 857-862.
75 Madkour, S.; Schönhals, A. In preparation.

CHAPTER 10 - Decoupling of Dynamic and Thermal Glass Transition in Thin Films of PVME/PS Blends

*Supporting information is given in Appendix II

DOI: http://dx.doi.org/10.1021/acsmacrolett.7b00625

Abstract

The discussions on the nanoconfinement effect on the glass transition and glassy dynamics phenomena have yielded many open questions. Here, the thickness dependence of the thermal glass transition temperature T_g^{therm} of thin films of a PVME/PS blend is investigated by ellipsometry. Its thickness dependence was compared to that of the dynamic glass transition (measured by specific heat spectroscopy), and the deduced Vogel temperature (T_0). While T_g^{therm} and T_0 showed a monotonous increase, with decreasing the film thickness, the dynamic glass transition temperature (T_g^{dyn}) measured at an accessible frequency showed a non-monotonous dependence that peaks at 30 nm. This was discussed by assuming different cooperativity length scales at these temperatures, which have different sensitivities to composition and thickness. This non-monotonous thickness dependence of T_g^{dyn} disappears for frequencies characteristic for T_0. Further analysis of the fragility parameter, showed a change in the glassy dynamics from strong to fragile, with decreasing film thickness.

10.1. Introduction

Miscible blends of amorphous polymers have attracted much attention in the past decades,[1-6] due to their numerous applications. For optimized applications, an understanding of how blending affects both glass transition and glass dynamics is essential.[7] Generally, the glass transition and the associated glassy dynamics has been a topical challenge in soft matter physics.[8-13]

For miscible binary polymer blends, the observed changes in their properties, compared to the corresponding homopolymers, have been discussed from several points of view.[14,15] Differential scanning calorimetry (DSC) shows a broad thermal glass transition, between that of both components. Here T_g^{therm} is defined as a glass transition temperature measured at the transition from the equilibrium melt state to the non-equilibrium glassy state. Furthermore, blending influences the underlying segmental dynamics (α-relaxation or dynamic glass transition) in two main directions.[7] First, a *symmetric broadening* of the α-relaxation as a function of frequency, compared to that of the homopolymers, is observed. Secondly, unlike the monotonous glass transition evidencing the miscibility of blends, segmental dynamics show *spatial dynamic heterogeneity*. These findings have been discussed by the combined effects of chain connectivity, which results in a self-concentration mechanism, and thermally driven concentration fluctuations.[7] For asymmetric polymer blends, with a large difference in the T_g^{therm} of the components, the dynamic heterogeneity is significantly enhanced. This was elaborated for Poly(methyl ethyl ether) (PVME) / Polystyrene (PS) blends.[5-7,-16,]Confinement of asymmetric miscible polymer blends into thin films leads to extra constrains. For films of few nanometers in thickness, solid interfaces and free surfaces could change local and effective concentrations, glassy dynamics, and the glass transition, from their bulk values. This could then alter macroscopic properties such as adhesion and wettability.[17] Furthermore, the surface tension of each component, with respect to air and the substrate plays an important role because of surface enrichment and preferential adsorption phenomena, which could further alter the compositional heterogeneities.[18] Despite the several studies on related systems, e.g. polymer/solvents and polymer/oligomers on the thickness dependence of the glass transition[19] and glassy dynamics[20] and the length scales[21-22] related to them, polymer/polymer blend films are rarely investigated in literature.

Thickness dependent measurements of the glass transition and glassy dynamics lead to contradicting results even for homopolymers. With decreasing thickness, T_g^{therm} of thin films can deviate substantially from the bulk value, where either an increase or a decrease of T_g^{therm} could be observed, depending on both the polymer and the substrate.[23-26]

The thickness dependence of T_g^{therm} is now generally discussed by an idealized three-layer model, where a spatial dynamically heterogeneous structure across the film is introduced.[27] It consists of a free surface layer, with enhanced dynamics at the polymer/air interface, a bulk-like layer and an irreversibly adsorbed layer at the polymer/substrate interface, with reduced mobility. Upon thickness decrease, the bulk-like layer decreases and the effect of one of the two other layers becomes dominant. Nevertheless, other parameters, e.g. annealing time, molecular weight, packing frustration, etc. should also be taken into account.[28] Although the above mentioned model should also apply for the dynamic glass transition, measured by broadband dielectric or specific heat spectroscopy (SHS)[29-33] and carried out at temperatures > T_g^{therm}, no thickness dependence was observed, in difference to the T_g^{therm}.[34-35]. It is worth to note that the related dynamic glass transition temperature T_g^{dyn} is measured at temperatures above the T_g^{therm} in equilibrium at a given measurement frequency. The different thickness dependencies of T_g^{therm} and T_g^{dyn} were partially discussed by showing that the thickness of the free surface layer decreases with increasing temperatures above T_g^{therm}. Thus, probing its influence on dynamic glass transition becomes difficult, due to the measurement conditions.[36,37]

Recently, the dynamic glass transition of thin films of the PVME/PS blend, with a composition of 25:75 wt%, was measured by SHS.[38] It was shown that T_g^{dyn} measured in the accessible frequency range depends non-monotonously on thickness, where T_g^{dyn} increases with decreasing film thickness, reaching a maximum value at 30 nm. With further decrease of the film thickness, T_g^{dyn} decreases. This result was discussed by elaborating the balance between an adsorbed and a PVME-rich free surface layer. Here, for the first time, the thermal glass transition of identically prepared thin PVME/PS films (200 nm – 8 nm) was measured by ellipsometry. The results were compared to the thickness dependence of the Vogel temperature (ideal glass transition temperature) estimated from the temperature dependence of the segmental dynamics measured by SHS. Furthermore, the fragility parameter is estimated and also discussed in its thickness dependence.

10.2. Experimental Methods

Polymers were purchased from Aldrich Inc. PVME was obtained as an aqueous solution (50-wt.%, M_w 10,455 g/mol, PDI=3). PS has a M_w of 524 kg/mol and a PDI of 1.04. A concentrated polymer solution of PVME and PS with the weight ratio of 25 to 75 was prepared as master solution in toluene. The thermal T_gs of the bulk materials were determined by DSC (10 K/min, second heating run) and were found to be 246 K, 376 K and 293 K for dried PVME (SI), PS, and PVME/PS 25:75-wt%, respectively.

Thin films were spin coated from diluted PVME/PS solutions, prepared from the same master solution. To ensure the removal of the stress induced during spin coating and any residual solvent,[39] all samples were annealed at $T_{g,Bulk}$+ 50 K for 72 h, in an oil-free vacuum. For the cleaning procedure of the wafers, spin coating conditions, and film thicknesses estimation see SI (figure S1 and S2). It was shown in reference [33 and 38] that these preparation conditions also lead to the formation of an immobilized layer adsorbed at the substrate with a thickness of ca. 4 nm (see below). For a further discussion of the different substrates used for SHS and ellipsometry, see SI.

Measurements were carried out by a polarizer-compensator sample analyzer (PCSA) ellipsometer (Optrel GbR, Sinzing, Germany) with a heating stage attached (for measurement conditions see SI). The ellipsometric angles $\psi(\lambda)$ and $\Delta(\lambda)$ were analyzed using a multilayer model (SI). Figure S3 shows the real and imaginary parts of the index of refraction including fits to the data. The obtained thicknesses are optical thicknesses, which are in good agreement with the ones measured by AFM (figure S1).

10.3. Results and Discussion

Figure 10.1 depicts the film thickness as a function of temperature for 9, 28, and 50 nm thick films. T_g^{therm} is defined as the intersection of the linear dependencies of the thickness in the supercooled and glassy regimes in accordance with literature procedures.[24,40]

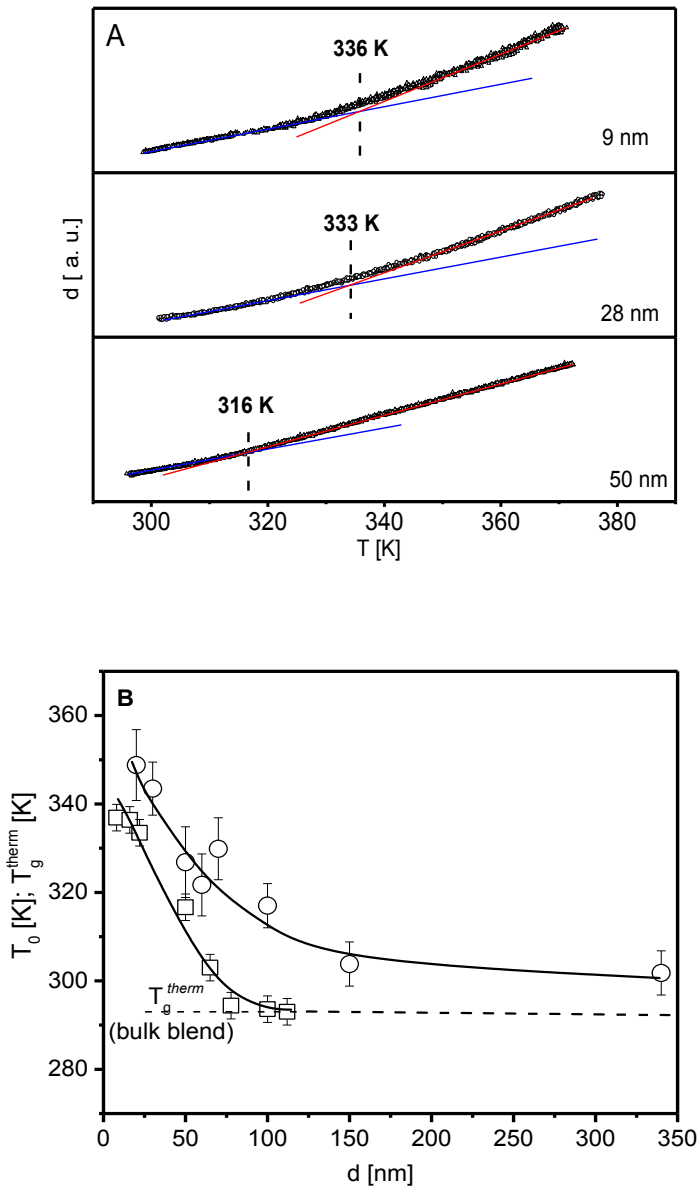

Figure 10.1. (A) *Thickness d as a function of temperature for the indicated film thicknesses. The dashed line marks* T_g^{therm}. **(B)** *Thickness dependency of* T_g^{therm} *– squares- and* T_0 *– circles. Typical error bars are given. The solid lines are guides for the eyes, while the dashed dotted line represents* $T_{g,DSC}^{therm}$ *of the bulk PVME/PS blend.*

The decrease in T_g^{therm} with decreasing film thickness for pure PS thin films on silicon is well established.[35,34,41] For the used PVME, preliminary results reveal that T_g^{therm} increases by 6 K with decreasing film thickness, down to 20 nm (Fig S4). Figure 10.1B shows that T_g^{therm} increases with decreasing film thickness down to 9 nm by approximately 50 K (experimental error ca. ± 3 K). This behavior is different from that reported for the dynamic glass transition measured for identically prepared PVME/PS films, probed by SHS in the

frequency range from 10 Hz to 10^4 Hz.[38] For the method and data analysis, see references [29,42]. The results are summarized in the relaxation map (figure 10.2), where the relaxation rate f_p is plotted versus inverse temperature. At the first glance, comparing only the data for 340 nm and 30 nm, the dynamic glass transition is shifted to higher temperatures for the thinner film. For films with 20 nm and 10 nm thicknesses, the segmental dynamics is then shifted back to lower temperatures. A closer inspection of the data for the 10 nm film reveals that there is a kind of crossover phenomenon defined by a crossing of the temperature dependence of the relaxation rates measured for the 10 nm film, with regard to the film of 340 nm. Such a crossover is also observed for films with thicknesses of 100 and 70 nm. At the moment, it is not clear whether this crossover behavior has a deeper meaning or not. On the one hand, if the former case is true, this observation might have some fundamental implications concerning the dynamic and thermal glass transition in thin films. On the other hand, such a crossover was not observed neither for homopolymers[29,30,31] nor for thin films of PVME/PS with a composition of 50:50 wt-%.[37] Therefore, further experimental investigations are necessary, including other blend systems, to draw further conclusions.

To discuss this thickness dependence, we consider $T_{g,320\,Hz}^{dyn}$ measured at a frequency of 320 Hz (inset figure 10.2), as an example. (Data for other frequencies 1720 Hz, 80 Hz, and 1 Hz are given in figure S5). For all measured frequencies, the corresponding T_g^{dyn} shows in principle the same thickness dependence as discussed here for 320 Hz. $T_{g,320\,Hz}^{dyn}$ increases with decreasing film thickness down to 30 nm. The maximum value reached at 30 nm is close to $T_{g,320\,Hz}^{dyn}$ of pure PS. With further decrease in thickness $T_{g,320\,Hz}^{dyn}$ decreases.

This behavior was discussed by considering that a PVME-rich layer forms at both interfaces. To confirm this assumption, X-ray Photoelectron Spectroscopy (XPS) measurements were carried out to estimate the PVME concentration at the free surface and the adsorbed layer. The PVME concentration at the free surface of film, was found to be 76 wt% (figure S6), whereas in the adsorbed layer it was estimated to be 100 wt% (figure S7). For the latter measurements, a second set of samples were used, where solvent leaching experiments were conducted to remove the bulk-like part of the film.[43] For further details on the XPS measurements as well as the solvent leaching experiments, see SI. These results are in agreements with literature data.[44,45]

In the light of this finding and due to mass conservation, a PS-rich layer in the middle of the film is formed. This PS-rich middle layer will have a slower segmental dynamics than the

as-formulated blend, leading to an increase in T_g^{dyn} till a thickness of 30 nm. This model is supported by the fact that the film with a thickness of 30 nm has a T_g^{dyn} close to that of pure PS.

For thicknesses lower than ca. 30 nm, the thicknesses and the composition of all 3 idealized layers are subjected to further changes leading to the observed decrease of T_g^{dyn}. Interestingly, at the lowest film thickness, T_g^{dyn} reaches a value which close to the value of the bulk. This would indicate that the averaged composition of the whole film is as formulated.

Further, here the Vogel/Fulcher/Tammann (VFT-) equation[46]

$$\log f_p = \log f_\infty - \frac{DT_0}{T - T_0} \tag{9.1}$$

is fitted to the data (figure 10.2). f_∞ is a fitting parameter and T_0 is the Vogel temperature. The parameter D is called the fragility parameter. It provides a quantity to classify glass-forming systems. The fitting was done in a two-step procedure. In the first step, all parameters were kept free. No systematic thickness dependence was obtained for log f_∞. To reduce the statistical error, in the second fitting step, the arithmetic average of log f_∞ was calculated and kept fixed during the fitting. Both procedures lead to similar thickness dependencies of T_0 and D. All parameters are summarized in Table S1 and S2.

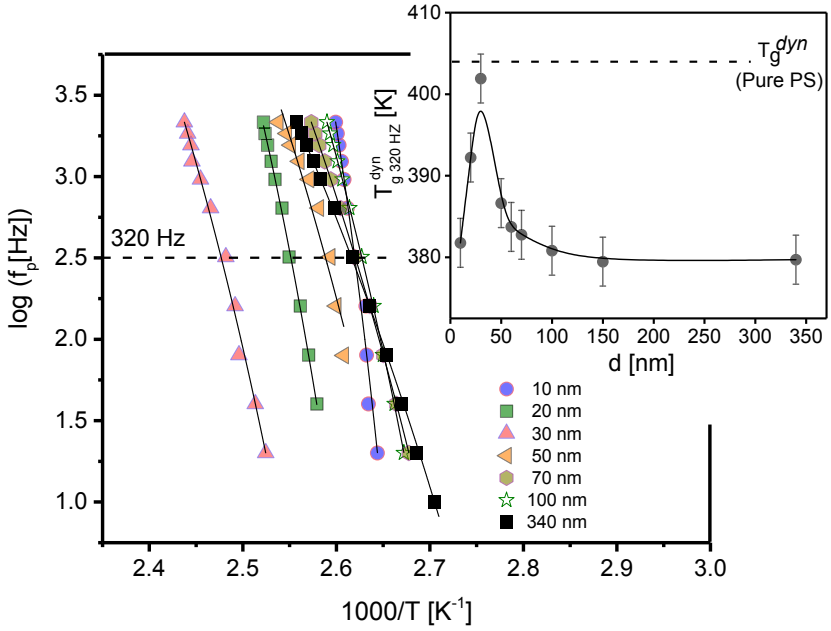

Figure 10.2. *Relaxation map of PVME/PS films for the indicated film thicknesses. The solid black lines are fits of the VFT equation to the corresponding data*. **Inset.** $T_{g,320\ Hz}^{dyn}$ *versus film thickness for PVME/PS blend films as an example. The line is guide for the eyes. The data were taken from reference [38].*

Table S1 reveals that T_0 depends on confinement. In difference to $T_{g,320\ Hz}^{dyn}$, it increases with decreasing film thickness, similar to the thickness dependence of T_g^{therm}. A comparable difference in the thickness dependence of T_0 and T_g^{dyn} was found for other systems.[47,48] Figure 10.1B depicts T_0 and T_g^{therm} as a function of thickness. Both temperatures increase with decreasing film thickness, contrary to the thickness dependence of T_g^{dyn} (inset figure 10.2). It should be noted that a similar decoupling of dynamic and thermal glass transition temperature was observed for other systems,[34,49] as it was also discussed in review publications.[28,50]

Now the question arises, *why do* T_g^{dyn} *measured at an accessible frequency and* T_0 *have different thickness dependencies, although both quantities were obtained from the same measurement?* As T_0 results from a dynamic measurement, it has a similar thickness dependence than T_g^{therm} estimated by ellipsometry (figure 10.1B). The segmental dynamics is not completely unrelated, which might be falsely concluded from the observed decoupling phenomenon. From the theoretical point of view, the glass transition is not completely understood till now.[13] Several theoretical approaches have been developed to understand the glass transition phenomenon. For an overview, see for instance references [8-11]. The

cooperativity approach to the glass transition was pioneered by Adam and Gibbs.[51] In the frame of the cooperativity approach to the glass transition,[52] the slowing down of glassy dynamics is described by a correlation length, which increases with decreasing temperatures.[53,54] At T_0, this correlation length is supposed to diverge. It is worth to note that dielectric measurements on blends have been used to estimate the cooperativity length for glassy dynamics also in its temperature dependence employing the temperature driven concertation fluctuation model.[55-57] Moreover, it was shown that this picture of cooperativity has relevance for confined systems.[58,59] The cooperativity approach is now used to discuss the different thickness dependencies of T_g^{dyn} and T_0. The SHS measurements were carried out at relatively high frequencies, which means at higher temperatures compared to T_g^{therm} and T_0. According to the theoretical approaches, at these temperatures, the cooperativity length scale is expected to be small compared to its value at T_g^{therm} or T_0. In other words, the comparison between the three different temperatures could elaborate the different sensitivities, of the different length scales, to changes in thickness and/or composition. At T_g^{dyn}, the cooperative length might be too small to be influenced by the change in thickness. Nevertheless, it is sensitive to compositional heterogeneities and senses the influence of the free surface layer at the air/polymer interface. At T_g^{therm} or T_0, the cooperativity length scale should be larger. Therefore, it becomes sensitive to thickness changes as well as to the influence of the adsorbed immobilized layer, which provides an additional glassy interface. In other words, the different thickness dependencies of the dynamic and thermal glass transition might also be a result of the different length scales, due to the different frequencies relevant for T_g^{dyn} and T_g^{therm} or T_0.

If these considerations have some relevance, the peak observed in the thickness dependence of T_g^{dyn} should disappear for frequencies, which are relevant for T_g^{therm} or T_0. These frequencies are not accessible in SHS measurements. To characterize the height of the peak $\Delta T_g^{dyn} = T_g^{dyn}(30\,nm)$ - $T_g^{dyn}(10\,nm)$ is considered in its frequency dependence (see figure 10.3A). ΔT_g^{dyn} decreases with decreasing frequency and reaches an extrapolated value of zero, at a frequency of 10^{-3} Hz. This means that for these frequencies, which are characteristic for T_g^{therm}, the peak observed in the thickness dependence of T_g^{dyn} disappears and the thickness dependence of T_g^{dyn} recovers that of T_g^{therm} and T_0.

In addition to T_g^{therm} and T_0, the fragility parameter D depends on film thickness; where D decreases with decreasing thickness (figure 10.3B). This means that the glassy dynamics of the films changes with decreasing thickness from a stronger to a fragile behavior.[60] A similar behavior was observed for thin films of a homopolymer by dielectric spectroscopy.[48] It should be noted that also an increase in the fragility with decreasing film thickness was observed.[24]

Extrapolating the thickness dependence of the fragility parameter to zero would yield a critical length scale value of ca. 5 nm (figure 10.3B). In the case that this is a valid extrapolation, this would point out to a dramatic change in the mechanism of the underlying molecular motions at this length scale. Interestingly, the fragility parameter becomes zero at approximately the same length scale, where $\Delta U_R \sim \Delta C_p \sim$ thickness, becomes zero indicating the formation of an immobilized layer at the substrate (fig S8),[37,38] which is further confirmed by XPS here.

10.4. Conclusion

In conclusion, the thicknesses dependencies of T_g^{therm} and T_g^{dyn} for thin films of PVME/PS 25:75 wt% blend were measured by ellipsometry and SHS,[38] respectively. Surprisingly, T_g^{dyn} measured at an accessible frequency shows a non-monotonous thickness dependence that peaks at 30 nm, T_0, deduced from the temperature dependence of the dynamic glass transition, showed a monotonous increase with decreasing thickness. The thickness dependence of T_0 was found to be similar to that of T_g^{therm}. The different thickness dependencies observed for T_g^{therm}, $T_g^{dyn}$and T_0 were linked to the different cooperativity length scales, related to the three temperatures. It was shown that the non-monotonous thickness dependence disappears at frequencies characteristic for T_0 or T_g^{therm}. Therefore, the thickness of T_0 is recovered for T_g^{dyn} measured at these extrapolated low frequencies. Further analysis of the fragility parameter, confirmed the conclusion, where the glassy dynamics of the thin films changed from fragile to strong, with decreasing film thickness.

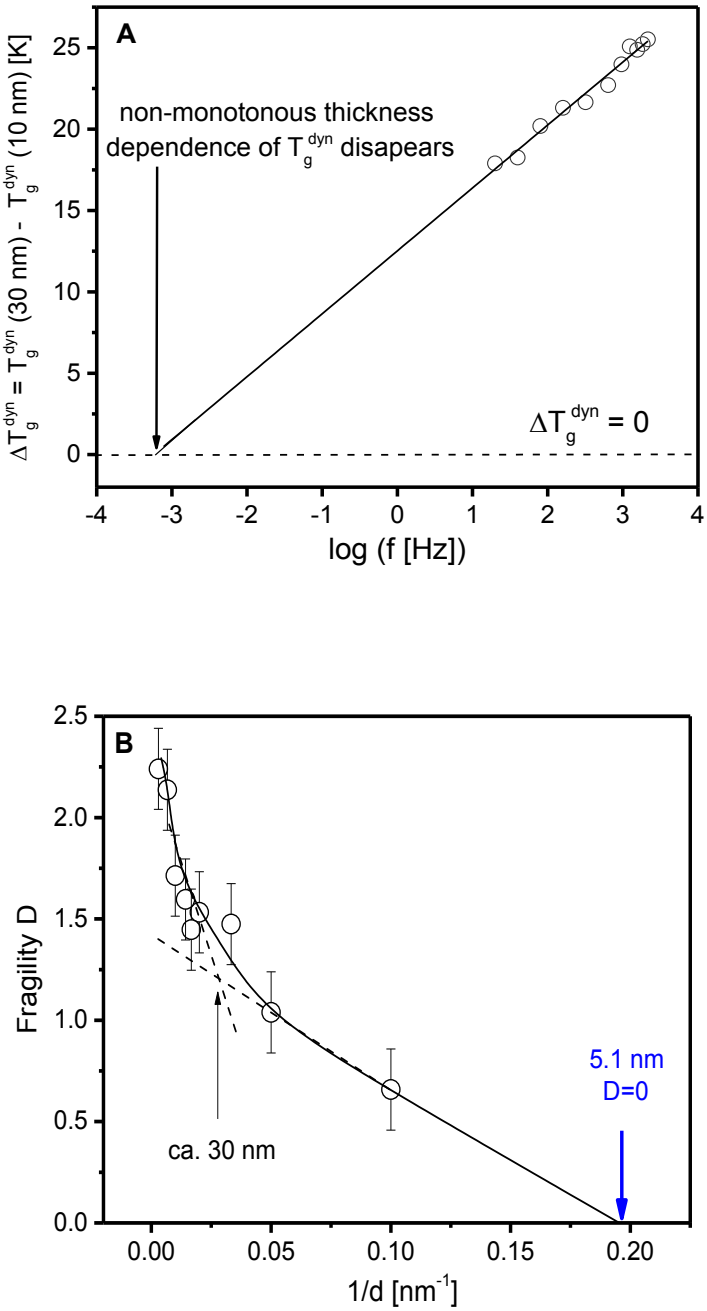

Figure 10.3. (A) ΔT_g^{dyn} *as function of the measuring frequency. The line is a linear regression to the data.* **(B)** *Fragility parameter D vs. inverse film thickness. The solid line is a guide for the eyes.*

References

1 Alegria, A.; Colmenero, J.; Ngai, K. L.; Roland, C. M. *Macromolecules* **1994**, *27*, 4486-4492.
2 Cendoya, I.; Alegria, A.; Alberdi, J. M.; Colmenero, J.; Grimm, H.; Richter, D.; Frick, B. *Macromolecules* **1999**, *32*, 4065-4078.
3 Takeno, H.; Kobayashi, M.; Aikawa, T. *Macromolecules* **2006**, *39*, 2183-2190.
4 Colby, R. H.; Lipson, J. E. G. *Macromolecules* **2005**, *38*, 4919-4928.
5 Alvarez, F.; Alegria, A.; Colmenero, J. *Macromolecules* **1997**, *30*, 597-604.
6 Arbe, A.; Alegria, A.; Colmenero, J.; Hoffmann, S.; Willner, L.; Richter, D. *Macromolecules* **1999**, *32*, 7572-7581.
7 Colmenero, J.; Arbe, A. *Soft Matter*, **2007**, *3*, 1474-1485.
8 Debenedetti, P. G.; Stillinger, F. H. *Nature* **2001**, *410*, 259–267.
9 Anderson, P. W. *Science* **1995**, *267*, 1617.
10 Ediger, M.; Harrowell, P. *J. Chem. Phys.* **2012**, *137*, 080901-080915.
11 Sastry, S.; Debenedetti, P. G.; Stillinger, F. H. *Nature* **1998**, *393*, 554-557.
12 Yin, H.; Madkour, S.; Schönhals, A. *Dynamics in confinement: Progress in Dielectrics*; Springer vol. 2. **2014**, Kremer, F. (Ed.).
13 McKenna, G.; Simon, S. *Macromolecules* **2017**, DOI: 10.1021/acs.macromol.7b01014.
14 Yin, H.; Schönhals, A.; *Polymer Blends Handbook;* Springer: Netherlands, **2014**, Utracki, L.; Wilkie, C. (Ed.)
15 Ngai, K.; Capaccioli, S. *J. Chem. Phys*. **2013**, *138*, 054903.
16 He, Y.; Lutz, T. R.; Ediger, M. D. *J. Chem. Phys.* **2003,** *119*, 9956-9965.
17 Napolitano, S.; Pilleri, A.; Rolla, P.; Wübbenhorst, M. *ACS Nano* **2010,** *4*, 841-848.
18 Jones, R. A. L.; Kramer, J. *Polymer* **1993**, *34*, 115-118.
19 Mangalara, J.; Simmons, D. *ACS Macro Lett*. **2015**, 4, 1134−1138.
20 Psurek, T.; Soles, C.; Page, K.; Cicerone, M.; Douglas, J. *J. Phys. Chem. B* **2008**, 112, 15980– 15990.
21 Ellison, C.; Ruszkowski, R.; Fredin, N.; Torkelson, J. *Phys. Rev. Lett.* **2004**, 92, 095702.
22 Riggleman, R.; Douglas, J.; de Pablo, J. *J. Phys. Rev. E* **2007**, 76, 011504.
23 Lupaşcu, M.; Picken, S.; Wübbenhorst, M. *J. Non-Cryst. Solids* **2006,** *352*, 5594-5600.
24 Fakhraai, Z.; Forrest, J. *Phys. Rev. Lett.* **2005,** *95*, 025701.
25 Sharp, J. S.; Forrest, J. *Phys. Rev. Lett*. **2003,** *91*, 235701.
26 Wang, J.; McKenna, G. B. *J. Polym. Sci., Part B: Polym. Phys.* **2013**, 51, 1343− 1349.
27 Ediger, M.; Forrest, J. A. *Macromolecules* **2014,** *47*, 471-478.
28 Napolitano, S.; Glynos, E.; Tito, N. B. *Rep. Prog. Phys.* **2017**, *80*, 036602.
29 Huth, H.; Minakov, A. A.; Schick, C. *J. Polym. Sci., Part B: Polym. Phys.* **2006,** 44, 2996-3005.
30 Yin, H.; Schönhals, A. *Soft Matter* **2012,** *8*, 9132-9139.
31 Yin, H.; Schönhals, A. *Polymer* **2013,** *54*, 2067-2070.
32 Tress, M.; Erber, M.; Mapesa, E. U.; Huth, H.; Müller, J.; Serghei, A.; Schick, C.; Eichhorn, K. J.; Voit, B.; Kremer, F. *Macromolecules* **2010,** *43*, 9937-9944.
33 Madkour, S.; Szymoniak, P.; Heidari, M.; von Klitzing, R.; A. Schönhals. *ACS Appl. Mater. Interfaces.* **2017**, 9, 7535-7546.
34 Boucher, V. M.; Cangialosi, D.; Yin, H.; Schönhals, A.; Alegria, A.; Colmenero, J. *Soft Matter* **2012,** 8, 5119-5122.
35 Yin, H.; Cangialosi, D.; Schönhals, A. *Thermochim. Acta* **2013,** *566*, 186-192.
36 Paeng, K.; Swallen, S.; Ediger, M. *J. Am. Chem. Soc.* **2011**, *133*, 8444–8447.
37 Yin, H.; Madkour, S.; Schönhals. A. *Macromolecules* **2015**, 48, 4936-4941.
38 Madkour, S.; Szymoniak, P.; Schick, C.; Schönhals. A. *J. Chem. Phys.* **2017**, *146*, 203321.
39 Reiter, G.; Hamieh, M.; Damman, P.; Sclavons, S.; Gabriele, S.; Vilmin, T.; Raphael, E. *Nat. Mater*. **2005,** *4*, 754-758.
[40] Glor, R.; Composto, J.; Fakhraai, Z. *Macromolecules*, **2015**, 48, 6682–6689.
41 Yoon, H.; McKenna, G. B. *Macromolecules* **2014**, 47, 8808−8818.
42 Madkour, S.; Yin, H.; Füllbrandt, M.; Schönhals, A. *Soft Matter* **2015,** 11, 7942-7952.
43 Napolitano, S.; Wübbenhorst, M. Nat. Commun. 2011, 2, 260.
[44] Ermi, B. D.; Karim, A.; Douglas, J. F. *J. Polym. Sci. Part B Polym. Phys*. **1998,** *36*, 191-200.
[45] Karim, A.; Slawecki, T. M.; Kumar, S. K.; Douglas, J. F.; Satija, S. K.; Han, C. C.; Russell, T. P.; Liu, Y.; Overney, R.; Sokolov, J.; Rafailovich, M. H. *Macromolecules* **1998,** *31*, 857-862.
46 Vogel, H. *Physikalische Zeitschrift*. **1921,** *22*, 645-646. Fulcher, G. S. *J. Am. Ceram. Soc.* **1925,** *8*, 339-355. Tammann, G.; Hesse, W. Z. *Anorg. Allg. Chem*. **1926,** *156*, 245-257.
47 Napolitano, S.; Lupascu, V.; Wübbenhorst, V. *Macromolecules* **2008,** *41*, 1061-1063.
48 Labahn, D.; Mix, R.; Schönhals, A. *Phys. Rev. E.* **2009**. 79, 011801-011809.

49 Fukao, K.; Miyamoto, Y. *Phys. Rev. E* **2000**, 61, 1743.
50 Priestey, R. D.; Cangialoso, D.; Napolitano, S. *J. Non-Cryst. Solids* **2015**, 407, 288-295.
51 Adam, G.; Gibbs, J.H. *J. Chem. Phys.* **1965**, 43, 139-146.
52 Donth, E.-J., *Springer*: Berlin, **2001.**
53 Berthier, L.; Biroli, G.; Bouchaud, J.-P.; Cipelletti, L.; El Masri, D.; L'Hôte, D.; Ladieu, F.; Pierno, *Science* **2005**, 310, 1797-1800.
54 Saiter, A.; Delbreilh, L.; Couderc, H.; Arabeche, K.; Schönhals, A.; Saiter, J.-M. *Phys. Rev. E*. **2010**, 81, 041805.
[55] Katana, G.; Zetsche, A.; Kremer, F.; Fischer, E. W. *ACS Polymer Preprints* **1992**, 33, 122-123.
[56] Katana, G.; Fischer, E. W.; Hack, T.; Abetz, V.; Kremer, F. *Macromolecules* **1995**, 28, 2714-2722.
57 Kumar, S. K.; Colby, R. H.; Anastasiadis, S. H.; Fytas, G. *J. Chem. Phys.* **1996**, 105, 3777-3788.
58 Zhang, C.; Guo, Y.; Priestley, R. D. *ACS Macro Lett*. **2014**, 3 (6),501−505.
59 Salez, T.; Salez, J.; Dalnoki-Veress, K.; Raphaël, E.; Forrest, J. *PNAS*, 2015, 112, 8227-8231.
60 Böhmer, R.; Nagi, K. L; Angell, C. A.; Plazek, D.J. *J. Chem. Phys*. **1993**, 99, 4201-4209.

CHAPTER 11 - Unraveling the Dynamics of Nanoscopically Confined PVME in Thin Films of a Miscible PVME/PS Blend

*Supporting information is given in Appendix III

DOI: http://dx.doi.org/10.1021/acsami.7b10572

Abstract

Broadband dielectric spectroscopy (BDS) was employed to investigate the glassy dynamics of thin films (7 – 200 nm) of a Poly (vinyl methyl ether) (PVME) / Polystyrene (PS) blend (50:50 wt%). For the BDS measurements, Nano-Structured Capacitors (NSC) were employed, where films are allowed a free surface. This method was applied for film thicknesses up to 36 nm. For thicker films, samples were prepared between Crossed Electrodes Capacitors (CEC). The relaxation spectra of the films showed multiple processes. The first process was assigned to the α-relaxation of a bulk-like layer. For films measured by NSC, the rates of the α-relaxation were higher compared to that of the bulk blend. This behavior was related to a PVME-rich free-surface layer at the polymer/air interface. A second process was observed for all films measured by CEC (process X) and the 36 nm film measured by NSC (process X2). This process was assigned to fluctuations of constraint PVME segments by PS. Its activation energy was found to be thickness dependent, due to the evidenced thickness dependency of the compositional heterogeneity. Finally, a third process with an activated temperature-dependence was observed for all films measured by NSC (process X1). It resembled the molecular fluctuations in an adsorbed layer found for thin films of pure PVME, thus it is assigned accordingly. This process undergoes an extra confinement due to frozen adsorbed PS segments at the polymer/substrate interface. To our knowledge, this is the first example where confinement induced changes were observed by BDS for blend thin films.

11.1. Introduction

In recent years, research on nanoscale confinement of polymers has witnessed topical investigations in attempt to tune polymer properties on demand.[1] One of the most studied forms of nanoconfinement are thin films, where confinement results from a reduction of the film thickness. For these systems, it is crucial to understand how confinement affects the glass transition phenomenon and the associated glassy dynamics, compared to the bulk behavior. This is due to the direct impact of these phenomena on many thin film-based technologies.[2-7] It has been observed that the thermal glass transition temperature (T_g^{therm}) of thin films of homopolymers and of polymer blends,[8-11] could deviate substantially from the bulk value. Please note that T_g^{therm} is defined here as the temperature measured by so-called static methods, e.g. ellipsometry,[12,13] fluorescence spectroscopy,[10] and dielectric expansion dilatometry,[14,15] where the system falls out of thermodynamic equilibrium from an equilibrium melt state to a non-equilibrium glassy state.[1,4] The thickness dependence of T_g^{therm} is now generally discussed by a idealized three-layer model.[1,12] This model considers a spatial dynamically heterogeneous structure across the film thickness, consisting of three idealized layers: I) A free surface layer with enhanced molecular dynamics at the polymer/air interface, II) a bulk-like layer in the middle of the film, and III) an irreversibly adsorbed layer at the polymer/substrate interface with a reduced mobility. With decreasing film thickness, the thickness of the bulk-like layer decreases and the effect of the remaining layers become dominant.[16] However, the prevalence of their effect is also correlated to other parameters for instance annealing time, molecular weight, packing frustration, and/or interfacial interactions with the substrate. The influence of these parameters was recently reviewed in reference [17].

Interestingly, the α-relaxation related to segmental dynamics (which can be characterized by a dynamic glass transition temperature T_g^{dyn}) of thin homopolymer films showed no thickness dependence, despite the fact that the three-layer model and the above-mentioned parameters should still apply. Note that T_g^{dyn} is estimated at temperatures above T_g^{therm} in thermodynamic equilibrium, by techniques that explore the segmental mobility, e.g. dielectric,[18-20] and specific heat spectroscopy (SHS).[21-23] This contradiction between the thickness dependence of T_g^{therm} and T_g^{dyn}has been partially conferred by showing that the molecular dynamics of the free surface layer becomes indistinguishable from that of the

bulk-like layer, at temperatures above T_g^{therm}. Thus, probing its influence on the dynamic glass transition becomes difficult, due to the measurement conditions.[16]

Aside from homopolymers, miscible polymer blends attract a lot of interest due to their numerous applications.[24] Generally, it is well accepted that the segmental dynamics of miscible polymer blends is affected in two main directions:[24] I) *symmetric broadening* of the relaxation functions compared to that of both homopolymers and II) *spatial heterogeneity* of the molecular dynamics. These experimental results are discussed by combining two sets of models: the self-concentration and the thermally driven concentration fluctuations model.[24] The mechanisms behind these models lead to a distribution of local glass transitions and relaxation times, due to spatial regions, which have different local compositions, compared to the average one.

Till now, investigations of the glassy dynamics of thin films of miscible polymer blends have not received the same attention as bulk blends, although their thin films could lead to new applications.[25] One has to consider that these systems are more complex than the homopolymers, due to the fact that even for the well-studied bulk blends, the molecular mobility is not completely understood. [26-39]

Here, the glassy dynamics of the bulk and of thin films of the miscible blend of Polystyrene (PS)/Poly(vinyl methyl ether) (PVME) with a composition of 50:50 wt% is investigated by Broadband Dielectric Spectroscopy (BDS). The used PVME/PS blend is asymmetric, with regards to the dipole moments, the glass transition temperatures (ΔT_g^{therm} = 130 K), and the molecular weights (1:50 folds) of both homopolymers. First, PS has a much weaker dipole moment compared to PVME, thus BDS measurements sense mainly the segmental dynamics of PVME, as affected by PS.[25,2828,31] Secondly, the asymmetry in the thermal glass transition temperatures and the molecular weights would enhance the dynamic heterogeneity. Further, the so-called surface enrichment phenomenon becomes important,[40] where the composition of the surface becomes dominated by the component with the lower surface tension with respect to air, to lower the Gibbs free energy of the whole system. For PVME/PS, PVME gets enriched at the surface, forming a self-assembled PVME-rich layer. This was evidenced for bulk blends by X-ray Photoelectron Spectroscopy (XPS)[41] and ellipsometry[42]. Recently,[43] it was shown, by a combination of SHS and XPS that for thin films of PVME/PS with a composition of 50:50 wt% (identical to the polymer blend used in this work), that the surface layer leads to a systematic decrease of T_g^{dyn} with decreasing

film thickness, at temperatures well above T_g^{therm} of the blend. Hence, the chosen system could also allow studying the influence of the mobile surface layer on the dielectric α-relaxation, which cannot be probed for thin films of homopolymers.

Besides the free surface, the dynamics and compositional heterogeneity at the polymer/substrate interface, are not completely understood. Granick et al. showed that for any non-repulsive polymer/substrate interaction, an irreversibly adsorbed thin layer, stabilized by the chain connectivity, is expected to form at the polymer/substrate interface.[44-46] Furthermore, Housmans et al.[47] revealed a spatially heterogeneous structure within such an adsorbed layer. The growth kinetics of this layer has a two-step adsorption regime with different time dependencies. At shorter times, the adsorption kinetics follows a linear time dependence, where the polymer segments adsorb directly to the substrate, at an energy cost of k_BT (k_B is Boltzmann's constant). This yields a "strongly-bounded" adsorbed layer,[48,49] with a higher density compared to that of the bulk.[50,51] At a crossover time, the kinetics of the adsorption process changes to a logarithmic time dependence. There, the adsorbed layer further grows by diffusion and/or changes in the conformation of the chains through the already existing layer, on the expense of their entropy. It should be noted here that the research on adsorbed polymer layers is not only academic but is also relevant to various applications.[52] For thin films of miscible polymer blends, such a spatially heterogeneous layer could directly influence the segmental dynamics and compositional heterogeneity of the whole film.

The segmental mobility of PVME and PS components as well as that of thin films of their blend was recently studied by SHS.[43] The segmental dynamics of pure PVME thin films was also recently investigated by a combination of BDS and SHS,[53] where two relaxation processes were found. Besides an expected α-relaxation with a bulk-like behavior, detected by both BDS and SHS, a second process with a completely different temperature dependence of the relaxation rates was observed. This relaxation process, detected only by BDS, was assigned to constraint segmental fluctuations in an irreversibly adsorbed layer at the polymer/substrate interface. Here, the dynamics of PVME segments as affected by PS for thin films of a PVME/PS blend with a composition of 50:50 wt% is studied and quantitatively compared to that of the pure PVME thin films.

11.2. Experimental Section

Materials

Polymers were purchased from Aldrich Inc. The PS had a molecular weight (M_w) of 524 kg/mol and a PDI of 1.04. PVME with a M_w of 10,455 g/mol and a PDI of 3 was obtained as a 50 wt % aqueous solution. For the sample preparation, PVME was dried in an oil free vacuum for 72 h at 303 K, then for another 96 h at 323 K. A concentrated polymer solution of PVME and PS with the weight ratio of the polymers of 50 to 50 wt% was prepared as master solution using toluene. A bulk film was prepared by casting from the master solution. The film was then dried in an oil free vacuum for 72 h at 313 K, then for another 96 h at 343 K. The T_g^{therm} of the bulk materials were determined by differential scanning calorimetry (DSC, 10 K/min, second heating run) to be 376 K, 246 K, and 273 K for PS, PVME, and PVME/PS 50:50 wt%, respectively. Thin films were prepared by spin coating. The film thickness was attuned by the concentration of the polymer solution. The diluted solutions were all prepared from the same master solution by the addition of toluene.

Spin coating and annealing procedure

Thin films were prepared by spin coating in a flow box to insure a dust-free atmosphere. The diluted solutions were filtered (Minipore, 0.2 μm) and then spin coated at a rotational speed of 3000 rpm and for 60 s. After the spin coating process, the samples were dried in an oil-free vacuum (10^{-4} mbar) and annealed at 323 K ($T_{ann}=T_{g,Bulk}+50$ K) for 72 h. This annealing procedure insures two main points: I) the removal of the solvent and II) the release of the induced stress during spin coating.[54] It is important to note that the quality of the topography of the films was controlled by AFM. All films showed low roughness and no dewetting or inhomogeneity down to 7 nm (see figure S1).

Methods and Sample preparation

Broadband dielectric spectroscopy (BDS): The dielectric properties of samples were characterized by a high-resolution ALPHA analyzer (Novocontrol) including a sample holder with an active head. The complex dielectric permittivity $\varepsilon^*(f) = \varepsilon'(f) - i\varepsilon''(f)$ was measured as a function of frequency f (range from 10^{-1} to 10^7 Hz). Here ε' and ε'' denote the real and imaginary (loss) part of the complex dielectric function, respectively. $i = \sqrt{-1}$ is the imaginary unit. The temperature of the samples was controlled by a Quatro cryosystem (Novocontrol), interfaced to the cryostat. The temperature stability is better than 0.1 K. Please note that all measurements took place in dry nitrogen atmosphere. For more experimental details, the reader is referred to reference [55].

Sample preparation:

Bulk samples: A bulk sample was prepared by melting the dried casted bulk film of PVME/PS between the contacting electrodes (two round gold plated brass electrodes with a diameter of 20 mm) in parallel plate geometry (see figure 11.1B-inset). Fused silica spacers were employed to control the sample thickness to be 50 μm.

Thin films:

Crossed electrodes capacitors (CEC) were used to measure capped films (see figure 11.2B-inset). A detailed description of the CEC and its preparation can be found in references [14,53]. In short, for CEC, films were spin coated on a thoroughly cleaned glass substrate with a flash-evaporated Al-electrode strip, (deposition rate >30 nm/s, strip width 2 mm, height 60 nm). This procedure was followed by the annealing of the films, according to the protocol given above. Finally, a second Al-electrode was thermally evaporated on top, perpendicular to the first one. The Al-strips are the two electrodes of the capacitor and the crossing region of the two Al-electrodes with the spin coated film defines the capacitor.

Nano-Structured capacitors (NEC) were used to measure supported films (see figure 4A-inset). A detailed description of this recently developed sample arrangement can be found in references [56,57]. The exact cleaning and sample preparation protocol followed can be found in references [53,56]. In short, for NSC, thin films were spin-coated on a thoroughly cleaned ultra-flat highly conductive silicon wafer. The sample preparation was finalized by placing a wafer, with nanostructured SiO_2 nano-spacers with heights of 35 nm or 70 nm, on top of the film. This procedure results in supported films with a free polymer/air interface.

Film thickness estimation:

A Cypher Atomic Force microscope (AFM) (Asylum Research, Santa Barbara, CA, USA) employing silicon cantilevers with a reflective coating of aluminum (AC160TS, Oxford Instruments) were used to measure the film thickness. For the *CEC*, the thickness of the first deposited Al-electrode was measured by estimating the step height of a scratch across it. After spin coating and annealing of the polymer film, the step height of a second scratch, obtained by cutting through the film on top of the Al-electrode, was measured. The film thickness was calculated as the difference between these two measurements.

NSC: Film thicknesses were estimated by AFM as described above, as well as by ellipsometry.

An ellipsometer based on a polarizer-compensator sample analyser (PCSA) (Optrel GbR, Sinzing, Germany) was used. Measurements were done at a fixed angle of incidence of 70

degrees, employing a laser light with a wavelength of 632.8 nm. The measurements were analysed using a multilayer model consisting of air/polymer film/SiO_2/Si-substrate. To minimise the number of fit parameters, firstly the thickness of the SiO_2 layer was estimated before spin coating the polymer film. This value (ca. 1.7 nm) was kept constant during the data analysis for the polymer film. A linear increase of the film thickness with the concentration of the solution was obtained, which is expected. Furthermore, the ellipsometry measurements agree with the AFM data (see figure S2).

11.3. Results and Discussion

Broadband Dielectric spectroscopy (BDS) senses the dipole fluctuations within a material. Figure 11.1A depicts a 3D plot of the dielectric loss spectra as a function of frequency and temperature for the bulk blend sample. Several dielectrically active processes are observed: I) At higher temperatures, the α-relaxation (dynamic glass transition), related to the cooperative segmental fluctuation, II) below the T_g^{therm}, a further peak starts to emerge during cooling. This process is assigned to the α´-relaxation, which is related to the restricted fluctuations of the PVME segments within the glassy PS.[58,59] III) At the lowest investigated temperatures (170 K), the observed peak is due to the β–relaxation for PVME, which is related to the localized fluctuations of the side chains. It is worth to note that the β–relaxation is known to be independent of the blending of PVME with PS.[24] Therefore, this process will not be discussed further. IV) At the highest investigated temperatures, conductivity contributions due to mobile charge carriers cause the increase of ε″ at low frequencies. All observations are in agreement with literature data in references [24,26,27].

Generally, concentration fluctuations are known to be strong for the asymmetric PVME/PS blends, causing broad spectra of the α-relaxation in the frequency domain. Thus, it is also important to analyze the dielectric spectra in the temperature domain, where the dielectric loss is plotted versus temperature at a given frequency. The complexity of this analysis was illustrated in references [59,60], where a contour plot analysis method was suggested. Here, in order to have a complete analysis, all dielectric data were analyzed in both temperature and frequency domain to insure a correct deconvolution and analysis of all relaxation processes. In the temperature domain, a Gaussian is fitted to the data to extract the temperature of maximum loss (see figure S3). Together with the measuring frequency, the relaxation map can be constructed. In the frequency domain, the data were analyzed by fitting the empirical formula of Havriliak/Negami (HN-function) to the data,[61] which reads

$$\varepsilon^*_{HN}(\omega) = \varepsilon_\infty + \frac{\Delta\varepsilon}{(1+(i\frac{\omega}{\omega_0})^\beta)^\gamma} \quad (11.1)$$

where ω_0 is related to the frequency of maximal loss f_p of the peak (relaxation rate). β and γ are shape parameters ($0<\beta\leq1$ and $0<\beta\gamma\leq1$), which describe the broadening and the asymmetry of the process. $\Delta\varepsilon$ is the dielectric strength. ε_∞ models ε' for $\omega>>\omega_0$ ($\omega=2\pi f$). Additionally, the conductivity contribution is considered by adding $\varepsilon'' = \sigma/(\omega^s\varepsilon_0)$ to the loss part of the dielectric spectra. Here σ is related to the DC conductivity, s is a parameter to model non-Ohmic effects with s=1 for Ohmic contacts and s<1 holds for a non-Ohmic behavior. ε_0 is the permittivity of vacuum. The reader is referred to reference [61] for further details. It is known that for homopolymers the analysis in temperature and frequency domain leads to identical results, see reference [62] and figure S4.

Figure 11.1B shows the relaxation map (log f_p versus 1/T) for bulk PVME/PS 50:50 wt% as measured by BDS and SHS, including the data for bulk PVME measured by BDS,[53] for comparison. Blending slows down the relaxation rates of the α-relaxation of PVME (shift to higher temperatures), compared to the pure PVME. In addition to the α-relaxation, the α'-relaxation is observed at temperatures above T_g^{therm} in agreement with data from reference [59], for higher PS concentrations. While the temperature dependence of the relaxation rates of the α-relaxation can be described by the Vogel/Fulcher/Tammann (VFT) equation[61]

$$\log f_p = \log f_\infty - \frac{B}{T-T_0} \quad (11.2)$$

(f_∞ and B are fitting parameters. T_0 is the Vogel temperature, empirically found to be 30-70 K below T_g^{therm}), the temperature dependence of the relaxations rates of the α'-relaxation could be approximated by an Arrhenius equation with an apparent activation energy E_a of 161 kJ/mol.

Despite the fact that both SHS and BDS probe the segmental dynamics, the relaxation rates measured by SHS are shifted by 13 K to higher temperatures, compared to the dielectric data. To discuss this effect, one has to keep in mind that SHS is sensitive to entropy fluctuations resulting from mobile segments of both PVME and PS, whereas BDS senses dipole fluctuations of PVME segments only. Hence, different aspects of the same process

are detected by both measurements techniques. In other words, SHS shows the mean relaxation rate of cooperatively fluctuating PS and PVME segments, as affected by one another. In contrast, BDS probes only the segmental fluctuations of PVME. This shift in the rates of the α-relaxations, measured by the two different methods, is an expression of the dynamic heterogeneity within the bulk blend sample.

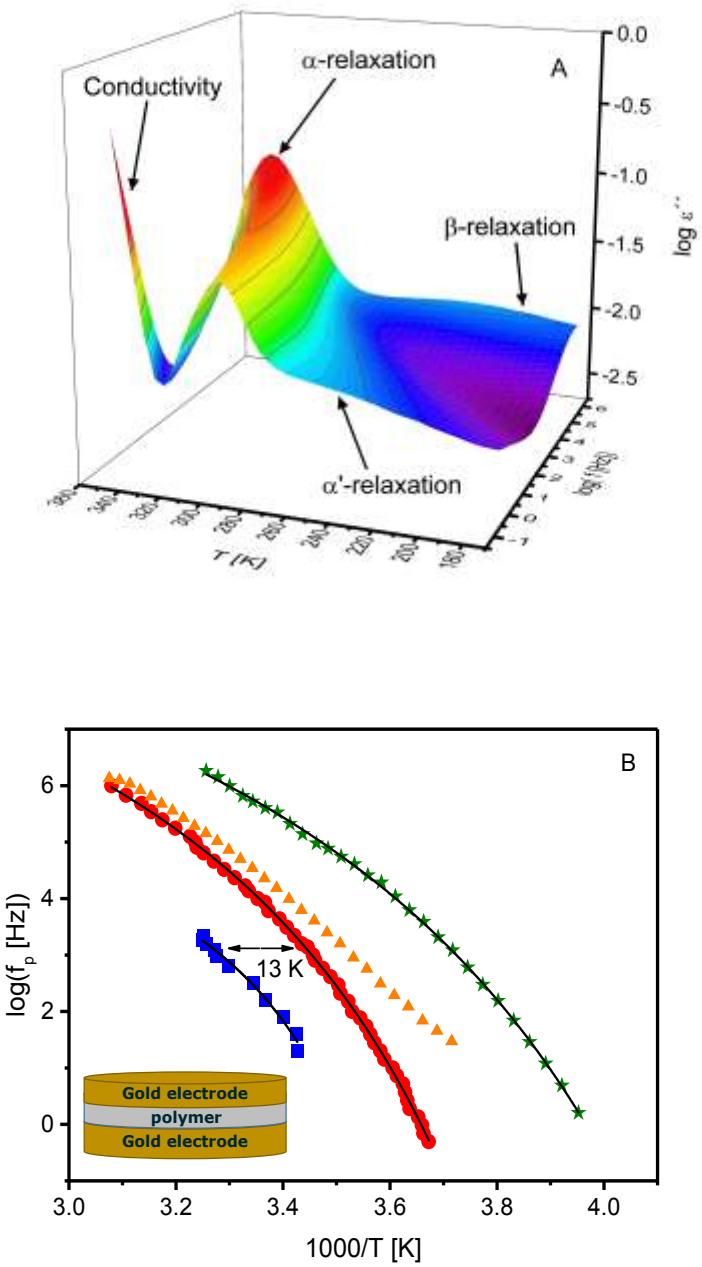

Figure 11.1. (A) *3D plot of the dielectric loss as a function of frequency and temperature for bulk PVME/PS. The peaks correspond to the indicated processes.* **(B)** *Relaxation map for bulk PVME/PS: red circles - α-relaxation (temperature domain analysis); orange triangles - α′-relaxation (frequency domain analysis), blue squares - bulk PVME/PS measured by SHS,[43] green stars - α-relaxation pure PVME measured by BDS.[53] The solid lines are VFT fits to the data.* **Inset.** *shows a schematic of a bulk sample in parallel plate arrangement - taken from reference [53].*

Thin films were measured by two sample arrangements: Crossed Electrode Capacitors (CEC) and Nano-Structured Electrode Capacitors (NSC) *(see experimental section)*. It is worth to note that CEC leads to capped films, whereas supported films can only be measured by NSC. Since one of the aims in this work is to compare the obtained results to those of SHS, recently reported in reference [43], NSCs were of preference, avoiding the questionable comparison of supported films with capped ones. Nevertheless, due to the limited spacer heights available (max. 70 nm), CEC were used to measure films thicker than 36 nm. It is worth to note that for NSC, a free surface had to be insured, even in the case of the complete sinking of the spacers into the film. Therefore, the heights of the spacers used in this work were at least twice the thickness of the measured film.

In general, the analysis of the dielectric loss for thin films in the frequency domain is quite similar to that of the bulk, discussed above. However, for thin films, one has to take into account an additional parasitic contribution due to the resistance R of the Al and/or that of the highly doped silicon electrodes (see figure 11.2A). This contribution results in an additional parasitic Debye-like loss peak with a characteristic time constant τ_{Res} = R*C (C = sample capacitance), observed as an increase in ε″ at high frequencies. For optimized sample geometries, the maximum position of this Debye-like peak $f_{Res} \sim 1/\tau_{Res}$ can be shifted outside the experimental frequency window.[14] For this reason, the Debye function was modeled by its low frequency tail and was taken into account in the model function for the analysis in the frequency domain, which now reads

$$\varepsilon^*_{Fit} = \varepsilon^*_{HN}(\omega) - i\frac{\sigma}{\omega^s \varepsilon_0} + iA\omega, \qquad (11.3)$$

where A is a parameter mainly due to τ_{Res}.

I) *Crossed Electrode Capacitors (CEC)* were used to measure capped films with thicknesses of 180, 130, 85, 48, and 36nm. For more details, see experimental section and reference [14].

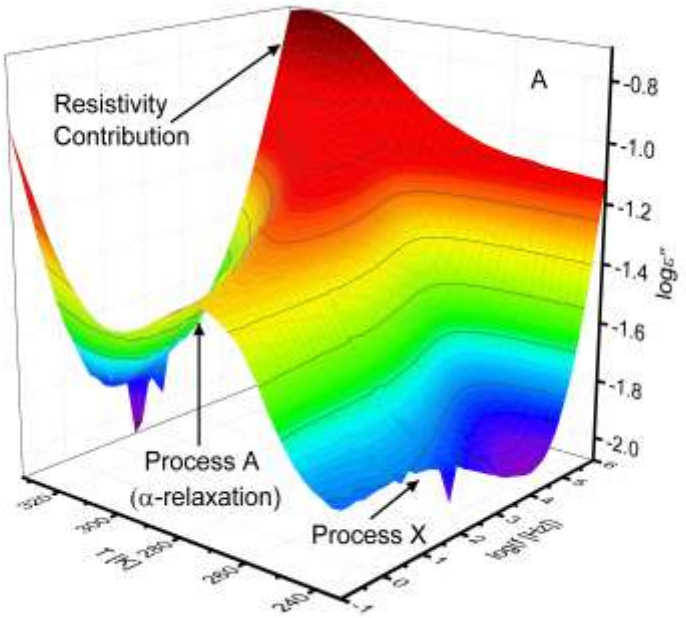
A
Resistivity
Contribution
Process A
(α-relaxation)
Process X
-0.8
-1.0
-1.2
-1.4
-1.6
-1.8
-2.0

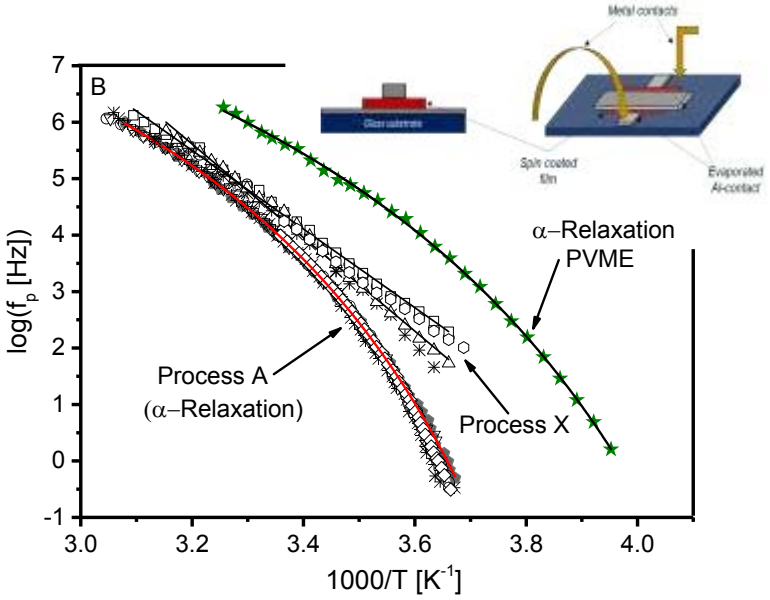
B
α–Relaxation
PVME
Process A
(α–Relaxation)
Process X
log(f_p [Hz])
1000/T [K^-1]
3.0
3.2
3.4
3.6
3.8
4.0
7
6
5
4
3
2
1
0
-1

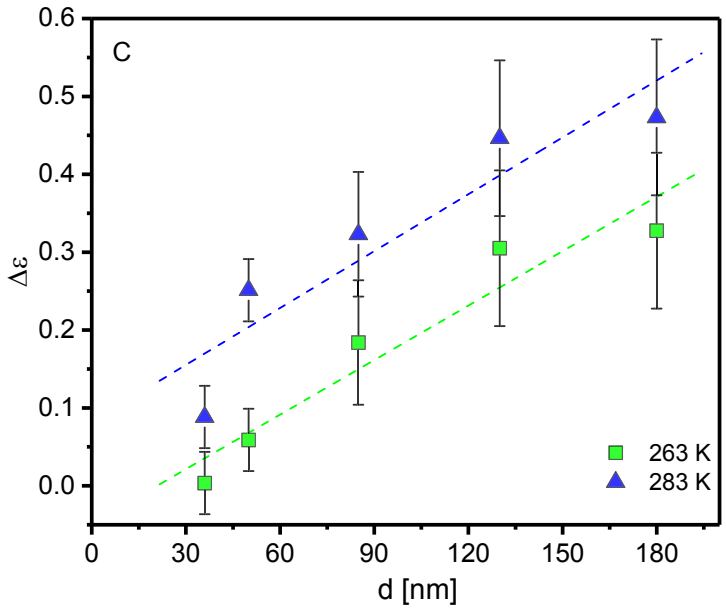

Figure 11.2. (A) *3D plot of the dielectric loss as a function of frequency and temperature for PVME/PS film with a thickness of 50 nm measured by CEC. The peaks correspond to the indicated processes*. **(B)** *Relaxation map of process A and X for all films measured by CEC. Black pentagon – bulk, asterisks – 180 nm, downside triangles -130 nm, squares – 85 nm, circles – 50 nm, and rhombuses - 36 nm. The red line is a common VFT fit to the α-relaxation, whereas the black lines are Arrhenius fits to the data of process X. Green asterisks - α - relaxation of pure bulk PVME.* **Inset** *shows a 3D schematic and a side view of the crossed electrode sample - taken from reference [53].* **(C)** *Dielectric strengths Δε for process X versus film thickness at 263 K – green squares - and 283 K – blue triangles. The dashed lines are linear regression to the data.*

Figure 11.2A shows a 3D plot of the dielectric loss spectra as a function of frequency and temperature for a 50 nm thick film measured by CEC. For all film thicknesses, one main relaxation (process A) is observed. Figure 11.2B depicts the relaxation rates of the main process A as function of reciprocal temperature for all film thicknesses. For comparison, the α-relaxation of the bulk blend is added. The relaxation map obtained for the CEC geometry reveals that the detected process is thickness independent down to the lowest film thickness. The observed process A superimposes, in its frequency and temperature dependence, with the α-relaxation of the bulk blend and can be well described by a common fit of the VFT equation[61] to the data, for all film thickness. Consequently, this process is assigned to the α-relaxation of the thin films.

In addition to α-relaxation of the bulk-like layer (process A), a further weak process (process X) was observed (see figure 11.2A). In difference to the temperature dependence of the relaxation rates of the α-relaxation, the temperature dependence of the relaxation rates of process X seems to be Arrhenius-like. In general the behavior of process X resembles that

of the α´-relaxation observed for the bulk blend (see figure 11.1B). This is further supported by the fact that the activation energy of process X estimated for the highest film thickness is 160 kJ/mol, which is similar to the bulk value. Moreover the dielectric relaxation strength Δε estimated for process X increases with increasing film thickness (see figure 11.2C). Therefore, it was concluded that process X is due to the α´-relaxation within the bulk-like layer. A similar result was found for films of PVME/PS blends but with a higher concentration of PVME[60], where only one film thickness (100 nm) was considered. The thickness dependence of the activation energy of process X will be discussed below, in detail.

II) *Nanostructured Electrode Capacitors (NSC)* were employed to measure supported thin films, with thicknesses of 36, 25, 12, and 7 nm. For more details, see the experimental section and references [53,56,57]. Samples with thicknesses of 36 and 25 nm were measured with 70 nm-high nanostructured SiO_2 spacers, whereas 12 and 7 nm thick films were studied with 35 nm spacers.

Figure 11.3A depicts a 3D plot for the dielectric loss ε´´ spectra as a function of frequency and temperature for a 36 nm thick film measured by NSC. Figure 11.3A shows 2 distinct independent processes indicated as two peaks. These two relaxation processes (process A and X1) were observed for all samples, measured by NSC. In order to assign and understand the origin of both processes, the two processes are discussed separately. It is important to note that process X1 is the dominant process in the frequency domain, thus this process was analyzed there accordingly. Nonetheless, process A was more or less submerged in the low frequency tail of process X1. However, due to its strong temperature dependence, it can be unambiguously analyzed in the temperature domain, see figures 11.3A, B, and 11.4A.

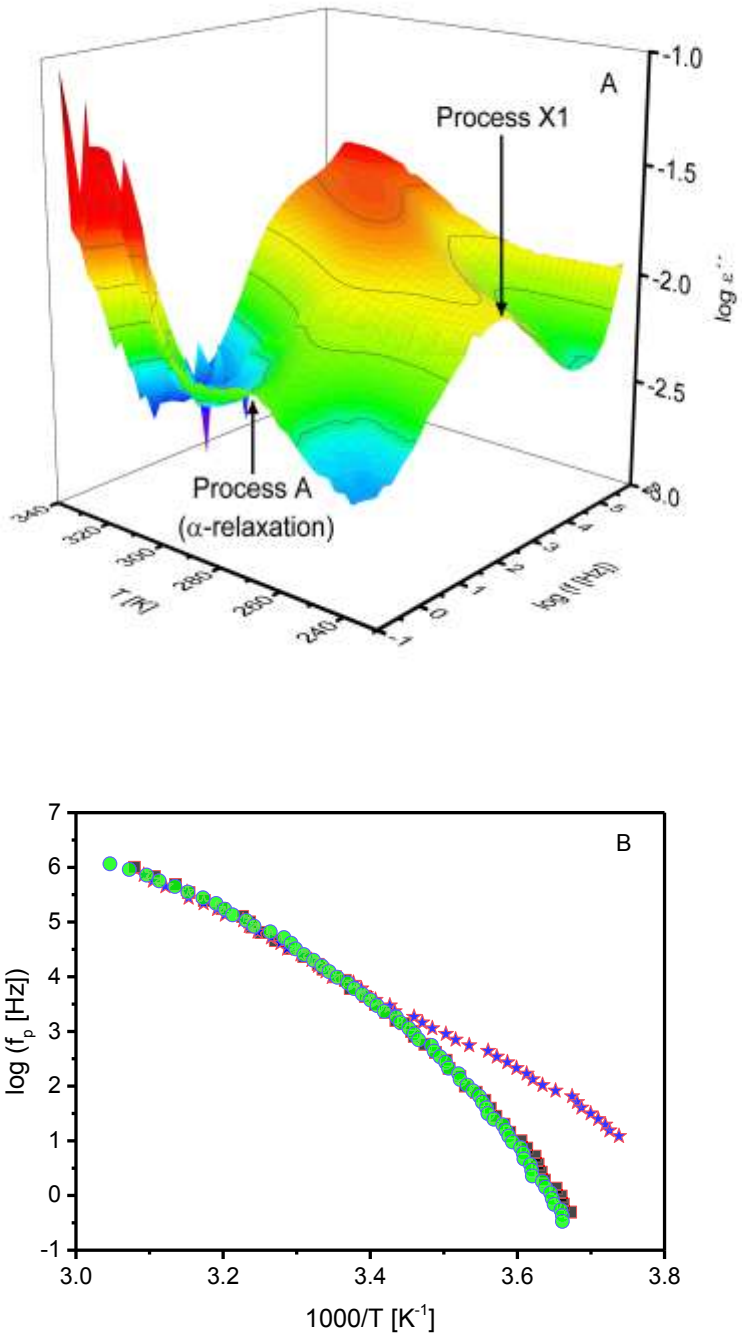

Figure 11.3. (A) *3D plot of the dielectric loss as a function of frequency and temperature for a 12 nm thick PVME/PS film measured by NSC.* (**B**) *Relaxation map of process A for a 36 nm thick film measured by NSC– blue stars, α-relaxation of 36 nm thick film measured by CEC – green circles, and α-relaxation of the bulk blend - black squares.*

First, *process A* is considered. Fig 11.3B shows the relaxation map for process A for 36 nm thick film measured by NSC. In addition, the relaxation rates for the α-relaxation for the bulk blend and that for a 36 nm thick film measured by CEC are included for comparison. As a first result, at high frequencies and/or temperatures, the relaxation rates of process A overlap with the α-process of the bulk and the data measured with CEC. Therefore, it is

concluded that process A corresponds to the α-relaxation of a bulk-like layer in the film. At lower frequencies and temperatures, the relaxation rates of the film measured by NSC are significantly higher, relative to that of the α-relaxation of the bulk and of the thin film measured by CEC for the same film thickness. Figure S5 depicts the dielectric loss spectra as in the temperature domain for the 36 nm thick film measured by NSC and bulk blend sample at 15 Hz. This figures shows that the peaks due to the α-relaxation are separated by 11 K. To discuss this behavior, one has to consider the following question: *How do the different sample arrangements and substrates affect the measured glassy dynamics?*

It is important to recall that for films measured by NSC, a PVME-rich layer with an enhanced molecular mobility is expected to form at the polymer/air interface, due to the surface enrichment phenomena.[41] Yin et al. recently showed by SHS that the free surface layer decreases the dynamic glass transition temperature of the whole film, with decreasing film thickness below 80 nm.[43] For films measured by NSC with thicknesses of 36 nm and below, the PVME-rich layer influences the dynamics of the whole film. This leads to an acceleration of the α-relaxation of thin films compared to that of the bulk for lower temperature (lower frequency < 10^4 Hz). Contrary, for the films measured by CEC, this free surface does not exist and therefore the relaxation rates of the observed α-relaxation superimpose with that of the bulk.

A more detailed inspection of figure S5 reveals that for the film measured by NSC, the spectra of α-relaxation is broadened at the high temperature side compared to that of the bulk. That might be due to an underlying relaxation process due to that of the bulk. Unfortunately, this process cannot be separated unambiguously.

Process X1 is first considered for low film thicknesses up to 25 nm. This process shows a completely different and independent temperature dependence of its relaxation rates than that of the α-relaxation. Figure 11.4A, shows the dielectric loss as a function of the measured frequency for two different temperatures, below and above T_g^{therm} of the blend, for a thin film with a thickness of 12 nm.

Figure 11.4B depicts the relaxation map of process X1 for film thicknesses of 7 and 12 nm. Moreover, the data for the α-relaxation for a 12 nm thick blend film were included. The relaxation rates of process X1 show an Arrhenius-like temperature dependence at temperatures above and below T_g^{therm}. This means that process X1 originates from localized

fluctuations rather than cooperative ones. Additionally, process X1 shows a change in the activation energy (see figure 11.4B).

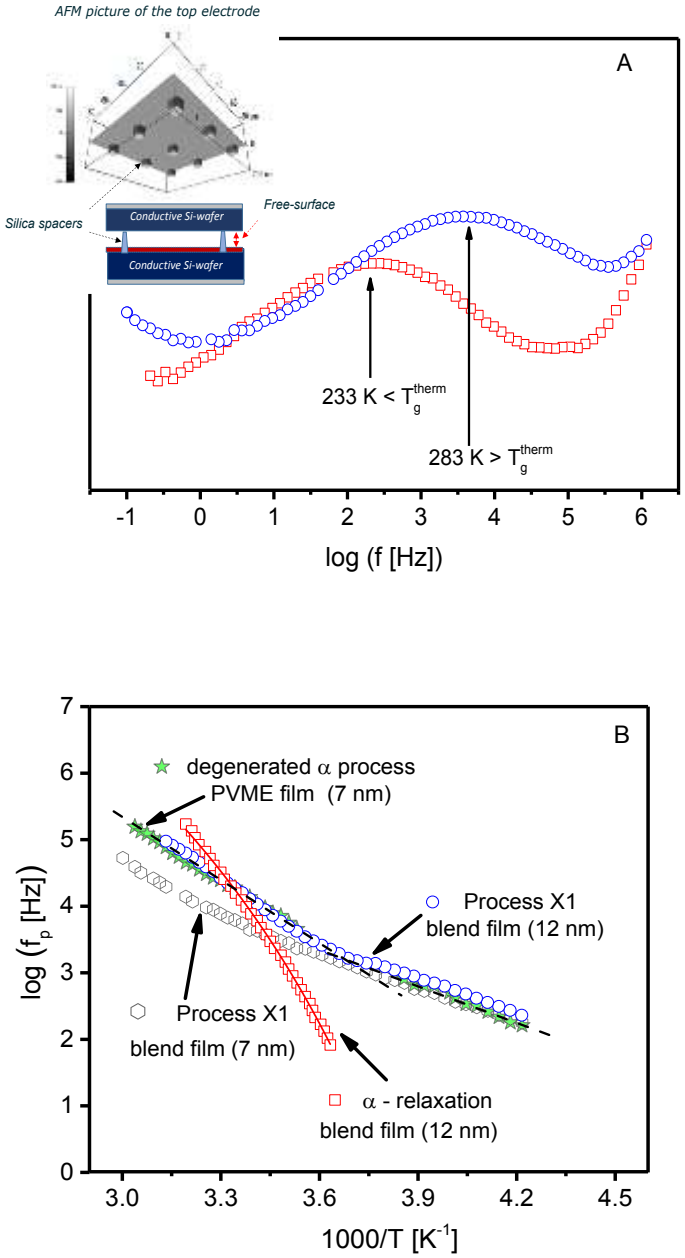

Figure 11.4. (A) *Dielectric loss spectra of process X1 for a 12 nm thick blend film as function of frequency for the indicated temperatures, which are above and below the* T_g^{therm} *of the bulk blend. The* ***inset*** *shows an AFM picture of the nanostructured top electrode with 70 nm spacers and a side view schematic of the nanostructured capacitor - taken from reference [53].* **(B)** *Relaxation map of process X1 for a 7 nm (black hexagons) and 12 nm (blue circles) thick blend films as well as the degenerated α-process assigned to the adsorbed layer of 7 nm thick pure PVME film - green stars. Dashed lines are guides for the eyes. Red squares - α-relaxation for a 12 nm thick PVME/PS blend film. The solid red line is a fit of the VFT equation to the data of the α-relaxation. PVME data were taken from reference [53].*

For the considered low film thicknesses (7 nm – 25 nm), at high temperatures, the temperature dependence of the relaxation rates of process X1 crosses that of the α-

relaxation. This result evidences that process X1 is independent of the α-relaxation of the bulk-like layer of the film.

To understand the behavior and the possible molecular reasons behind process X1 for low film thicknesses, one should reconsider the relaxation of thin films of pure PVME, which was recently studied by NSC as well.[53] It is worth to note that the used PVME is identical to the one employed here. For these pure PVME thin films, two relaxation processes were also found. The temperature dependence of the relaxation rates of the one process obeys the VFT law and overlaps with that of bulk PVME. This process was assigned to the α-relaxation of a bulk-like layer of the films. The relaxation rates of the second process had an Arrhenius-like behavior. This process was assigned to restricted or constrained fluctuations in an irreversible adsorbed layer at the substrate independently of the α-relaxation of the bulk-like layer. The relaxation rates of this process for a 7 nm thick film of pure PVME, were also added to figure 11.4B. A reconsideration of the data of the latter process also reveals a change in the temperature dependence for the 7 nm thick film of pure PVME.

Furthermore, for the considered low film thicknesses, the relaxation rates of process X1 are close in their frequency and temperature dependence to that of the process assigned to the restricted fluctuations of the pure PVME film (degenerated α-relaxation). This would imply that process X1 should have a similar molecular origin. Hence, for low film thicknesses, process X1 is assigned to restricted fluctuations of PVME segments irreversibly adsorbed to the substrate. In addition, the dielectric strength Δε for process X1 increases with increasing temperature (see figures S6). This is contrary to what would be expected for a regular α-relaxation process; where Δε was found to decrease with increasing temperature. Recalling that according to the Debye theory of dielectric relaxation, the dielectric strength is proportional to the number density of the involved dipoles.[45] Therefore, the observed behavior for the temperature dependence of Δε can be rationalized by considering that the segment/substrate interaction will decrease with increasing the temperature. Thus, with increasing temperature, more dipoles become mobile, contributing to the increase of the dielectric strength. For further information, the reader is referred to references [53,63]. This further supports the molecular origin of process X1. It should be noted that a similar line of argumentation was employed to understand the behavior of ultra-thin polystyrene films.[64]

Further, with this approach, this experimental finding would support the hypothesis that a PVME-rich layer is formed at the polymer/substrate interface. To confirm this assumption, X-ray Photoelectron Spectroscopy (XPS) measurements (see SI) were carried out to estimate the PVME concentration at the adsorbed layer. For these measurements, solvent leaching experiments were conducted to remove the bulk-like part of the film, see figure S8.[18] For further details of the solvent leaching experiments, see SI. The XPS measurements unveils the composition of the adsorbed layer to be ca. 100% PVME, see figure S9. This is contrary to what was assumed in references [43,65]. There, a PS-rich layer was postulated, at the polymer/substrate interface. This conclusion was based on the fact that a PVME-rich layer self-assembles at the polymer/air interface as well as the assumption that the bulk-layer keeps its as-prepared composition, independent of thickness. Nonetheless, the possibility of a PVME-rich layer at the polymer/substrate interface, which would require the bulk-like layer to experience a thickness dependent compositional alteration, is in accordance with references [66-70].

As discussed above, a change in the activation energy is observed, for both films (PVME - 7 nm, PVME/PS 7 nm and 12 nm), in the vicinity of T_g^{therm} of the blend (273 K), see figure 11.4B. In general, a decrease in the activation energy would indicate a further localization of the fluctuations of the segments. Since this change in the activation energy is observed for both PVME and the blend films, it is concluded that this further confinement is not related to PS.

To explain this change in the activation energy, *two different scenarios* are considered. First, this behavior could be due to further confinement between the strongly bounded adsorbed layer and the bulk-like layer. A second explanation emerges from a recent molecular dynamics simulation (MDS) study on a 10 nm film of 1,4-polybutadiene confined between two graphite walls.[71] In the vicinity of an attractive solid interface, it was shown that the adsorbed chains could change their conformation from a type B polymer (net dipole moment along the chain backbone is zero) to a type A´ polymer (having a net dipole moment, parallel to the end-to-end vector). This would then allow for the detection of the relaxation rates associated with desorption and adsorption of segments at the polymer/substrate interface by BDS. However, it was concluded, for highly entangled polymers, the characteristic time scale involved for this adsorption kinetics is much longer than the polymer reptation dynamics. For an untangled polymer, similar to the PVME used in this work and keeping in mind that the adsorbed layer is ca. 100 % PVME, the time scale of the desorption/adsorption

process could probably be much shorter. Assuming that the PVME segments could get converted to a type A´, process X1 could also be related to the desorption kinetics of the segments at the interface, below T_g^{therm}. This might be further evidenced by the E_a value reported for the desorption/adsorption process by molecular dynamic simulations of 27 kJ/mol,[72] which is similar to the value 29 kJ/mol found for process X1, below T_g^{therm}. As discussed in the introduction, the adsorbed layer consists of two parts characterized by two different time dependencies of the adsorption process,[43] this would also include conformational changes of the polymer chains within the part of the layer formed in the logarithmic part of the adsorption process due to fluctuations of tails and loops - referred to below as "loosely-bounded" layer.[50,47] Above T_g^{therm}, the restricted fluctuations of the PVME segments irreversibly adsorbed to the substrate become more pronounced, as the temperature increases (see discussion above). Nonetheless, the reason behind the temperature, at which the activation energy changes, is still not clear and requires further investigations. However, the fact that it takes place in the vicinity of T_g^{therm} of the blend is probably coincidental and has more to do with the glassy dynamics and/or other relaxation processes taking place within the strongly-bounded part of the adsorbed layer.

III Process X for 36 nm film measured by CEC vs. NSC: Figure 11.5A depicts the dielectric loss spectra in the temperature range of process X1 for the 36 nm thick PVME/PS film for different temperatures, measured by NSC. A closer look on the data reveals that process X1 convolutes two processes within; process X1 at the higher frequency side and process X2 at the lower frequency side. Further, with increasing temperature, process X2 gains intensity, becoming the dominating process at high temperatures and shifts to higher frequencies with a higher activation energy, compared to that of process X1, see figure 11.5A. It is worth to note that process X2 could only be observed for films thicker than 36 nm, see figure 11.5B.

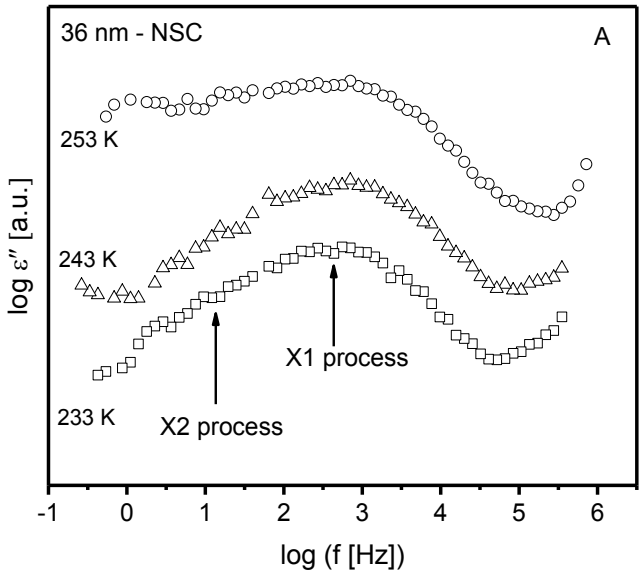
36 nm - NSC
A
253 K
243 K
233 K
X1 process
X2 process
log ε″ [a.u.]
log (f [Hz])
-1
0
1
2
3
4
5
6

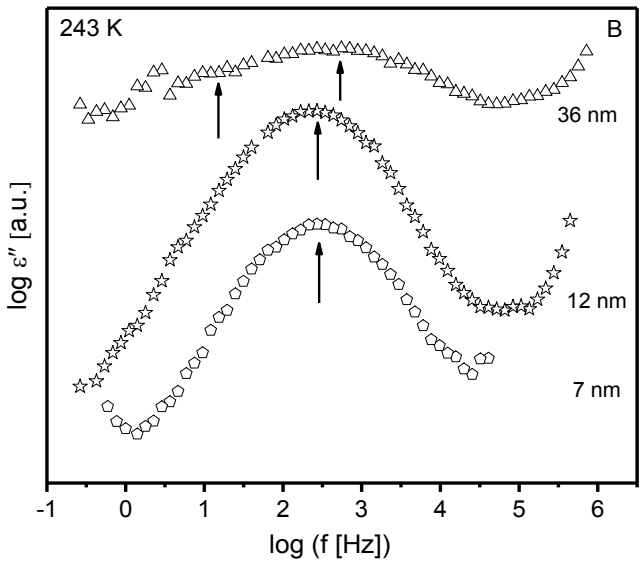
243 K
B
36 nm
12 nm
7 nm
log ε″ [a.u.]
log (f [Hz])
-1
0
1
2
3
4
5
6

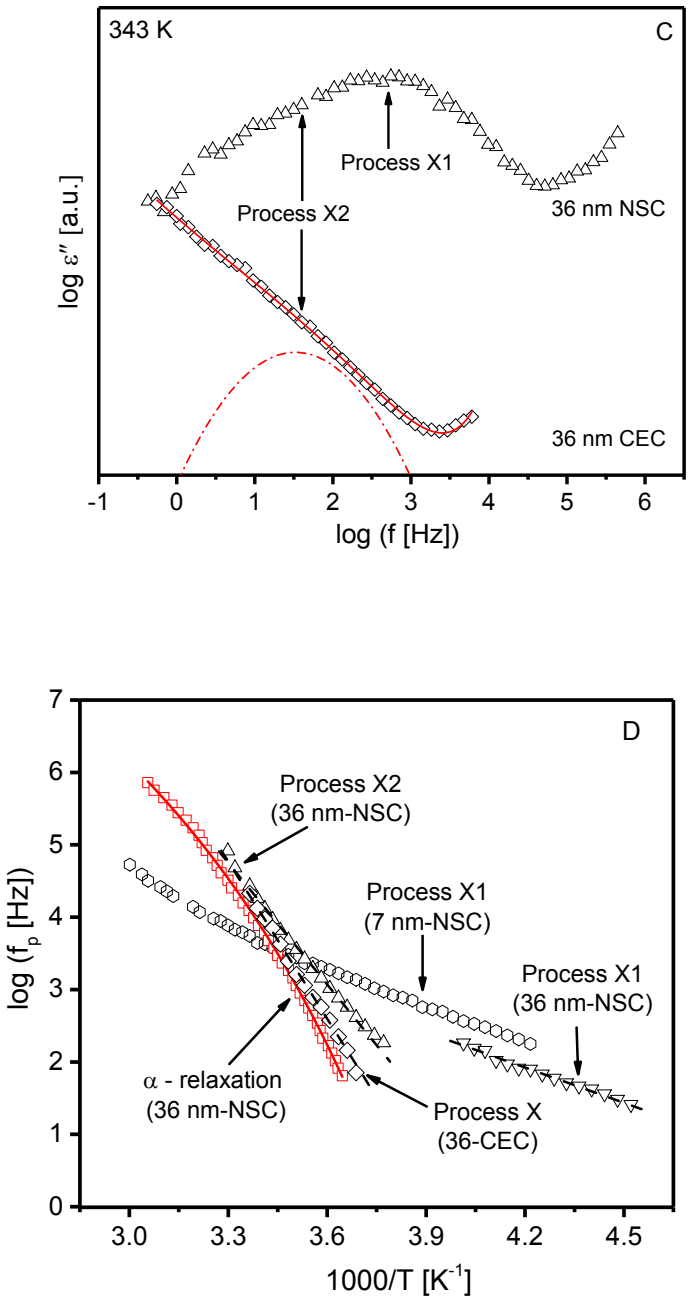

Figure 11.5. (A) *Dielectric loss spectra as function of frequency of process X for a 36 nm thick blend film measured at different temperatures (squares – 213 K; triangles – 223 K, circles – 233 K). The arrows point to the indicated processes.* **(B)** *Dielectric loss spectra for films measured by NSC with thicknesses of 36 nm – triangles, 12 nm – stars and 7 nm – pentagons.* **(C)** *Dielectric loss spectra for 36 nm films measured by CEC – rhombuses and NSC – triangles at 343 K. The solid line is a fit to the data consisting of the HN-function and a power law due to the high frequency tail of the α-relaxation. The dashed line indicates the process X2 deconvoluted from the fit data* **(D)** *Relaxation map for the 36 nm thick blend film measured by NSC showing the α-relaxation –squares, process X2 and X1 –triangles. The solid line is a VFT fit to the α-relaxation, whereas the dashed lines are linear regressions to processes X1 and X2. In addition, the process X for the 36 nm film measured by CEC – rhombuses- as well as process X1 for 7 nm blend film –hexagons- were added for comparison.*

As discussed above, process X was observed for films capped between two aluminum electrodes. However, in that case, its dielectric strength is much lower than that for films prepared on silica substrates (see figure 2A). Figure 11.5C compares the dielectric spectra of process X1 and X for a 36 nm thick film measured by NSC and CEC, respectively. Firstly, process X1 is not observed for the 36 nm thick sample measured by CEC. Therefore, it was concluded that process X1 should be related to the SiO_2 surface like for films in the thickness range from 7 nm to 25 nm. In reference [53], the interaction energies between PVME and both substrates were estimated by contact angle measurements. It was found, that the interaction energy between PVME and aluminum (0.66 mJ/m^2) is much smaller than that between PVME and SiO_2 (2.73 mJ/m^2). This means that the adsorption or segregation of PVME segments to aluminum is much weaker than that of silica, leading to a thinner and weaker adsorbed or even only a segregated layer for the same annealing conditions.[17] In other words, the observed process X1 for all films investigated by NSC further supports the conclusion that process X1 could be due to the localized molecular fluctuations of adsorbed PVME segments at the SiO_2 surface.

Secondly, figure 11.5D further shows that process X2 measured by the NSC coincidence with the process X measured by CEC. In the latter case, process X was assigned to the α′-relaxation of a bulk-like layer in the film. Therefore, process X2, observed by the NSC, is also assigned to the α′- relaxation of a bulk-like layer. This conclusion is further supported by the fact that the estimated activation energies for process X, measured by CEC, and process X2, studied by NSC, are similar.

IV) Combined discussion of α′-relaxation measured by CEC (process X) and NSC (process X2): In figure 11.6, the estimated activation energies E_a are plotted as a function of inverse film thickness. With decreasing film thickness, the activation energy of the α′-relaxation decreases. This behavior could be rationalized by recalling that for all measured films, both interfaces are PVME rich.[60,65] This concerns the segregation of PVME to both Al substrates of the CEC was well as the adsorbed PVME layer (polymer/substrate interface) and the self-assembled PVME-rich layer at the polymer/air interface of the 36 nm thick sample measured by NSC. Therefore, due to mass conservation, a PS-rich layer in the middle of the film is formed. With decreasing the film thickness to 36 nm, the bulk-like layer decreases, while the thickness of the layer adsorbed at the interface(s) will probably remain more or less the same.[73] Consequently, the PS concentration within the bulk-like layer will increase with decreasing the film thickness. The increase in the frozen PS segments would impose further

confinement on the PVME segments, which would yield a decrease in the value of E_a. This line of argumentation is further supported by the results found for the α´- relaxation of bulk PVME/PS samples, where the concentration of the blend was varied.[59] There it was found that the activation energy of the α´- relaxation decreases with increasing PS concentration. To evidence the thickness dependent compositional heterogeneities, XPS measurement on the free-surface of the blend films (with varying film thicknesses) were commenced, see SI. Preliminary results show that the PVME-rich free surface layer of a 60 nm thick film has a PVME concentration of ca. 66 wt% (see figure S7 and SI), in contrast to 84 wt% measured for 200 nm films.[43] (One has to keep in mind here that the given values are the average compositions over the penetration depth of XPS, which is ca. 10 nm.) This is in line with reference [65] and directly confirms the change of the compositional heterogeneities with decreasing the film thickness. A systematic study of the PVME concentration at both interface for different substrates and blend composition is currently on going and will be published elsewhere.

Nevertheless, it is worth to mention that around ca. 30 nm, several investigations have reported unexpected changes in the thickness dependence of glass transition[10,74] and the glassy dynamics.[66] It is worth to note that the extrapolated activation energy for process X2 becomes zero at a length scale of ca. 15 nm. This would indicate that process X2 do not exist anymore for films thinner than 15 nm.

On the other hand, the activation energy of process X1 has a completely different thickness dependence (see figure 11.6). For the films in the thickness range from 7 nm to 25 nm, the activation energy was taken at temperatures above T_g^{therm}. Please recall that process X1 was assigned to originate from PVME fluctuations within the adsorbed layer. The slight decrease in the activation energy with decreasing film thickness, in the thickness range from 7 nm to 25 nm, generally implies that the adsorbed PVME segments undergo further confinement upon thickness reduction. Again, such confinement could only be enforced by PS segments. This is concluded from the fact that the degenerated α-relaxation of the pure PVME thin films is thickness independent down to lowest measured film thickness of 7 nm. At the length scale of ca. 10 nm, the thickness of the adsorbed layer is bound to decrease slightly, taking place, at first, on the expense of the thickness of the "loosely-bounded" part of the adsorbed layer. This would have to happen to conserve the mass of the film. Accordingly, this would mean that with decreasing the film thickness, free volume sites would start to appear at the interface, which could then be filled with PS segments. This

scenario would result in an increase in the PS content, within this part of the adsorbed layer; where the PS segments feel an extra confinement due to the adsorption at the interface, which leads to a further decrease of the activation energy.

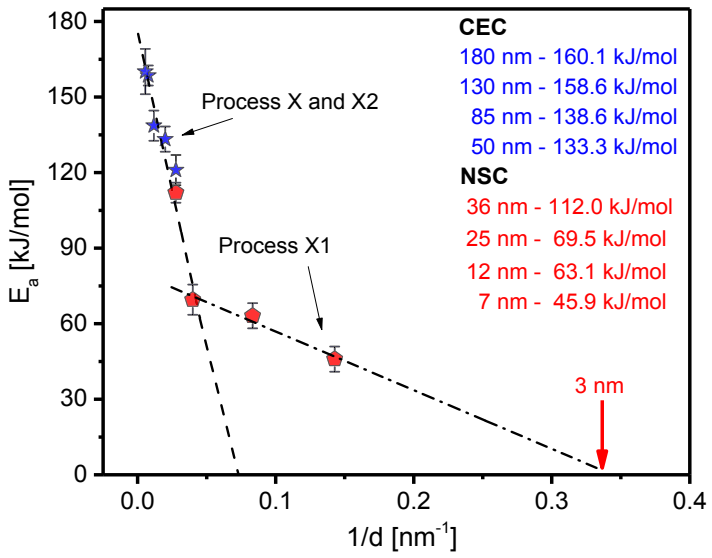

Figure 11.6. *Activation energy E_a as a function of inverse thickness for samples measured by CEC – blue stars and NSC – red pentagons. Typical error bars are given. The dashed and the dashed dotted line are guide to the eyes. The arrow highlights the extrapolated value of E_a to zero.*

In Figure 11.6, the thickness dependence of E_a is extrapolated to zero. This leads to a second characteristic length scale of ca. 3 nm. Interestingly this corresponds approximately to the thickness of an adsorbed layer of ca. 4 nm found in solvent leaching experiments, see figure S8 and SI.

11.4. Conclusion

Broadband dielectric spectroscopy (BDS) was employed to investigate the glassy dynamics of thin films (7 nm – 180 nm) of a Poly (vinyl methyl ether) (PVME) / Polystyrene (PS) blend with a composition of 50:50 wt-%, which is miscible in bulk. BDS measurements of thin films were carried out employing Crossed-Electrode Capacitors (CEC) and Nano-Structured Capacitors (NSC). The former method was employed to measure films thicker than 36 nm, whereas thinner films were measured by the latter arrangement. It is important to note that the NSC allows the films to have a free surface, contrary to the CEC arrangement, where the films are capped between two Al electrodes.

All thin films measured by both arrangements showed multiple relaxation processes. I) An *α-relaxation* process was observed, for all thin films studied, that is related to the α-

relaxation of the bulk blend. This process showed no thickness dependency and followed a VFT behavior. For films measured by NSC, at high temperatures, this α-relaxation coincided in its frequency and temperature dependence, with the α-relaxation of bulk blend. At lower frequencies and/or temperatures the relaxation rates are higher than that of the bulk. This enhancement was related to a PVME-rich layer at the polymer/air interface, which causes the acceleration of the α–process at lower temperatures compared to the bulk and films measured by CEC, where the free surface does not exist. This was found to be in agreement with reference [43].

II-A.) For CEC, *process X* was observed at temperatures above and below T_g^{therm} of the bulk blend. This process was relatively weak and its intensity (dielectric strength) was found to decrease with decreasing film thickness. For the thickest films, the E_a of this process resembled that of the α´- relaxation in bulk. Consequently, process X was assigned to the α´- relaxation within the bulk-like layer, originating from the localized fluctuations of the PVME segments within a frozen PS scaffold.

II-B.) For NSC, process X1 was observed. For the 36 nm film, it was shown that process X1 convoluted a second process (process X2), at the lower frequency side. Process X2 was only observed for the 36 nm film. Its activation energy and frequency/temperature dependence was similar to that of process X, observed for the same film thickness measured by CEC. Therefore, it was assigned to the α´- relaxation originating from the bulk like layer. For thinner films, process X1 was the dominant process in the dielectric loss spectra. Its relaxation rates had an Arrhenius-like temperature-dependence, completely independent from the α-relaxation. Astonishingly, the behavior of its relaxation rates as a function of temperature resembles that of the degenerated α-process of pure PVME thin films.[53] Therefore, this process was assigned to the restricted PVME fluctuations taking place in the mobile part of the adsorbed layer. Further, XPS measured on a leached blend film of a 200 nm thick film directly evidenced a 100% PVME film at the polymer/substrate interface, thus validating the comparison.

Furthermore, a closer look on the activation energies of process X and X2 (α´- relaxation) for the different film thicknesses revealed that this process undergoes and extra confinement. This extra confinement was traced to the increase in PS concertation within the bulk-like layer, with decreasing the film thickness. This thickness dependent compositional heterogeneity would have to occur to conserve the mass of the film. XPS

measurements on the free surface of a 60 nm vs. 200 nm blend films evidenced the change in the composition of the free surface with decreasing the film thickness. On the other hand, the E_a of process X1 showed a completely different thickness dependence. For the latter process it was concluded that this process undergoes two extra confinement effects, in addition to the thickness reduction. I) Confinement between the strongly bounded part of the adsorbed layer and the bulk-like layer. This was deduced from the decrease of the activation energy (E_a) of process X, with decreasing temperature, for the same film thickness. II) Confinement due to frozen PS segments within the adsorbed layer. This was concluded by showing that the E_a, decreases systematically with decreasing the film thickness. These findings also point to thickness dependent changes in the composition of the adsorbed layer. Hence, the importance of studying the dynamics and compositional heterogeneity of the adsorbed layers, which could strongly influence the overall glass transition and glassy dynamics of thin film. To our knowledge, this is the first investigation probing the molecular dynamics of an adsorbed layer for thin polymer blend films.

References

1 Ediger, M.; Forrest, J. A. *Macromolecules* **2014,** *47*, 471-478.
2 Debenedetti, P. G.; Stillinger, F. H. *Nature* **2001**, 410, 259–267.
3 Anderson, P. W. *Science* **1995**, 267, 1617.
4 Ediger, M.; Horrowell, P. *J. Chem. Phys.* **2012**, 137, 080901-080915.
5 Angell, C. A. *Science* **1995**, 267, 1924-1935.
6 Sastry, S.; Debenedetti, P.G.; Stillinger, F.H. *Nature* **1998**, 393, 554-557.
7 Yin, H.; Madkour, S.; Schönhals, A. Dynamics in Confinement: Progress in Dielectrics, Springer vol. 2. **2014**, Kremer, F. (Ed.).
8 Keddie, J. L.; Jones, R. A.; Cory, R. A. *Faraday Disc.* **1994**, 98, 219-230.
9 Keddie, J. L.; Jones, R. A; Cory, R. A. *Euro Phys Lett*. **1994**, 27, 59-64.
10 Ellison, C.; Torkelson, J. *Nat Mater.* **2003**, 2, 695-700.
11 Fakhraai, Z.; Forrest, J. *Phys. Rev. Lett.* **2005**, 95, 025701-025707.
12 Forrest, J.; Dalnoki-Veress, K. *Adv. Colloids Interface Sci.* **2001**, 94, 167-196.
13 Efremov, M.; Kiyanova, A.; Last, J.; Soofi, S.; Thode, C.; Nealey, P. *Phys. Rev. E.* **2012**, 86, 021501-021505.
14 Yin, H.; Napolitano, S.; Schönhals, A. *Macromolecules* **2012**, 45, 1652-1662.
15 Lupaşcu, V.; Picken, S.; Wübbenhorst, M. *J. Non-Cryst. Solids* **2006**, 352, 5594-5600.
16 Paeng, K.; Swallen, S.; Ediger, M. *J. Am. Chem. Soc.* **2011**, *133*, 8444–8447.
17 Napolitano, S.; Glynos, E.; Tito, N. B. *Rep. Prog. Phys.* **2017**, *80*, 036602.
18 Napolitano, S.; Wübbenhorst, M. *Nat. Commun.* **2011**, 2, 260.
19 Tress, M.; Erber, M.; Mapesa, E.; Huth, H.; Müller, J.; Serghei, A.; Schick, C.; Eichhorn, K.; Voit, B.; Kremer, F. *Macromolecules* **2010**, 43, 9937−9944.
20 Labahn, D.; Mix, R.; Schönhals, A. *Phys. Rev. E.* **2009**. 79, 011801-011809.
21 Huth, H.; Minakov, A.; Schick, C. D. *J. Polym. Sci., Part B: Polym. Phys*. **2006**, 44, 2996–3005.
22 Yin, H.; Schönhals, A. *Soft Matter* **2012**, 8, 9132-9139.
23 Madkour, S.; Yin, H.; Füllbrandt, M.; Schönhals, A. *Soft Matter* **2015**, 11, 7942-7952.
24 Colmenero, J.; Arbe, A. *Soft Matter*, **2007**, *3*, 1474-1485.
25 Russell, T.; Chai, Y. *Macromolecules* **2017**, 50, 4597-4609.
26 Ngai, K.; Capaccioli, S. *J. Chem. Phys*. **2013**, *138*, 054903.
27 Alegria, A.; Colmenero, J.; Ngai, K. L.; Roland, C. M. *Macromolecules* **1994**, *27*, 4486-4492.
28 Cendoya, I.; Alegria, A.; Alberdi, J. M.; Colmenero, J.; Grimm, H.; Richter, D.; Frick, B. *Macromolecules* **1999**, *32*, 4065-4078.
29 Takeno, H.; Kobayashi, M.; Aikawa, T. *Macromolecules* **2006**, *39*, 2183-2190.
30 Watanabe, H.; Urakawa, O. *Korean-Australian Rheol. J*. **2009;** *21*, 235-244.
31 Green, P. F.; Adolf, D. B.; Gilliom, L. R. *Macromolecules* **1991**, *24*, 3377-3382.
32 Colby, R. H.; Lipson, J. E. G. *Macromolecules* **2005**, *38*, 4919-4928.
33 Urakawa, O.; Fuse, Y.; Hori, H.; Tran-Cong, Q.; Yano, O. *Polymer* **2001**, *42*, 765-773.
34 Chung, G. C.; Kornfield, J. A.; Smith, S. D. *Macromolecules* **1994**, *27*, 5729-5741.
35 Wang, D.; Ishida, H. *Macromol. Chem. Phys.* **2007,** *208*, 2222-2228.
36 Dionisio, M.; Fernandes, A. C.; Mano, J. F.; Correia, N. T.; Sousa, R. C. *Macromolecules* **2000**, *33*, 1002-1011.
37 Wang, J.; Roland, C. M. *Polymer* **2005**, 46, 4160-4165.
38 Alvarez, F.; Alegria, A.; Colmenero, J. *Macromolecules* **1997**, *30*, 597-604.
39 Arbe, A.; Alegria, A.; Colmenero, J.; Hoffmann, S.; Willner, L.; Richter, D. *Macromolecules* **1999**, *32*, 7572-7581.
40 Jones, R. A. L.; Kramer, J. *Polymer* **1993**, *34*, 115-118.
41 Bhatia, Q. S.; Pan, D. P.; Koberstein, J. T. *Macromolecules*, **1988**, 21, 2166–2175.
42 Thomas, K. R.; Clarke, N.; Poetes, R.; Morariu, M.; Steiner, U. *Soft Matter* **2010**, 15, 3517-3623.
43 Yin, H.; Madkour, S.; Schönhals. A. *Macromolecules* **2015**, 48, 4936-4941.
44 Santore, M. *Curr. Opin. Colloid Interface Sci.* 2005, 10, 176-186.
45 Granick, S. *Eur. Phys. J. E* **2002**, 9, 421-424.
46 O'Shaughnessy, B.; Vavylonis, D. *J. Phys.: Condens. Matter* **2005**, 17, 63-99.
47 Housmans, C.; Sferrazza, M.; Napolitano, S. *Macromolecules* **2014**, 47, 3390−3393.
48 Gin, P.; Jiang, N.; Liang, C.; Taniguchi, T.; Akgun, B.; Satija, S. K.; Endoh, M. K.; Koga, T. *Phys. Rev. Lett.* **2012**, 109, 265501.
49 Asada, M.; Jiang, N.; Sendogdular, L.; Gin, P.; Wang, Y.; Endoh, M. K.; Koga, T.; Fukuto, M.; Schultz, D.; Lee, M.; Li, X.; Wang, J.; Kikuchi, M.; Takahara, A. *Macromolecules* **2012**, 45, 7098-7106.
50 Jiang, N.; Shang, J.; Di, X.; Endoh, M. K.; Koga, T. *Macromolecules* **2014**, 47, 2682-2689.

51 Jiang, N.; Endoh, M.; Koga, T.; (Ed.) Napolitano, S. Structures and Dynamics of Adsorbed Polymer Nanolayers on Planar Solids: Non-equilibrium Phenomena in Confined Soft Matter, *Springer International*, Switzerland, **2015**, 129.
52 Napolitano, S.; Sferrazza, M. *Adv. Colloid Surface Sci.* **2017**, https://doi.org/10.1016/j.cis.2017.02.003.
53 Madkour, S.; Szymoniak, P.; Heidari, M.; von Klitzing, R.; A. Schönhals. *ACS Appl. Mater. Interfaces.* **2017**, 9, 7535-7546.
54 Reiter, G.; Hamieh, M.; Damman, P.; Sclavons, S.; Gabriele, S.; Vilmin, T.; Raphael, E. *Nat. Mater*. **2005,** *4*, 754-758.
55 Schönhals, A.; Kremer, F. Broadband Dielectric Measurement Techniques and Theory of Dielectric Relaxation. In Broadband Dielectric Spectroscopy; Kremer, F.; Schönhals, A., Eds.; *Springer*, Berlin, **2002**, 01-57.
56 Tress, M.; Mapesa, E.; Kossack, W.; Kipnusu, W.; Reiche, M.; Kremer, F. *Science* **2013**, 341, 1371−1374.
57 Serghei, A.; Kremer, F.*Rev. Sci. Instrum.* **2008**, 79, 026101-026107.
58 Lorthioir, C.; Alegria, A.; Colmenero, J. *Phys. Rev. E* **2003**, 86, 031805-031809.
59 Sharma, R. P.; Green, P. F. *Macromolecules* **2017**, DOI:10.1021/acs.macromol.7b00092
60 Yang, H.; Green, P. F. *Macromolecules* **2013**, 46, 9390-9395.
61 Schönhals, A.; Kremer, F. Analysis of Dielectric Spectra and The Scaling of the Dynamics of Glasses and Supercooled Liquids. In Broadband Dielectric Spectroscopy; Kremer, F.; Schönhals, A., Eds.; *Springer*, Berlin, **2002**, 01-57.
62 Schlosser, E.; Schönhals, A.; Carius, H.E.; Goering, H. *Macromolecules* **1993**, 26, 6027-6032.
63 Füllbrandt, M.; Purohit, P.; Schönhals, A. *Macromolecules* **2013**, 46, 4626−4632.
64 Napolitano, S.; Wübbenhorst, M. *J. Phys. Chem.* B **2007**, 111, 9197-9199.
65 Tanaka, K.; Yoon, J.-S.; Takahara, A.; Kajiyama, T. *Macromolecules* **1995**, 28, 934-938.
66 Madkour, S.; Szymoniak, P.; Schick, C.; Schönhals. A. *J. Chem. Phys.* **2017**, *146*, 203321.
67 Ogawa, H.; Kanaya, T.; Nishida, K.; Matsuba, G. *Polymer* **2008**, 49, 2553-2559.
68 Ogawa, H.; Kanaya, T.; Nishida, K.; Matsuba, G. *Polymer* **2008**, 49, 254-262.
69 Ermi, B. D.; Karim, A.; Douglas, J. F. *J. Polym. Sci. Part B Polym. Phys*. **1998,** *36*, 191-200.
70 Karim, A.; Slawecki, T. M.; Kumar, S. K.; Douglas, J. F.; Satija, S. K.; Han, C. C.; Russell, T. P.; Liu, Y.; Overney, R.; Sokolov, J.; Rafailovich, M. H. *Macromolecules* **1998,** *31*, 857-862.
71 Solar, M.; Paul, W. *Soft Matter.* **2017**, 13, 1646-1653.
72 Solar, M.; Binder, K.; Paul, W. *J. Chem. Phys*. **2017**, 146, 203308.
73 Bal, J.; Beuvier, T.; Unni, A.; Panduro, E.; Vignaud, G., Delorme, N.; Chebil, M.; Grohens, Y.; Gibaud, A. *ACS Nano* **2015**, 9, 8184-8193.
74 Zhang, Y.; Glor, E. C.; Li, M.; Liu, T.; Wahid, K.; Zhang, W.; Riggleman, R. A.; Fakhraai, Z. *J. Chem. Phys.* **2016,** *145*, 114502.

CHAPTER 12- Conclusion & Outlook

12.1. Conclusion

Despite the controversial discussions about the nanometric confinement effect on the properties of thin films, many details remain not understood and/or experimentally unproven. Generally, it is well known that the thermal glass transition temperature (T_g^{therm}) of thin films of homopolymers and of polymer blends could deviate substantially from the bulk value. Nowadays, the thickness dependence of T_g^{therm} is generally discussed in the framework of an idealized three-layer model. This model considers a spatial dynamically heterogeneous structure across the film thickness, consisting of three layers: I) A free surface layer with enhanced molecular mobility at the polymer/air interface, II) a bulk-like layer in the middle of the film, and III) an adsorbed layer at the polymer/substrate interface with a reduced mobility. With decreasing film thickness, the thickness of the bulk-like layer decreases and the effect of the remaining layers become dominant. However, recently, it was shown that the prevalence of their effect is also correlated to other parameters such as annealing time, molecular weight, packing frustration, interfacial interactions with the substrate, and compositional heterogeneity.

The aims of this dissertation is to achieve a deeper understanding of the confinement in thin films effects on the glass transition and glassy dynamics, which goes beyond the effects of the increased surface-to-volume ratio presented in the three-layer model, and take into account the aforementioned parameters. This work presents a complex framework governing nanoconfinement is thin polymer films, which is supported by a large body of experimental evidence and simulations, as well as the results presented in chapters 7 to 11.

The research work presented here investigates the influence of nanoconfinement on the glass transition and glassy dynamics of thin polymer films of both homopolymers and polymer blends using a combination of volume sensitive methods and surface analytical techniques. The main two volume sensitive methods used were Broadband Dielectric Spectroscopy (BDS) and Specific Heat Spectroscopy (SHS). For the BDS measurements, a recently designed and adapted nano-structured electrode capacitor (NSC) was employed to study the glassy dynamics, from the kinetic point of view. This sample arrangement allowed measuring thin supported films with a free polymer/air interface. Additionally, SHS employing AC-chip calorimeter was used to investigate the segmental dynamics of the thin

films from the thermodynamic point of view. The results of both methods were quantitatively discussed.

First, the thickness dependence of the segmental dynamics (α-relaxation, related to a dynamic glass transition temperature T_g^{dyn}) of Poly(2-vinyl pyridine) (P2VP) films down to 10 nm were investigated by SHS. This study was carried out to affirm the long-standing discussion regarding the thickness independency of T_g^{dyn} of thin homopolymer films and the molecular reasons behind it. The results showed that through a traditional analysis method, some of the information within the data could be lost due to different errors, and T_g^{dyn} is thickness independent within the experimental error. Nevertheless, through a new derivative-based method, a slight decrease (7 K) in T_g^{dyn} was evidenced, for the first time, with decrease film thickness. This verified that the SHS could indeed provide useful insights to study the confinement effects on the overall segmental dynamics of the film. However, despite the slight confinement effect, it could not be confirmed whether the evidenced confinement effect was due to a free surface (the layer at the polymer/air interface) or an increase in the free volume, at the polymer/substrate interface, due to the short annealing time used, compared to the terminal relaxation time of the polymer.

Consequently, a low molecular weight Poly(vinyl methyl ether) PVME was specifically selected to insure the well annealing of the thin films, necessary to form adsorbed layer, within a reasonable time. Films down to 7 nm of the low molecular PVME were investigated by both BDS and SHS. The BDS measurements showed two dielectrically active relaxation processes. Besides an expected thickness-independent process, assigned to the α-relaxation of a bulk-like layer (also confirmed by SHS), a second process with a completely different temperature dependence was observed. Unexpectedly, the temperature dependence of the relaxation rates of the second process obeyed an Arrhenius-like temperature dependence. This process was not observed by SHS and was related to the constrained segmental fluctuations in a layer, which is irreversibly adsorbed at the substrate with a heterogeneous structure. Its molecular fluctuations undergo a confinement effect resulting in the localization of the segmental dynamics. This was the first report on the molecular dynamics of an adsorbed layer in thin films.

The investigations on thin homopolymer films, presented in chapter 7 and 8, revealed the difficulty of probing the segmental dynamics of the free surface layer in these systems. This is due to the fact that above T_g^{therm}, which is the temperature range at which the segmental

dynamics are probed, the segmental dynamics of the free surface layer are indistinguishable from that of the bulk. However, by carefully selecting an asymmetric polymer blend system, the effect of the free surface layer on the overall segmental dynamics could be probed. This is due to the surface enrichment phenomenon, which results in a different composition at the polymer/air interface, compared to the bulk: Therefore, inducing adequate contrast between the segmental dynamics of the free surface and that of the bulk-like layer.

Accordingly, the second part of this dissertation focused on asymmetric polymer blend systems. An identical PVME, to the one studied in chapter 8, was blended with the well-studied Polystyrene (PS) in two compositions; 50:50 wt% and 25:75 wt%. First, the thin films of the blends were studied with SHS and compared to one another. There, it was shown that for the thin films of the 25:75 wt% blend, their segmental dynamics were dependent on the film thickness. It was shown that down to 30 nm thicknesses, T_g^{dyn} of the whole film was strongly influenced by the surface enrichment phenomenon taking place at both interfaces. This phenomena resulted in the segregation of some of the PVME at the interfaces, creating PVME-rich interfaces. Therefore, due to the mass conservation, a PS-rich bulk-like layer was present yielding a systematic increase in T_g^{dyn}, with decreasing the film thickness. However, at a thickness of ca. 30 nm thickness, the influence of the mobile PVME-rich surface layer became more pronounced. This resulted in a systematic decrease in T_g^{dyn} with the further decrease of the film thickness, below 30 nm. This is different from what was found for the thin films of the 50:50 wt% blend system, where $T_g^{dyn}$was found to decrease systematically with decreasing the film thickness. Furthermore, X-ray Photoelectron Spectroscopy (XPS) measurements confirmed that for both blends, their free surfaces are PVME-rich. However, measurements on their adsorbed layers (obtained by solvent leaching experiments), have shown that for both blend systems the PVME concentration is 100%. This is contrary to the long-standing assumption in literature that PS-rich layer forms at the SiO_2/polymer interface.

Moreover, the thickness dependence of T_g^{therm} of thin films of the 25:75 wt% blend was investigated by ellipsometry. Its thickness dependence was compared to that of T_g^{dyn} (measured by SHS), and the deduced Vogel temperature (T_0). While T_g^{therm} and T_0 showed a monotonous increase, with decreasing the film thickness, T_g^{dyn} measured at an accessible frequency showed a non-monotonous dependence that peaks at 30 nm. This was discussed by assuming different cooperativity length scales at these temperatures, which have different

sensitivities to composition and thickness. For the first time, it was shown that the thickness dependence of T_g^{dyn} could recover that of the T_g^{therm} at frequencies characteristic for T_0. This vividly elucidated the coupling/decoupling behavior of the glass transition and glassy dynamics as a function of frequencies or time scales, which has been controversially discussed for decades now.

Finally, thin films of the 50:50 wt% blend were studied by BDS, where capped and supported films were both investigated by Crossed-Electrode Capacitors (CEC) and Nanostructured Capacitors (NSC), respectively. The results were quantitatively discussed with the SHS ones as well as that of thin films of pure PVME. On the on hand, the combination of BDS and SHS provided a unique insight to study the different aspects of the glassy dynamics and its relationship to the dynamic heterogeneities. For PVME/PS blends, BDS is sensitive only to the segmental dynamics of PVME, as affect by PS, due to the negligible dipole moments of PS, compared to PVME. Whereas, SHS is sensitive to all the mobile segments of PVME and PS. Comparing that data from both methods elaborated the dynamics heterogeneity within the blend samples.

On the other hand, the BDS dielectric spectra of the films showed different dielectrically active processes. The first process was assigned to the α-relaxation of a bulk-like layer. For films measured by NSC, the rates of the α-relaxation were higher compared to that of the bulk blend. This behavior was related to the PVME-rich free-surface layer at the polymer/air interface. A second process was observed for all films measured by CEC (process X) and the 36 nm film measured by NSC (process X2). This process was assigned to fluctuations of constraint PVME segments by PS. Its activation energy was found to be thickness dependent, due to the evidenced thickness dependency of the compositional heterogeneity. Finally, a third process with an activated temperature-dependence was observed for all films measured by NSC (process X1). It resembled the molecular fluctuations in an adsorbed layer found for thin films of pure PVME, thus it is assigned accordingly. For the latter process, it was concluded that this process undergoes two extra confinement effects, in addition to the thickness reduction. I) Confinement between the strongly bounded part of the adsorbed layer and the bulk-like layer. This was deduced from the decrease of the activation energy (E_a) of process X, with decreasing temperature, for the same film thickness. II) Confinement due to frozen PS segments within the adsorbed layer. This was concluded by showing that E_a, decreases systematically with decreasing the film thickness.

The results of the thin films of the polymer blends point out to an extra parameter (compositional heterogeneity) to be considered when discussing the confinement effect on the glass transition and glassy dynamics. The findings clearly show that the local concentration (at a molecular level) changes drastically, with decreasing the film thickness. Moreover, they point to thickness dependent changes in the composition of the adsorbed layer. Hence, the importance of studying the dynamics and compositional heterogeneity of the adsorbed layers, which could strongly influence the overall glass transition and segmental dynamics of thin film.

12.2. Outlook

The next challenge to endeavor would be to draw a compositional "map" of the thin films of the blends, as a function of film thickness. This could be done through combining angle-dependent XPS measurements with time-of-flight Secondary Ion Mass Spectrometry (TOF-SIMS). In addition, BDS measurements, employing the NSC, of the naked irreversibly adsorbed layer solvent-leached from different film thicknesses, would allow for "mapping" the segmental dynamics as a function of thickness, at the polymer/substrate interface. Through BDS, XPS, and TOF-SIMS results, a full picture of the compositional heterogeneities as well as their deriving molecular mechanism could be drawn. This could help answering the long-standing question of *what are the molecular reasons behind the deviations and the compositional heterogeneities observed for thin polymer blend films?*

Furthermore, it was recently shown that the irreversibly adsorbed layer could have great potential for multiple technological applications. For instance, it was shown that adsorbed layers could have enhanced physical, mechanical, and thermal properties, compared to bulk, making them appealing candidates for lubricants, adhesives, and functional coatings applications.[1-5] These properties are closely related to the polymers intermolecular interaction, molecular weight, and chain and segmental mobility (e.g. α-relaxation). BDS measurements employing NSC, would allow for studying the molecular dynamics of the leached adsorbed layers. If the potential systems and or materials are of interest from the scientific and/or application point of view, i.e. block-copolymers, such studies could serve as both models for fundamental research as well as potential system for technological applications.

References

1 Lučić, S.; Kovačević, V.; Hace, D. *Int. J. Adhes. Adhes.* **1998**, 18, 115.
2 Zou, H.; Wu, S.; Shen, *J. Chem. Rev*. **2008**, 108, 3893.
3 Ellison, C. J.; Mundra, M. K.; Torkelson, J. M. *Macromolecules* **2005**, 38, 1767.
4 Soga, I. *J. Coat. Technol.* **2003**, 75, 53.
5 Zou, D. Q.; Yoshida, H. J. *Therm. Anal. Calorim*. **2010**, 99, 21.

Appendix I. - Supporting Information for Chapter 8

DOI: http://dx.doi.org/10.1021/acsami.6b14404

Atomic force microscopy (AFM)

A

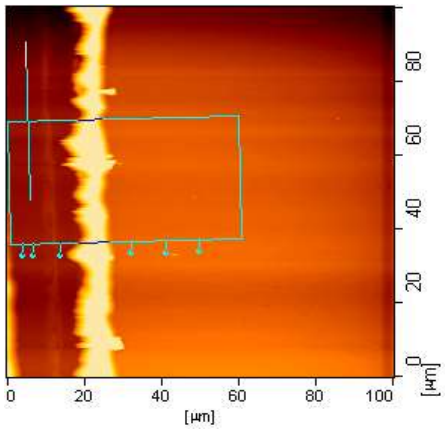

B

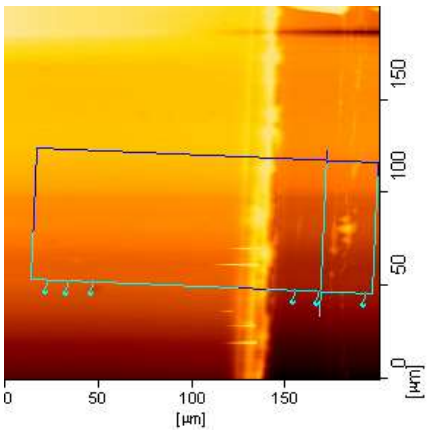

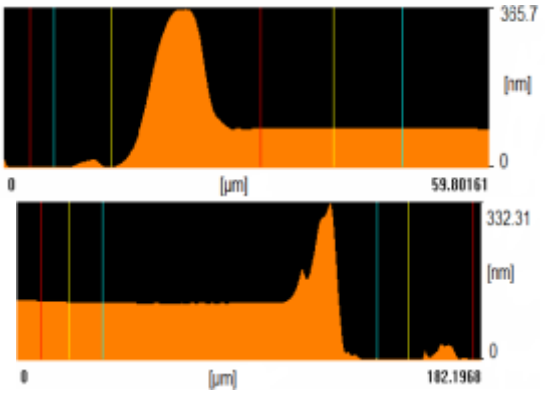

Figure S1. AFM image of a scratch across (**left**) the Al-electrode and (**right**) PVME film on the same Al-electrode **(A)**, cross section view **(B)** of the rectangular area indicating that the average thickness of the film in the marked scratch was ca. 50 nm. No sign of dewetting was found.

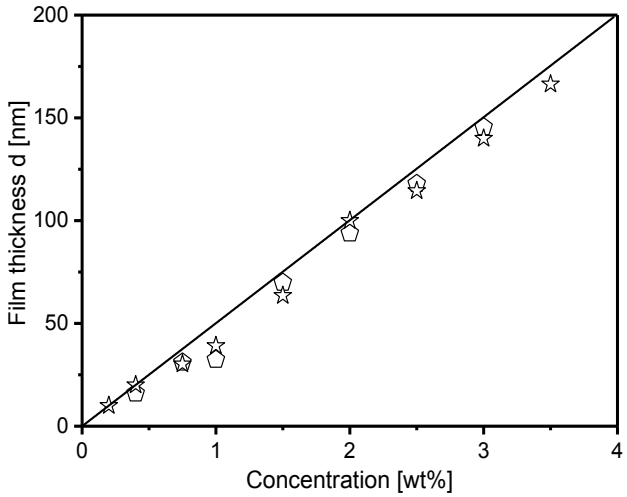

Figure S2. *Film thickness versus concentration of the polymer solution. Stars - ellipsometry thicknesses of PVME; black circles - thickness values estimated by AFM. The solid red line represents a common linear regression of the data.*

Broadband Dielectric Spectroscopy (BDS)

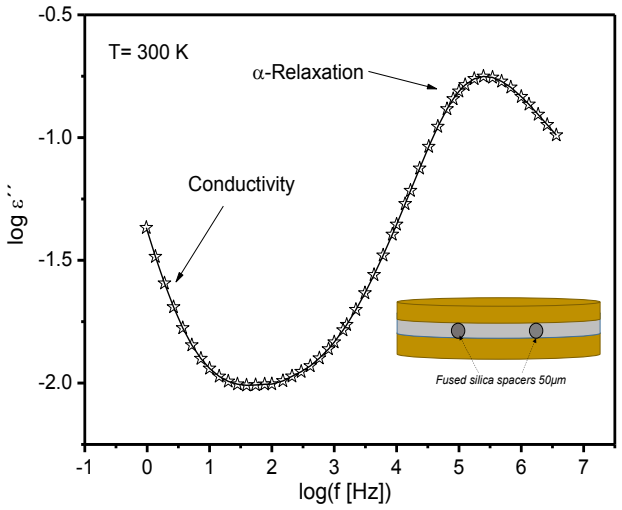

Figure S3. *Dielectric loss spectra for bulk PVME at 300 K- stars. The solid line is a fit of equation 3 to the data.* **Inset**. *Schematic of the sample geometry used to measure bulk PVME.*

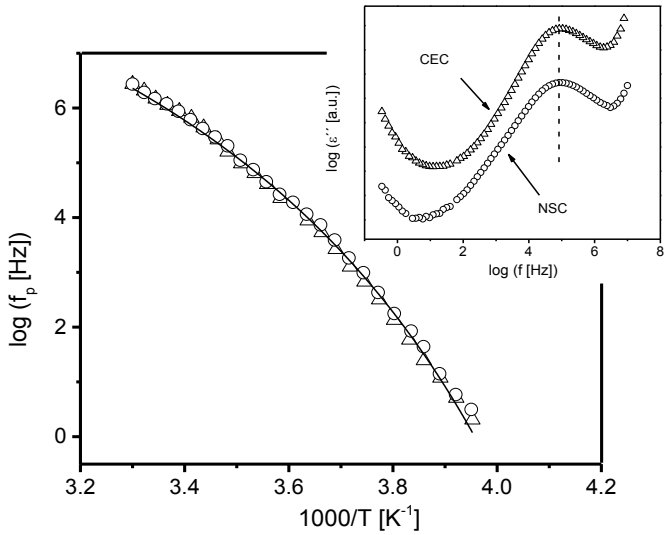

Figure S4. *Relaxation map of ca. 50 nm PVME films measured by CEC –triangles and NSC –circles. The solid line is a common VFT fit to the data.* **Inset.** *Dielectric loss spectra at 293 K for a ca. 50 nm PVME ultrathin film using the CEC - triangles and NSC – circles. The curves are shifted along the y-scale for sake of clearness.*

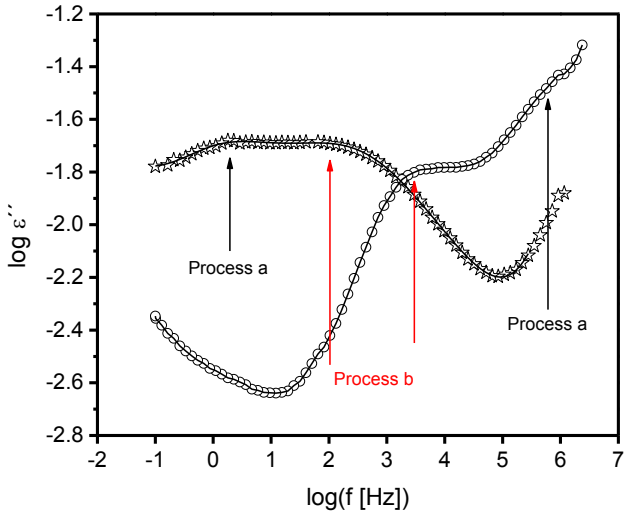

Figure S5. *Dielectric loss spectra at 305 K -circles and 253 K -stars for a ca. 7 nm PVME thin film using the NSC. The solid lines are fits for the data using equation 3. Process (a) α-relaxation of PVME and process (b) the relaxation of the segments within the part of the adsorbed layer with logarithmic time dependence.*

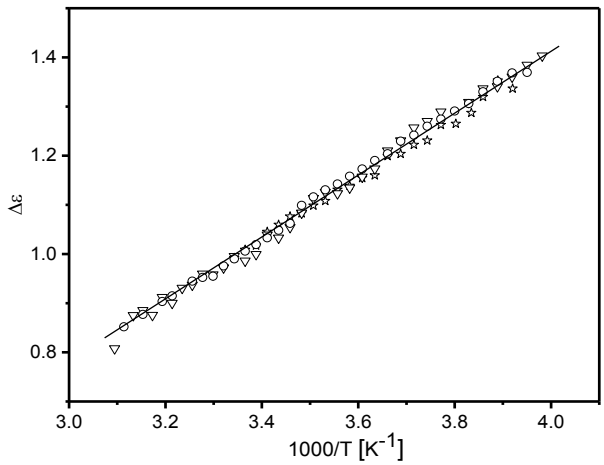

Figure S6. *Dielectric strength for PVME ultrathin films in CEC with thicknesses of 160 nm– circles, 110 nm- upside triangles and 50 nm – stars. The solid lines are linear fits to the data.*

Contact angle measurements (CAM)

$$(1+\cos\theta_i)\gamma_{L,i} = 2[(\gamma_{PVME}^{LW}\gamma_{L,i}^{LW})^{\frac{1}{2}} + (\gamma_{PVME}^{+}\gamma_{L,i}^{-})^{\frac{1}{2}} + (\gamma_{PVME}^{-}\gamma_{L,i}^{+})^{\frac{1}{2}}] \qquad \text{(S6)}$$

$$a_i\gamma^{PVME} = 2[b_i(\gamma^{LW}_{PVME})^{\frac{1}{2}} + c_i(\gamma^{+}_{PVME})^{\frac{1}{2}} + d_i(\gamma^{-}_{PVME})^{\frac{1}{2}}] \quad \text{(S2)}$$

$$\frac{(1+cos\,\theta_i)\gamma_{L,i}}{2\sqrt{\gamma^{LW}_{L,i}}} = \sqrt{\gamma^{P}_{S}}\,\frac{\sqrt{\gamma^{P}_{L,i}}}{\sqrt{\gamma^{LW}_{L,i}}} + \sqrt{\gamma^{LW}_{S}} \quad \text{(S3)}$$

Table S1. *Contact angle values of the test liquids used for poly(vinyl methyl ether).*

Test liquids	*Contact angle*
Glycerol	89.9°
HDEC	13.3°
PEG	64.6°
TDEC	7.4°

Table S2. *Total surface energies* γ^{Total} *and their dispersive* γ^{LW} *and polar* γ^{p} *components for PVME,* SiO_2 *and* AlO_2 *surfaces of the capacitors*.

	γ^{Total} [mJ m^{-2}]	γ^{LW} [mJ m^{-2}]	γ^{P} [mJ m^{-2}]
PVME	27.4	26.01	1.36
AlO_2	30.4	26.5	3.9
SiO_2	47.0	44.6	2.3

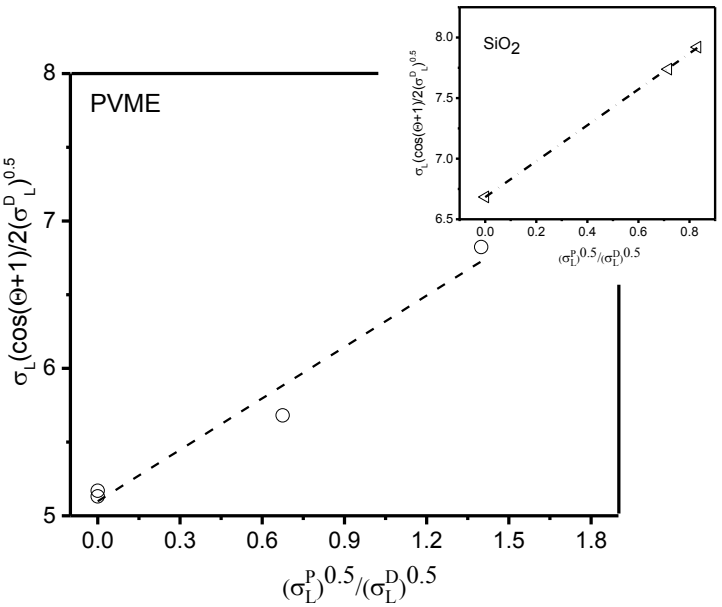

Figure S7. *Owens/Wendt plot according to Equ. (S3). The polar and dispersive components of the solid surface energy are estimated by linear regression. Results are presented in Table S1.*

Appendix II – Supporting Information for Chapter 10

DOI: http://dx.doi.org/10.1021/acsmacrolett.7b00625

Samples Preparation

Drying of Pure PVME: As-purchased PVME (aqueous 50-wt%) was dried in an oil free vacuum for 72 h days at 303 K, then for another 96 h at 323 K.

Si-wafer cleaning: Silicon wafers, with a natural silica layer, were sonicated in acetone for 15 min, for preliminary cleaning and removing of the photoresist layer, followed by nitrogen purging. Next, the cleaned wafers were put in an oxygen plasma for 300 s at 30 watts to burn off remaining organic contamination and activate the silicon oxide layer. As a final step, a carbon dioxide snow jet gun was used to further clean the wafer down to the microscale.

Thin Film preparation: The films were prepared by toluene dilution of the same master solution. Thin films were spin coated from the filtered (Minipore, 0.2 μm) diluted PVME/PS solutions, at 3000 rpm for 60 s, on to the cleaned silicon wafers. Film thicknesses were attuned by changing the solution concentration. After spin coating, all samples were dried in an oil-free vacuum (10^{-4} mbar) and annealed at 313 K ($T_{ann}=T_{g,Bulk}+ 50$ K) for 72 h, in order to remove the stress induced during spin coating and any residual solvent.[42]

Roughness of the different substrates: The substrates for SHS are different than the ones used in ellipsometry. While the substrates used for the former measurements are flat (roughness 0.43 nm rms) the roughness in the central area of the empty sensor used for the SHS measurements is rather large, ca. 3.5 nm rms (Zhou DS, Huth H, Gao Y, Xue G, Schick C. Macromolecules 2008, 41,7662). At the first glance, one could think that comparing results could be problematic. However, it was shown that for such high roughness values, the film follows the roughness of the substrate. This means that for a thickness of ca. 10 nm,

the roughness of the film on the sensor in comparable to that of a film prepared on a wafer (Huth H, Schick, C, personal communication). Moreover, the data measured with rough and flat surfaces agree (see figure 10.1B).

Film Thickness Estimation:

Films thicknesses were measured using a polarizer-compensator sample analyzer (PCSA) ellipsometer (Optrel GbR, Sinzing, Germany). The wavelength of the laser light was 632.8 nm and the angle of incidence was fixed to 70 degrees. The thickness and topography of the films were double checked by atomic force microscopy (AFM) after the measurement. The film thicknesses obtained by AFM were in a good agreement with the ellipsometry results (see fig. S1).

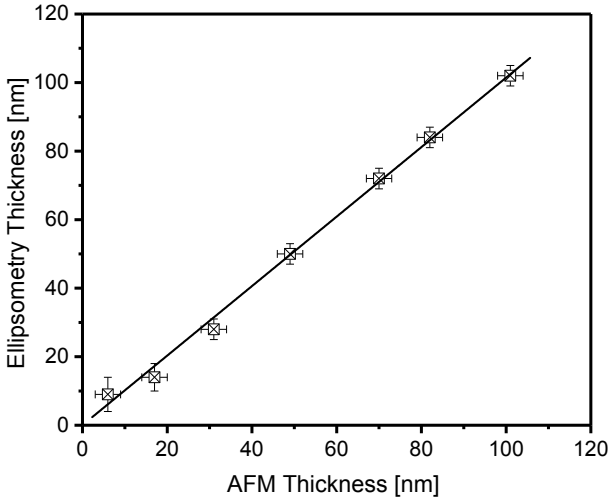

Figure S1. *Film thickness estimated by Ellipsometry versus AFM. Typical error bars are given. The solid line represents a common linear regression of the data*.

The prepared films showed a low surface roughness and no sign of dewetting or phase separation, even after heating to the maximum temperature reached during the measurement (see fig. S2).

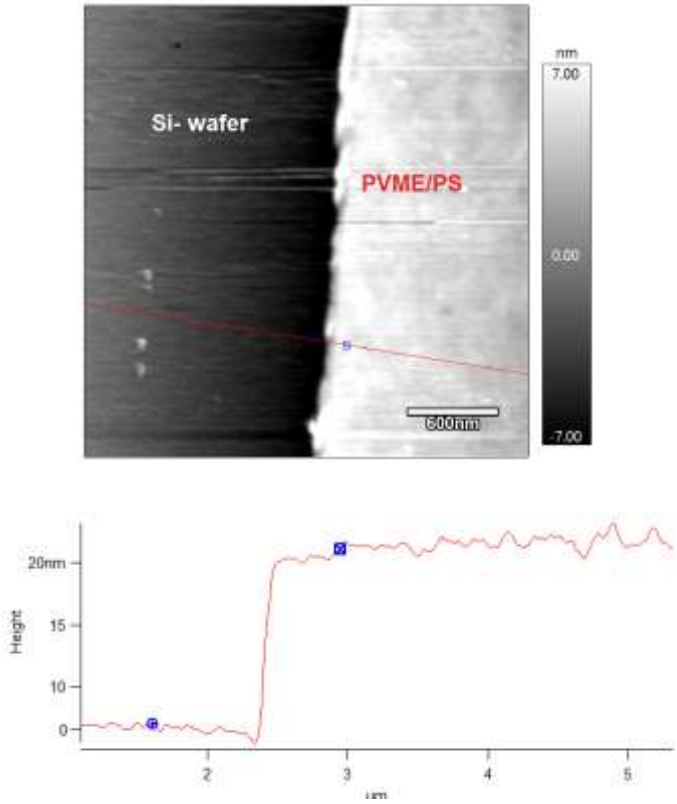

Figure S2. *AFM image of (top panel) top view and (bottom panel) cross section view of scratch across a PVME/PS (25:75-wt%) thin film with a thickness of 20 nm after annealing at T= 338 K for 72 hours. No sign of dewetting or phase separation is observed.*

Ellipsometry

Temperature dependent measurements conditions

Thin PVME/PS films can undergo phase separation. Therefore, the maximum temperature reached during the measurement was 383 K, which is below the cloud temperature, 448 K, of PVME/PS 25:75-wt%, measured for a 100 nm thick film. The heating/cooling rates were kept constant at 0.2 K/min.

Ellipsometry model

The analysis of the measurements employed a simplified multilayer model, consisting of air/polymer film/SiO_2/Si-substrate. To reduce the number of free fit parameters, the thickness of the SiO_2 layer was determined before spin coating the polymer film and then this value (ca. 1.7 nm) was kept constant during the data analysis for the polymer film.

It is important to note that an optimized model shall take into account the different compositional gradients within the film, which probably varies with decreasing the film thickness. This was concluded from references [Madkour, S.; Szymoniak, P.; Schick, C.;

Schönhals. A. J. Chem. Phys. 2017, 146, 203321 and Yin, H.; Madkour, S.; Schönhals. A. Macromolecules 2015, 48, 4936.] where the compositional change is mostly influenced by the surface enrichment effect, as the system attempts to reduce its Gibb's free energy [Jones, R. A. L.; Kramer, J. Polymer 1993, 34, 115-118].[18] An optimized model is currently under development and will be published elsewhere. It is worth to mention that the applied model will only influence the absolute values of the thickness but not its temperature dependence, which is addressed here. Further, it is important to note that the obtained thickness from the ellipsometry model are the optical thickness, which reflects the true thickness of the films. Please remember that the deduced optical thicknesses and the thicknesses measured by AFM are in a good agreement.

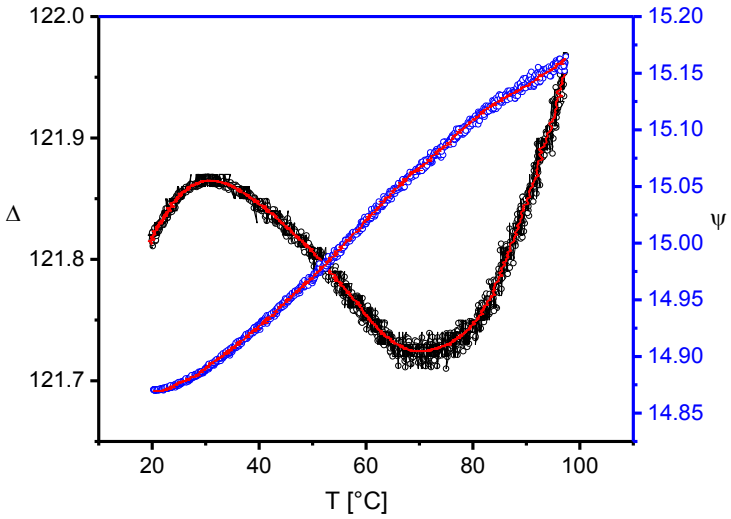

Figure S3. *A typical plot of the raw ellipsometry data measured at wavelength of 632 nm and angle of incidence of 70°. This data is for a 50 nm film of a PVME/PS 25:75-wt% blend. The model explained above was used to fit every point of the raw data. The solid red lines are the yielded fits.*

Preliminarily ellipsometric results of pure PVME thin films showing an increase in T_g^{therm} of pure PVME with decreasing film thickness.

Sample preparation: PVME thin films were prepared by spin coating, as explained above. After spin coating process, the samples were dried in vacuum (10^{-4} mbar, oil-free) and annealed at 313 K ($T_{ann}=T_{g,Bulk}+67$ K) for 72 h. It is important to note that AFM topography images revealed that films have low roughness down to 7 nm. Further, no inhomogeneities nor dewetting was observed.

The thickness of these films was verified using ellipsometery (M-2000 DI J. A. Wollam). The raw ellipsometric angles Ψ and Δ data were fitted to a Cauchy model ($n=A+B/\lambda^2$, K = 0). Where n and K are the real and imaginary indices of refraction. For the temperature measurements, the films were mounted onto a heating stage, inside a chamber, that was attached to the ellipsometer, to allow reaching lower temperatures (measurements were carried out from 200 K to 340 K). The heating/cooling rate was 1K/min. Both the heating and cooling rates were maintained using a liquid nitrogen cooling system. The closed chamber with the heating stage was purged with dry nitrogen gas throughout the experiment.

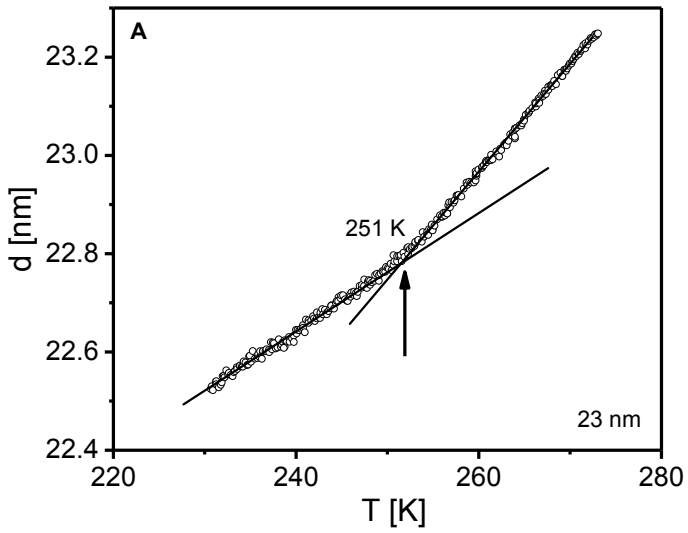

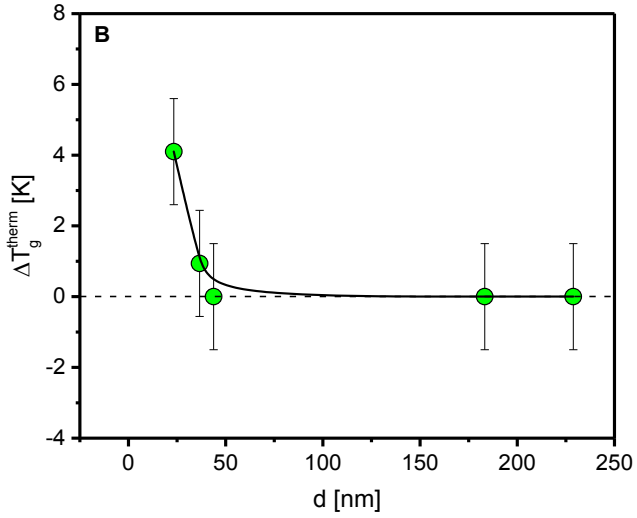

Figure S4. (A) *Thickness d as a function of temperature for a 23 nm thick PVME film, as an example. The arrow marks* T_g^{therm}. **(B)** ΔT_g^{therm} *for pure PVME thin films. The dashed line represents* T_g^{therm} *of bulk PVME measured by DSC.*

Thickness Dependency of T_g^{dyn} at Different Measuring Frequencies

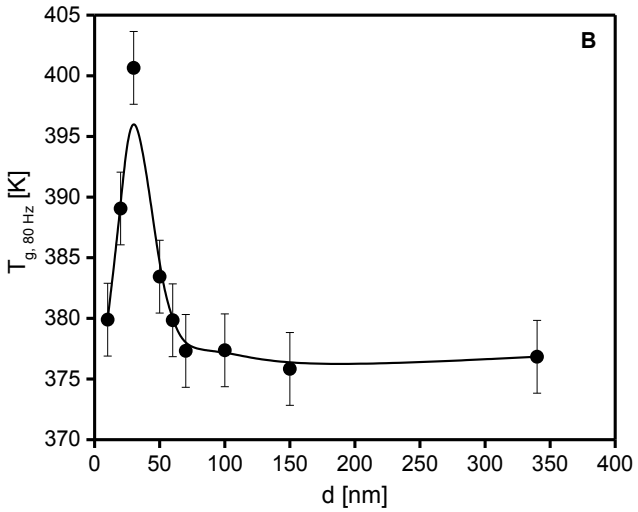

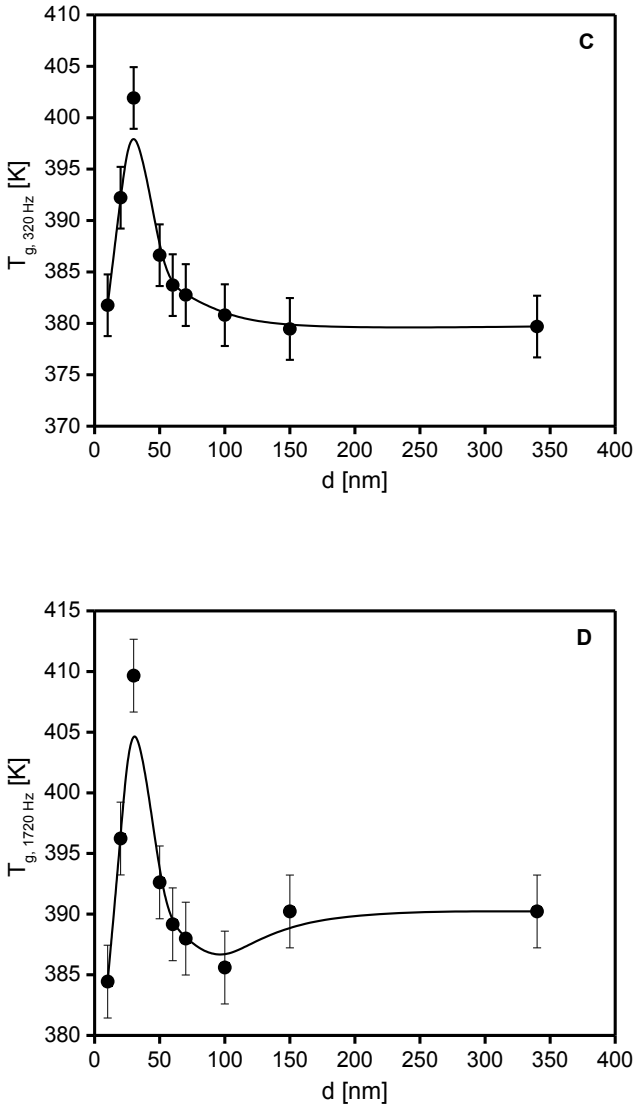

Figure S5. (**A**) $T_{g,1\,Hz}^{dyn}$ *extrapolated from the VFT fit lines* (**B**) $T_{g,80\,Hz}^{dyn}$ (**C**) $T_{g,320\,Hz}^{dyn}$ (**D**) $T_{g,1720\,Hz}^{dyn}$ *versus film thickness for all PVME/PS blend films measured. The lines represent the average values. The data were taken from reference [38]. Error bars are given. For all measured frequencies, the corresponding* T_g^{dyn} *shows in principle the same thickness dependence as discussed for 320 Hz.*

X-ray Photoelectron Spectroscopy (XPS)

XPS investigations were carried out with an ESCALAB 220iXL (ThermoFisher) using monochromatic Al K α radiation (1486.6 eV). The samples were fixed with a double adhesive Carbon tape on a stainless steel sample holder. The peaks were fitted by Gaussian−Lorentzian curves after Shirley background subtraction. The electron binding energy was referenced to the Ti 2p3/2 peak of TiO_2 at 458.8 eV. To quantitatively analyze

the peaks, the areas were determined and divided by the element-specific Scofield factor and the analysator-depending transmission function.

To confirm the PVME-rich interfaces (free surface and adsorbed layer) directly, XPS measurements were employed. It is worth to note that XPS measures only ca. 6 nm through the film.

Measurements of the free surface layer were conducted on a 228 nm film of PVME/PS 25:75 wt%. The estimation of the PVME concentration depends on the fact that PVME contains oxygen, in contrast to PS. Fig. S6 shows the C1s XPS-spectrum of the blend. The C-H and C-O bonds can be observed as separated peaks. The peaks were then fitted by Gaussian−Lorentzian curves after Shirley background subtraction to estimate the areas of both peaks ($I_{C\text{-}O}$ and $I_{C\text{-}H}$). For the weight fraction w of PVME, one obtains[43]

$$\frac{I_{C-O}}{I_{C-H}} = \frac{2w/M_{VME}}{\frac{8(1-w)}{M_S} + \frac{3w}{M_{VME}}} \qquad \text{(S7)}$$

where M_{VME} and M_S are the molecular weights of the repeating units of PVME and PS, respectively. The concentration of PVME was calculated to 76 wt% at the air/polymer interface. Thus, the PVME-rich surface layer is confirmed.

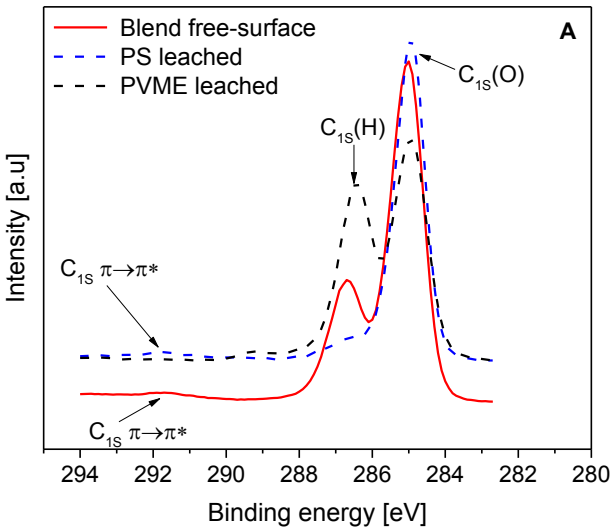

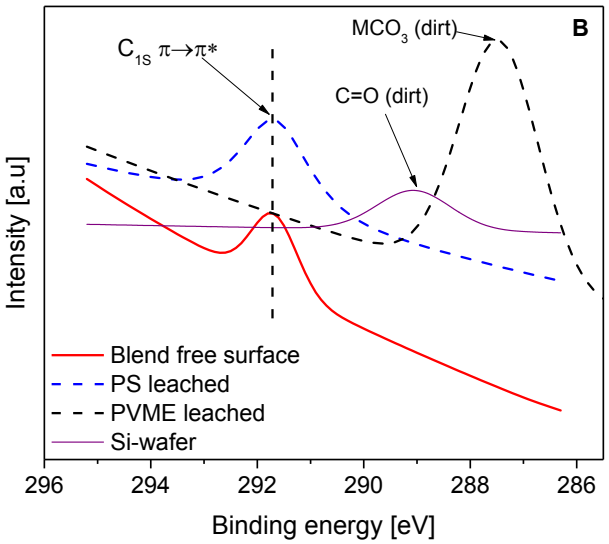

Figure S6. (**A**) *XPS C1s spectra for the free surface layer of PVME/PS 25:75 wt%. – red solid line, pure PS – dashed blue line, pure PVME – black dashed line.* (**B**) *XPS C1s π-π* spectra for the same samples, in addition to a clean Si-wafer as a reference – solid purple line. Please note that the C1s – π-π* peak is only observed for the blend free surface and the PS leached film.*

To measure the concentration of PVME within the *adsorbed layer*, XPS measurements were carried out on a second batch of samples, identically to the one used for the free-surface measurements, as explained above. Moreover, 220 nm films of pure PVME and pure PS, were prepared, for the comparison of the XPS measurements. Both samples, were prepared under identical spin coating conditions, as explained above. Pure PVME film was annealed at $T = T_g + 67$ K, whereas Pure PS was annealed at $T = T_g + 50$ K, for 72 hr in oil free-vacuum. This was then followed by solvent leaching of all samples, to unveil their *irreversibly adsorbed layer.*

Preparation of the irreversibly adsorbed layer was done employing solvent-leaching experiments (also called Guiselin brushes experiments). Toluene was used as the leaching-solvent, for all samples. First, all samples were dipped into separate toluene baths for 20 mins. This was then followed by a two-step process I) resining with toluene II) fast drying with dry nitrogen. Finally, the samples were annealed for 20 mins at $T = T_g + 50$ K. For a more detailed explanation, the reader is referred to ref. [41]. The yielded adsorbed layers were then checked by AFM, no sign of dewetting was seen. The thickness of this layer was found to be ca. 4 nm for PVME and PVME/PS blend, whereas it was found to be ca. 9 nm for PS.

XPS measurements carried out on *the irreversibly adsorbed layer* were conducted in identical manner, as explained above. However, since the thickness of the PVME film is thinner than the penetration range, of the X-rays, through the sample, it is expected that the surface of the wafer will also contribute the output signal, including any traces of dirt that might be there despite the thorough cleaning of the wafers. Consequently, in addition to analyzing the C1s peak, as it was done for the free surface, the C1s – π-π* peak, characteristic only for PS, was check and compared to a leached pure PS and pure PVME samples, as well as a cleaned Si-wafer. See fig. S7 and its inset.

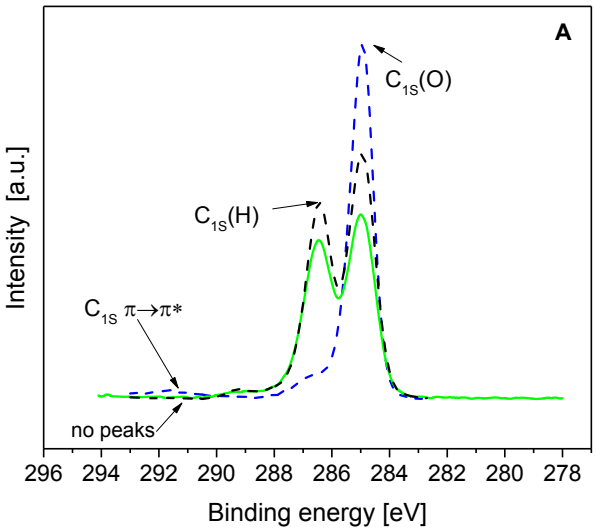

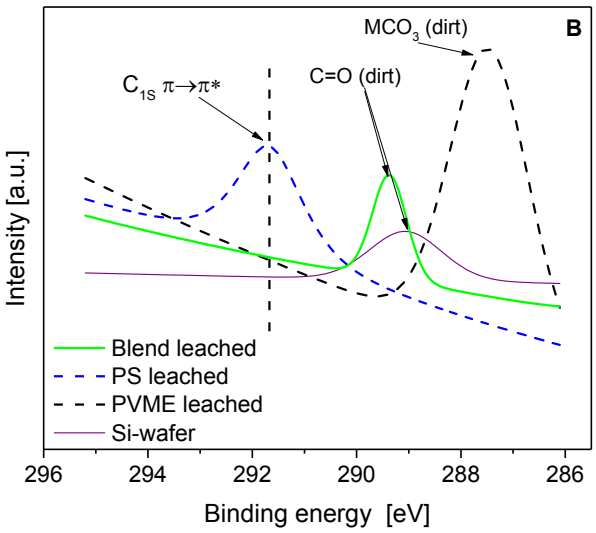

Figure S7. (**A**) *XPS C1s spectra for the irreversibly adsorbed layer of PVME/PS 25:75 wt%. – solid green line, pure PS – dashed blue line, pure PVME – black dashed line.* (**B**) *XPS C1s π-π* spectra for the same samples, in addition to a clean Si-wafer as a reference – solid purple line. Please note that no C1s – π-π* peak is not observed for the blend and PVME leached films, contrary to the pure PS leached film.*

The PVME concentration calculated from the C1s peaks (fig. S7) and according to equation S1, yields 106 wt%. This value evidence the Si-wafer, or possible organic dirt on the surface, contribution to the signal. Nevertheless, the value hints at a highly enriched PVME adsorbed layer. Furthermore, checking the C1s π-π* peak, and comparing it to that of pure PS and pure PVME leached films (inset fig S7), reveals that no C1s π-π* peak exists for the adsorbed layer of the blend, similar to the pure PVME. This is contrary to the free surface of the same blend, see inset fig. S6, as well as the leached pure PS film. Consequently, this directly evidence that the PVME concentration within the adsorbed layer is ca. 100 wt%, for this blend system.

Results of the all-free VFT fits

Table S1. *Estimated VFT parameters, for the fitting process where all parameters where kept free. SHS (nom) d is the thickness of the samples for SHS. Ellip. d is the thickness of the samples measured ellipsometry.*

SHS (nom.) d [nm]	Ellip. d [nm]	T_g^{therm} [K]	log (f_∞ [Hz])	A [K]	T_0 [K]	D
10	9	333.9	10.8	194.5	356.3	0.5
20	14	336.4	9.5	225.4	357.8	0.6
30	28	333.5	9.8	356.5	352.91	1.0
50	50	316.6	9.6	294.5	341.0	0.9
60	72	303.6	11.8	574.1	321.7	1.8
70	84	294.2	12.2	568.8	322.2	1.8
100	102	393.0	11.2	579.0	314.9	1.8
150	148	393.0	10.8	626.8	306.0	2.0
340	-	393.0	11.6	699.5	300.5	2.3

Table S2. *Estimated VFT parameters, for the fitting process where the arithmetic average of log f_∞ was calculated from the first step and kept fixed during the fitting.*

SHS (nom.) d [nm]	Ellip. d [nm]	T_g^{therm} [K]	log (f_∞ [Hz])	A [K]	T_0 [K]	D
10	9	333.9	10.9	233.0	354.0	0.7
20	14	336.4	10.9	362.4	348.8	1.0
30	28	333.5	10.9	506.4	343.5	1.4
50	50	316.6	10.9	500.9	326.8	1.5
60	72	303.6	10.9	473.9	327.2	1.5
70	84	294.2	10.9	526.5	329.9	1.6
100	102	393.0	10.9	543.2	317.0	1.7
150	148	393.0	10.9	647.6	303.8	2.1
340	-	393.0	10.9	676.2	301.8	2.2

$U_R \sim \Delta C_p$ as a function of thickness

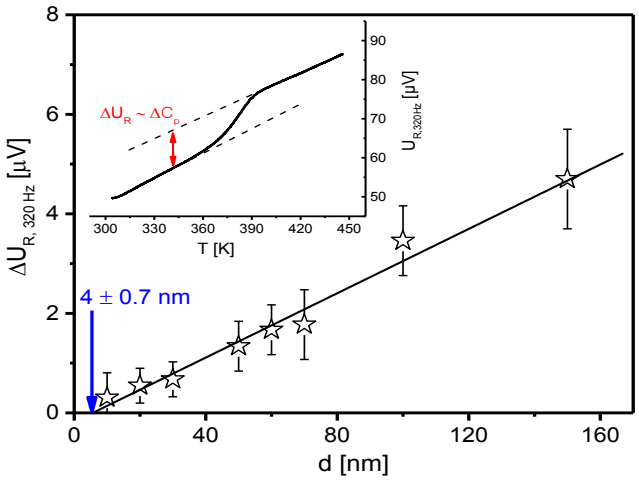

Figure S8 *ΔU_R versus the film thickness d for a frequency of 320 Hz for PVME/PS films. The solid line is a linear regression to the data.* **(Inset)** *Real part of the complex differential voltage U_R versus temperature for a 100 nm film measured at 320 Hz. The data are taken from reference [38].*

Appendix III – Supporting Information for Chapter 11

DOI: http://dx.doi.org/10.1021/acsami.7b10572

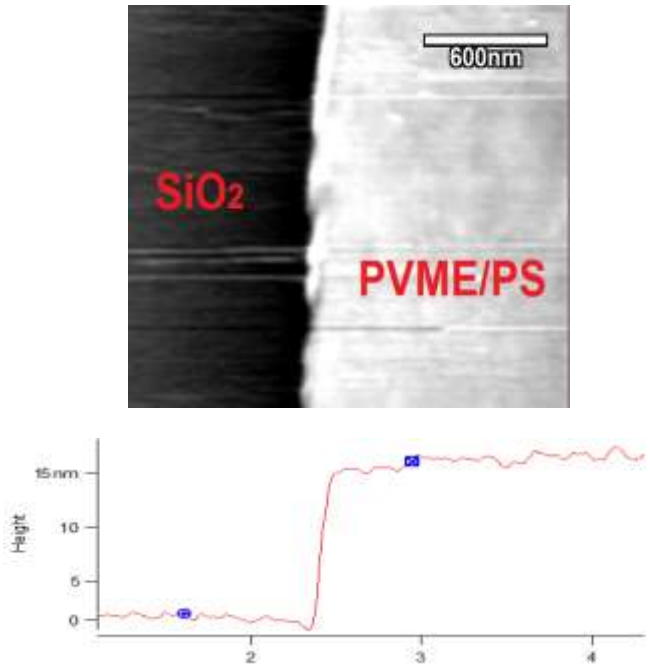

Figure S1. *AFM image (top panel) and the step height (bottom panel) of a scratch across a PVME/PS thin film with a thickness of 12 nm after annealing at T= 223 K for 72 hours. No sign of dewetting or phase separation is observed.*

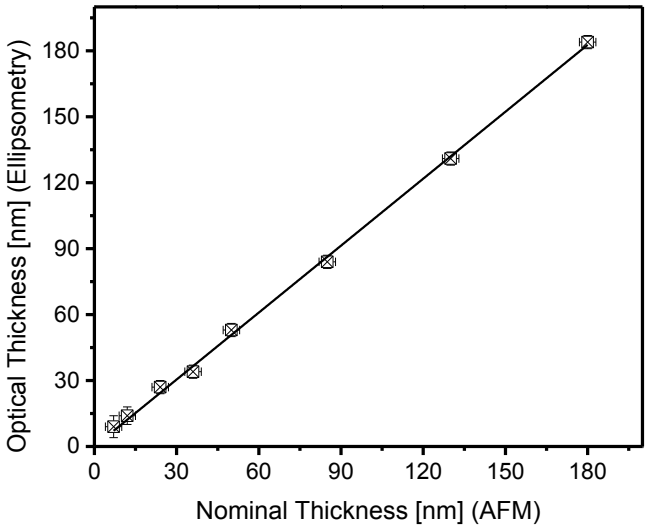

Figure S2. *Film thickness estimated by Ellipsometry (optical thickness) versus AFM (Nominal thickness). Typical error bars are given. The solid line represents a common linear regression of the data with a linearity factor of 0.997.*

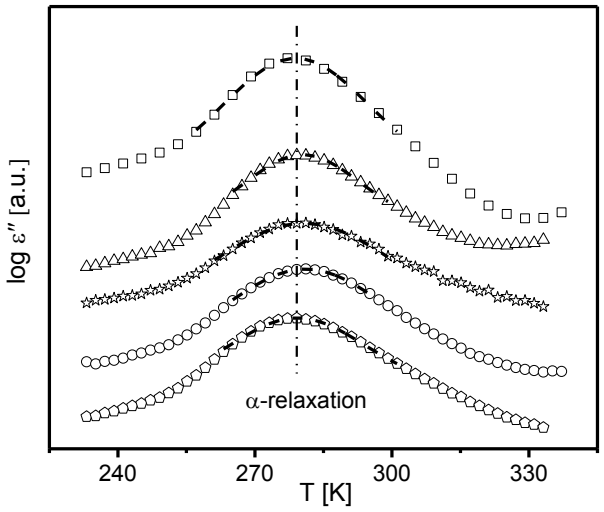

Figure S3. *Dielectric loss spectra in the temperature domain, for blend thin films measured in CEC at a frequency of 10 Hz. Triangles – 180nm, stars, 130 nm, circles -85 nm, and pentagons – 50 nm. The bulk blend sample – squares- is added for comparison. The dashed lines are Gaussians fitted to the peaks*.

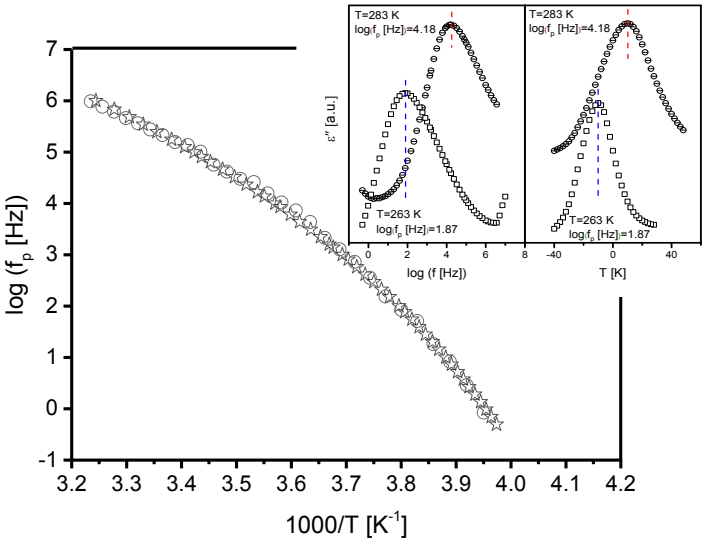

Figure S4. *Relaxation map of bulk pure PVME analyzed in both frequency – circles- and temperature – stars- domains. Data taken from ref. [51]. Inset: dielectric loss in both the temperature and frequency domains*.

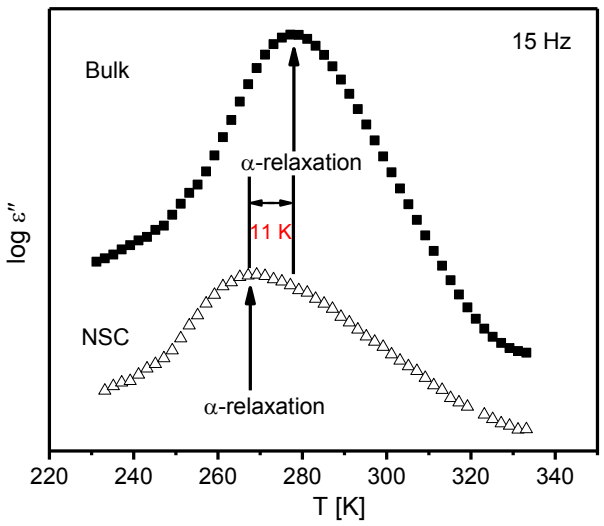

Figure S5. *Dielectric loss spectra in the temperature domain, for 36 nm thick blend films measured by NSC – open triangles and bulk PVME/PS –solid squares at a frequency of ca. 15 Hz. The arrows indicate the corresponding processes. The peak corresponding to the α-relaxation is shifted by 11 K.*

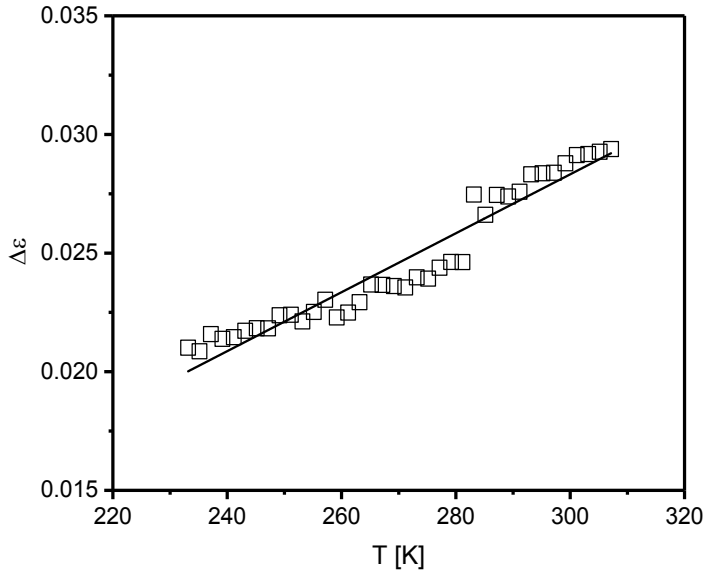

Figure S6. *Dielectric strength for process X for a 7 nm thick films, measured by NSC. The solid line is a linear regression to the data.*

X-ray photoelectron spectroscopy (XPS)

XPS investigations were carried out with an ESCALAB 220iXL (ThermoFisher) using monochromatic Al K α radiation (1486.6 eV). The samples were fixed with a double adhesive Carbon tape on a stainless steel sample holder. The peaks were fitted by Gaussian−Lorentzian curves after Shirley background subtraction. The electron binding energy was referenced to the Ti 2p3/2 peak of TiO_2 at 458.8 eV. To quantitatively analyze the peaks, the areas were determined and divided by the element-specific Scofield factor and the analysator-depending transmission function.

To directly evidence the PVME-rich interface at the polymer/air (free surface layer) and polymer/substrate interfaces (adsorbed layer), XPS measurements were employed. It is worth to note that the penetration depth of XPS is ca. 10 nm through the film.

Measurements of the free surface layer were conducted in ref. [43] for a ca. 200 nm blend film. There the PVME concertation was found to be 84 wt% at the free surface. Here, a thin blend film with a thickness of 60 nm was measured, see figure S7, and compared to the 200 nm film. The estimation of the PVME concentration depends on the fact that PVME contains oxygen, in contrast to PS, where the C-H and C-O bonds could be observed as separated peaks in the C1s spectra. The peaks could then fitted by Gaussian−Lorentzian

curves after Shirley background subtraction to estimate the areas of both peaks (I_{C-O} and I_{C-H}). For the weight fraction w of PVME, one obtains:

$$\frac{I_{C-O}}{I_{C-H}} = \frac{2w/M_{VME}}{\frac{8(1-w)}{M_S} + \frac{3w}{M_{VME}}} \quad \text{(S8)}$$

where M_{VME} and M_S are the molecular weights of the repeating units of PVME and PS, respectively. The concentration of PVME for the 60 nm film was estimated to be 66 wt% at the air/polymer interface.

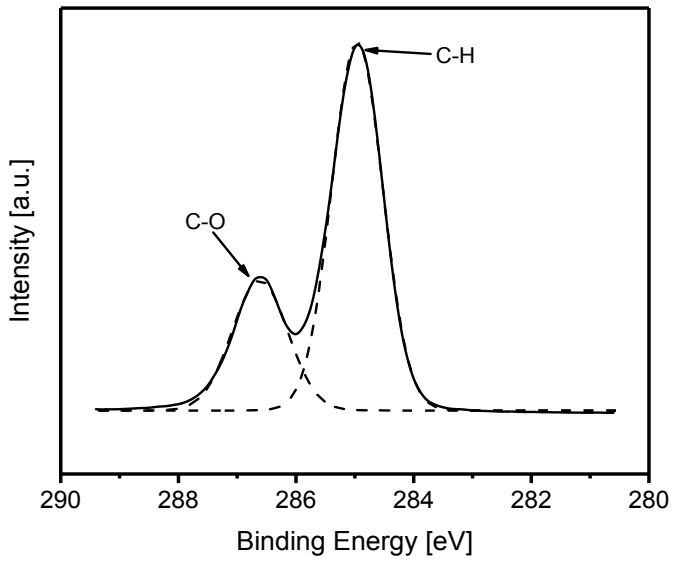

Figure S7. *XPS C1s spectra for the free surface layer of film of PVME/PS 50:50 wt%. with a thickness of 60 nm. The dashed lines represent the fitted Gaussian−Lorentzian. The PVME concertation was calculated according to equation S1 and found to be 66 wt%.*

To measure the concentration of PVME within the *adsorbed layer*, XPS measurements were carried out on a second batch of samples, identically to the one used for the free-surface measurements, as explained above. Moreover, 220 nm films of pure PVME and pure PS, were prepared, for the comparison of the XPS measurements. Both samples, were prepared under identical spin coating conditions, as explained above. Pure PVME film was annealed at $T = T_g + 67$ K, whereas Pure PS was annealed at $T = T_g + 50$ K, for 72 hr in oil free-vacuum. This was then followed by solvent leaching of all samples, to unveil their *irreversibly adsorbed layer.*

Preparation of the irreversibly adsorbed layer was done employing solvent-leaching experiments (also called Guiselin brushes experiments). Toluene was used as the leaching-

solvent, for all samples. First, all samples were dipped into separate toluene baths for 20 mins. This was then followed by a two-step process I) resining with toluene II) fast drying with dry nitrogen. Finally, the samples were annealed for 20 mins at T = T_g + 50 K. For a more detailed explanation, the reader is referred to ref. [18]. The yielded adsorbed layers were then checked by AFM, no sign of dewetting was seen. The thickness of this layer was found to be ca. 4 nm for PVME and PVME/PS blend (fig. S7), whereas it was found to be ca. 9 nm for PS.

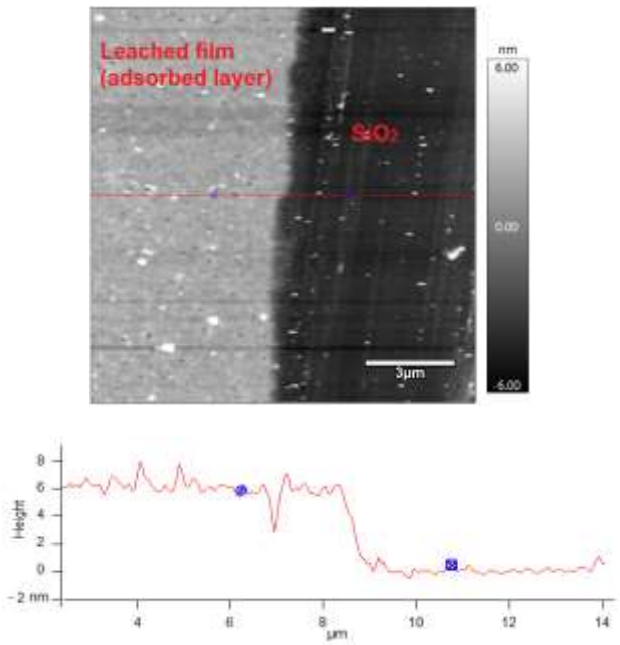

Figure S8. *AFM image (top panel) and the step height (bottom panel) of a scratch across a leached film from a PVME/PS 200 nm thick film. The thickness of the leached layer is ca. 4.5 nm. No sign of dewetting or phase separation is observed.*

XPS measurements carried out on *the irreversibly adsorbed layer* were conducted as explained above. However, since the thickness of the PVME film is thinner than the penetration range, of the X-rays, through the sample, it is expected that the surface of the wafer will also contribute the output signal, including any traces of dirt that might be there despite the thorough cleaning of the wafers. Consequently, in addition to analyzing the C1s peak, as it was done for the free surface,[43] the C1s – π-π* peak, characteristic only for PS, was check and compared to a leached pure PS and pure PVME samples, as well as a cleaned Si-wafer. See fig. S9B

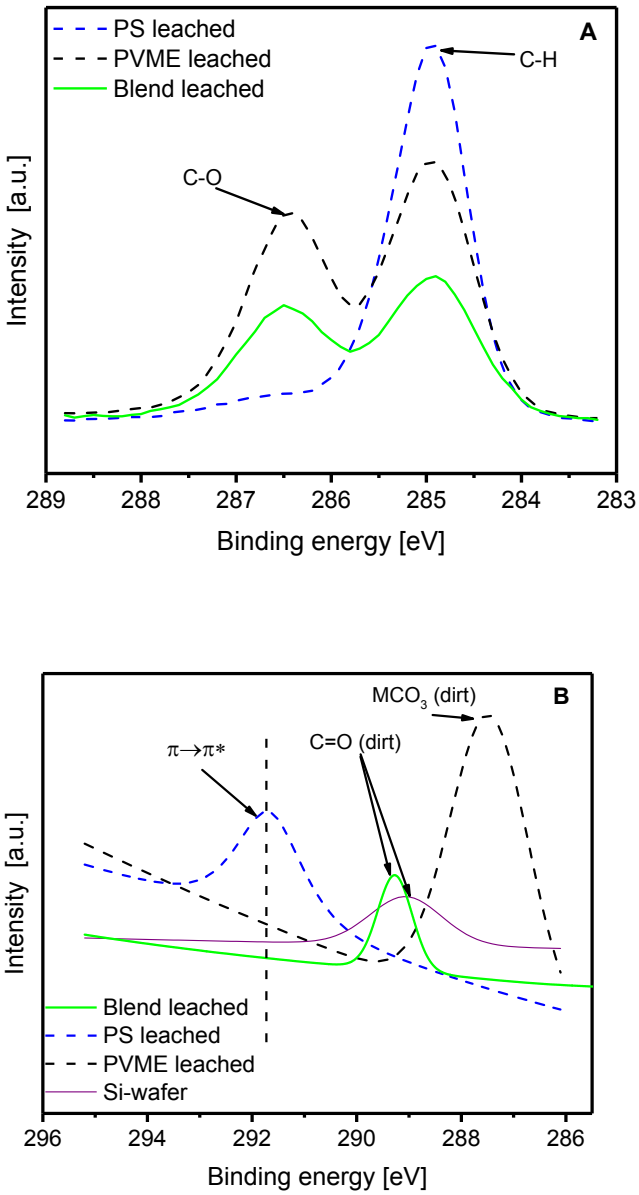

Figure S9. (**A**) *XPS C1s spectra for the irreversibly adsorbed layer of PVME/PS 50:50 wt%. – solid green line, pure PS – dashed blue line, pure PVME – black dashed line.* (**B**) XPS C1s π-π* spectra for the same samples, in addition to a clean Si-wafer as a reference – solid purple line. Please note that no C1s – π-π* peak is not observed for the blend and PVME leached films, contrary to the pure PS leached film.

The PVME concentration calculated from the C1s peaks (fig. S9) and according to equation S1, yields 109 wt%. This value evidence the Si-wafer, or possible organic dirt on the surface, contribution to the signal. Nevertheless, the value hints at a highly enriched PVME adsorbed layer. Furthermore, checking the C1s π-π* peak, and comparing it to that of pure PS and pure PVME leached films (fig S9B), reveals that no C1s π-π* peak exists for the adsorbed layer of the blend, similar to the pure PVME. This is contrary to the leached pure PS film.

Consequently, this directly evidence that the PVME concentration within the adsorbed layer is ca. 100 wt%, for this blend system.

Appendix IV

List of Abbreviations, Symbols and Constant

List of Abbreviations

DSC	Differential scanning calorimetry
CAM	Contact Angle Measurements
BDS	Broadband dielectric spectroscopy
SHS	Specific heat spectroscopy
XPS	X-ray photoelectron spectroscopy
AFM	Atomic force microscopy
VFT	Vogel-Fulcher-Tammann-equation
WLF	Williams-Landel-Ferry-equation
HN	Havriliak-Negami function
CRR	Cooperatively rearranging region
TCF	Temperature driven concentration fluctuations
SC	Self-concentration
PC	Poly(bisphenol A carbonate)/Polycarbonate
PS	Polystyrene
PVME	Poly(vinyl methyl ether)
P2VP	Poly(2-vinyl pyridine)
PMMA	Poly(methyl methacrylate)
M_w	Molecular weight
M_c	Critical molecular weight for entanglements
Al / AlO_x	Aluminum / Aluminum oxide
SiO_2	Silicon dioxide (Silica)
SiN	Silicon nitride
CEC	Crossed Electrode Capacitor
NSC	Nanostructured Capacitor

List of Symbols

τ	Relaxation time
T_g	Glass transition temperature
T_g^{therm}	Thermal glass transition temperature
T_g^{dyn}	Dynamic glass transition temperature
T_0	Vogel temperature
η	Viscosity
$f_{p,\alpha}$; $f_{p,\beta}$	α-relaxation rate; β-relaxation rate
E_A	Activation energy
c_p	Specific heat capacity
ρ	Density
ξ	Cooperative length of CRR
V_f	Free volume
V	Actual volume
V_0	Theoretical volume
E	Electric field
D	Dielectric displacement
P	Polarization
P_∞	Induced polarization
μ	Permanent dipoles
ε^*	Complex dielectric function
ε'; ε''	Real and imaginary part of the complex dielectric function
$\Delta\varepsilon$	Dielectric strength
F	Onsager's parameter
g	Kirkwood-Fröhlich correlation factor
ω	Angular frequency
f	Frequency
U_R	Amplitude of the complex differential voltage
φ	Phase angle of the complex differential voltage
θ	Contact angle
γ	Interfacial energy
d	Film thickness

List of Constants

k_B	Boltzmann constant ($k_B = 1.381\times10^{-23}$ m^2 kg s^{-2} K^{-1})
R	Ideal gas constant ($R = 8.314$ Jmol^{-1}K^{-1})
ε_0	Dielectric permittivity constant in vacuum ($\varepsilon_0 = 8.854\times10^{-12}$ AsV^{-1}m^{-1})
N_A	Avogadro number ($N_A = 6.022\times10^{23}$ mol^{-1})

List of Publications

Publications Included in Dissertation

1. **S. Madkour**, H. Yin, M. Füllbrandt, A. Schönhals. Calorimetric Evidence for A Mobile Surface Layer in Ultrathin Polymeric Films: Poly(2-vinyl pyridine). *Soft Matter* **2015**, 11, 7942-7952.
2. **S. Madkour**, P. Szymoniak, M. Heidari, R. von Klitzing, A. Schönhals. Unveiling the Dynamics of Self-Assembled Layers of Thin Films of Poly(vinyl methyl ether) (PVME) by Nanosized Relaxation Spectroscopy. *ACS Appl. Mater. Interfaces*. **2017**, 9, 7535-7546.
3. **S. Madkour**, P. Szymoniak, C. Schick, A. Schönhals. Unexpected Behavior of Ultra-thin Films of Blends of Polystyrene/Poly(vinyl methyl ether) Studied by Specific Heat Spectroscopy. *J. Chem. Phys*. **2017**, 146, 203321
4. **S. Madkour**, P. Szymoniak. A. Hertwig, M. Heidari, R. von Klitzing, S. Napolitano, M. Sferrazza, A. Schönhals. Decoupling of Dynamic and Thermal Glass Transition in Thin Films of PVME/PS Blends. *ACS Macro Letters* **2017**, 6, 1156-1161.
5. **S. Madkour**, P. Szymoniak, J. Radnik, A. Schönhals. Unraveling the Dynamics of Nanoscopically Confined PVME in Thin Films of a Miscible PVME/PS Blend. *ACS Appl. Mater. Interfaces.* **2017**, 9, 37289-27299.

Related Publications

1. H. Yin, **S. Madkour**, A. Schönhals. Unambiguous Evidence for a Highly Mobile Surface Layer in Ultrathin Polymer Films by Specific Heat Spectroscopy on Blends. *Macromolecules* **2015**, 48, 4936– 4941.
2. P. Szymoniak, **S. Madkour**, A. Schönhals. Dielectric Investigations of Nanoscopically Confined PVME in Thin Films of PVME/PS 25:75-wt% Blend. To be submitted to *Macromolecules* **2017**.
3. **S. Madkour**, A. Hertwig, A. Schönhals. The growth kinetics and Glassy Dynamics of Irreversibly Adsorbed PVME Layers. *In preparation*.

List of Awards

Best Poster Presentation: *"Dielectric Investigations on Carbon Nanomembranes"* at the 9th International Conference on Broadband Dielectric Spectroscopy and its Applications. Pisa, Itlay, **2016**.

Other Publications

Peer reviewed articles

1. S. Omara, M. Abdel Rehim, A. Ghoneim, **S. Madkour**, A. Thünemann, G. Turky, A. Schönhals. Preparation of Hyperbranched polymers/Kaolinite nanocomposites: Study of the glass transition by dielectric and specific heat spectroscopy. *Macromolecules*, **2015**, 48, 6562–6573.
2. **S. Madkour**, I. Melnichuk, A. Choukourov, I. Krakovský, H. Biederman, A. Schönhals. In situ Nanocalorimetric Investigations of Plasma Assisted Deposited Poly(ethylene oxide)-like Films by Specific Heat Spectroscopy. *J. Phys. Chem. B,* **2016**, 120, 3954–3962.
3. **S. Madkour**, A. Choukourov, D. Nikitin, I. Gordeev, A. Schönhals. In situ calorimetric measurements of multi-layered Cu NPs/PEO nanocomposite films by specific heat spectroscopy. To be submitted to *J. Phys. Chem. B*, **2017**.
4. S. Omara, **S. Madkour,** M. Abdel Rehim, A. Youssef, A. Thünemann, G. Turky, A. Schönhals. In situ polymerization of HBP/ nanocomposites: Dielectric relaxation studies. To be submitted to *Macromolecules*, **2017**.
5. **S. Madkour**, P. Penner, X. Zhang, A. Gölzhäuser, A. Schönhals. Dielectric Investigations of Carbon Nanomembranes. To be submitted to *ACS Nano*, **2017**

Book Chapter

1. H. Yin, **S. Madkour**, A. Schönhals. Dynamics in confinement: Progress in Dielectrics, **2014**, 2, F. Kremer (Eds.), *Springer*.

Conference Contributions

Invited Talks

1. **S. Madkour**, P. Szymoniak, A. Schönhals. In-Situ Probing of the Dynamics of Irreversibly Adsorbed Layers in PVME Thin Films. *8 IDMRCS*, Wisla, Poland, **2017**.
2. **S. Madkour**, P. Szymoniak, A. Schönhals. Unveiling the Heterogeneous Structure of Miscible Polymer Blend Confined in Ultrathin Films Via Nanosized Relaxation Spectroscopy. *UPenn Seminar*, Philadelphia, PA., USA, **2017**.

Oral Presentation

1. **S. Madkour**, P. Szymoniak, A. Schönhals. Unveiling the Dynamics of Self-Assembled Layers of Ultra-Thin Films of PVME by Nano Relaxation Spectroscopy. *APS March meeting*, New Orleans, La., USA, **2017**.
2. **S. Madkour**, P. Szymoniak, A. Schönhals. Dielectric and Thermal Relaxation Behavior of Ultra-Thin Films of Poly(vinyl methyl ether) – Evidence of an Adsorbed Layer. *9th International Conference on broadband dielectric spectroscopy and its applications*, Pisa, Italy, **2016**.
3. **S. Madkour**, P. Szymoniak, A. Schönhals. Behavior of Ultra-Thin Films of Blends of Polystyrene/ Poly(vinyl methyl ether) by Nanosized Relaxation Spectroscopy. *9th*

International Conference on broadband dielectric spectroscopy and its applications, Pisa, Itlay, **2016**.

4. **S. Madkour**; P. Szymoniak; M. Heidari; R. von Klitzing; A. Schönhals. Evidence of a three-layered structure in ultra-thin PVME and PVME/PS blend films by nano-sized relaxation spectroscopy. March spring meeting, *German Physics Society (DPG)*, Regensburg, Germany, **2016**.
5. **S. Madkour**; H. Yin; M. Füllbrandt; A. Schönhals. Dynamic glass transition of ultrathin poly(2-vinyl pyridine) films. March spring Meeting, *German Physics Society (DPG)*, Berlin, Germany, **2015**.

Poster presentation

1. **S. Madkour**, P. Penner, X. Zhang, A. Gölzhäuser, A. Schönhals. Dielectric Investigations on Carbon Nanomembranes. *9th International Conference on Broadband Dielectric Spectroscopy and its Applications*. Pisa, Italy, **2016**.
2. **S. Madkour**, P. Szymoniak, A. Schönhals. Evidence of a Three-Layered Structure in Ultrathin PVME and PVME-PS Blend Films by Nanosized Relaxation Spectroscopy. *14th Lähnwitzseminar on Calorimetry*, Rostock, Germany, **2016**.
3. **S. Madkour**, H. Yin, A. Schönhals. Calorimetric Glass Transition of Ultra-Thin Poly(2-Vinyl Pyridine) Films. *8th International Conference on Broadband Dielectric Spectroscopy and its Applications*, Wisla, Poland, **2014**.
4. **S. Madkour**, H. Yin, A. Schönhals. Specific Heat Spectroscopy Characterization of Dynamic Glass Transition in Ultra-Thin Poly(2-Vinyl Pyridine) Films. *Polydays Conference: Beyond Self-Assembly - Making Polymeric Materials More Versatile*. Berlin, Germany, **2014**.
5. S. Omara, M. Abdel Rehim, A. Ghoneim, **S. Madkour**, G.Turky, A. Schönhals. The Effect of Preparation Method on the Physical Properties of the Nanocomposites Based on Hyperbranched Polymers. Spring Meeting, *German Physics Society (DPG).* Berlin, Germany, **2015**